Análisis integrado del impacto de la variabilidad ambiental en las condiciones del fondo marino en el Mediterráneo durante el Último Ciclo Glacial

Santiago Casanova Arenillas

Tesis Doctoral

2023

Directores:

Francisco Javier Rodríguez Tovar

Francisca Martínez Ruiz

Programa de Doctorado en Ciencias de la Tierra

UNIVERSIDAD DE GRANADA

Departamento de Estratigrafía y Paleontología

Editor: Universidad de Granada. Tesis Doctorales
Autor: Santiago Casanova Arenillas
ISBN: 978-84-1195-124-1
URI: https://hdl.handle.net/10481/88714

Table of Contents

Acknowledgements/

Agradecimientos

En primer lugar es importante que primeramente agradezca a los sistemas e instituciones que me han permitido realizar y terminar este trabajo. He disfrutado estos años de un contrato de formación del profesorado por el que tengo que agradecer al Ministerio de Educación y Universidades (FPU17/01207), asi como de dos ayudas a la movilidad enmarcadas en el mismo programa. También el trabajo de esta tesis se ha integrado a lo largo de estos años en proyectos de investigación (P18-RT-4074), gracias a los cuales he dispuesto de los medios para poder llevar a cabo parte del proceso.

Como todo en la vida, el llegar a ciertos objetivos nunca es resultado solo del esfuerzo de uno mismo, sino que es el resultado conjunto de éste y el apoyo recibido durante el camino. Muchas personas me han acompañado durante el proceso que me ha llevado aquí y parte del mérito siempre recaerá en estas. Personalmente llegar a término con éxito esta etapa que ha sido la realización de los estudios que se presentan en esta tesis no ha sido siempre fácil y nunca habría llegado al final sin el apoyo de todas estas personas e instituciones.

Mi más sincero agradecimiento a mis dos directores de tesis, al Dr. Francisco Javier Rodríguez Tovar y la Dra. Francisca Martínez Ruiz, los cuales me dieron en primer lugar la oportunidad de iniciar este camino y me han acompañado, colaborado conmigo y formado, mostrando siempre mucha paciencia y apoyo lo cual siempre agradeceré. Sin ellos nada había sido posible.

He de agradecer también a la Universidad de Southampton (UK) y a los Doctores Paul Wilson y Chuang Xuan, gracias a los cuales pude realizar mis estancias durante el doctorado, las cuales me ayudaron en gran medida a completar mi formación como científico. Agradezco a su vez a todas aquellas personas del *National Oceanography Centre* en Southampton que me dieron formación y apoyo durante mis 6 meses allí.

También tengo que agradecer mucho a las personas con las que he podido trabajar en conjunto durante esta tesis, especialmente al Dr. José Noel Pérez Asensio, a Ricardo Monedero Contreras y al Dr. Víctor Villasante Marcos con los cuales fue un placer colaborar.

También he de agradecer todo ese apoyo que si no enmarcado en un ámbito laboral o investigador ha sido para mí igualmente importante para seguir adelante. Tengo mucho que agradecer a todas las personas que me han acompañado a lo largo de estos años y que son más de los que puedo nombrar. Agradezco por supuesto a mi familia, mis padres y hermanas, por su apoyo incondicional y presencia constante. también tengo muchísimo que agradecer a Marilo, mi principal acompañante y apoyo, que ha estado ahí en cada momento de este proceso que ella ha tenido que vivir muy de cerca. Agradezco a todos los amigos que han estado ahí, los

que estaban ya y los que se fueron uniendo, con especial mención a todos los que me llevo de esta etapa, para mi probablemente la cosa más importante que me llevo de este periodo. Agradezco a todos los compañeros que ahora ya considero amigos que han pasado por la becaría de paleo, los que estaban antes de mi llegada y me acogieron como uno más, y los que fueron llegando y los que se quedan tras de mí. Agradezco a todos los compañeros del Departamento que me han hecho fácil estar donde he estado. A todos y a todos los que me dejo, gracias.

Abstract

The Last Glacial Cycle is one of the most interesting periods for environmental studies, presenting some of the most complete records of climatic and environmental changes that can be analogous to the current anthropogenic climate change. In addition, the Mediterranean area presents a highly interesting setting for palaeoceanographic, paleoclimatic and palaeoenvironmental studies, situated and impacted by both the north, middle and equatorial latitudes climate systems and presenting al the oceanographic characteristics of a big ocean with much faster reaction times.

The layers rich in organic carbon, such as the sapropels in the Eastern Mediterranean Sea and their counterparts in the Western Mediterranean, the Organic Rich Layers (ORL), represent one of the most interesting phenomena within the recent geological record of the Mediterranean Sea Basin. These events have occurred over the past 3 million years as a consequence of the restriction of the waters of deep parts of the Mediterranean basins in response to climatic changes. This doctoral thesis presents a comprehensive analysis of these layers during the Last Glacial Cycle, with a particular focus on the ORLs, which have received less attention in past works, with the objective of deciphering the environmental changes and oceanographic and climatological triggers of these events in the Mediterranean. Additionally, a comparative examination between events in the West and East Mediterranean Sea basins is conducted, elucidating the temporal evolution of both basins and differences in the external factors leading to the deposition of these layers.

In the present thesis, a multiproxy approach is employed to assess the stated objectives, integrating inorganic geochemistry and palaeontological proxies, in particular, the ichnological features observed on core surfaces. Novel ichnological analysis tools have been developed through image analysis, which have been applied in conjunction with traditional ichnological and geochemical analysis techniques on three cores from the Alboran Sea and one core from the Ionian Sea, near the Gulf of Sirte.

Through the different projects completed during this thesis, some particular and general conclusions have been obtained. It has been observed that the relationship between ORLs and sapropels is intricate, and they generally respond asynchronously to climatic events, with no clear correlation between the bottom water conditions in the eastern and western events found, indicating a differential response to climatological variations over the Last Glacial Cycle. Sapropel depositions are more influenced by the African Monsoon cycles, while ORLs exhibit a more coherent response to the warm-cold cycles of the Last Glacial Period. Further, differences between the different ORLs and sapropels have been found, indicating variable conditions and important differences between the events that produced their deposition, with at least 3 main typologies of ORLs described. The utility of a multiproxy analysis, encompassing geochemical and paleontological data, in deep-sea core studies has been

confirmed. Furthermore, the value of continuous ichnological analysis has been underscored in comparison with other indicators and in complementing other data in the analysis of marine sediment cores.

Resumen

El Último Ciclo Glacial es uno de los períodos más interesantes desde el punto de vista científico para el estudio de cambios paleoambientales. De este periodo se pueden encontrar algunos de los registros más completos de cambios climáticos y ambientales, los cuales se pueden equiparar como análogos del cambio climático antropogénico actual. Además, el área mediterránea se presenta como un escenario muy interesante para estudios paleoceanográficos, paleoclimáticos y paleoambientales, situada e impactada por los sistemas climáticos de latitudes norte, media y ecuatorial y presentando todas las características oceanográficas de un gran océano con tiempos de reacción mucho más rápidos.

Las Capas Ricas en Carbono Orgánico, como los sapropeles del Este del Mar Mediterráneo y sus equivalentes del Oeste del Mediterráneo, conocidas como Organic Rich Layers (ORL) en su acepción inglesa, son uno de los eventos más interesantes que se pueden encontrar en el registro geológico reciente del Mar Mediterráneo. Estos eventos ocurrieron durante los últimos 3 millones de años como resultado del aislamiento de las partes profundas de las cuencas mediterráneas, impedida su renovación, un fenómeno que ocurre en respuesta a cambios oceanográficos inducidos por cambios climáticos. En esta tesis doctoral se ha realizado un análisis detallado de estos intervalos sedimentarios durante el Último Ciclo Glaciar, prestando una especial atención a las ORLs, las cuales habían sido menos estudiadas. También se realiza una comparación entre los eventos ocurridos en el Oeste y el Este del Mediterráneo, comprobando cómo se comportan ambas cuencas a lo largo del tiempo y analizando las diferencias en las causas que llevaron al depósito de estas capas.

En esta tesis, para alcanzar los objetivos propuestos, se ha utilizado una aproximación multi-indicador, combinando indicadores de geoquímica inorgánica y paleontología, especialmente información icnológica. Se han desarrollado nuevas herramientas de análisis icnológico a través del análisis de imágenes, las cuales se han integrado con otras técnicas tradicionales de análisis icnológico y geoquímico en 3 sondeos del Mar de Alboran y en un sondeo del Mar Jónico, cercano al golfo de Sidra.

A través de los diferentes proyectos realizados durante esta tesis se han obtenido algunas conclusiones particulares y generales sobre las ORLs y la dinámica del mar Mediterráneo. Se ha observado que la relación entre ORL y sapropels es compleja, respondiendo de forma general de forma asincrónica a eventos climáticos, no existiendo una correlación clara entre las condiciones del agua del fondo en los eventos orientales y occidentales estudiados. Por tanto, se observa una respuesta diferencial a las variaciones climatológicas durante el último Ciclo Glacial entre el este y el oeste del mar Mediterráneo. Los sapropeles están claramente controlados por los ciclos del monzón africano, mientras que los ORL exhiben una respuesta más coherente con los ciclos de transición rápida cálido-frío del último período glacial. Además, se han encontrado diferencias entre los diferentes ORL y sapropels, lo que indica importantes

diferencias en las condiciones del fondo marino durante la deposición de las diferentes capas, encontrándose al menos 3 tipologías principales de ORL atendiendo a sus características sedimentológicas y icnológicas. Se ha confirmado la utilidad de un análisis multi-indicador, que abarque datos geoquímicos y paleontológicos, en estudios de núcleos de aguas profundas. Además, se ha subrayado el valor del análisis icnológico continuo en comparación con otros indicadores y para complementar otros datos en el análisis testigos de sedimentos marinos.

PART 1

INTRODUCTION AND BACKGROUND

Chapter I

Introduction

I.1. Motivation

I.1.1. Why?

The environmental changes that occurred over the Last Glacial Cycle in the Mediterranean Sea have been investigated during the elaboration of this PhD thesis. The motivation behind this PhD thesis arises from the necessity for a deeper comprehension of the impact of climate change on the deep-sea environments in marine basins. During this text, the focus will be put on the reconstruction of past environmental changes, specifically on the variations in the oxygenation of deep-sea bottom waters that have occurred as a response to the past climate changes in the Mediterranean region. The presented research is significant for comprehending the influence of past and present climate variability in marine settings, thus shedding light on the consequences and impacts of climate change.

Significant consensus exists today in the scientific community that human-produced emissions of greenhouse gases like CO_2 and CH_4 have resulted in a constant increase in their concentration in the atmosphere, induced by the insufficient capacity of the earth's systems to absorb them at the same rate (IPCC, 2021). As a result, important changes in the Earth's atmosphere, oceans, and land surface have been occurring since the initiation of the Industrial Revolution around 1750 of the Common Era, significantly affecting from the past to the future the planet's biosphere and cryosphere (IPCC, 2021). For instance, CO_2 has reached 417 ppm in 2022 and is expected to increase much further under the current emission rate. Under the worst emissions scenarios proposed in the IPCC (2021), CO_2 levels will surpass those of the Miocene by the end of the century, reaching levels not seen since the Eocene millions of years ago by the middle of this millennium (e.g., Rae et al., 2021). This rapid change will have unexpected consequences, with some worrisome results already being observed. For instance, over the last decades, absolute global temperature maximums over the previous records are constantly being reached, entering uncharted territory for the Earth's climate.

Making the situation even more worrying, the rapid warming of the atmosphere due to CO_2 has the potential to reach "tipping points" (Lenton et al., 2008), events of accelerated changes, not easily predictable, that result from the triggering of positive feedback loops. Some of these tipping points could be the halting of important ocean currents like the Atlantic Meridional Overturning Circulation (AMOC), the melting of one or several ice caps, or the liberation of methane in the permafrost due to increased temperatures (Lenton et al., 2008; Lenton and Ciscar, 2013). Reaching one or more of these points will mean dramatic changes and could be considered as points of no return for the current trend. Thus, the rapidly accelerating anthropogenic climate change poses a significant threat to economies and societies worldwide, presenting immense challenges to adapt. Scientific knowledge can inform decision-making and policy processes related to climate change, allowing us to better prepare for and mitigate its impacts.

It is important to understand how and when future change events will develop with the intention of being able to deal with the challenges that a rapidly changing planet presents. However, due to the complexity of the climate system, with the interconnectedness of the oceans, atmosphere, biosphere, and continents over extended periods, understanding the Earth's systems and the prediction of the future is extremely complicated. Continuous collaboration within the scientific community is essential to achieving these objectives. Scientists must integrate their efforts to enhance the understanding of climate change by refining models, collecting new data, and improving data-gathering techniques. The earth science disciplines play a very important role in the necessary collective effort, as it is crucial to know and understand the past in order to predict what the future holds. Many of the driving forces behind past global changes are similar to the stressors we are experiencing today, albeit at different rates of change. Therefore, reconstructing past Earth dynamics at various temporal resolutions is crucial for finding analogues for current climate change, understanding the Earth's response, identifying important tipping points and feedback mechanisms, and predicting ecological and environmental consequences.

During this thesis, the focus will be put on the ocean's environmental changes over time. Understanding how oceans have evolved during past climatic transitions is important in the climate context, where some of the first signals of important alterations are already occurring. Oceans cover approximately 70% of the Earth's surface and contain approximately 97% of the planet's surface water, one of the most, if not the most, important component of the Earth's system. They face important challenges in the future. For instance, they face warming, deoxygenation, and acidification, all impacting important ecosystems. All these threats are strongly influenced by human-made stressors, like the changing climate and its decades-long cumulative impact, and the effect is expected to be further amplified in the future (Halpern et al., 2019). In addition, due to the slow reaction times, oceans can potentially produce dramatic fast climate changes and be the cause of reaching certain of the previously mentioned tipping points (Allison and Bassett, 2015); for example, if important currents stop, altering the global or region atmospheric patterns, or if deep cold parts of the ocean that have been absorbing the

warming of the atmosphere get too warm to continue regulating the climate and induce rapid climate changes, or a reduction of the mixing of the oceans limits oxygen availability in the deep ocean and leads to a lack of nutrients at the surface; all these and other dramatic processes are known to have happened in the past (e.g., Clark et al., 2002; Alley et al., 2003; Rousseau et al., 2022).

Among the many problems related to the oceans in a warming world, deoxygenation due to increased stratification is one major problem already occurring as a result of climate change (Polovina et al., 2008; Stramma et al., 2012; Breitburg et al., 2018) with the potential for the creation of anoxic conditions in several parts of the oceans (Roegner et al., 2011). For instance, the oceans have averaged 2% or more of oxygen loss in the last 50-100 years just by temperature increases reducing oxygen solubility (Levin, 2018). For the issue of ocean dysoxia and its potential impact on human societies, of special interest is the study of anoxic basins and an understanding of the processes that have regulated the anoxic events in the geological record (e.g., Hennekam et al., 2020; Dermawan et al., 2022). Other climate change consequences in the oceans will include important shifts in primary productivity with unknown consequences on marine resources and the global carbon cycle (Bopp et al., 2013) or the disappearance of the Arctic summer sea ice, increased methane venting from the deep ocean sediments, acidification, warming and rising sea level (Bijma et al., 2013).

All the presented problematics and challenges make the significance of paleoenvironmental and paleoclimatic studies undeniably significant, focused on past oceanic environments, such as the one presented in this PhD thesis.

I.1.2. Where, When and How?

Among the many areas of the world that will undergo challenging scenarios in the future, the Mediterranean showcases important consequences and faces important challenges, with the surface temperature increasing steadily over the last decades (Pastor et al., 2020). In addition, the Mediterranean region is intensely populated, with more than 160 million people living in it (UNEP/MAP and Plan Bleu, 2020). This area is one of the more highly menaced areas for climate change, defined as a hot spot for future global warming (Giorgi, 2006).

Also, this sea is very interesting from a scientific point of view as a laboratory for studies on palaeoclimate and palaeoceanography, and even though its particularities will be developed in detail in the next chapter (Chapter II), some of them deserve to be mentioned here, as crucial factors that render this sea an exceedingly captivating backdrop for the objectives of this thesis. The Mediterranean constitutes a complex and dynamic system shaped by atmospheric, oceanic, and terrestrial processes, in which all the marine phenomena that occur at the ocean scale are also observed (e.g., Robinson and Golnaraghi, 1994; Bergamasco and Malanotte-Rizzoli, 2010). However, as it is a small basin with short residence times, reactions occur much faster than in open oceans (Schroeder et al., 2017), making it more susceptible to climate change. As a result,

the Mediterranean Sea shows modifications in its dynamics more rapidly than other oceans, which is what gives it its high interest for palaeoclimatology and palaeoceanography as an analogue to open oceans (Bethoux et al., 1999). Thus, the Mediterranean region reacts to environmental changes faster than other regions since oceans present longer residence times and prolonged reaction times; these are some of the characteristics that make the Mediterranean an exceptional place to investigate future climate changes (Lejeusne et al., 2010). In addition, the Mediterranean location is exceptional for the study of climate interconnections between different regions at a global scale, like the connection of the Mediterranean climate, the North Atlantic oscillation, or the Monsoons (Lionello et al., 2006). Furthermore, and related to the focus of this thesis on oxygenation of deep ocean basins, the deep ventilation of the Mediterranean Sea has been highly variable in the geological time scale in response to climate changes (e.g., Cramp and O'Sullivan, 1999; Sierro et al., 2005; Rogerson et al., 2008; Rohling et al., 2015), also being susceptible to climate pattern shifts in recent decades (e.g., Roether et al., 1996; Tsimplis et al., 2006; Schroeder et al., 2008, 2012).

The period studied in this thesis, the Last Glacial Cycle, from the end of the Penultimate Glaciation to the Holocene, is particularly interesting in palaeoclimate reconstructions. It is characterised by rapid climate changes (e.g., Rasmussen et al., 2014), which makes it a suitable analogue for investigating future anthropogenic climate changes. The Mediterranean is known to have responded very fast to these changes, leaving a continuous record even of short-duration variations (Schroeder et al., 2017). Over the Last Glacial Cycle, these significant environmental responses to the rapidly fluctuating climate are known to have also produced one of the main impacts associated with climate change, such as oxygen depletion, which in turn resulted in changes in water mass circulation (Schroeder et al., 2017; Schroeder and Chiggiato, 2022). This period is likewise of special interest in human evolution, as modern humans embarked from Africa during the cooling phase of the Last Glaciation, subjected to important regional climate changes (e.g., Stewart and Stringer, 2012), and where climatic shifts were a primary trigger of human dispersion (e.g., Müller et al., 2011).

The reconstruction of past climates requires reliable proxies for appropriate interpretation of physical, chemical, and biological conditions. Such reconstructions are essential to improve our understanding of current environmental conditions and predictions. This calls for improving the current proxies and developing new ones, as well as new ways of integrating different proxies. In this regard, the thesis (see Chapter I.2) is aimed at contributing to palaeoenvironmental reconstructions by using a multiproxy approach, incorporating multiple lines of evidence from different sources, including abiotic ones, such as bulk sediment geochemical composition and biogenic proxies, including ichnological features. The combination of these different proxies will afford a comprehensive and robust understanding of bottom water conditions in the Mediterranean over the Last Glacial Cycle and allow for identifying key drivers and patterns of variability. Additionally, using this integrated multiproxy approach will provide a new and improved understanding of the bottom water conditions in the Mediterranean and their role in shaping the regional climate system.

I.2. Objectives

This thesis explores how climatic changes have impacted the deep Mediterranean over the Last Glacial Cycle, spanning from the Penultimate Glaciation's Termination to the Holocene epoch's onset. It also attempts to understand further what processes trigger the deep-water restriction in the Mediterranean basins in a transect from west to east.

The proposed objectives will significantly contribute to advancing our comprehension of the effects of climate change on marine environments and emphasise the significance of ancient records in accomplishing this task. These objectives are the following:

- The primary aim of this study is to reconstruct the variations in oxygen conditions in bottom waters in different settings of the deep Mediterranean Basin over the Last Glacial Cycle by studying several sediment cores and using a multiproxy approach that combines ichnological features with geochemical information.
- Understand the relationship between changes in deep-sea oxygen content and climate variations and gain insights into the processes influencing oxygen levels and their link to global climate dynamics. Particular attention is given to the rapid climate changes that occurred during the Last Glaciation, such as the Heinrich Events.
- Gaining insights into the spatial variations of environmental conditions and processes within the Mediterranean Basin over the Last Glacial Cycle, also establishing a West-East transect_to assess how these variations evolve across different basins.
- Evaluating palaeoceanographic changes that account for the observed variability and gaining an understanding of the continental and atmospheric configurations that trigger these changes.
- Assessing and evaluating the used palaeoproxies, in particular the potential of integrating automatic image analysis into the ichnological study workflow in well cores and evaluating new methodologies for describing and recognising organic-rich layers in well cores, utilizing easily accessible data such as colour analysis, ichnological features in well-core images, and XRF core scanner outputs.

I.3. Thesis structure

This thesis comprises 11 chapters grouped into four sections.

Part 1 Introduction and Background.

This section corresponds to the thesis introduction, presenting the motivation, the main characteristics of the studied region, and the state of the art in the knowledge of the Mediterranean sediment records. Section I groups the three first chapters.

Chapter I provides the background and foundation for the motivation of this research.

Chapter II consists of a review of the current knowledge about the Mediterranean climate and oceanographic characteristics, including sedimentary processes occurring in the deep basin, as well as the knowledge of palaeoenvironments, including "Sapropels" and "Organic Rich Layers" deposition.

Chapter III presents an update of geochemical and ichnological proxies in palaeoenvironmental studies, focusing on the proxies used in this thesis.

Part 2 Materials and Methods.

In this section, the materials used for the thesis, as well as the main methodologies applied, are presented; it comprises two chapters.

Chapter IV presents the studied materials, including sites and sediment records. It also focuses on sampling and analytical methods.

Chapter V concerns the methodology for the ichnological analysis and presents a method (published in Computers and Geosciences) for the automatic analysis of images from well-core surfaces.

Part 3 Results and Discussion.

Here, the main research results are grouped into four chapters; two include already published papers, one is a submitted manuscript, and the last chapter corresponds to work that is still in progress.

Chapter VI focuses on the evolution of the ichnological features in the deep Alboran Sea Basin over the Last Glacial Cycle, including a comparison between two Ocean Drilling Program (ODP) Sites located at the east and the west of the Alboran Ridge.

Chapter VII presents the Organic Rich Layers' characteristics for the same two ODP records using ichnological features and colour analysis.

Chapter VIII consists of a multiproxy approach including ichnological features, inorganic geochemistry, palaeomagnetic susceptibility, and foraminifera assemblages to study the evolution of the Western Alboran Sea Basin over the last 35 kyr, with a particular focus on the ORL1 formation.

Chapter IX includes the ichnological and geochemical analysis of a sediment record in the Eastern Mediterranean Basin, spanning the time interval from Termination II to the Early Holocene.

Part 4 Integrated Discussion and Conclusion.

The fourth section presents a general and integrative discussion (Chapter X) and conclusions (Chapter XI).

Chapter II

The Mediterranean Over the Last Glacial Cycle: climate, oceanography, and sedimentation

II.1. The Mediterranean Sea general setting

The Mediterranean Sea is a semi-enclosed marginal sea between Europe and Africa, between 45° and 30° North. This basin covers 2470000 km^2, with an average depth of 1500 m and a maximum depth of 5267 m at the Calypso Deep in the Levantine Basin (Woodward, 2009). The abyssal plains cover 1159644 km^2 and have a mean depth of 2534 m, with slopes that do not usually reach more than 1 degree (Schroeder and Chiggiato, 2022).

The Mediterranean Basin is subdivided into two main sub-basins, the Eastern and Western Mediterranean basins (Fig. II.1). The dynamics of the Mediterranean are affected by its narrow connection with the Atlantic Ocean via the Gibraltar Strait, which narrows down to a minimum width of 14 km at a depth of 880 m (Bryden and Kinder, 1991) and to a minimum depth of 170 m on the Camarinal Sill (Woodward, 2009). Western and Eastern basins are separated by the wide Sicily Strait of about 145 km, with an average depth of 130 m (Wüst, 1961). It is connected to the Marmara Sea at the NE by the Dardanelles Strait, which has an average depth of 55 m and is 1.2 km wide (Woodward, 2009), and through it to the Black Sea. These characteristics are unique to the Mediterranean, with no other marginal sea having such a reduced connection to the global ocean with a similar large size (e.g., Lionello, 2012). In addition, the Mediterranean presents multiple minor subbasins, presenting different insolation grades. For instance, in the Western Mediterranean, several basins can be differentiated (Fig. II.1): the Alboran Sea Basin, the Gulf of Lions, the Algerian Basin, the Balearic Basin, the Ligurian Basin, and the Tyrrhenian Basin. The Eastern Mediterranean can be divided into several other basins, such as the Adriatic Basin, the Ionian Basin, the Aegean Basin and the Levantine Basin.

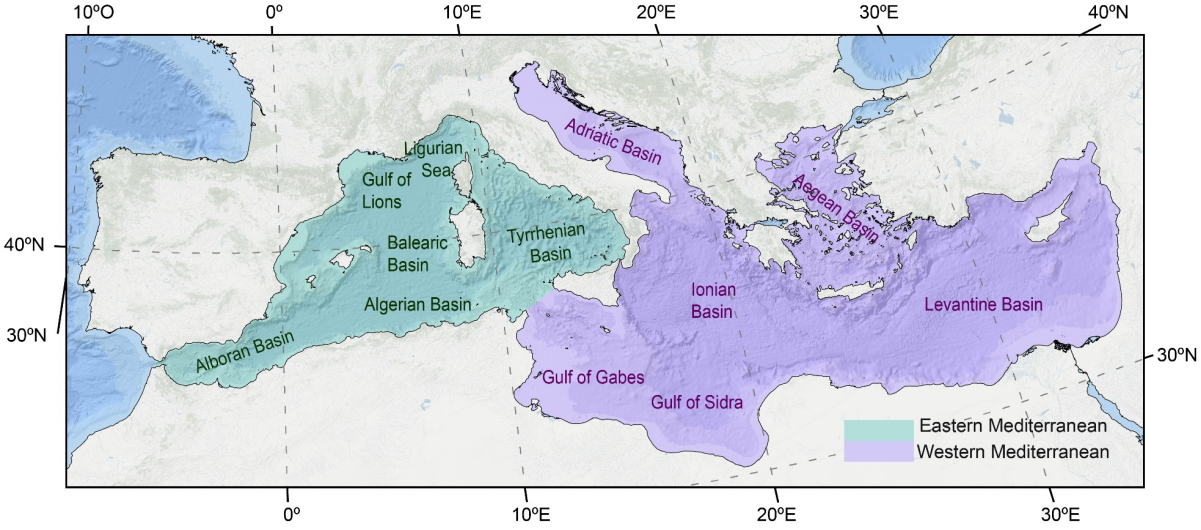

Figure II.1. Mediterranean basins.

The Mediterranean comprises the westernmost part of the Alpine Himalayan orogenic belt. It can be considered a relic ocean basin formed as a result of the closure of the Tethys Ocean, which began with the convergence of the Africa and Eurasia plates during the Cretaceous period (Dercourt et al., 1986). This process still occurs today at rates over 1 cm/year but generally around 5 mm/year (Nocquet and Calais, 2004). The movement northwards of the African plate after its counterclockwise rotation in the Miocene (23 My) has been the main factor controlling the Mediterranean orography and characteristics, closing the Tethys Ocean and progressively creating a more restricted basin (e.g., Rögl, 1999). Today, the African plate is subducting under the European plate. Due to the variable velocities in different subduction zones, a rollback occurs (Leeder et al., 2003); thus, the primary movement occurs obliquely to the main compression direction (Rosenbaum et al., 2002; Rosenbaum and Lister, 2004). This rollback gives the basin an observable shape and produces its division into two differentiable basins at East and West (Fig. II.1), separated by Italy and the Sicily Channel. The Calabrian and Hellenic arcs in the Eastern Mediterranean Basin are the central zones of active subduction and tectonic activity in the Mediterranean today.

Vulcanism has occurred since the beginning of the Quaternary, mainly in the line between Tuscany, Sicily and Pantelleria volcanic region, even though it has had a much wider distribution over the past, appearing in the Hellenic and Calabrian arcs (Paterne et al., 1988, 2008; Pe-Piper and Piper, 2002). This vulcanism has produced the deposition of ash layers that can be recognised in abyssal areas and can cover more than 100 km^2 for the most explosive eruptions (Aksu et al., 2008; Satow et al., 2015).

As a result of this complex geologic history, the basin is surrounded by several mountain ranges resulting from the collision of Africa and Europe, the most important being the Alps in Europe. The orography of the Mediterranean Sea margins and the sea basin plays a significant role in shaping its distinct climatic and oceanographic characteristics. These surrounding mountain ranges significantly influence atmospheric dynamics by affecting wind patterns and storm movements (Lionello, 2012). Furthermore, the intricate distribution of islands and peninsulas within the Mediterranean gives rise to a complex system of currents, with circulation organized into sub-basin scale gyres (for a more comprehensive description, see Chapter II.3).

II.2. Climate variability over the Last Glacial Cycle

II.2.1. General characteristics of the present Mediterranean climate

The Mediterranean region is situated in a transitional zone between tropical and mid-latitude climate systems. This unique position enables the basin to exhibit characteristics influenced by the interaction between these two systems, which has resulted in the development of the general Mediterranean climate across various temporal and spatial scales (Fig. II.2; Lionello et al., 2006). This transitional nature makes the Mediterranean an exceptional location for studying changes in global dynamics and exploring the interconnections between different atmospheric components as well as several zones of the planet.

In this regard, significant changes are recognized across the Mediterranean. For instance, the dynamics of the northern Mediterranean are primarily influenced by the North Atlantic Oscillation (NAO) and other teleconnections with mid-latitudes, while the south and east of the Mediterranean are rather subjected to variations in the high-pressure belt corresponding with the north pole flank of the Hadley cells and the African Monsoon activity (Hoerling et al., 2004; Xoplaki et al., 2004; Lionello et al., 2006). The resulting climatic transition from north to south can be seen in the local Köppen climate classifications, which range from the mid-latitudinal temperate climates corresponding to the categories Cfa, Cdb, Cfc, Csa, Csb, that can be found in the northern margin to the boreal or polar climates appearing in the mountain ranges (Fig. II.3), advancing south to arid and semiarid climates corresponding to the types BSh, BsSk, BWh, BWh (Fig. II.3). Orography also has an important influence on climate. For instance, the numerous mountain ranges around the basin (Fig. II.4) produce sharper climatic responses over time and favour wind channelling (Lionello et al., 2006).

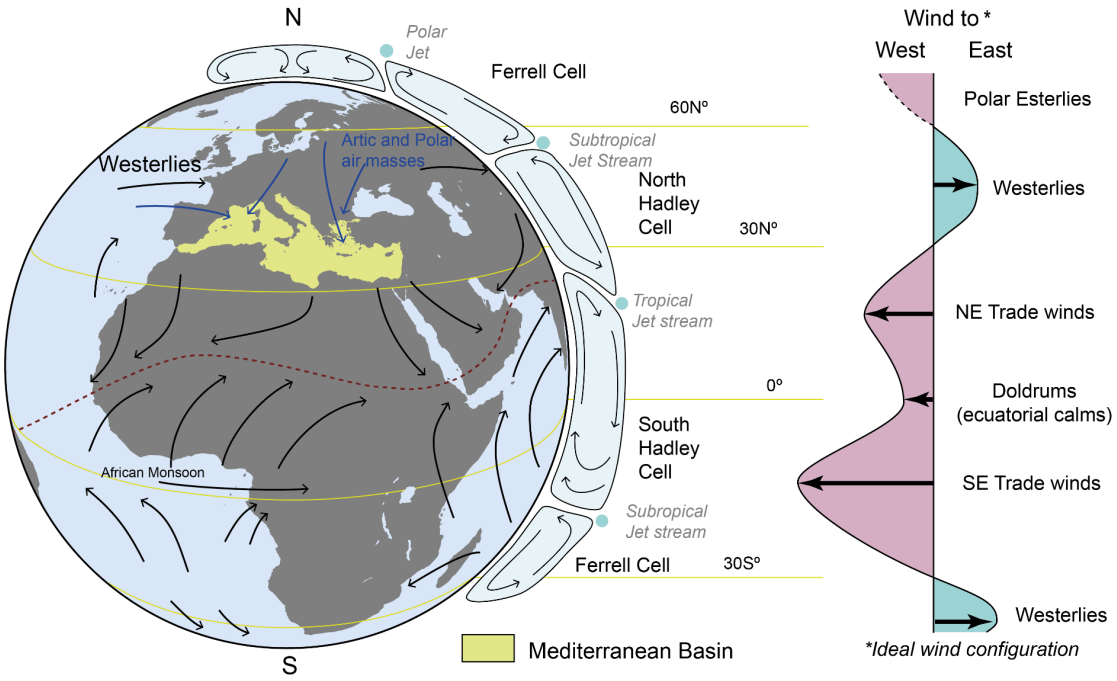

Figure II.2. The situation of the Mediterranean in the global atmospheric patterns today. The presented wind circulation corresponds to the summer atmospheric configuration (black) and some winter winds (blue). Modified and restructured after Rossignol-Strick (1985), Sarmiento and Gruber (2006), and Rohling et al. (2008).

The present-day Mediterranean climate is characterized by pronounced seasonal variability, with dry summers and more humid winters. The seasonal variability also stems from the geographical location of the Mediterranean in the boundary between the subtropical climate systems and the temperate mid-latitude climate systems that occur in the high-pressure north pole flank of the Hadley Cell (e.g., Lolis et al., 2002; Lionello et al., 2006; Lionello, 2012). In summer, the North Atlantic Oceanic High (the Azores High) extends its influence over the Mediterranean region, displacing the storm track northward and bringing dry and hot summers (Rodwell and Hoskins, 2001; Schroeder and Chiggiato, 2022); during this period, the Atlantic influence can penetrate south sometimes, bringing humidity to the Western Mediterranean but rarely reaches the Eastern basin (Rohling and Hilgen, 1991). During winter, the boundary, the high-pressure north pole flank of the Hadley cell, is displaced southward (e.g., Lionello, 2012; Schroeder and Chiggiato, 2022), the region enters under the influence of the westerlies and the Mediterranean storm track is established, bringing winter precipitation to the Mediterranean region due to the storms coming from the Atlantic (e.g., Trigo et al., 1999; Lionello et al., 2006, 2016; Flocas et al., 2010; Campins et al., 2011). These cyclones can also track eastward and bring rain to the far East Basin. However, important cyclogenesis inside the Mediterranean Basin is responsible for the rains in the Eastern Basin (e.g., Rohling et al., 2015; Lionello et al., 2016).

II.2.2. Large-scale atmospheric forcing of past and present Mediterranean climate

The most important climatic patterns that influence the Mediterranean region are the North Atlantic Oscillation (NAO), East Atlantic (EA) pattern, East Atlantic-West Russia (EA-WR) pattern, Mediterranean Oscillation (MO) and the Mediterranean Meridional Oscillation (MMC) (Criado-Aldeanueva and Soto-Navarro, 2020). Other large-scale patterns like monsoons have impacted the Mediterranean climate over larger cycles and geological times.

The NAO index is a fundamental mode of climatic variability in the northern hemisphere, defined by the dipole between the Azores High and the Iceland Low (Loon and Rogers, 1978; Lifland, 2003), with the variation over time of the strength of this dipole produces the oscillation known as the NAO (Salby, 2011; Criado-Aldeanueva and Soto-Navarro, 2020).

These variations in the NAO index have implications for the position of the Atlantic Jet (Fig. II.2), subsequently impacting the westerlies' intensity and direction (Criado-Aldeanueva and Soto-Navarro, 2020). During the NAO positive phase, the dipole between pressures at the north and tropical Atlantic gets stronger, with the increase in pressure in the Azores High and decrease in the Iceland Low; this intensifies the westerlies strength, increasing the humidity transport, and at the same time, the jet stream and this the storm track is pushed to the north. This phase results in more humid winters in the north of Europe and drier conditions in the south and the Mediterranean (Jones et al., 1997; Serreze et al., 1997; Mariotti and Arkin, 2007; Salby, 2011). Positive NAO has been observed to affect oceanography, reducing water convention in the north of the basin (Josey, 2003; Papadopoulos et al., 2012). In the negative phase of NAO, there is a suppression in the dipole between Azores High and Iceland Low; this results in weaker westerlies and the pushing of the storm track to the south. There will be colder and drier conditions in the north of Europe due to the placement of arctic air masses further south and wetter conditions in the south due to the storm track pushing the humidity of the Atlantic to the area (Jones et al., 1997; Serreze et al., 1997; Mariotti and Arkin, 2007; Salby, 2011).

The NAO is the major factor influencing the Mediterranean climate at decadal scale (Xoplaki et al., 2004), mainly on humidity, with less impact on temperature variations (Pozo-Vázquez et al., 2001).

The EA pattern is a large-scale atmospheric circulation pattern that also plays a critical role in shaping the climate of the North Atlantic region (Trigo et al., 2008; Mellado-Cano et al., 2019). The EA represents the sea-level pressure anomaly over the region between Greenland and the British Islands–Baltic Sea area. The EA pattern is characterised by a sea-level monopole structure with high-pressure anomalies south and west of Ireland (Trigo et al., 2008; Comas-Bru and Hernández, 2018). This pattern is linked to changes in the strength and position of the North Atlantic jet stream, modulating the NAO action centres, which, in turn,

affects the temperature and precipitation patterns over the North Atlantic region (e.g., Moore and Renfrew, 2012).

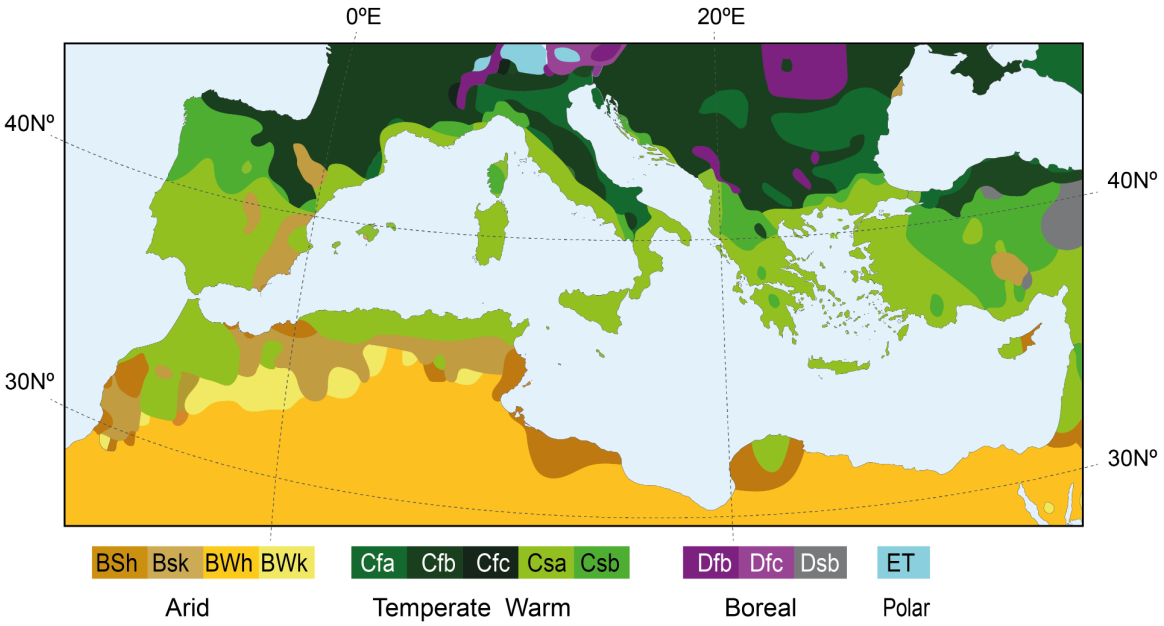

Figure II.3. Mediterranean region climates attending the Köppen classification.

Figure II.4. Mediterranean orography with the indication of some of the main mountain ranges.

When EA is positive, it results in a negative sea level pressure anomaly, which produces strong cyclonic winds over the North Atlantic; in contrast, negative EA results in positive anomalies and induces the flow of cold, dry air to the northeast, producing strong gradients in sea-air temperature and humidity and leading to heat loss in the Mediterranean Basin (Criado-Aldeanueva and Soto-Navarro, 2020). In recent times, the EA has had more impact on the heat loss of the northern Mediterranean than the NAO pattern and thus might have also been more important over geological time scales in wind-induced water convention (e.g., Josey et al., 2011), as discussed in the next section. The EA is fundamental in controlling the north-westerly winds affecting the Mediterranean Basin's north. Thus, through this pattern, the deep-water convection in the Mediterranean Sea has been correlated to the Atlantic Climatic oscillations.

The EA-WR pattern comprises the sea level pressure anomalies in the North Sea surrounded by two poles of opposite anomalies in the western North Atlantic and West Russia (Criado-Aldeanueva and Soto-Navarro, 2020). This pattern has a special influence in the Eastern Mediterranean Basin; a positive EA-WR index enhances the northerlies over the Eastern Mediterranean and the southerlies over the Western Mediterranean. As the nature of these winds is opposite, with the northerlies being dry and cold while the southerlies are warm and humid, during a positive phase, it induces the formation of a dipole in the Mediterranean produced by the differences in heat loss between the basins (e.g., Josey et al., 2011).

The MO represents the dipolar behaviour of the atmosphere between the Eastern and Western Mediterranean. The MO is one of the main controls of the Mediterranean climate, a pressure seesaw that goes west to east and is more active during winter and spring (Lolis et al., 2002). This index correlates well with the NAO (Criado-Aldeanueva et al., 2014). The MO is associated with a negative NAO index and with wet conditions in the Mediterranean (Lolis et al., 2002; Dünkeloh and Jacobeit, 2003). A way to understand the MO is as the oscillation in the difference in the pressure at sea level over the Western Mediterranean (correlated with the westerlies) and, thus, highly correlated with the cyclogenesis inside the basin and over the Eastern Mediterranean. Interestingly, the MO is influenced by the NAO and also by other systems like the East Atlantic west Russian pattern or the Scandinavian climates, in which oscillations have been detected in the Mediterranean pressure systems influencing the pressure over both basins (Papadopoulos et al., 2012).

The MMC represents the circulation of cold and dry north winds inside the basin over winter, causing intense cyclogenesis due to the warm Mediterranean Sea. These systems explain most cyclones forming in the Mediterranean Basin, which are generated inside the basin (Trigo et al., 1999).

The Africa Monsoons System is another important part of the Mediterranean climate, and over time, it has major control of Quaternary sediment records. At present, monsoons occur in different regions between 40°N and 30°S (Fig. II.5). These areas are delimited by a summer-minus-winter precipitation difference that is over 300 mm and a proportional summer

precipitation threshold exceeding 55% of the annual total (Wang and Ding, 2008). Differential heat transfers between the continent and the ocean, changing between seasons, are the primary driver of monsoon oscillation. Over low latitudes, the weaker Coriolis force allows the circulation to be more thermally controlled. Thus, the circulation inside the Hadley Cell is not uniform. The monsoon circulation develops in summer over tropical continental land masses, which becomes hotter in summer while the sea maintains colder, generating a low-pressure centre over the continent and a high-pressure centre over the ocean. The monsoon displaces the Intertropical Convergence Zone (ITCZ) to the north, and the dominant winds blow from the ocean to the land, sending humidity to the continent (Salby, 2011). The configuration in winter is the opposite. Due to its distinct land-ocean configuration, topography, and atmosphere-ocean-land interactions, each regional monsoon has distinctive characteristics, and multiple monsoon zones exist at present (Fig. II.5; Wang et al., 2017).

African and Asian monsoon systems can impact the Mediterranean during summer when the Atlantic moisture advection diminishes. The Hadley cell moves north and reduces its strength (Lionello et al., 2006), allowing the monsoons' influence over the Mediterranean, which is more important in the Eastern than on the Western basins. This influence does not extend to the northern coast of the basin, where the Eastern Atlantic is the main factor influencing the humidity in summer (Dünkeloh and Jacobeit, 2003). Dry and hot summers in the Western Mediterranean positively correlate with the monsoon regime, with the sea temperature increasing the humidity over the Sahel area.

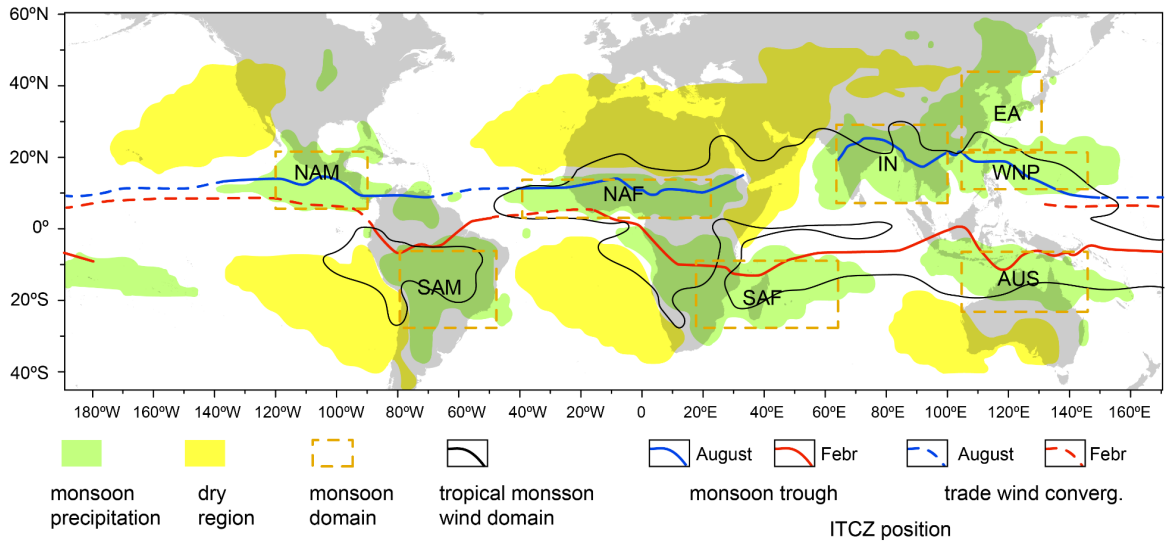

Figure II.5. Regional monsoon precipitation domains. Dry regions where precipitation is below 150 mm are shown. The blue and red lines indicate the ITCZ variation between February and August. The wind domains indicate an annual reversal of 850 hPa in the zonal winds. There are 8 monsoon domains presented (Wang et al., 2017). NAM: North American, SAM: South American, NAF: North African, SAF: South African, IN: Indian, EA: East Asian, WNP: Western North Pacific, AUS: Australian.

Monsoons have been highly irregular over geological time scales, with variability responding to changes in the ocean-atmosphere dipoles, the solar flux (solar radiation and solar incidence), volcanos, greenhouse gases, and surface reconfigurations (ice sheets, orographic changes or sea level; Wang et al., 2017). In the Mediterranean, monsoons have had a great influence on sediment records, in particular triggering events like the sapropel formation (see II.4.2). African Monsoons have influenced the Mediterranean even if the system itself did not penetrate the basin, as it can significantly influence the discharges from the Nile and increase the precipitation in source areas. Also, it can change the humidity and vegetation in dust source areas and, over certain time intervals, penetrate further north, reactivating riverine systems in the north of Africa that discharged in the Mediterranean basins (Larrasoana et al., 2003; Rohling et al., 2015; Crocker et al., 2022).

II.2.3. Mediterranean palaeoclimate

II.2.3.1. Forcings of the glacial variability

The main forcing in glacial variability is the cyclic variation in Earth's orbital parameters, as defined by the Milankovitch cycles, which have important consequences on the insolation received in different latitudes and on total insolation (e.g., Hays et al., 1976; Hoffman et al., 2017; Meyers and Malinverno, 2018; Westerhold et al., 2020). The Milankovitch hypothesis posits that variations in seasonal insolation resulting from cyclical shifts in the orbital precession, Earth's obliquity, and eccentricity are responsible for the Quaternary glaciations (e.g., Berger, 1988; Ridgwell et al., 1999), and have influenced Earth since the Proterozoic to the present (e.g., Hays et al., 1976; Le Treut and Ghil, 1983; Berger, 1988, 1992; Imbrie et al., 1993; Berger et al., 2016). The precession is defined by the change in the position of the Earth's axis concerning the orbital plane. This variation changes the direction of the Earth's axis with a period of 26 kyr (Pälike, 2005). The obliquity is defined by the angle of the axis with the perpendicular plane between 22° and 24.5° (Pälike, 2005), determining less low-latitude solar radiation (e.g., Bosmans et al., 2015). The obliquity defines a primary period of 41 kyr and additionally at 24 kyr and 54 kyr periods. When this angle increases, the amplitude of the seasonal insolation cycle rises, with more insolation in summer and less in winter. Thus, this cycle significantly influences the glacial cycles (Pälike, 2005). The obliquity cycles repeat over a glacial cycle but phase with eccentricity and precession, significantly influencing the beginning and end of glaciations (e.g., Bajo et al., 2020). The eccentricity controls the orbital ellipse shape with a long period of 400 kyr and short periods of 95 kyr and 123 kyr (Hays et al., 1976; Pälike, 2005; Meyers and Sageman, 2007). Eccentricity has not a big influence on summer insolation, but it does influence the amplitude of the precession cycle (see below; Berger and Loutre, 1991; Loutre et al., 2004), which, in turn, will play an important role in beginning and end of the glacial cycle and thus has been correlated with the 100 kyr cyclicity observed in the last million year glaciations (e.g., Ridgwell et al., 1999; Lisiecki, 2010).

While orbital parameters play a fundamental role in driving the ice ages and serve as their ultimate cause, climate variation over time is influenced by a complex interplay of internal and external feedback mechanisms (Maslin, 2016). For instance, the glacial periods of the Quaternary are not all the same duration and intensity, and a complex interaction between ice growth and atmospheric greenhouse gases is responsible for different reactions of the system to equal orbital parameters (e.g., Hays et al., 1976; Ruddiman, 2006). Moreover, the Earth's systems have demonstrated variable responses to orbital cycles throughout geological history, responding to changes in the land masses' configuration, ocean currents' rearrangement, opening of connexion between oceans, and orogenies, among others.

The previously described present Mediterranean climate appeared at 3.2 Ma with the development of the "glacial mode" in the Northern Hemisphere (e.g., Shackleton and Opdyke, 1977) and got more persistent after 2.8 Ma (Suc, 1984). Mediterranean glacial cycles are influenced by astronomical cycles, first by 41 kyr of obliquity forcing and later in time and to the present by 100 kyr of eccentricity forcing after the Mid-Pleistocene at 1 Ma (Ruddiman et al., 1989). Thus, over the last 10 cycles, the glacial cycles have primarily been characterized by the 100 kyr eccentricity cycle and the radiation flux in the Northern Hemisphere. Low atmospheric CO_2 levels and minimum solar radiation have triggered glacial expansion during the beginning of each cycle, further enhanced by internal feedback such as increased albedo (e.g., Hughes and Gibbard, 2018).

II.2.3.2. The Last Glacial Cycle

The Last Glacial Cycle, on which this thesis focuses, includes the Last Interglacial Period (Eemian, 132-116 ka; Shackleton et al., 2003) and the Last Glacial Period, which corresponds to the Glacial stadial (GS) that spans from the end of the Eemian interglacial (116 ka) to the beginning of the Holocene (11.7 ka; Fig. II.6) thus being completed interglacial-glacial cycle. However, this term could also refer to the cycle that formed the Last Glacial Period and the Holocene. This thesis focuses on records that include the Holocene, so the term Last Glacial Cycle is used to refer to the last 132 kyr.

The Last Glacial Cycle was a period of significant climatic fluctuations characterised by the growth and retreat of continental ice sheets. During this time, global temperatures were, on average, several degrees Celsius cooler than today, and sea levels were up to 130 m lower due to the amount of water locked up in ice caps (Siddall et al., 2003; Grant, 2013). The cycle was punctuated by abrupt climate changes and rapid warming and cooling episodes, driven by astronomical changes, internal ocean patterns, and ice sheets' internal systems (e.g., Rousseau et al., 2022). The Last Glacial Cycle profoundly impacted Earth's landscapes, ecosystems, and human societies, shaping the world we know today.

The interglacial periods are warmer, with higher sea levels and higher CO_2 concentrations between the colder glacial cycles. The last two interglacials have been well defined using $\delta^{18}O$ records (e.g., Shackleton and Opdyke, 1973; Andersen et al., 2004; Rasmussen et al., 2014).

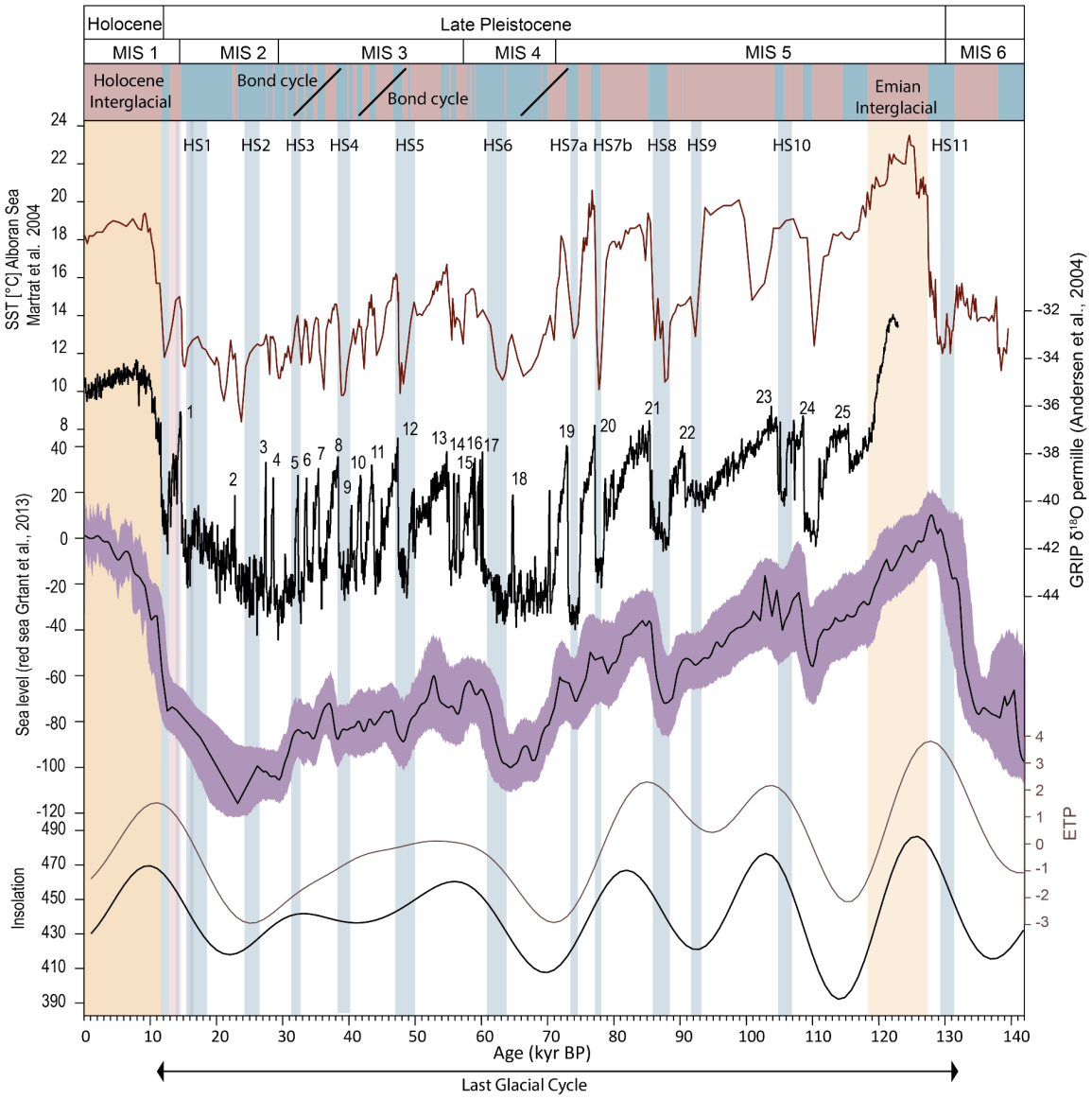

Figure II.6. Last Glacial Cycle through Mediterranean surface temperature, $\delta^{18}O$, sea level, precession, and insolation. Data for temperature from Martrat et al. (2004); Greenland Ice Core Project (GRIP) $\delta^{18}O$ data from Andersen et al. (2004); sea level at the Red Sea from Grant (2013). The numbers over the $\delta^{18}O$ represent the recognised DO Cycles over the Last Glacial Cycle. HS: Heinrich Stadial, MIS: Marine Isotope Stage.

This Last Glacial Cycle includes 5 Marine Isotope Stages (MIS; Fig. II.6), where odd numbers represent the warm (interglacial) phases while even numbers represent the more glacial phases (Railsback et al., 2015). The ice sheets that characterised the glaciations reached the maximum extent in two periods, early in the cycle during the MIS4 (73-60 ka; Hughes et al., 2013) and during the Last Glacial Maximum (LGM) at the end of the period (26-19.5 ka; Clark et al., 2009).

Pleistocene long cycles of glaciation and deglaciation are related to the Milankovitch astronomical cycles. However, the millennial-scale (sub-Milankovitch) climate variability is not directly correlated with these phenomena (e.g., Dansgaard, 1987; Dansgaard et al., 1993), even though it ultimately responds to other interplays inside the Earth's complex system between the oceans, the cryosphere, and the atmosphere (e.g., Rousseau et al., 2022). This low amplitude variability includes the Dansgaard-Oeschger oscillations (DO) and the Heinrich Events (HE).

II.2.3.2.1. Centennial and millennial variability over the Last Glacial Cycle

The Eemian and Holocene are the last two interglacial periods. The Eemian interglacial was warmer than the Holocene, or it had been previously, until the human impact on global climate. The major glacial-interglacial oscillations of the Pleistocene had important impacts on the Mediterranean environment; the interglacials are periods of ice sheets retreat and global temperatures increase; in the Mediterranean, there was extensive tree growth, indicating more humidity, warmer conditions, and more insolation (Combourieu Nebout et al., 2009). During the Eemian, global temperatures were about 1-2°C warmer than pre-industrial levels, and sea levels were higher than today by about 6-9 meters (Siddall et al., 2003; Rasmussen et al., 2014). The Holocene interglacial began around 11,700 years ago and continues today, characterised by more stable and higher global temperatures and higher sea levels than during the glacial cycle. Humans developed agriculture, civilisations, and modern societies during this interglacial period. One of the most notable differences between the Eemian and Holocene is their stability and temperatures; the Eemian was warmer and more variable, with several abrupt cooling and warming events (Fronval and Jansen, 1997; Andersen et al., 2004). During glacial periods, the fixed Anticyclonic Highs over the North European Ice Sheet and the colder sea surface resulted in colder and drier conditions over the Mediterranean, with lesser vegetation cover and increased seasonality in the precipitation. In addition, the sea level was much lower than today, up to 120m below the present level in the Last Glacial Period (Siddall et al., 2003; Grant, 2013). The sea level also has an important impact on the Mediterranean oceanography.

In addition to these broad glacial-interglacial transitions, millennial and centennial climate variations occurred during the Quaternary. Abrupt climate oscillations punctuated the Last Glacial Period; the so-called Dansgaard-Oeschger Cycles (DO), which can be correlated with the Greenland stadial/interstadial cycles, and their presence has been recognised in northern hemisphere ice records and ultimately respond to variations in the Atlantic Meridional Overturning Circulation (stopping, starting, slowing or accelerating) and its influence in the Ice Sheets and the northern hemisphere (e.g., Dansgaard et al., 1984, 1993; Dansgaard, 1987;

Broecker et al., 1990; Bond et al., 1992; Cacho et al., 1999; Andersen et al., 2004; Bagniewski et al., 2017). Twenty-five abrupt warming events were identified in the Greenland ice cores during the Last Glacial Cycle (Fig. II.6; Rasmussen et al., 2014). These oscillations are enclosed in a longer and higher-level cycle, the Bond Cycle (Bond et al., 1993), that, in their idealised form, consists of successive phases of rapid warming followed by slow cooling, stadial(cold) - interstadial(warm) transitions, also known as DO as has been described above. The Bond cycle ends with a final rapid cooling; as the Bond Cycle progresses, the phases reach colder temperatures until finally, in the last and colder cooling, a HE occurs; these last stadial can be named Heinrich Stadial (Fig. II.7). The cycle ends with a rapid warming phase leading to much higher temperatures (Alley, 1998). The duration of DO cycles is not constant over the Last Glacial Cycle; the DO Cycles last between 500 and 4000 years in MIS 3 and 4, while they are significantly longer in the MIS 5 (Fig. II.6). Warmings of up to 7° C to 16° C characterise the DO cycles in Greenland and are usually followed by a more gradual cooling (Wolff et al., 2010). Notably, for its use as anthropogenic climate change analogues, the global climate changes associated with these transitions occurred within a few decades throughout the northern hemisphere (Corrick et al., 2020). These periods of variability may be considered as part of the background spectrum of climate variability; they result from complex and still not fully understood interactions between the orbital forcing and internal forcings affecting the carbon cycle and ice sheets, in other words, a combination of external forcing with the internal cyclicity of the ice sheets (e.g., Rousseau et al., 2022). These cycles are an important link between the astronomical forcing and the internal climate dynamics (e.g., Hodell et al., 2023).

In the Mediterranean region, the Dansgaard-Oeschger transition is associated with cold and dry conditions in the stadial phases and more warm and wet conditions in the interstadial phases (e.g., Fletcher et al., 2010; Sánchez Goñi and Harrison, 2010; Rodrigo-Gámiz et al., 2011; Jiménez-Espejo et al., 2014; Martínez-Ruiz et al., 2015; García-Alix et al., 2021; Sánchez Goñi, 2022). The climate during stadial/interstadial climate oscillations is associated with the migration of the storm track, which moves south during interstadials in response to the AMOC stopping and the reduction of the Azores-Iceland dipole (Fig. II.8; Toucanne et al., 2015). This process could be considered analogous to the NAO oscillation (see II.2.2) but on longer timeframes and much bigger changes in current and atmospheric configuration. In addition, the timing of the Mediterranean precipitation maxima, which comes from the migration south of the storm track during interglacials, coincides with the timing of the monsoon maxima that occurs insolation maxima over the northern hemisphere, with positive feedback occurring between these two elements that induce higher winter precipitation during the monsoon maxima periods (Toucanne et al., 2015).

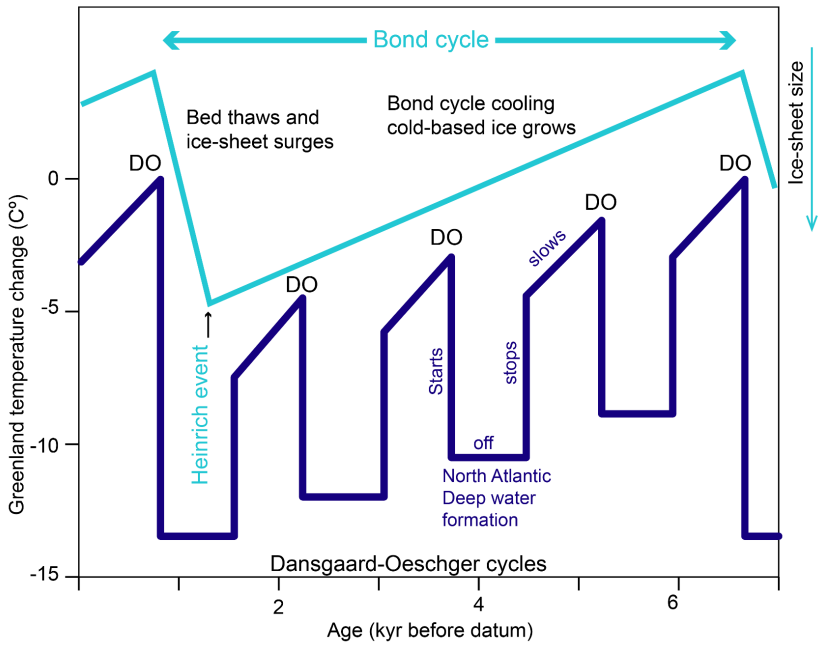

Figure II.7. Idealised Bond cycle from Alley (1998).

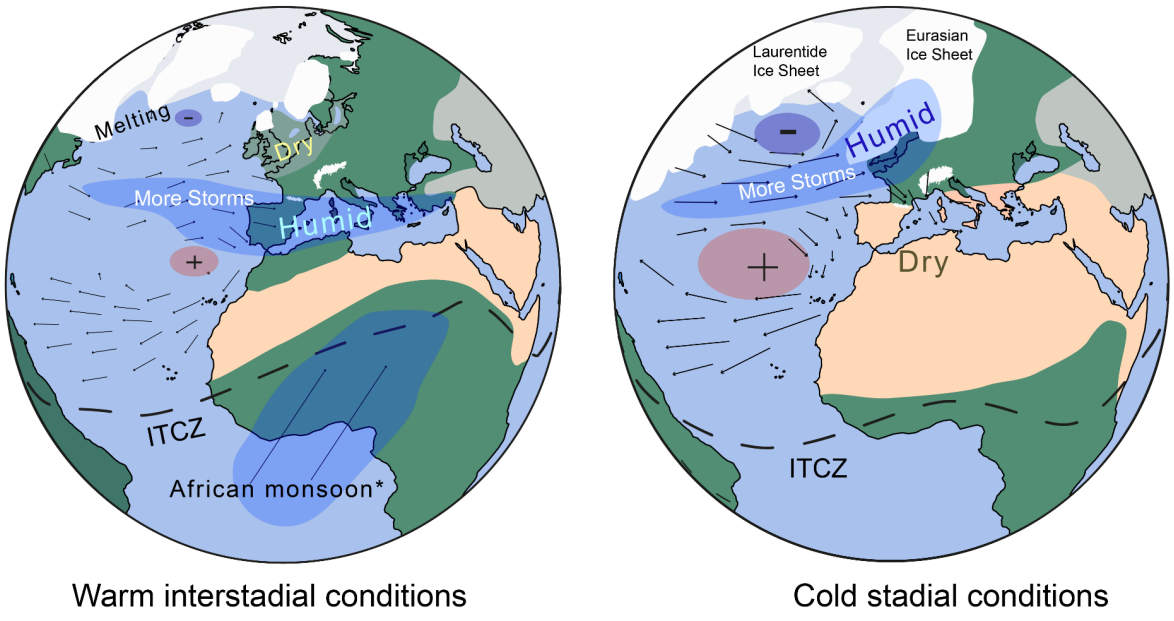

Figure II.8. Glacial/interstadial transition and its influence on the storm track position and the humidity over the Mediterranean Basin. Figure elaborated from conceptual models of several origins: e.g., Moreno et al. (2005), Menviel et al. (2014, 2020)—ice sheet extension during GS and GI cycles obtained from Batchelor et al. (2019). ITCZ (Intertropical Convergence Zone). *ITCZ migration and African monsoons reaching north do not have to occur during all interstadials, as they are controlled by the isolation cycle, not by the bond cycle.

In the Mediterranean region, the Dansgaard-Oeschger transition is associated with cold and dry conditions in the stadial phases and more warm and wet conditions in the interstadial phases (e.g., Fletcher et al., 2010; Sánchez Goñi and Harrison, 2010; Rodrigo-Gámiz et al., 2011; Jiménez-Espejo et al., 2014; Martínez-Ruiz et al., 2015; García-Alix et al., 2021; Sánchez Goñi, 2022). The climate during stadial/interstadial climate oscillations is associated with the migration of the storm track, which moves south during interstadials in response to the AMOC stopping and the reduction of the Azores-Iceland dipole (Fig. II.8; Toucanne et al., 2015). This process could be considered analogous to the NAO oscillation (see II.2.2) but on longer timeframes and much bigger changes in current and atmospheric configuration. In addition, the timing of the Mediterranean precipitation maxima, which comes from the migration south of the storm track during interglacials, coincides with the timing of the monsoon maxima that occurs insolation maxima over the northern hemisphere, with positive feedback occurring between these two elements that induce higher winter precipitation during the monsoon maxima periods (Toucanne et al., 2015).

Another important climatic phenomenon during the Northern Hemisphere glacial transitions, and part of the Bond Cycles are the HEs, which are the massive, repeated episodes of iceberg discharge that occurred every 1000 to 7000 years in the North Atlantic (Heinrich, 1988; Sánchez Goñi, 2022). These iceberg rafts disaggregated from the Laurentide Ice sheet, cooled the ocean surface, impacted the global climate (Bond et al., 1993) and left a debris deposition signature recognised over the Atlantic (Heinrich, 1988). These events have been associated with decreased AMOC strength (Henry et al., 2016), affecting the climate over the entire hemisphere. For instance, in the continent, they responded as other stadial periods with cold and dry conditions but no glacial growth in the Mediterranean area due to low humidity (Allard et al., 2021).

II.3. Mediterranean oceanographic setting

II.3.1. Main characteristics of the Mediterranean Sea circulation

Despite its relatively small size and marginal location, the Mediterranean Sea exhibits a well-developed thermohaline circulation. Nielsen (1912) was the first to provide a comprehensive review of Mediterranean oceanography, recognising its unique features and importance as a region of study, being followed by many others in the next decades (Wüst, 1961; Stanley, 1972; Robinson et al., 1992; Bethoux and Gentili, 1994; Bethoux et al., 1999; Millot, 1999; Millot and Taupier-Letage, 2005; Schroeder et al., 2012; Pinardi et al., 2015, 2019; Somot et al., 2018, among many others).

Circulation in the Mediterranean is driven by wind stress and thermohaline forcing (e.g., Robinson and Golnaraghi, 1994), which is forced by evaporation and precipitation. A thermohaline cycle is established, starting and finishing at the Strait of Gibraltar and flowing throughout the entire basin. There is a constant surface flux of Atlantic water entering the basin while a saline outflow leaves the basin below; the velocity and relative volume of these two fluxes are regulated by the net evaporation of the basin and the net riverine and precipitation inputs, as the Atlantic influx is entering the basin forced by this water loss. The outflow compensates for the difference in salinity being created by the evaporation. However, even with the constant exchange with the Atlantic, there is no compensation for the salinity increase inside the basin, and the Mediterranean is more saline than the Atlantic (e.g., Schroeder et al., 2022). Thus, the circulation of the Mediterranean Sea can be described as anti-estuarine, which means evaporation exceeds precipitation and constant water enters from the Atlantic to maintain the sea level. Present total evaporation increases towards the east over the basin, with estimated averages of 1.45 my−1 (Malanotte-Rizzoli and Bergamasco, 1991) and 1.36–1.57 my−1 (Bethoux et al., 1990; Bethoux and Gentili, 1999) and evaporation and precipitation ranges of 0.92–1.57 my−1 and 0.26–0.70 my−1, respectively (Adloff et al., 2011; Criado-Aldeanueva et al., 2012). The overall Mediterranean excess of evaporation over freshwater input (E (evaporation)–P (precipitation)–R (runoff)) has been estimated at ~ 1.0 my−1 (Bethoux et al., 1999), 0.75 my−1 (Gilman and Garrett, 1994), or 0.56-0.66 my−1 (Bryden and Kinder, 1991), or between 0.42 and 1.23 my−1 (Criado-Aldeanueva et al., 2012).

There are substantial differences between subbasins, and the variable E-P-R in different zones of the Mediterranean creates a pump system that will drive the Mediterranean thermohaline circulation through time and space and determine the water exchange with the Atlantic Ocean (Bethoux and Gentili, 1999; Bethoux et al., 1999; Millot et al., 2006; Skliris et al., 2007). For instance, due to substantial freshwater inputs from the Rhone and Ebro rivers, the Po River, and the Black Sea, northern regions such as the Gulf of Lions and the Adriatic and Aegean seas have relatively low E-P-R values. In contrast, the Eastern Mediterranean southern regions have high E-P-R values (Bethoux and Gentili, 1994). The disparities between the basins and the overall surplus of evaporation basin-wide contribute to a noticeable rise in surface water salinity from west to east (e.g., Wüst, 1961; Adloff et al., 2011; Mikolajewicz, 2011).

The Mediterranean today suffers net evaporation and cooling, as is evident by the difference between the inflow and outflow; the Atlantic inflow is warmer and less saline, while the outflow is colder and much more saline (Gascard and Richez, 1985), and the inflow is 50% higher in volume than the outflow (Bethoux and Gentili, 1994).

Even if small, the Mediterranean is an important part of the global ocean as a pump of saline water injected into the North Atlantic from the Gibraltar Strait. The leaving flux is known as the Mediterranean Outflow Water (MOW), which has an important role in the AMOC (e.g., Hernández-Molina et al., 2014; Sierro et al., 2020) as well as in the global ocean circulation (Fig. II.9). The MOW can be traced in the North Atlantic at a depth of around 1000 m as a

warm and saline layer that can be considered an important element preconditioning the formation of North Atlantic Deep Water (Rohling et al., 2009).

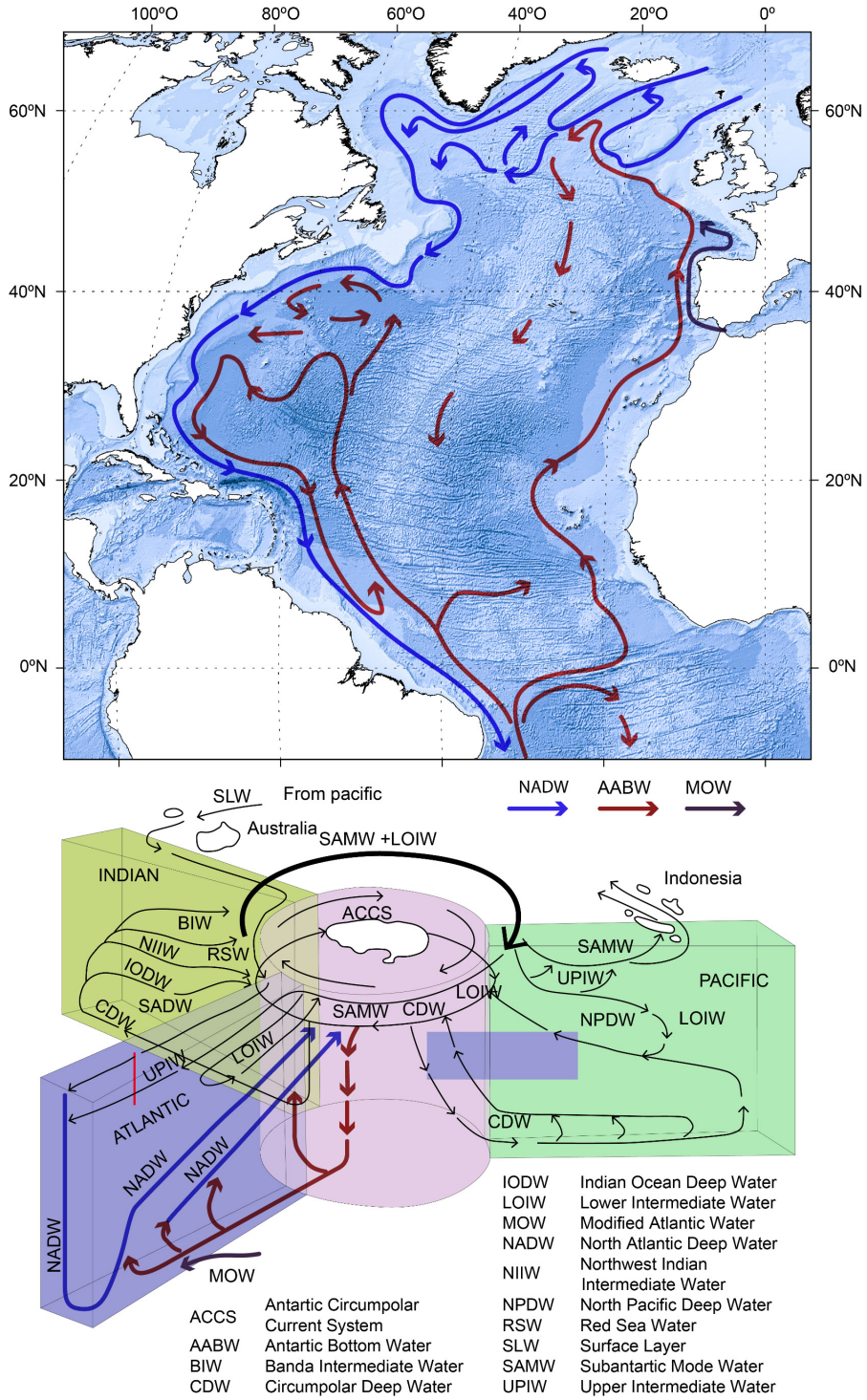

Figure II.9. Configuration of the deep marine circulation of the Atlantic (above). Schematic configuration of the global marine convection (below). Modified from Schmitz (1996).

III.3.2. Mediterranean overturning circulation

The water masses distribution in the Mediterranean can be presented as 3 layers that flow at different depths and that differ in origin, circulation pattern, salinity and temperature; these are the Modified Atlantic Water (MAW), the Levantine Intermediate Water (LIW) and the Mediterranean Deep Water (MDW) which is subdivided between the two main sub-basins of the Mediterranean into the Western and Eastern Mediterranean Deep Water (WMDW and EMDW; Fig. II.10, e.g. Wüst, 1961; Millot and Taupier-Letage, 2005; Schroeder et al., 2012; Pinardi et al., 2015, 2019; Schroeder and Chiggiato, 2022).

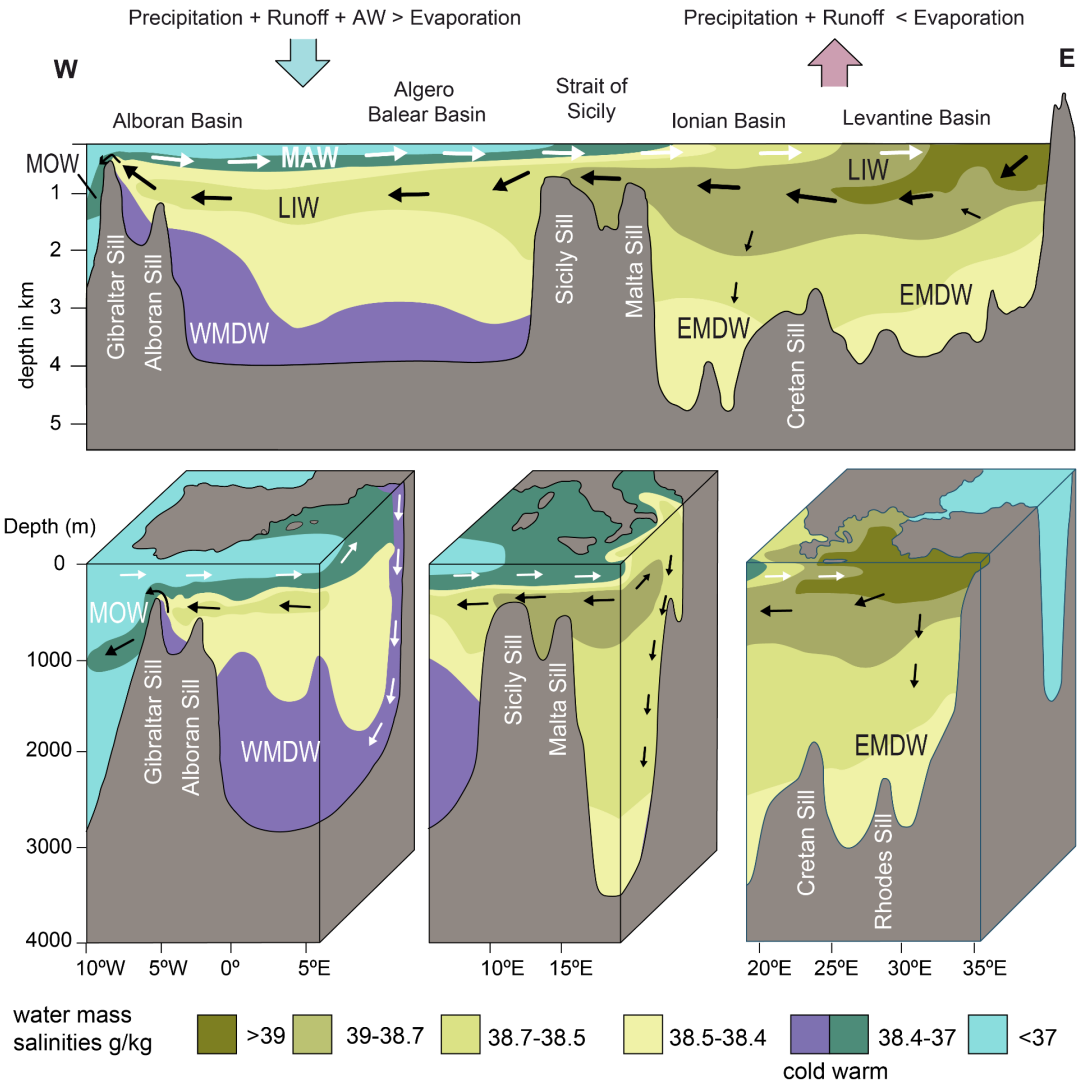

Figure II.10. The current vertical disposition of the water masses in the Mediterranean (after Wüst, 1961; Cramp and O'Sullivan, 1999) has been subjected to changes over time, but the general flow is assumed to be similar for the Last Glacial Cycle. MAW: Modified Atlantic Water, LIW: Levantine Intermediate Water, WMDW: Western Mediterranean Deep Water. EMDW: Eastern Mediterranean Deep Water.

As it enters the basin through the Gibraltar Strait, the Atlantic Water (AW) starts mixing with the more saline intermediate layer (Fig. II.10), creating the MAW. The surface water flows under the influence of the dominant winds, and upon entering the basin, the water accelerates, creating a high-velocity jet that, under the Coriolis force effect, initiates the creation of the Alboran gyres and the associated coast upwelling areas; this jet current general circulation pattern consists in a meandering through Alboran gyres in its way to the Balearic Basin (Fig. II.11; Heburn and La Violette, 1990; Béranger et al., 2005). Upon entering the Balearic Basin, the MAW Atlantic Jet is split into two stems, one flowing along the African coast and the other towards the Balearic Islands (Fig. II.11; Pinardi et al., 2015). The northward stem will eventually reach the Tyrrhenian Sea and the northern coast and participate in the formation of the Mediterranean Deepwater (Rohling et al., 1998; Send et al., 1999; Pinardi et al., 2015), while the other stem will continue east, parallel to the African coast and cross the Sicily channel towards the Levantine Basin (Pinardi et al., 2015). Upon crossing the Sicily Channel and entering the Ionian Sea, the current divides again into two branches, with a branch flowing north to the Tyrrhenian Sea and eventually westwards following the European coast (Pinardi et al., 2015). On the way eastward of the MAW, it will suffer from evaporation and mixing with underlying water and gets warmer and saltier (Fig. II.10; Bethoux, 1979; Pinardi and Masetti, 2000; Durrieu de Madron et al., 2011).

Once the mixed and saline MAW reaches the Levantine Basin, and under the influence of the cold north winds that occur during winter, especially in the Cyprus and Rhodes gyres (Fig. II.11), the saline MAW reaches enough density to sink to middle depths of 150 m to 600 m by open sea cyclonic sinking, generating the LIW (Fig. II.12; e.g., Roether and Schlitzer, 1991; Lascaratos et al., 1993; Roether et al., 1996; Tsimplis and Bryden, 2000; Kubin et al., 2019). One important characteristic of this water mass is that it represents the maximum salinity throughout the water column (Wüst, 1961; Béranger et al., 2010). The LIW flows east to west anticlockwise under the influence of the Coriolis force through the main basins (Figs. II.10 and II.11; Millot and Taupier-Letage, 2005; Schroeder et al., 2012). It crosses the Ionian Sea, where one part flows back to the Eastern Mediterranean Basin, and the other part enters the Western Mediterranean Basin through the Sicily Channel, entering the Balearic Basin and the Tyrrhenian Sea (Fig. II.11). The LIW reaches the Ligurian Sea and Gulf of Lions and then flows close to the Balearic Islands towards the Alboran Sea, flowing then close to its northern margin and reaching the Gibraltar Strait, where it mixes with the WMDW and the MAW to form the MOW (Figs. II.10; Pinardi et al., 2015). The LIW properties depend on the formation process and the water characteristics in the source area, influencing the MOW features and impacting MDW production (e.g., Wu and Haines, 1996; Incarbona and Sprovieri, 2020; Sierro et al., 2020).

The colder and less salty MDW flows below 600-1000 m depth and is divided in two by the Sicily Channel (Millot, 1999), the WMDW at the west and the EMDW at the east. Each basin has different origins for these deep waters (Béranger et al., 2010), and for this reason, they do not have equal characteristics; for instance, the EMDW is saltier and denser than the WMDW

(Schroeder et al., 2022). Like in the case of the LIW, the sinking of deep water will come from the buoyancy loss and the momentum fluxes that will produce cyclonic sinking (Figs. II.10) and the process of cascading (Durrieu de Madron et al., 2013).

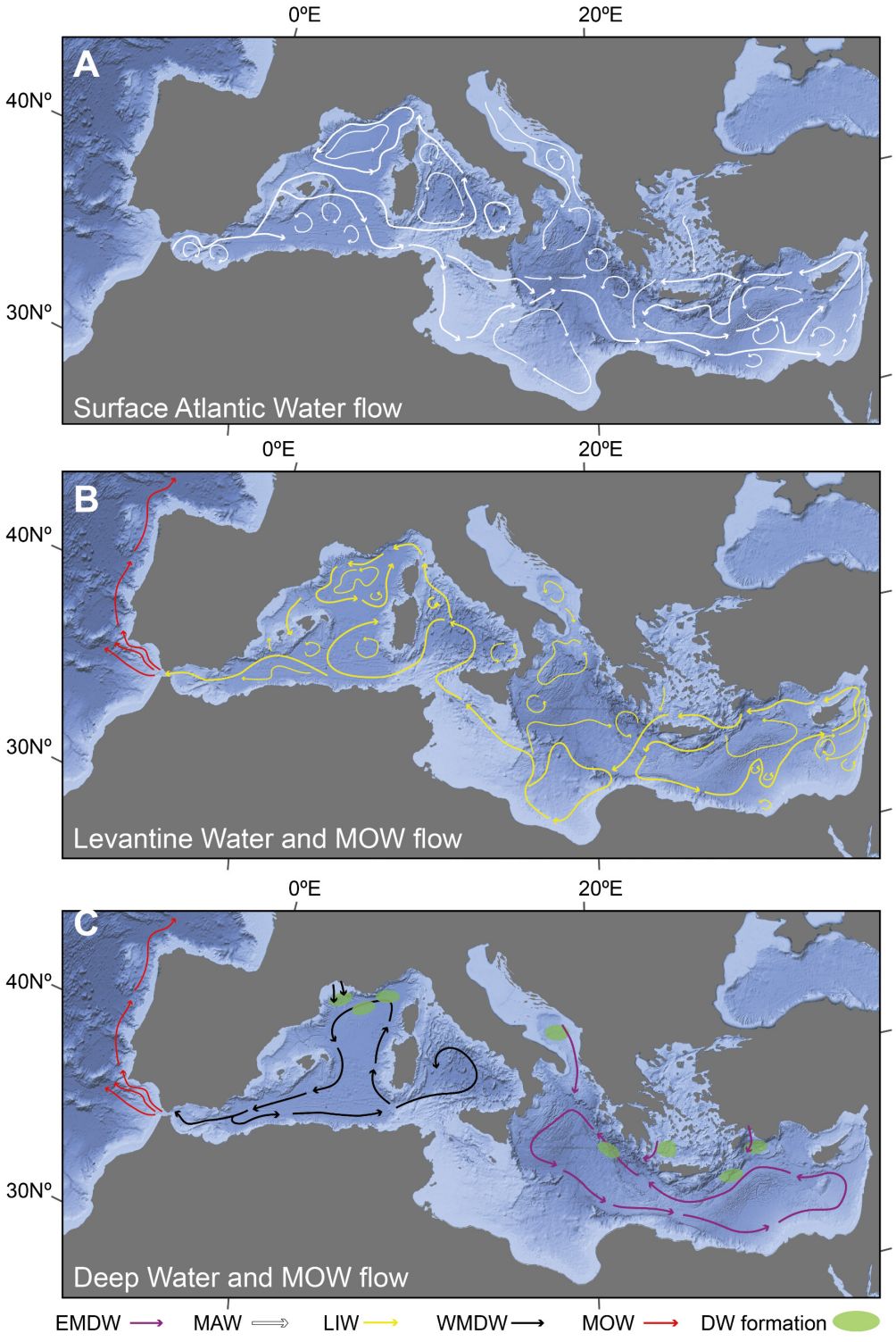

Figure II.11. Main water masses circulation patterns in the Mediterranean Sea. MAW and LIW water paths based on Pinardi et al. (2015). Intermediate and deep water formation points are indicated in the green areas. EMDW: Eastern Mediterranean Deep Water, MAW: Modified Atlantic Water, LIW: Levantine Intermediate Water, WMDW: Western Mediterranean Deep Water, MOW: Mediterranean Outflow Water.

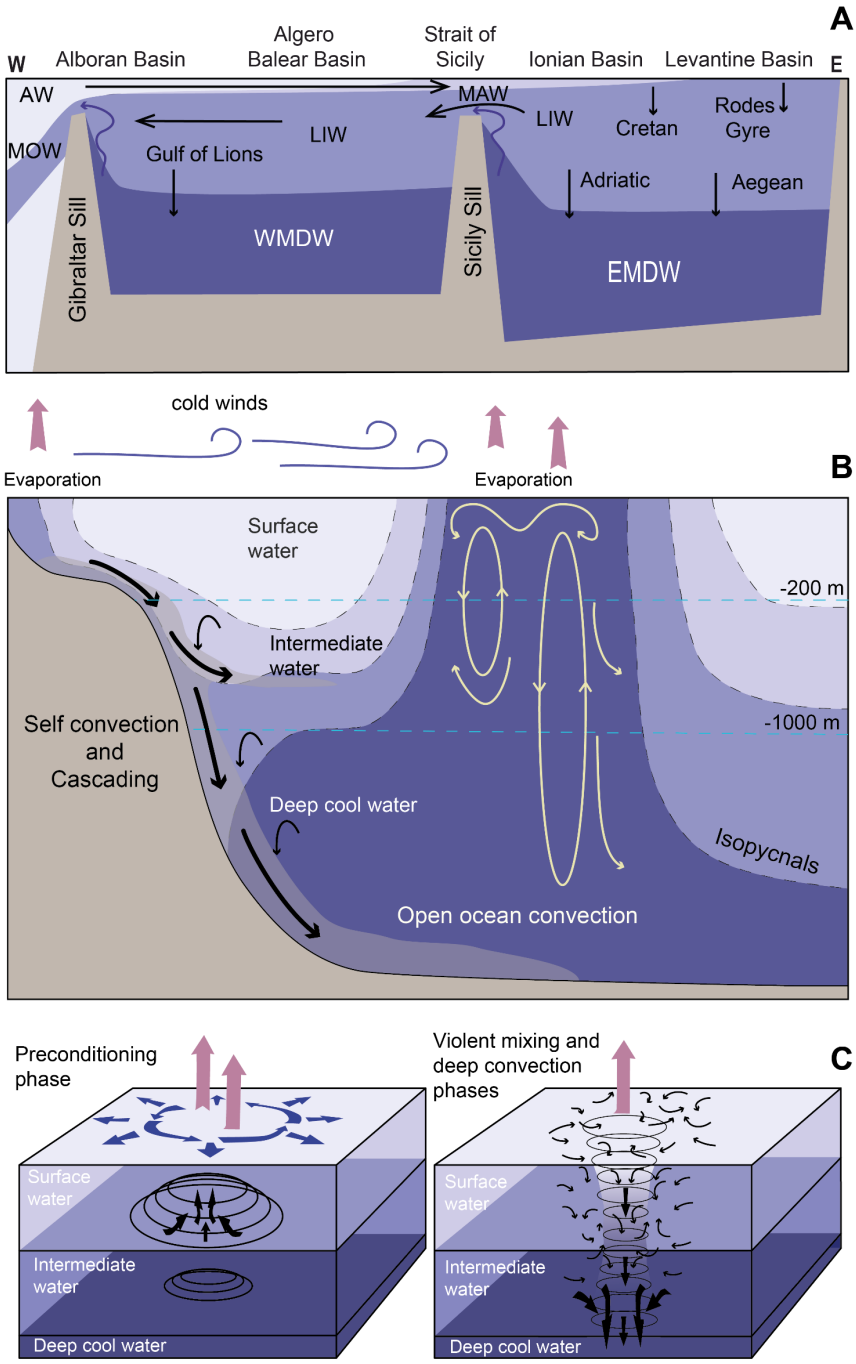

Figure II.12. (A) Simplified schematic overturning circulation in the Mediterranean and the main exchange places between water masses. (B) Deep water formation processes in the basin's north margins, modified from Pusceddu et al. (2010). (C) Sketch of cyclonic sinking in deep water (Rohling et al., 1998; Woodward, 2009). AW: Atlantic Water, MAW: Modified Atlantic Water, MOW: Mediterranean Outflow Water, LIW: Levantine Intermediate Water, WMDW: Western Mediterranean Deep Water, EMDW: Eastern Mediterranean Deep Water.

In regions subjected to intense winds, such as the Gulf of Lions and the Ligurian, the Aegean and Cretan Seas, and the southern portion of the Turkish coast, evaporation rates increase (Medoc Group et al., 1970; Pinardi and Masetti, 2000; Josey et al., 2011; Pinardi et al., 2015), while the humid air masses from the Atlantic produce weak evaporation in the Algerian and Moroccan margins (Criado-Aldeanueva et al., 2012). Regional wind systems' strength and variation over the sinking areas affect the amount of deep-water production, and their properties also give them kinetic momentum (Millot, 1990; Cisneros et al., 2019; Amitai et al., 2021). During winters, polar and continental air masses are canalised through valleys that traverse the mountain ranges of the northern Mediterranean margin, directed towards the centre of the Mediterranean; for example, during the winter and spring, intense cold and arid wind flows impact the Gulf of Lions ('Mistral'), the Adriatic ('Bora'), and the Aegean Sea ('Vardar'), causing intense evaporation and cooling and then considerable heat loss (Maheras et al., 1999; Casford et al., 2003; Ulbrich et al., 2012). The WMDW is produced in the Gulf of Lions and the Ligurian Sea, where a cyclonic gyre is formed (Fig. II.11; Pinardi et al., 2015). The cold and dry winds from the north will force the WMDW production by cascading and cyclonic sinking (Fig. II.12). These occur through the preconditioning of the surface water by evaporation and then the mixing due to the wind force cyclonic gyre, ventilating the deep basin (Medoc Group et al., 1970; Somot et al., 2018; Cisneros et al., 2019). The EMDW is also formed in winter by similar processes, but it occurs in the Adriatic (the main origin) and the Aegean Sea (Schott et al., 1996; Millot, 1999; Schroeder et al., 2008), with the relative contribution of these areas to the total production of EMDW, influencing the salinity as the Aegean water has more salt content (Roether et al., 1996, 2007; Rohling et al., 2009).

Dense water formation is a complex process. Preconditioning by the characteristics of the surface water or the LIW is of great importance (e.g., Krokos et al., 2014; Bensi et al., 2016; Cisneros et al., 2019). Sea surface temperature also impacts the composition and rate of formation of deep-sea water (Bouvier et al., 2010). Also, the freshwater budget of the Mediterranean governs surface water salt content and has an important influence on deep water formation. Freshwater discharges tend to reduce the formation rates of dense water, thereby influencing the MOW velocity at Gibraltar (Bethoux and Gentili, 1999; Bethoux and Pierre, 1999; Josey, 2003; Skliris et al., 2007; Criado-Aldeanueva et al., 2012). Another important element to consider is the salinity of the Atlantic influx; for example, during Heinrich, it is known that the surface of the Atlantic and thus the Atlantic influx in the Mediterranean was less salty and thus affected the buoyancy and dense water sinking (e.g., Sierro et al., 2005).

Sea level fluctuations also play a crucial role; the interplay between sea level changes, strait depth, and global oceanic connections has important implications for the Mediterranean Sea circulation and water masses characteristics (Schroeder et al., 2022). For instance, during sea-level lowlands, the flow area in Gibraltar Strait is diminished, increasing the residence times of the water in the Mediterranean and then the salinity (Rohling, 1994). The MOW will be more saline during these low-stand phases and thus could have moved at deeper depths in its flow along the Iberian Margin (Sierro et al., 2020).

II.4. Organic rich sediments in the Mediterranean

II.4.1. Fate of organic matter in marine environments

Photosynthetic activity in terrestrial and marine ecosystems is the primary organic carbon source that eventually accumulates in marine sediments. This organic matter (OM) reaches the deep sea through gravitational settling, originating from continental areas via rivers and through productivity within the water column (e.g., Middelburg et al., 1993; Hedges and Keil, 1995; Arndt et al., 2013). The fate of OM in the deep sea and the amount preserved in sediment records display high spatial and temporal variability. Diverse, complex factors influence the degradation or preservation of OM (LaRowe et al., 2020). Therefore, understanding the past variations in preservation and predicting future changes is crucial, as organic matter preservation plays a significant role in the global carbon cycle and the sequestration of atmospheric CO_2 (LaRowe et al., 2020).

Figure II.13 (Einsele, 2000) illustrates an idealized model of the oceans' organic matter cycle. The first 100 meters of the water column, where light penetration allows for primary productivity, is the primary source of OM production (excluding river discharges). As OM is exported from the euphotic layer and sinks into the deeper water column, it undergoes remineralization by various organisms ranging from bacteria to marine pluricellular organisms. This process releases CO_2 and nutrients into the water column, facilitating their reuse in biogeochemical cycles (Einsele, 2000). In certain cases, erosion and lateral transport of OM - rich sediments can occur through turbidites, nepheloid layers from slopes, or strong bottom water currents (e.g., Kusch et al., 2010; Arndt et al., 2013). The amount of OM that continues its descent through the water column is often referred to as the benthic flux or the rain rate (Einsele, 2000; Fig. II.13). The primary production level and the efficiency of downward remineralization influence this flux. Once the OM reaches the benthic boundary layer, it is deposited in the sediment and can undergo various pathways; it can be remineralized, leading to the rereleasing, or conserved and buried effectively in the sediment (e.g., Canfield, 1994; Arndt et al., 2013).

Once the OM has reached the seafloor, it suffers chemical, biological, and physical processes, making it a complex reaction-transport issue (e.g., Middelburg et al., 1993; Arndt et al., 2013; LaRowe et al., 2020). Factors such as deposition rate (e.g., Tromp et al., 1995), activity of benthic communities (e.g., Aller, 1982), organic matter composition (e.g., Dauwe et al., 2001), availability of certain chemicals in the environment (e.g., Canfield, 1994; Arndt et al., 2013), or physical protection (e.g., Kennedy et al., 2002), among many others, influence OM preservation. In addition, external crucial factors affecting OM preservation are oxygen availability or the transport process until the final resting place (e.g., Canfield, 1994; Arndt et al., 2013). The process suffered by the OM during its transport reduces the potential for

degradation during burial, making it more refractory by consuming more labile parts (Arndt et al., 2013).

The role of oxygen in OM preservation varies depending on the specific environmental conditions. In marine environments with high rates of OM deposition, such as those near continental upwellings, oxygen content in the bottom water has limited influence. This is because anaerobic degradation processes dominate, particularly during burial (e.g., Canfield, 1994; Arndt et al., 2013). However, in abyssal plains where sedimentation rates are considerably lower, the decomposition of OM can occur over extended periods, allowing for a predominance of more efficient aerobic processes. Thus, in oxygenated bottom waters, OM is consumed in the oxidation zone (e.g., Hesse and Schacht, 2011). However, in suboxic bottom environments, it follows anaerobic and less efficient degradation paths that increase preservation, making the bottom water's oxygen content a crucial factor influencing preservation in these areas (e.g., Canfield, 1994; Arndt et al., 2013).

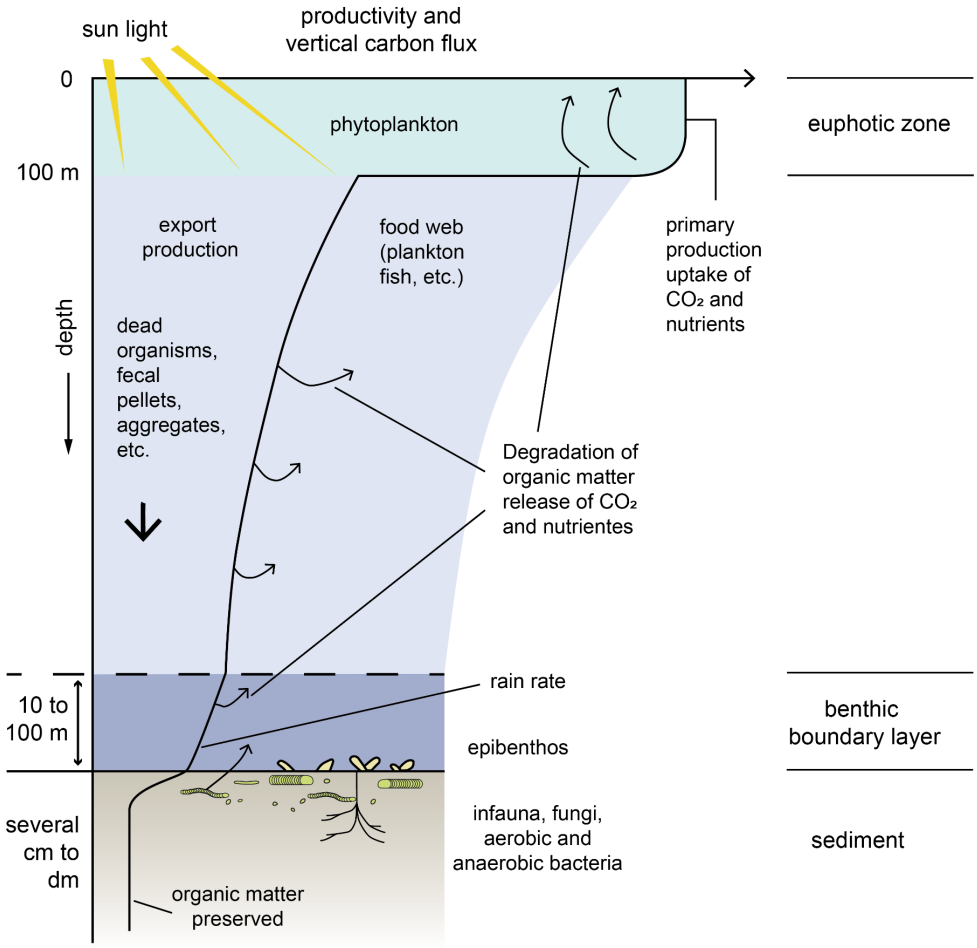

Figure II.13. Representation of the processes suffered by the organic matter in the water column and the sediment. The figure was slightly modified and redrawn from Einsele (2000).

Oxygenation and carbon fluxes in the Mediterranean are influenced by several factors, including terrestrial transported carbon by rivers, primary ocean productivity, lateral advection of carbon particles, upwelling events, and organic matter remineralisation in the water column (Hedges et al., 1997; Hedges and Oades, 1997; Thunell et al., 2007). Productivity induced by deep water convention is also a factor to be considered (Murray, 2006; McCave, 2007) and can be an important process, especially in the Western Mediterranean (Ausín et al., 2015b).

II.4.2. Sapropels and Organic Rich Layers

In the Mediterranean, sapropels and Organic Rich Layers (ORLs) represent exceptional examples of deposits linked to climate change events. This periodic widespread deposition of organic-rich sediments over periods of several thousands of years can be considered a modern analogue of the black shales in the Mesozoic oceans. Sapropels and ORLs present increased organic carbon concentrations that contrast with surrounding organic-poor sediments and occur (quasi-) periodically in the sedimentary sequences of the last 13.5 million years, at least the sapropels of the Eastern Mediterranean Basin (e.g., Rossignol-Strick et al., 1982; Krijgsman et al., 1995; Lourens et al., 1996; Cramp and O'Sullivan, 1999; Sierro et al., 1999; Hilgen et al., 2003). Sapropels and ORLs present similarities; however, they are not considered exactly equivalent, with important differences in their development and causes. Moreover, they appear out of phase and in different periods most of the time (e.g., Rohling et al., 2015).

In general, the thickness of sapropel layers ranges from a few millimetres to more than a metre. Sapropels have been deposited intermittently from the Neogene and through the Quaternary, with the most recent occurring between 10.8–6.1 kyr BP (Cita et al., 1977; Thunell et al., 1977; Kidd et al., 1978; Rossignol-Strick et al., 1982; Rossignol-Strick, 1985; Hilgen, 1991; Rohling and Hilgen, 1991; Van Os et al., 1994; Lourens et al., 1996; Nijenhuis et al., 1996; Emeis et al., 2000; Meyers, 2006; de Lange et al., 2008; Rohling et al., 2015; Grant et al., 2022). The term "sapropel" was introduced by Wasmund (1930) to describe lacustrine sediments deposited in environments where benthic fauna is absent and bottom water has dissolved H_2S. Later, Kidd et al. (1978) expanded the definition to include marine sediments with over 2% total organic carbon (TOC) and sediment layers over 1 cm thick. Subsequent studies in the Eastern Mediterranean have shown that sapropels can occur in shallower depths and have lower TOC values (Sigl et al., 1978; Hilgen, 1991; Murat, 1999). Some authors have proposed different TOC values to define sapropels, such as a lower limit of 0.5% (Hilgen, 1991) or using colour changes in combination with TOC values that contrast with the surrounding sediment (Sigl et al., 1978; Murat, 1999). Furthermore, the characteristics of these layers have broadened to include sediments with no lamination or dark colouration, as initially proposed (Cramp and O'Sullivan, 1999). Thus, sapropels are sediment layers with over 2% TOC content, while layers with 0.5-2% TOC are defined as sapropelic sediments (Sigl et al., 1978). Sapropels commonly present an absence of benthic foraminifera and are preceded by a faunal association indicative of bottom-water oxygen depletion (Casford et al., 2003). When observed in marine records,

sapropels can be recognised by a distinct colour ranging from dark grey to olive green or black (Rohling et al., 2009). However, many times, they appear oxidised with a reddish colour (Löwemark et al., 2006; De Lange et al., 2008); sapropels can be thus erased from the sediment record by postdepositional oxidation, or their thickness appears truncated (Higgs et al., 1994). Postdeposition oxidation can fully remove all visual evidence of sapropels.

During the Last Glacial Cycle, 5 sapropels have been recognised (Fig. II.14). The timing of Mediterranean sapropel deposition is controlled by maxima in Northern Hemisphere summer insolation during precession minima, which leads to higher monsoon intensity over the North African continent (e.g., Ziegler et al., 2010; Grant et al., 2016). Intensified monsoons increased runoff from North Africa into the Mediterranean Sea, especially through the Nile (Rohling et al., 2015; Grant et al., 2022). Most of the organic matter from sapropels comes from marine origins, indicating enhanced productivity due to nutrient availability from the Nile discharge (Gallego-Torres et al., 2010). Moreover, the freshening of the upper layer and its thickening, reaching the nutrient-rich surface water deeper zones, facilitated photosynthesis across a larger portion of the water column, thus increasing productivity (Rohling et al., 2015; Zwiep et al., 2018). It is also now widely accepted that the formation of sapropel layers has another primary driver in the disruption of the Deep Mediterranean Overturning Circulation, which occurred in conjunction with the increased productivity and that reaches levels of deep-water renewal even ten-fold lower than the present (Andersen et al., 2018). In summary, buoyancy gain resulting from surface water freshening insolated the EMDW, leading to extended oxygen depletion. In addition, Nile-borne nutrients facilitated increased productivity and enhanced benthic flux, further promoting oxygen consumption and organic matter accumulation at depth, and promoting the formation of sapropels (e.g., Rossignol-Strick, 1985; Rohling and Hilgen, 1991; Calvert et al., 1992; Rohling, 1994; Thomson et al., 1999; Weldeab et al., 2003; Meyers, 2006; Gallego-Torres et al., 2010; among others). In addition, other climatic, oceanographic, and ecological responses broadly preconditioned the basin for sapropel deposition, such as the sea level or the north winds (Rohling et al., 2015). In general, the sapropel deposition is initiated abruptly, and it is assumed that it occurs after reaching a tipping point where positive feedback mechanisms are triggered (Rohling et al., 2015). However, the beginning of the sapropel is preceded by preconditioning periods of variable duration that can reach more than a millennium, where short-duration low oxygen events occur gradually more frequently, followed by increasingly slower recovery of oxygenated conditions (e.g., Andersen et al., 2020; Hennekam et al., 2020) and, as mentioned above, the process leads to the abrupt restriction of the bottom waters.

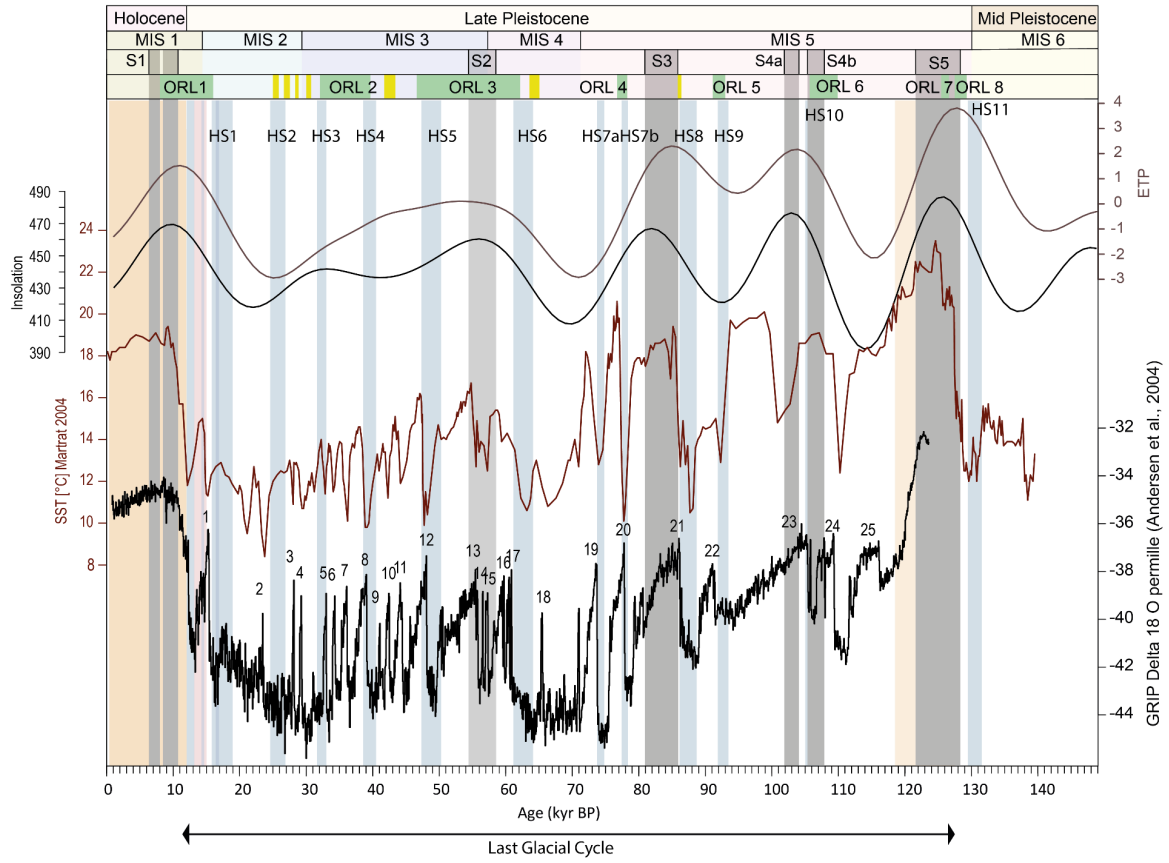

Figure II.14. Main sapropels (S1 to S5) and Organic Rich Layers (ORL1 to ORL8) in core 977 from Leg 161 ODP expedition in the Last Glacial Cycle. The numbers over the δ18O represent the recognised DO Cycles over the Last Glacial Cycle. HS: Heinrich Stadial, MIS: Marine Isotope Stage, ORL: Organic Rich Layer (green for previous studies, yellow for this thesis), S: Sapropel.

Sapropels present important differences in duration, total organic carbon or preservation, probably due to changes in monsoon strength over North Africa and associated freshwater runoff into the Mediterranean Sea (Sweere et al., 2021). For example, S5 can be considered the most strongly developed sapropel of the Last Glacial Cycle (Benkovitz et al., 2020), while the "glacial" sapropels that occur in insolation maxima in the middle of glacial periods are generally less developed. Also, the deposition was not spatially homogeneous. For instance, the water column with important oxygen depletion is variable during sapropels, and the shallower zones below 300 m in the Mediterranean were not anoxic during all the sapropels events. Some shallower sapropels present characteristics that indicate that the anoxia was periodically interrupted (Reitz and de Lange, 2006; De Lange et al., 2008; Filippidi et al., 2016). In contrast, deeper zones presented stronger and more generalised oxygen depletion throughout all the sapropel events (e.g., Thomson et al., 1999; Reitz and de Lange, 2006; De Lange et al., 2008; Filippidi et al., 2016; Wu et al., 2019; Monedero-Contreras et al., 2023).

In the Western Mediterranean, the layers rich in organic carbon have been defined as Organic Rich Layers (ORLs) and present important differences compared to sapropels. ORLs are primarily recognized in the Alboran Sea Basin (the westernmost basin of the Mediterranean

Sea). They have been observed in records spanning the last 2.7 million years. ORLs do not occur synchronously with the sapropels at least over the last 130,000 years (Fig, II.14; Murat, 1999; Cacho et al., 2002) and do not appear to follow the insolation maxima cycles (von Grafenstein et al., 1999; Cacho et al., 2002; Rogerson et al., 2008; Rohling et al., 2015). Moreover, the background TOC content in the Alboran Sea Basin is elevated, exceeding the typical 0.3% value for oxygenated open ocean environments (Stein, 1990), ranging from 0.4% to 0.5% (Murat, 1999). As a result, during the ODP expedition from Leg 161 and 160, Murat (1999) established a lower limit of 0.8% TOC to define these sediment layers with increased organic carbon in the Western Mediterranean.

The occurrence of ORLs is primarily associated with low oxygenation of the WMDW during deglaciation periods and warm interglacials. In the Western Mediterranean, deep-water ventilation seems to be more related to climatic changes in the Northern Hemisphere, such as the D-O and HEs (Sierro et al., 2005; Frigola et al., 2008; Jiménez-Espejo et al., 2008; Rogerson et al., 2008), however, although HEs can impact oxygenation levels, they might not be significant enough to produce organic-rich layers, but probably have a potential to precondition the basin for the ORL deposition (Sierro et al., 2005; Rogerson et al., 2008). However, there is a significant lack of studies of ORLs before the Last ORL (ORL1), so some more work is still necessary to assess HEs' influence on ORLs. In general, ORLs are not fully anoxic, as those from the Tyrrhenian Sea are the only ones considered truly anoxic in the Western Mediterranean (Krishnamurthy et al., 2000).

Many other elements also have importance in ORL deposition. Primary productivity has also been linked to the formation of ORLs in the global geological record and may sometimes be more important than anoxic conditions (Pedersen and Calvert, 1990; Kuypers et al., 2002). Sedimentation rates also play a crucial role in organic matter preservation and must be considered (Müller and Suess, 1979), being quite high, especially in the Alboran Sea, where the sedimentation rates probably played a major role in the deposition of the last ORL (e.g., Mesa-Fernández et al., 2022).

Overall, deep ventilation has been highly affected by the wintertime climate conditions and thus has been highly variable over time. During the Last Glacial Cycle, the periods of more intensified and more frequent north winds are correlated with DO stadials and have a positive correlation with the intensity of these events (Cacho et al., 2002; Frigola et al., 2008; Rogerson et al., 2008). It has been observed that cold events, even of short duration, have the potential to reactivate and accelerate deep Mediterranean currents and cause an interruption in the Mediterranean sapropels and ORLs formation (Zirks et al., 2019; Pérez-Asensio et al., 2020).

Chapter III

Use of geochemical and ichnological proxies for palaeoenvironmental conditions

III.1. Geochemical composition on marine sediments as a tool

The elemental composition of sediments and sedimentary rocks is a valuable tool for palaeoenvironmental reconstructions, giving insights into sediment sources, mode and direction of sediment transport, past climates, ocean circulation, organic production, seafloor environments, oxygenation, and even post-depositional modifications.

Geochemical proxies have developed significantly since their first utilisation in the XIX century in some of the first marine expeditions (Murray and Renard, 1891; Correns, 1937; Bramlette and Bradley, 1940; Arrhenius, 1952). After that, sedimentologists discovered that deep-sea sediment lithology and mineralogy might identify glacial sequences in sedimentological records (Bramlette and Bradley, 1940), and from then on, geochemical proxies in marine records were utilised to recognise sedimentary record alterations by enriching or depleting components (Goldberg, 1954; Goldberg and Arrhenius, 1958; Wedepohl, 1960; Degens, 1965; Berner, 1971). Today, geochemical analysis is broadly used in the study of marine sediments, and many geochemical relations have been analysed for sediment provenance studies (Dymond et al., 1992; Dypvik and Harris, 2001; Thomson et al., 2006; Bout-Roumazeilles et al., 2013; Martínez-Ruiz et al., 2015, among many others) or, more specifically, trace metals for reconstructing palaeoredox conditions (Jenkins, 2003; Tribovillard et al., 2006; Hennekam et al., 2019; Algeo et al., 2020; Algeo and Li, 2020; Sweere et al., 2021, among many others).

In general, marine sediments involve very different materials, comprising lithogenous components, crystalline and non-crystalline phases from continental surfaces, soil-derived components, crustal rocks from the sea floor, biogenic, hydrogenous and cosmogenous

components, inorganic components directly precipitated from the seawater, meteoric material, and diagenetic phases formed after accumulation (Calvert and Pedersen, 2007). Thus, the composition of marine sediments depends on multiple factors, like the amount of humidity in the continental area that controls weathering and erosion, the type of the substrate, characteristics of the basin, currents, geographical location (on the continental platform or in a distal abyssal area), biological productivity in the basin, insolation, temperature, among others. Moreover, the bulk sediment composition will be narrowly related to the climate and the region. Authigenic precipitation is also significant for the sediment composition. Under certain environmental conditions, some minerals will precipitate from the interstitial waters inside the sediment. These produce, for example, enrichment in certain trace metals like U, Mo, and Cr, among others, under certain circumstances, as they are soluble in seawater and become insoluble under oxygen depletion.

Mediterranean's sediment inputs, like fluvial discharge, aeolian supply, and productivity, influence and produce significant compositional changes. As the variation in these factors comes mainly from climatic changes, geochemical proxies can be applied to interpret climate variations and the related environmental (ecological and depositional) conditions.

Thus, the composition of the sediments is quite complex, and the elemental composition will reflect an ample range of diverse factors. Many efforts have been devoted to unravelling the component mixtures and gaining insight into sedimentary deposits (Calvert and Pedersen, 2007). When analysing the lithogenous fraction, which comes from Earth's crust erosion, diverse factors should be considered, such as differential erosion, type of erosion, sorting, and processes during transport, among other factors (Calvert and Pedersen, 2007). The use of a conservative element is the best methodology to separate the lithogenous fraction. Aluminium has been revealed particularly useful in this regard since it has very similar concentrations in most of the rocks from the upper crust (e.g., Wedepohl, 1971; Taylor and McLennan, 1985; Calvert and Pedersen, 2007), and it is also conservative during weathering of rocks and soils because of the clay formation (Bohn et al., 1979). For these reasons, it is one of the most commonly used elements for the normalisation of elemental data and obtention of the relative composition of the lithogenous fraction, providing qualitative information about enrichments and depletions and correcting the dilution factor (Calvert and Pedersen, 2007). Occasionally, titanium has been used as a conservative element for normalising bulk sediment. However, titanium content is inconsistent across various rock types (Calvert and Pedersen, 2007); for instance, it is enriched in a factor of five or more in mafic rocks with respect to silicic rocks (Wedepohl, 1995). Moreover, titanium is transported in Ti-bearing heavy minerals like rutile, which enriches it in the fine fraction and has sometimes been used as a grain size proxy (Spears and Kanaris-Sotiriou, 1976). Thus, aluminium is the preferred element for normalising the lithogenic fraction in this thesis, with titanium being utilised when insufficient aluminium data are available.

III.2 Proxies for terrigenous input in the Mediterranean Basins

III.2.1. Variability of the sediment inputs

Climate change will be one of the main forces influencing ocean sediment composition. In the Mediterranean, the varying climate over the geological times has considerably influenced runoff, vegetation cover, water mass and circulation. There are many examples of these influences, from seasonal to millennial-scale, with significant composition variations in the sediments. For instance, important measurable variations are defining the glacial-interglacial transitions or the Dansgaard-Oesger cycles that are known to have very important consequences not just for the temperature but for the precipitation in the Mediterranean Basin (Dinarès-Turell et al., 2003; Martínez-Ruiz et al., 2015).

Global climate change can also be reflected in sediment composition. Several factors, such as sea-level changes driven by climate change and glacial-interglacial transitions, can influence sediment dynamics. During high sea levels, when the sea inundates the continental platform, it creates additional accommodation space, reducing the amount of sediment reaching the deep basin.

These variations in sediment deposition patterns can provide valuable insights into past climatic conditions and environmental changes. By studying sediment composition and variations in sedimentation rates, a better understanding of the impacts of climate change on sediment records can be obtained. The terrigenous fraction will have different compositions resulting from the transport distance, mode of transport, erosion type (chemical or physical), mineralization, and grain size, among others. These differences leave an imprint in the geochemical signatures that can be used to infer the importance of each process and correlate it to climatic and oceanographic parameters.

In this research, the sediment components are related to several origins. The terrigenous fraction originates from the erosion of landmasses and is transported to the Mediterranean Basin. The terrigenous is sedimented along other fractions, like the biogenic fraction — primarily composed of carbonate and, in some areas, from opal— and the authigenic input — minerals precipitated in the water column and sediments. Consequently, geochemical proxies can be used to understand further the complexities associated with the variability of different inputs (see Fig. III.1 as a sketch of variable inputs in the Mediterranean Basin and some diagnostic elements).

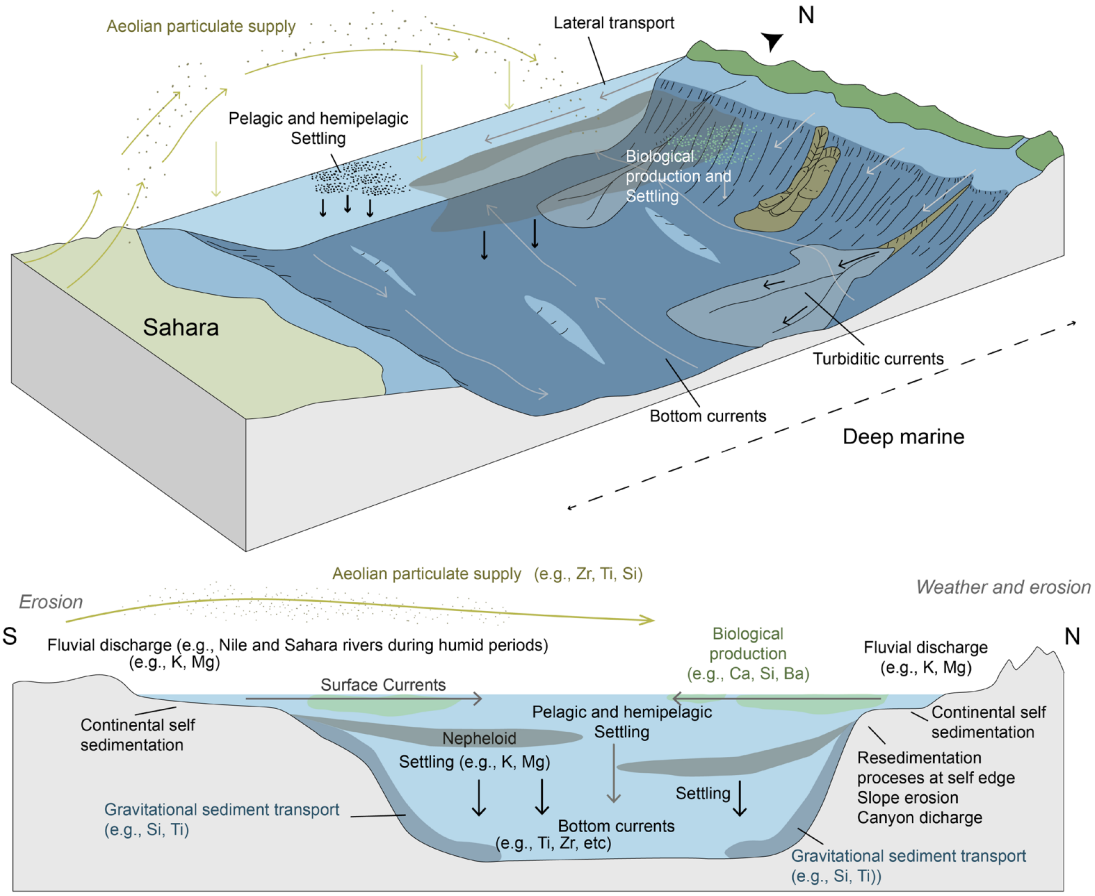

Figure III.1. Different sediment origins in the Mediterranean Basin. In addition, the main elements associated with the different inputs contributing to the sediment bulk composition are shown.

III.2.1. The terrigenous fraction

There are two primary pathways through which sediments of the terrigenous fraction can reach their final deposition in the deep sea: riverine and aeolian inputs. Another important sediment input to the basin, especially in the east and central Mediterranean, is the episodic deposition of volcanic material from the active volcanic regions of the Italian and Aegean areas (Narcisi and Vezzoli, 1999). The terrigenous input can be reconstructed from various elemental ratios commonly used to indicate sediment sources and sedimentological processes (Tribovillard et al., 2006; Calvert and Pedersen, 2007; Algeo and Tribovillard, 2009; Martínez-Ruiz et al., 2015).

Fluvial input

The rivers transport most of the sediment that reaches the sea worldwide (Milliman and Meade, 1983). These sediments originate from erosion and weathering of landmasses and are carried by rivers and their associated discharge into the ocean. At present, the total freshwater discharge to the Mediterranean is around 450 km^3 (Vörösmarty et al., 1998), with an average

sediment load of 10^9 tons per year (Poulos et al., 2002). However, these have been highly variable in the past. Several rivers discharge in the Mediterranean Sea, with the most significant discharges coming from the more humid European margin. Today's main rivers are Nile, Rhone, Po, Ebro, Tevere, Adije, and Vijose, presented in order of total discharge volume. There are many others, but they are of less relative importance.

Generally, the riverine material accumulates in the continental platform, and a part of it can bypass the platform to reach the deep basin or be eroded from the continental platform margins by, for example, storms. This transfer to the deep basin occurs through gravitational fluxes, nepheloid layers, or aided by current transport both at the surface or at the bottom and can extend over vast distances (Fig. III.1). In the deepest zones, as the ones studied in this thesis, most of the terrigenous fluvial material comes from lateral advection, current transport and nepheloid layer deposition, with the rare contribution of turbiditic gravitational fluxes. However, some basins, like the Balearic Basin, include abundant turbidite layers (Rothwell et al., 2006), sometimes with individual layers several meters thick, like the one described in the LGM (Cattaneo et al., 2020). Thus, the riverine input in the deep Mediterranean Basin will be influenced mainly by the precipitation on the continent and the sea level, and it has been observed to increase during warmer periods when the atmospheric patterns favour intensified westerlies in the Mediterranean Basin (e.g., Cacho et al., 2002; Bout-Roumazeilles et al., 2013) or what will be equivalent to a negative NAO today. In the Eastern Mediterranean, the Monsoon activity is a main factor controlling the riverine inputs, especially the variations in the Nile discharge (e.g., Wu et al., 2018).

Regarding the geochemical proxies to reconstruct this input, the potassium enrichment (K/Al ratio) has been used as a proxy for fluvial input since this ratio reflects the illite and detrital K-feldspar content. These minerals are present mainly in river runoff (Martínez-Ruiz et al., 2015), and thus their increase is usually correlated with humid periods and a significant transport by rivers, with the enhanced terrigenous fraction against the carbonate fraction (Jiménez-Espejo et al., 2007; Martínez-Ruiz et al., 2015).

Aeolian inputs

The terrigenous fraction can also reach the deep sea through aeolian (wind) transport. Fine-grained particles, such as dust and silt, can be lifted by wind from terrestrial surfaces, including deserts, arid regions, and coastal areas, and transported over long distances before eventually settling in the deep sea. Dust arriving in the Mediterranean Basin comes from highly dust-productive areas like the Sahara (e.g., Middleton and Goudie, 2001; Dinarès-Turell et al., 2003; Zielhofer et al., 2017). The Sahara Desert is the main dust source (Goudie and Middleton, 2001); yearly, 2000 metric tons of dust are emitted into the atmosphere (Shao et al., 2020). Wind intensity is essential in controlling Saharan input, with a strong correlation between wind intensity, the NAO, the ITCZ, and the Sahel drought (Evan et al., 2016). On the millennial scale, the migration of the ITCZ in latitude can explain important variations in dust transport. When the ITCZ is situated northward, a negative anomaly in the north of Africa appears,

increasing dust transport (Sabatier et al., 2020). The aeolian dust can constitute an essential part of the detritic fraction in areas with very low riverine inputs.

Some elements like zirconium, rubidium or titanium tend to accumulate in the particulate fraction as they are more abundant in weathering-resistant elements (Oldfield, 2003). For this reason, Saharan dust is enriched in certain chemical weathering-resistant minerals, such as zircon. The aeolian input into the Mediterranean basins is one of the significant contributors to the terrigenous fraction of the sediments due to its proximity to the Sahara Desert (Moreno et al., 2002). Zirconium has been interpreted as characteristic of the erosion of soils during dry periods, thus allowing the use of the Zr/Al ratio as an aeolian input proxy (Bout-Roumazeilles et al., 2013). Although silica can come from biogenic production, in the Mediterranean, it mostly comes from aluminosilicates (Masqué et al., 2003; Martínez-Ruiz et al., 2015). Si/Al ratio can be used as an aridity proxy in the Mediterranean as a proportion between quartz against other aluminosilicates (Jiménez-Espejo et al., 2007, 2008; Rodrigo-Gámiz et al., 2011). Thus, elemental ratios like Zr/Al ratio, Si/Al ratio or even Ti/Al ratio have been used to reconstruct aeolian input fluctuations.

III.2.2 Carbonate fraction

Three factors control the ocean's carbonate cycle: dissolution, productivity in the surface water, and dilution by terrigenous or non-carbonate organic remains (Hoogakker et al., 2004). The skeletal remains of microorganisms can be more than 75% of the constituents of the sediment in open sea pelagic environments (Hüneke and Henrich, 2011). In the Mediterranean, the carbonate content is attributed mainly to productivity and dilution by terrigenous inputs. The carbonate content can be low related to increased input of terrigenous sediments or low productivity; at the same time, high productivity or low terrigenous inputs will produce decreased carbonate content (e.g., Van Os et al., 1994).

The carbonate production of the Mediterranean is dominated by red algae and sea grass on the coasts (e.g., Michel et al., 2018). However, significant carbonate production in the open seawater column comes from planktonic organisms like foraminifera, pteropods, or dinoflagellates. Carbonate productivity has been important in the Mediterranean during interglacials (e.g., Weldeab et al., 2003). Moreover, some authors proposed that non-carbonate mediated productivity (opal, diatoms) during glacial periods was also higher in contrast to carbonate producers (Hoogakker et al., 2004).

The Ti/Ca ratio served to evaluate the relative variations between the terrigenous and carbonate fractions. It is commonly used as a proxy for increased continental runoff and sediment transport, rising with enhanced terrigenous input and the relative importance of the lithogenous fraction in the sediment (Arz et al., 1998; Bahr et al., 2005; Calvert and Pedersen, 2007; Jaeschke et al., 2007; Litt et al., 2009; Pierau et al., 2010; Govin et al., 2012; Stuut et al., 2014; Rothwell and Croudace, 2015). It has also recently been used as a proxy for current

intensity in the Western Mediterranean due to the currents' potential for transporting fine terrigenous sediments (Mesa-Fernández et al., 2022). Within the terrigenous fraction, some ratios can also be used to distinguish between different source areas and transport processes.

III.2.3 Redox conditions and authigenic minerals

Many trace metals also accumulate in sediments by precipitation in the water column, leading to authigenic enrichments (e.g., Calvert and Pedersen, 2007). This precipitation from seawater is caused by complex changes in pH, salinity, temperature, and oxygen, as well as by the availability of these metals in the seawater (e.g., Tribovillard et al., 2006).

Many redox-sensitive elements like As, Cu, Mo, Ni, Re, U, V, and Zn are concentrated in sediments deposited during periods of oxygen restriction, inducing reduced conditions in the sediment or when a significant volume of organic matter is buried, allowing post-depositional reduced conditions (Vine and Tourtelot, 1970; Calvert and Pedersen, 1993; Algeo and Maynard, 2004; Tribovillard et al., 2006). These oxygen variations in the water column and sediments can be reconstructed from trace metal ratios (e.g., Calvert and Pedersen, 1993, 2007; Jones and Manning, 1994; McLennan, 2001; Tribovillard et al., 2006; Algeo and Liu, 2020). Sapropels are excellent examples of such variations. They show enrichments in redox-sensitive elements such as Mo, S, Re, As, Cu, Ni, Sb, and Fe, reflecting, in some cases, a strong sulfidation in the water column. The trace metal content of anoxic basins is mainly controlled by the availability of trace metals in the water column and sedimentation rate (e.g., Brumsack, 2006).

Even though some elements exhibit limited enrichment within the suboxic zone, bulk authigenic enrichment of the redox-sensitive elements occurs within the euxinic zone. However, since the threshold value associated with a given elemental proxy can vary considerably between depositional systems, redox proxies must be internally calibrated for each palaeodepositional system under investigation (Algeo and Li, 2020).

The different enrichments of these elements can be used to define past oxygen conditions (Fig. III.2) and have been applied in this thesis to describe events of low oxygenation in the Mediterranean Basin related to the ORL and sapropel formation (Morford and Emerson, 1999; Tribovillard et al., 2006; Algeo et al., 2020; Algeo and Li, 2020; Algeo and Liu, 2020).

Uranium and molybdenum are probably some of the most valuable elements for the study of redox conditions in marine settings (e.g., Emerson and Huested, 1991; Crusius and Thomson, 2000; Vorlicek et al., 2004; Algeo and Tribovillard, 2009; Helz et al., 2011; Algeo and Liu, 2020). U and Mo can precipitate where bottom waters are oxygenated due to respiration, lowering the pore water oxygen concentration (e.g., McManus et al., 1998, 2005; Singh et al., 2011).

Continuous exposure to relatively high oxygen bottom waters in open ocean locations with low sedimentation rates, notably 2 cm/kyr, might cause authigenic uranium to reoxidize and permeate out of the sediment (i.e., burndown), erasing any archival evidence of its precipitation

(Mangini et al., 2001; Jacobel et al., 2017, 2020; Costa et al., 2018). In these cases, any interpretation of redox conditions should be avoided since the latter preservation bias is tricky to discern and even more difficult to account for or rectify (Jacobel et al., 2020). However, considering these biases, it is possible to use redox proxies to partially reconstruct oxygenation conditions when we dispose of proxies that reflect the possible displacement of the signals, like the Mn/Al ratio in cases of oxygen penetration, but the results should always be used with precaution.

Another known effect, especially important in very high-resolution studies, is when the anoxic/oxic interface occurs at a certain depth in the sediment, the enrichment might occur then several centimetres below the sediment-water interface (Mangini et al., 2001; McManus et al., 2005) and thus the displacement should be considered when doing time scaled interpretations in comparison with other proxies. In some open ocean environments, it has been shown that the interface could be situated up to 50 cm below the seafloor (King et al., 2000). Thus, this aspect must be considered when using trace metals as palaeoredox proxies.

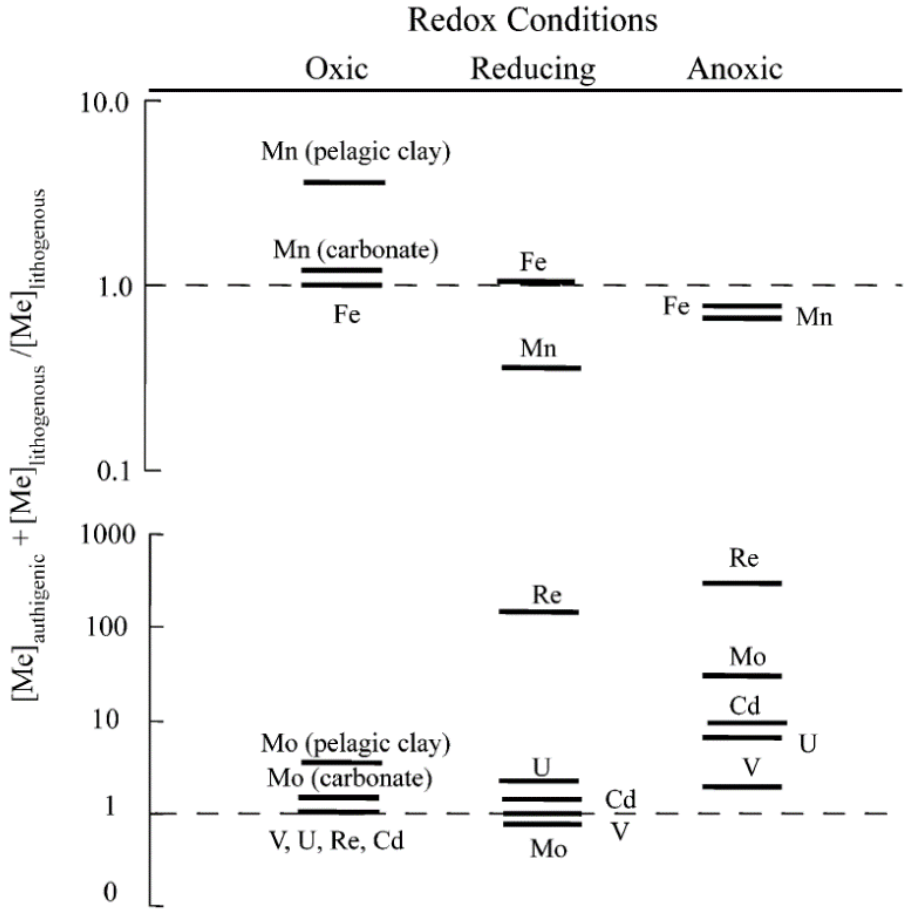

Figure III.2. Trace metal concentration under redox conditions (Calvert and Pedersen, 2007).

III.2.4 Barium proxies and productivity

Ba has been broadly used as a proxy for productivity (e.g., Dymond et al., 1992), and it is a key proxy in the area for defining the Eastern Mediterranean sapropel deposition even after oxidation processes (e.g., Thomson et al., 1999; De Lange et al., 2008). Ba precipitates as barite in the water during organic matter decay. Thus, it correlates well with productivity (Schoepfer et al., 2015). Ba excess from biogenic origin has also been used as a proxy for palaeoproductivity in the Alboran Sea Basin (e.g., Rodrigo-Gámiz et al., 2011; Martínez-Ruiz et al., 2015).

Ba is generally well preserved in oxic sediments, though it may become mobile under reducing diagenetic conditions (De Lange et al., 1994). Under sulphate-reducing conditions, it can be dissolved at a certain depth below the sediment surface, removed or diffused, and reprecipitated outside its original interval (Tribovillard et al., 2006; Griffith and Paytan, 2012). In some deep sites in the Eastern Mediterranean (Van Santvoort et al., 1997), it has been observed that Ba has been partially mobilised and reprecipitate up and below a sapropel or in the oxidation front due to the pyrite dilution upwards, becoming a "diagenetic barite front" at greater sulphate concentrations (De Lange et al., 1994). Ba remobilisation is not particularly significant in the Mediterranean due to pore water sulphate concentration, though important remobilisation has been reported in the Black Sea (Henkel et al., 2012).

Barite precipitation in the water column is linked to biological processes, particularly bacterial activity (Martínez-Ruiz et al., 2018). Thus, its enrichment in the sediments against the terrigenous fraction has been associated with high export productivity (Dymond et al., 1992; McManus et al., 1998; Tribovillard et al., 2006; Griffith and Paytan, 2012; Schoepfer et al., 2015; Carter et al., 2020; Horner et al., 2021; Whitmore et al., 2022) and has been broadly used as indicative of palaeoproductivity in the Mediterranean basins (e.g., Sternberg et al., 2007; Rodrigo-Gámiz et al., 2011; Martínez-Ruiz et al., 2015).

III.3. Ichnological analysis in well core

From the end of the XX century and the beginning of XXI, the ichnological analysis has been considered a powerful tool for studying past environmental changes (Ekdale et al., 1984; Buatois and Mángano, 2011; Knaust and Bromley, 2012). It is especially useful for supporting sedimentological and stratigraphic interpretations and then sedimentary basin research, for instance, in the differentiation of deep-sea deposits like the pelagites, turbidites, and contourites (e.g., Wetzel and Uchman, 2012; Rodríguez-Tovar, 2022), with the contourites in the centre of this characterisation today (Rodríguez-Tovar and Hernández-Molina, 2018; Rodríguez-Tovar et al., 2019b; Rodríguez-Tovar, 2022).

The axis of ichnological studies resides in the relationship between trace fossils and palaeoenvironmental conditions. Trace fossils, which reflect tracemaker behaviour, record the response to biotic and abiotic factors (e.g., salinity, oxygen, nutrients, hydrodynamic energy,

rate of sedimentation, and substrate, among others; Rodríguez-Tovar, 2022). Two main paradigms supporting the usefulness of the ichnological analysis have been developed, such as the ichnofabric approach and the ichnofacies model. The ichnofabric approach embraces any textural or structural aspect resulting from bioturbation and bioerosion at any scale (Ekdale and Bromley, 1983; Rodríguez-Tovar and Dorador, 2015; Rodríguez-Tovar et al., 2020a). It considers trace fossil assemblage and other ichnological features such as cross-cutting relationships, tiering or degree of bioturbation (Fig. III.3; Buatois and Mángano, 2011; Ekdale et al., 2012; Knaust, 2017). The ichnofacies model (Seilacher, 1964, 1967) is based on identifying certain features shared by ichnotaxa during a long time span that can be related to particular environmental conditions (Buatois and Mángano, 2011).

Ichnofacies characterisation integrates data from ichnological, sedimentological, stratigraphical and taphonomical information. Both the ichnofabric approach and the ichnofacies model determine the usefulness of ichnology in very different fields, including palaeoecology, sedimentology, evolutionary palaeoecology, palaeoceanography and palaeoclimatology (Mángano and Buatois, 2012).

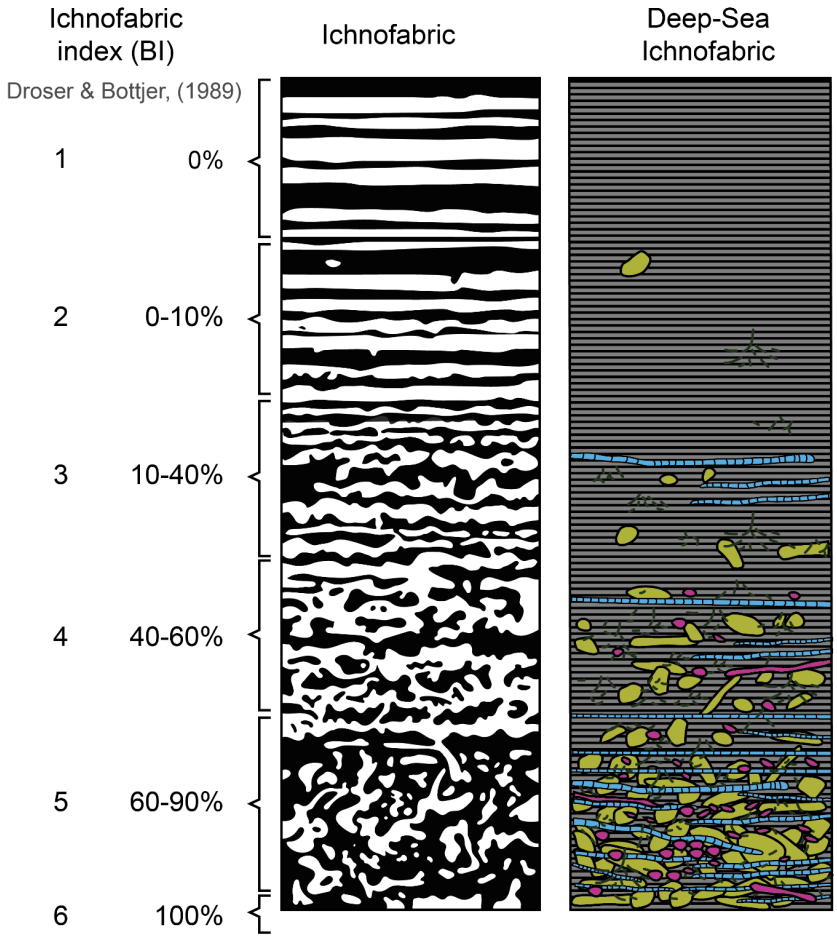

Figure III.3. Representation and appearance of "Generic Shelfal" and "Deep–Sea" ichnofabrics, including ichnofabric indexes according to the scheme of Droser and Bottjer (1989).

Particularly, the ichnological information has proven to be a very useful proxy for the characterization of past anoxic events as was seen for the Faraoni Event (upper Hauterivian; Rodríguez-Tovar and Uchman, 2017), the Bonarelli Event (Cenomanian-Turonian boundary; Uchman et al., 2008, 2013a, 2013b; Rodríguez-Tovar et al., 2009, 2020b; Rodríguez-Tovar and Uchman, 2011; Monaco et al., 2012, 2016) and the Toarcian Oceanic Anoxic Event (Early Toarcian; i.e., Rodríguez-Tovar and Uchman, 2010; Reolid et al., 2014; Miguez-Salas et al., 2017, 2018; Rodríguez-Tovar et al., 2017, 2019c). Thus, in the research conducted here, ichnological features, including ichnotaxonomy, degree of bioturbation, cross-cutting relationships, or ichnological assemblage, will be interpreted in terms of benthic flux and oxygen content in an integrative approach with other studied proxies.

Ichnological analysis of well-core surfaces is especially interesting as it offers an accessible and affordable way to approach the environmental variations and sediment characteristics. However, this research entails particular limitations related to core properties, such as the narrow-exposed surface, the two-dimensional core slabs, or the usual absence of complete structures (e.g., Knaust, 2012; Dorador and Rodríguez-Tovar, 2014a; Rodríguez-Tovar and Dorador, 2014). Thus, ichnotaxonomical classification is sometimes difficult due to the scarcity/absence of diagnostic criteria or ichnotaxobases (Bromley et al., 1990, 1996; Bertling et al., 2006; Knaust, 2012, 2017), determining a generalized ichnotaxonomical classification at the ichnogenus level (Bromley et al., 1990, 1996). Ichnological research in cores from modern marine deposits is particularly difficult because of the unconsolidated character of the sediment and the weak differentiation between biogenic structures and host sediment (Dorador and Rodríguez-Tovar, 2015).

In this thesis, an ichnological study has been conducted following the methodology previously proposed and tested to improve the visibility of trace fossils, allowing qualitative and quantitative analysis of ichnological features in the well core (Dorador and Rodríguez-Tovar, 2014a, 2016a, 2018; Rodríguez-Tovar and Dorador, 2015). The images from the core surface were treated using Photoshop™ software (Dorador and Rodríguez-Tovar, 2014b) based on modifications to image features, such as contrast, brightness, vibrance, saturation, exposure, lightness, and colour balance. After improving the images, the observed traces were manually or automatically selected for their ichnotaxonomic identification. After ichnotaxonomical classification, bioturbation quantification was conducted using a semiautomatic methodology that was recently developed (see Chapter V).

The main differentiated ichnogenera in the studied cores have been (Fig. III.4); *Chondrites* von Sternberg, 1833, *Planolites* Nicholson, 1873, *Scolicia* Quatrefages, 1849, *Thalassinoides* Ehrenberg, 1944, and *Zoophycos* Massalongo, 1855. *Chondrites* are distinguished by clusters of small, millimetre-sized, circular to subcircular sections, occasionally overlapping other traces (such as *Thalassinoides*). *Planolites* are characterised by circular or subcircular, unlined burrows less than one centimetre in diameter. The fill lacks structure and is typically darker in colour than the adjacent sediment. *Scolicia* is recognised as large, cm-thick, elliptical cross-sections with a central ridge or as a series of indistinct lamellar back-fill structures in 10-40 cm

thick bioturbated intervals. *Thalassinoides* are observed as comparatively greater circular, subcircular, or elongated burrow sections, typically > 1 cm long. *Zoophycos* appear as elongated structures, mainly horizontal, that can cut the entire diameter of the core surface. In some cases, the characteristics of internal spreite have been observed, but not always. Usually, the trace is darker than the host sediment.

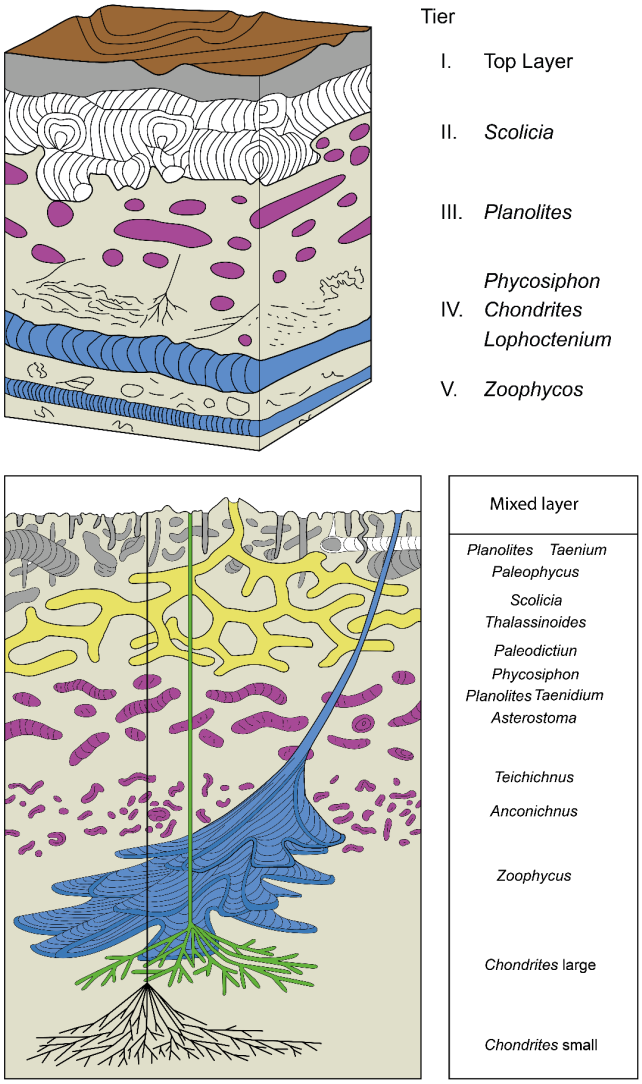

Figure III.4. Schematic representation of tiering levels (vertical partitioning of the habitat) in deep marine environments (Ekdale and Bromley, 1991; Bromley, 1996), including the recognized ichnotaxa (Chondrites, Planolites, Scolicia, Thalassinoides Zoophycos).

PART 2

MATERIALS AND METHODS

Chapter IV

Materials and main methodologies

IV.1. Data sources and materials

IV.1.1. Materials

In this thesis, diverse sediment records from the Westernmost Mediterranean (Alboran Sea basin) and the Eastern Mediterranean at the Ionian Sea (Table IV.1; Fig IV.1) have been studied.

In the Western Mediterranean, the studied sediment records are cores recovered at Sites 977 and 976 recovered during Leg 160 of the ODP in 1996 (housed in the IODP Bremen Core Repository, Germany), and core GP03 recovered during the Gasalb oceanographic cruise onboard the R/V Pelagia in November 2011 (housed in the Andalucian Institute of Earth Sciences). Core LC10 was obtained during the Marion Dufresne cruise 81 in the Eastern Mediterranean as part of the MAST II PALAEOFLUX programme in February 1995 (housed, sampled, and scanned at the British Ocean Core Research Facility in Southampton).

All the studied cores consist of pelagic mud and hemipelagic facies (see corresponding chapters for details).

IV.1.2 Data and age models

Part of the conducted research uses data previously obtained from online repositories like Pangaea.de and the JOIDES Resolution Repository for the core photographs.

For sites 977 and 976, the used age model is presented by Martrat et al. (2004, 2014) based on radiocarbon dating and tie points from the isotopic curve. For GP03, the age model from the twin core GP04 (Morcillo-Montalbá et al., 2021) was used to establish a linear interpolation based on several tie points from the Ba/Al record.

For core LC10, the age model was done by establishing tie points with the sapropel onset and demise and $\delta^{18}O$ profiles. The top part of the LC10 core is missing. The presence of the sapropel 1 from the Eastern Mediterranean is detected on the top, with an age of the top of the core inferred to be 5000 ka.

Table IV.1. Locations and a brief description of the studied cores

Core	Location	Coordinates and depth	Description
GP03	Western Alboran Sea	35.787° N, 4.534° W 1306.5 mbsl	Dark greenish hemipelagic mud clays with some foraminifera and shell fragments
976	Western Alboran Sea	36.205° N, 4,313° W 1108 mbsl	Greenish hemipelagic nannofossil-bearing clay
977	Eastern Alboran Sea	36.0317° N, 1.955° W 1984 mbsf	Greenish hemipelagic nannofossil clay and calcareous silty clay
LC10	Ionian Sea	35,212° N, 16.581° E 1322 mbsf	Greyish-yellow to olive-grey foraminifer-rich mud and nannofossil ooze slightly to strongly bioturbated

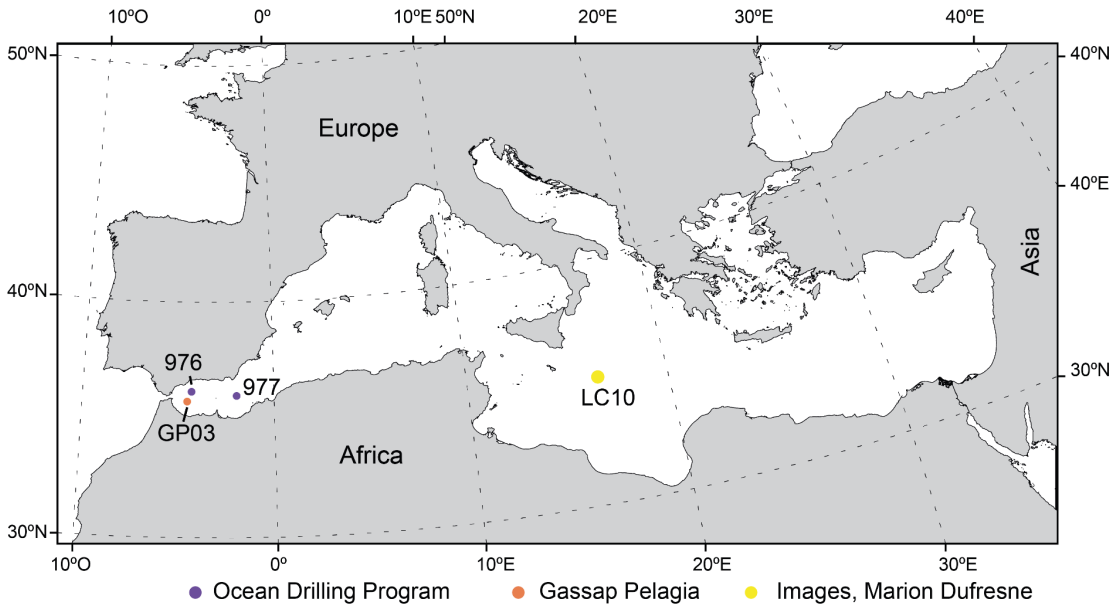

Figure IV.1. Location of the studied sediment records.

IV.2. Sampling and analysis

IV.2.1. Sampling

The first step included XRF core scanner analysis of some of the cores and the acquisition of high-resolution images and radiographs in the case of the LC10 core. Prior to the preparation of the discrete samples for the different analyses, cores were described and sampled, and then samples were dried following the steps shown in Figure IV.2; the dried samples from GP03 and LC10 cores were prepared for XRF analyses to determine major element composition. The analyses were performed at the Andalusian Earth Science Institute using X-ray fluorescence (XRF) and wavelength dispersive spectrometry (WDXRF) Bruker AXS Pioneer.

IV.2.2. Analysis

X-ray fluorescence core scanner (XRF)

XRF scanning is a non-destructive technique that only requires preparation of the surface of the core, flattening the surface and eliminating possible cracks that could create data distortion. A comparison was made with data obtained from discrete sample analysis to ensure the reliability and quality of the results obtained from the core scanner. This technique was used to analyse core GP03 and cores LC10 and GP03. GP03 was analysed using an Avaatech III Core Scanner system (Serial No. 21) at the CORE LAB laboratory of the University of Barcelona. LC10 was scanned at the National Oceanography Centre in Southampton using a COX Analytical Systems Itrax X-ray Fluorescence (XRF). This equipment also obtains a high-resolution optical image of the sample surfaces and an X-radiograph to evaluate sample-wide density contrasts.

X-Ray Imaging Scanner

A GeoTek ScoutXcan X-Ray Imaging Scanner was used to obtain X-ray 2D photographs of some of the studied cores. The X-Ray Imaging Scanner requires no specific sample preparation before imaging. Samples of round and half-round cores can be scanned. The X-Ray Imaging Scanner accommodates core samples between two movable limbs. Other samples not secured between the moving arms will be deposited in a transparent X-ray tray. The sample is positioned between the two movable arms and then fed through the X-ray imaging area in the machine's centre, where a powerful X-ray source sends X-rays through the sample to the detector at the bottom of the instrument. Multiple 2D radiographs can be captured by rotating the limbs about their axes. The software composes these images into a pseudo-three-dimensional laminography. The laminograph illustrates the X-Ray Imaging Scanner's enhanced imaging capabilities compared to the standard radiograph in the middle. Density contrasts are

significantly more distinct. Detailed descriptions of the core can be derived from these images. In addition, sampling can be more precisely targeted when specific characteristics of interest are identified.

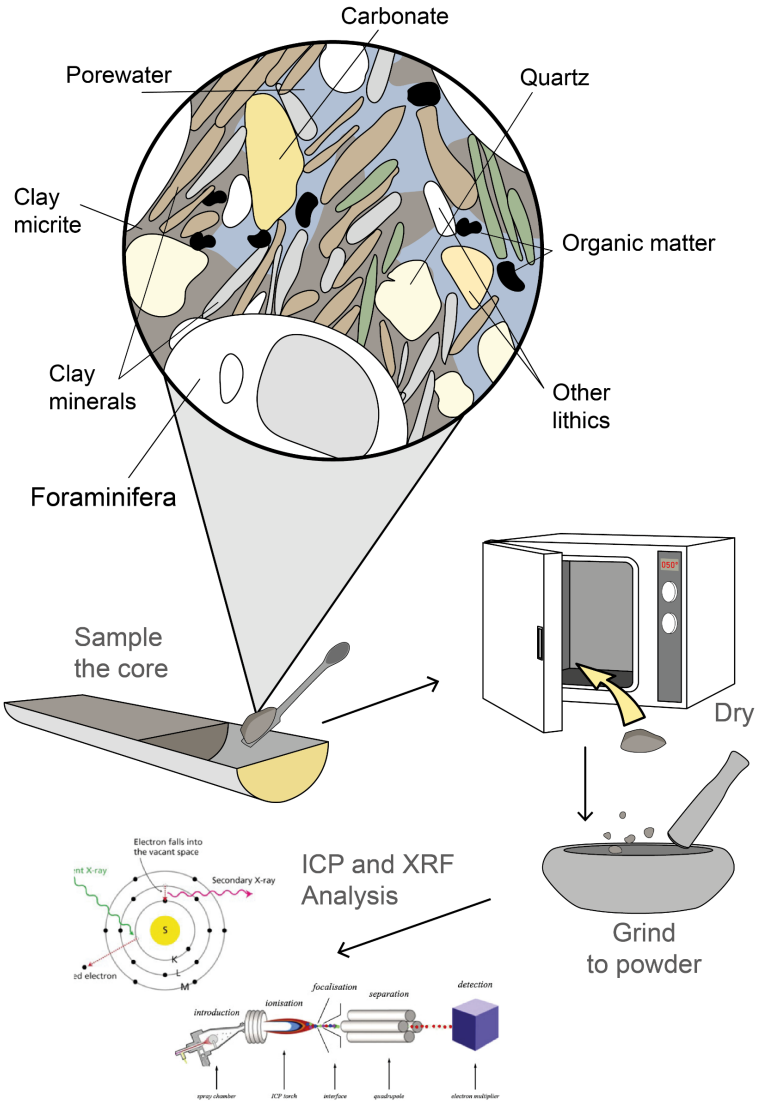

Figure IV.2. Procedure of ICP-MS and XRF analyses of discrete samples.

Wavelength dispersion X-Ray fluorescence (WDXRF)

The GP03 and LC10 cores were also analysed by WDXRF to determine the major elements' composition. The major elements' composition was determined for this study at the Andalusian Earth Science Institute.

Samples were prepared as fused beads melting 0.9 g of calcined bulk sediment with lithium tetraborate. The instrument used was an S4 Pioneer BRUKER with a maximum power of 4 kW and equipped with an Rh anode X-ray tube (60 kV, 150 mA), three analyser crystals (OVO- 55; LiF 200 and PET) and a collimator of 0.26° and 0.46°, and an analytical detection limit of 0.1% and an instrumental error <1%.

Inductively coupled plasmas mass spectrometry (ICP-MS)

GP03 and LC10 samples were digested in HCl, H_2O_2, HNO_3 and HF in a Teflon-lined vessel at 180°C, evaporated and then diluted in 100 ml bi-distiller water with 4%vol HNO3. Trace elements were measured using ICP-MS, NexION 300d (Perkin Elmer) and Sciex Elan 5000 (Perkin Elmer) at the Centre of Scientific Instrumentation of the University of Granada. The internal standards for Rh and Re were used in this study. The instrument error was ±2% for an elemental concentration of 50 ppm.

Magnetic properties analysis

Magnetic susceptibility was obtained at the Material and Environmental Magnetism Laboratory (Laboratorio de Magnetismo de Materiales y Magnetismo Ambiental, Instituto Geográfico Nacional). Magnetic susceptibility was obtained from discrete samples every 2.5 cm along the core. Samples were dried at 40°C low-frequency (LF, 0.465 kHz), and magnetic susceptibility was measured ten times for each sample using Bartington MS3/MS2B dual-frequency equipment. The average mass-normalised values and standard deviations were calculated and plotted.

High-resolution images and digital visibility enhance ichnological analysis

For the ichnological analysis, high-resolution images were obtained and then treated under the methods proposed in previous works (Dorador and Rodríguez-Tovar, 2016a, 2018) (see Chapter V for a detailed description).

Chapter V

Applied ichnology in sedimentary geology: Python scripts as a method to automatise ichnofabric analysis in marine core images

Computers & Geosciences
Volume 136, March 2020, 104407

https://doi.org/10.1016/j.cageo.2020.104407

S. Casanova-Arenillas [a], F.J. Rodríguez-Tovar [a], F. Martínez-Ruiz [b]

[a] Departamento de Estratigrafía y Paleontología, Universidad de Granada, Campus Fuentenueva s/n, 18002, Granada, Spain

[b] Instituto Andaluz de Ciencias de la Tierra (IACT), Consejo Superior de Investigaciones Científicas-Universidad de Granada (CSIC-UGR), Avda. de las Palmeras 4, 18100, Armilla, Granada, Spain

Abstract

Image analysis has been successfully applied in core research, especially in studies from modern deposits, to enhance the visibility of ichnological features and characterise ichnoassemblages and ichnofabrics. Its application to ichnological research provides useful information for marine core studies, hence sedimentary geology, but also for hydrocarbon exploration. Here we develop a new methodology, using Python programming language, which significantly improves the ichnological analysis. The method automatises the process of obtaining continuous ichnological information, in this case, about the percentage of bioturbation as a key aspect of the ichnofabric approach. The method affords the possibility of automatically generating continuous percentage and other index records using pixel counts in previously treated images. The resulting data sets are easy to correlate with the information usually obtained from cores (e.g., geochemical, and mineralogical data). Such an integration of different proxies for to the field of sedimentary geology especially in the use of ichnological analysis, making it easier for the researcher, less time consuming, and more likely to be undertaken. The coding and sharing of open software tools allow for great flexibility, giving researchers in ichnology or related fields the option to implement new features, develop more complex tools to improve the package, and share findings with the scientific community.

V.1. Introduction

The ichnofabric approach is understood as the integration of multiple lines of information on an original sedimentary fabric together with the bioturbation and bioerosion fabrics, and the taphonomic filter (Taylor et al., 2003; Buatois and Mángano, 2011; Ekdale et al., 2012), is essential in applied ichnology as a tool for sedimentary basin research. Since the first papers on ichnofabrics (Ekdale and Bromley, 1983; Ekdale et al., 1984), this approach has been developed in several ways, including the use of semi-quantitative flashcards to evaluate the intensity of bioturbation (Droser and Bottjer, 1986, 1989; Bottjer and Droser, 1991), the visualisation of ichnofabrics based on graphic illustrations (Bromley and Ekdale, 1986; Taylor and Goldring, 1993; Taylor et al., 2003), the use of computer-aided analysis to improve the visualisation of key features (Magwood and Ekdale, 1994), and the recent application of digital image treatment to characterise ichnological properties (Dorador and Rodríguez-Tovar, 2014a, 2014c, 2014b; Rodríguez-Tovar and Dorador, 2014; Dorador and Rodríguez-Tovar, 2016b; Dorador et al., 2016; Dorador and Rodríguez-Tovar, 2018; Miguez-Salas et al., 2019). Lastly, the use of Python in fore-core image analysis has been shown helpful in previous works, i.e., Timmer et al., 2016a, 2016b.

The ichnofabric approach became especially informative in the second half of the twentieth century based on its application on cores; at this time, many cores were available due to the increase of scientific ocean expeditions (e.g., ODP, IODP). Such efforts provided an extensive

dataset of subsurface sediments where bioturbation is commonly present. Certain limitations specific to logged cores, e.g., a narrow-exposed surface, two-dimensional core slabs, or the usual absence of complete structures, may impede ichnological research to some extent; but at the opposite end of the scale lie such benefits as a more detailed observation of the infilling material of traces, the cross-cutting relationships, and the distribution and abundance of bioturbation structures. Several techniques like X-ray, magnetic resonance, computer tomography, microtomography, and high-resolution digital photography can be applied for ichnological analysis on cores (Dorador and Rodríguez-Tovar, 2018), altogether providing for a large number of images to be studied. However, in most cases deriving ichnological information from the images can entail tedious or repetitive work not usually done in detail. This research aims to present a method that adds a tool for image treatment and high-resolution ichnofabric analysis, which implies a significant advance for ichnological research on cores with scientific (e.g., sedimentary geology) and economic (e.g., reservoir exploration) implications.

V.2. Methods

V.2.1. Background

Back when computers began featuring image analysis, their use and capabilities were similar in all technical and scientific fields. Yet in recent years the potential of computers, the available resources, and new techniques have become more field specific. The method presented here, using Python programming language and its libraries, builds on previous advances in the ichnological analysis of cores, enhancing the visibility and quantification of bioturbational features (Dorador and Rodríguez-Tovar, 2018), providing an automatic analysis of the images.

Python is a sound program language on which to base this project. It was well suited to the development of scripts for geoscientists who integrate programming into their workflow. It has a clear and easily understandable code easy to learn, an active and growing community of users (especially in academia), and multiple and versatile modules. All these features support the election/use of Python for the present research and suggest a promising future for this programming language for geoscience research purposes.

For such reasons, many users in the scientific field are switching from other major software packages and programming environments (e.g., MATLAB, R, or Stata) to adopt Python as their primary one (Stata Corp, n.d.; The R Foundation, 1999; The MathWorks, 2019). Python is overtaking data science, machine learning and artificial intelligence, and it may well surpass the rest of the languages in the near future (Robinson, 2017). It can therefore be seen as a language for the future of science, particularly when there is a need to manage data sets (Perkel, 2015).

Evaluating the intensity of bioturbation is a main aspect of the ichnofabric approach. Semi-quantitative indices such as the Bioturbation Index (BI) (Reineck, 1963; Reineck and Singh, 1967; Taylor and Goldring, 1993) and the ichnofabric indices (ii) (Droser and Bottjer, 1986, 1989) are used, both mainly based on the percentage of the bioturbated surface. The Bioturbation Index (Reineck, 1963; Reineck and Singh, 1967) establishes seven grades of bioturbation: from 0 (0%; no bioturbation) to 6 (100%; complete bioturbation). In turn, ichnofabric indices (ii) (Droser and Bottjer, 1986; Bottjer and Droser, 1991) rely on comparison with a series of flashcards where five ichnofabric indices are illustrated, from 1 (0%) to 5 (60–100%), while 6 would designate complete burrow homogenisation (Knaust, 2012). Under both approaches, the amount of bioturbation is gauged by the naked eye, so that an element of subjectivity is always involved. Characterising the percentage of bioturbated surface in a semiautomatic way, using a computer package, contributes to a simpler, faster and more objective ichnofabric analysis, as part of a complete ichnofabric analysis including other sedimentological, ichnological and taphonomical information (Buatois and Mángano, 2011; Ekdale et al., 2012; Knaust, 2012).

The present method marks a new step for the semiautomatic evaluation of the percentage of the bioturbated surface. We use Python script integrated with other tools in a program (Casanova-Arenillas, 2019) to build a tool that can be shared with a greater scientific community in the coming years.

V.2.2. Script functioning

The flow of the script is simplified in Figure V.1 showing the main steps.

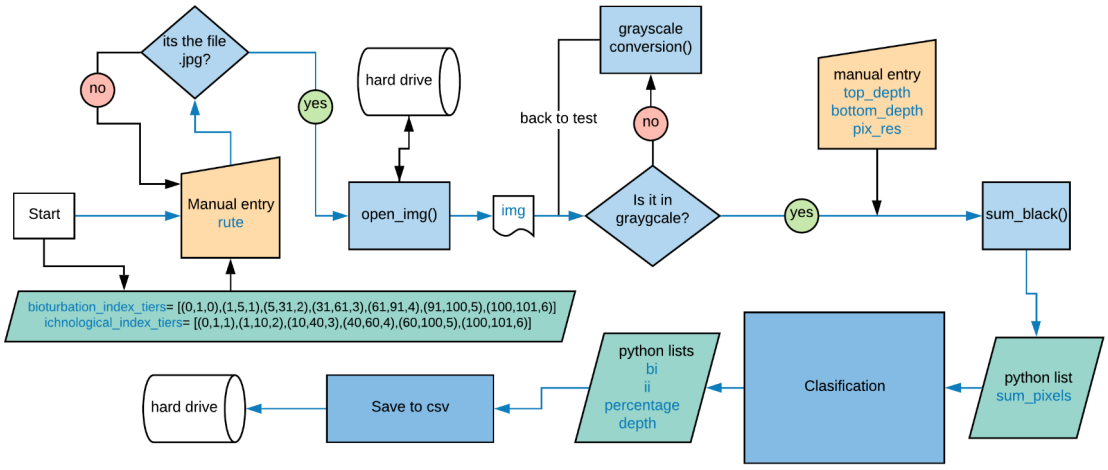

Figure V.1. Schematic program flow, the process can be repeated for more than one section. To see the code, access the database in Zenodo (Casanova Arenillas, 2019).

Before running the script, the method calls for a previous interpretation of the bioturbation in the image. Then, we conduct a manual or semiautomatic selection of the bioturbation features and those pixels assigned to bioturbation are coloured in black (value 0 in the greyscale). To increase the visibility and selection of the structures we suggest following the guidelines proposed in previous research (Dorador and Rodríguez-Tovar, 2014c).

The script runs (as seen in Fig. V.1) as follows: First of all, the image is opened as a jpg and converted to grayscale if it is in RGB. Then, the greyscale image, using the Image module (Clark, 2019), to a NumPy Array, a matrix structure that lends itself to efficient computations (van der Walt et al., 2011), to construct a matrix of any given dimensions. We chose to use a NumPy "array" rather than build a "list" type, because arrays are more reliable for arithmetic operations and, also, provide a better foundation for future expansions of the methodology. After this, the script will carry an automated pixel count line by line, from bottom to top, of the studied interval (reviewing the manual entering the depth of the top and bottom of the section to assign depths to the data obtained), continuously obtaining the percentage of bioturbation. This could be done for every line of pixels. Otherwise, preferably, a data point can be generated every few (horizontal) lines of pixels, representing the mean value along the vertical interval. The adequate number of pixels per point would depend on the resolution of the image (see below). A larger number of lines involved in the mean would translate as fewer points generated and a curve with less "noise". That is, the number of lines can be modulated and adapted to different situations and resolutions, its optimum value depending on the features focused upon.

The obtained data can be saved in a data frame to be plotted using Python tools (e.g., matplotlib) (Hunter, 2007) or exported to an external file (e.g., CSV module). In the test script accessible in (Casanova-Arenillas, 2019) the program will save them as a CSV file. They can thus be directly correlated with multiple logging data, from geochemical, mineralogical, or gamma-ray analyses, for instance.

Fig. V.1 offers a visual concept of the flow, to illustrate script functioning. The frame shown in Fig. V.2A could represent a studied section with black pixels corresponding to bioturbation structures. The program extracts the sum of black pixels and then calculates the percentage of bioturbation for every line. Afterwards, the program can be configured to generate mean values for several lines: in Fig. V.2A the number would be 10 lines, giving a mean value of 40%, whose assigned depth is the middle point (Assigned Depth in Fig. V.2A). In Fig. V.2B, we have an example of how the script works with the images, as a matrix with elements with value 0 counted as bioturbation (coloured in blue) in the figure.

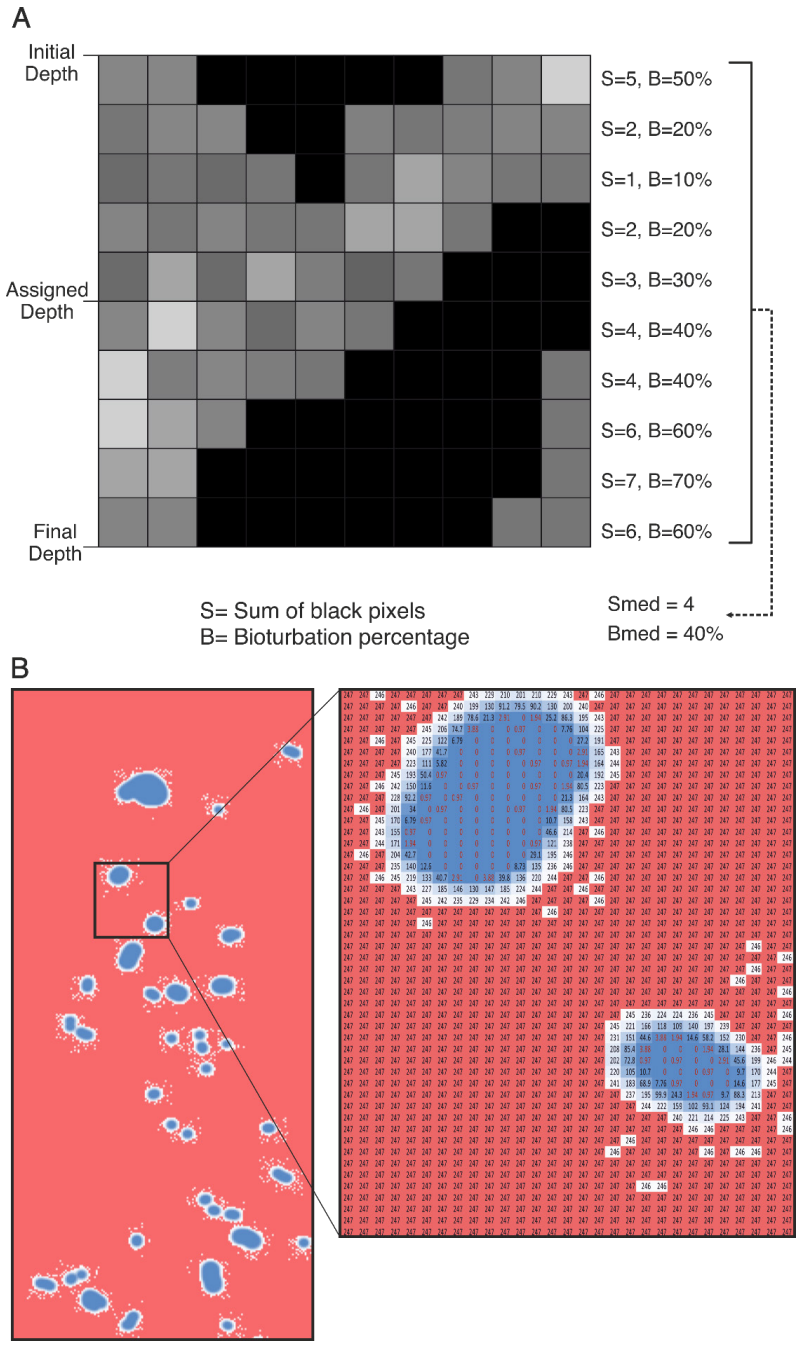

Figure V.2. A: Graphic concept of the method Smed and Bmed are the data generated if the script is assigned to take 10 lines for every data point. B: Example of the values of the pixels in a grayscale image. Values of pixels from 0 to 255, values under 1 (coloured as blue in the image) will be selected as black and counted as bioturbation. (For interpretation of the references to colour in this figure legend, the reader is referred to the Web version of this article).

V.3. Results

The method has been tested early in its development, on real and simulated images, to check its functionality. Four examples of variable quality were selected to better appraise the results of the technique: a) an idealised image (artificially created) to test the method potential (Fig. V.3), b) two different real images, one with low trace visibility (Fig. V.4) and another from a consolidated core and good trace visibility (Fig. 5.5), and c) an example of a potential comparison between the bioturbation plots obtained and other proxies (Fig. V.6).

V.3.1. Case studies

The first example is an idealised image created to test the script (Fig. V.3). In addition to the percentage of bioturbation, we included the most usually applied indexes of the amount of bioturbation to quantify the Bioturbation Index (BI) (Reineck, 1963; Taylor and Goldring, 1993), and the ichnofabric indices (ii) (Droser and Bottjer, 1986). In this idealised image, we illustrate the potential of the method to generate continuous plots and datasets that can be correlated with other proxies to improve the interpretations.

The second selected example is shown in Figure V.4. Here the method was applied to images of the 977A hole from the Ocean Drilling Program Leg 161 (Shipboard Scientific Party, 1996a), which took place in the Alboran Sea (Western Mediterranean) to conduct studies of convergent plate-tectonic boundaries. The images were taken on board during the ODP Expedition and digitalised at a later date. Resolution is low, and the core surface is somewhat rugged and irregular, making observation of trace fossils difficult. Still, useful data can be derived, evidencing the usefulness of this methodology.

Two vertical sampling intervals were chosen, 1-pixel and 100-pixel the latter to make the results easier to interpret reducing the noise and producing a smoother line. In addition. In addition, Bioturbation Indices (BI) (Taylor and Goldring, 1993) and ichnofabric indices (ii) (Dorador et al., 2016) parameters were introduced, based on the 100-pixel interval curve.

Firstly, the image was enhanced by applying high-resolution digital image treatment. This increased visibility facilitates the selection of bioturbational features in a semiautomatic way (A in Fig. V.4), after which the conversion to the grey scale was conducted (B in Fig. V.4), and finally, the percentage of bioturbation was obtained (C in Fig. V.4). Variations in the percentage of bioturbation become clear when plotting the data; indeed, they appear quite detailed, at a short-period scale.

The third case (Fig. V.5) corresponds to a core recovered from Site M0077 (Chicxulub impact crater, Yucatan Peninsula, Mexico) drilled by the IODP/ICDP Expedition 364 in April and May 2016 (Morgan et al., 2016; Lowery et al., 2018). The example offers a high-resolution image of cores from consolidated sediments where ichnological features are visible. After

image treatment and conversion to the greyscale, like in the previous example, two curves are present for the percentage of bioturbation, one for 1-pixel evaluation and the other for the 100-pixel interval. It is important to note that as the resolution of the image increases, the number of pixels representing a feature likewise increases, so the interval of pixels needed to produce a good, smoothed line is greater. For comparison, the percentage of bioturbation for the 100-pixel interval curve is correlated with the corresponding BI (Taylor and Goldring, 1993) and ii (Droser and Bottjer, 1986).

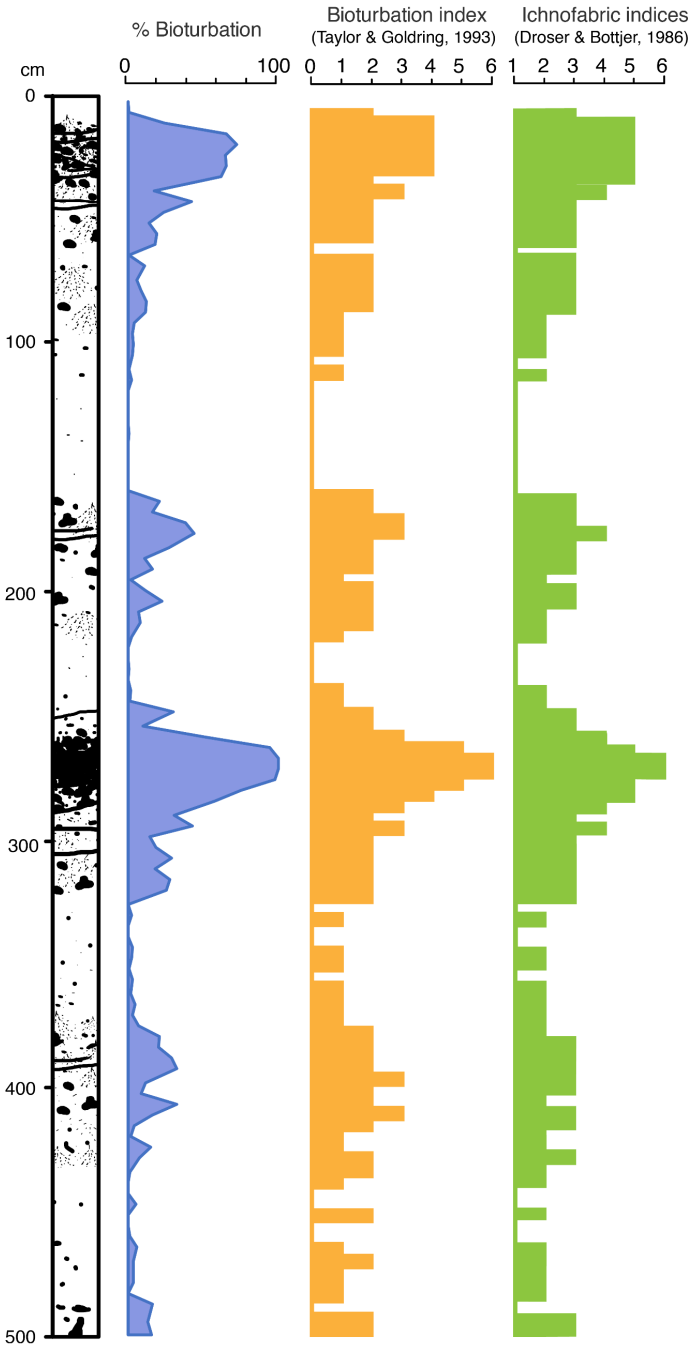

Figure V.3. Idealised example to show the method. The image has been created to show the potential to see and plot changes along the core. The method plots the variations and cycles of bioturbation along a core, generating a useful dataset.

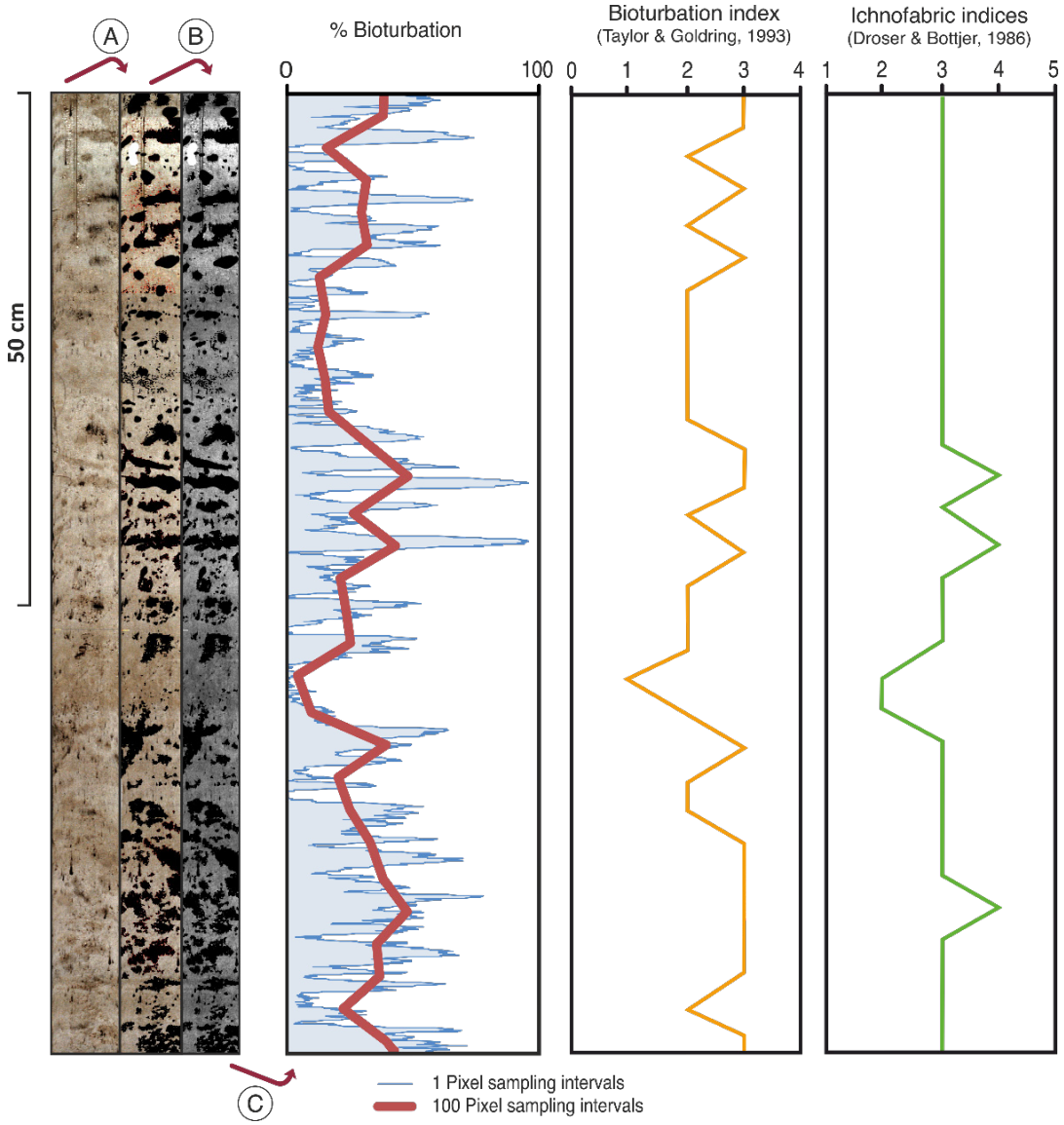

Figure V.4. 977 core study: low-resolution images. (A) High-resolution image treatment and selection of the bioturbation. (B) Greyscale conversion. (C) Generation of data frame and plots (percentage of bioturbation and correspondence with Bioturbation Index and ichnofabric indices).

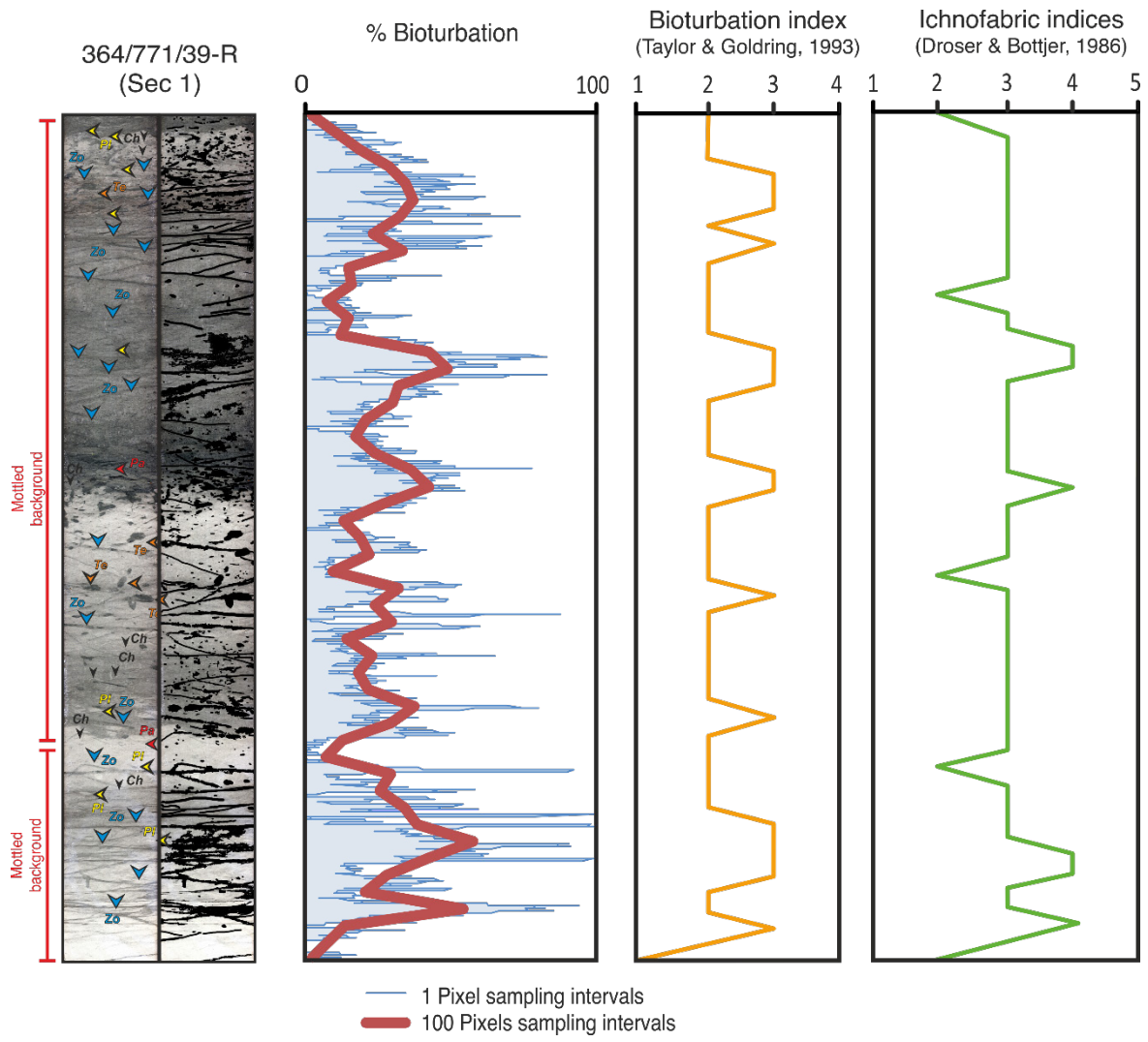

Figure V.5. Site M0077 core study: high-resolution image. From left to right: High-resolution image treatment with an indication of the differentiated ichnotaxa (*Ch* = *Chondrites*, *Pa* = *Palaeophycus*, *Pl* = *Planolites*, *Te* = *Teichichnus*, *Zo* = *Zoophycos*, and mottled background), greyscale conversion, generation of data frame and plots (percentage of bioturbation) and correlation with Bioturbation Index and ichnofabric indices scales.

To test the potential of the method in palaeoenvironmental studies, a new example is presented (Fig. V.6), applying the method to the first 26 m of core 977 (corresponding to the Last Glacial Cycle) (Shipboard Scientific Party, 1996a). Following the steps already explained, the method gave a continuous record of the percentage of bioturbation for the 26 m of the core, with a 100-pixel resolution interval. Core depth was converted to age interpolating in the age model from Martrat et al. (2004). The obtained curve thus represents variations in the percentage of bioturbation throughout the core. This curve was correlated with Sea Surface Temperatures (SST) from the Alboran Sea (Martrat et al., 2004.) and from the origin of the Mediterranean deep water, namely the Gulf of Lions (Cortina et al., 2015) the result can be seen in Figure V.6.

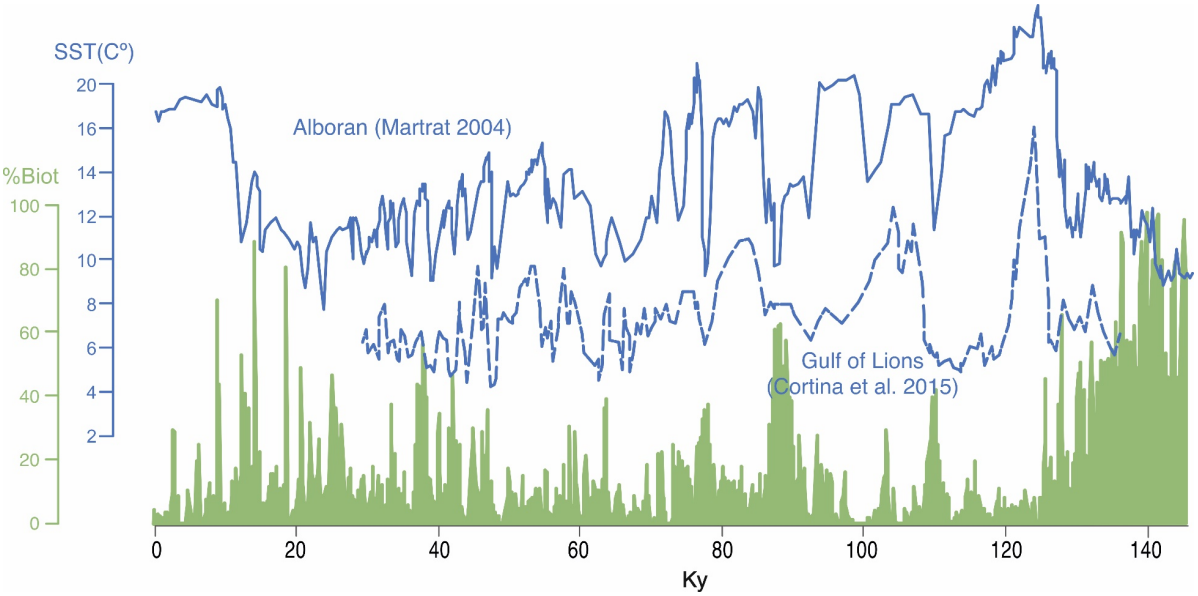

Figure V.6. Percentage of bioturbation (green) along the Last Glacial Cycle and Holocene obtained using the methodology applied to images of the 977A hole from the Ocean Drilling Program leg 161 (Shipboard Scientific Party, 1996) and its relationship with Sea Surface Temperatures (blue) from the Alboran Sea (Martrat et al., 2004) and Gulf of Lions (Cortina et al., 2015).

V.4. Discussion

Ichnological research, particularly the ichnofabric approach, necessarily involves the integration of a variety of features. The percentage of bioturbation is fundamental information, traditionally obtained through semi-quantitative analysis, which is subjective, tedious and time-consuming. It can now be evaluated in a more objective, fast and easy, semiautomatic way.

As illustrated in the examples, the methodology can provide a continuous record of the analysed data. This stands as a significant improvement upon previous methods, mainly applied in a discontinuous way, implying some loss of information from the non-studied intervals. The possibility of fine-tuning the resolution is furthermore very useful, allowing a researcher to choose the spacing best suited for the samples and objectives at hand. Such flexibility, ease, and speed are outstanding features of the methodology put forth. Its adaptability to an easily understandable code also permits one to create specific data frames to fit research objectives, e.g., to highlight more or less bioturbated sections, or a particular BI or ii value associated with particular events.

The possibility of obtaining a continuous record increases its usefulness and suggests new means of advancing along this approach, through a comparison of results with traditional proxies (geochemical or isotope data) obtained continuously in the core record. As illustrated in Figure V.6, the continuous data set can easily match with other sets and proxies indicating distribution over time. In the case study, the curve of the percentage of bioturbation obtained —by applying the method to the first 26 m (140 kyr) of the core 977 from ODP— was matched against Sea Surface Temperatures from the Alboran Sea (Martrat et al., 2004) and the source of the Mediterranean's deep water, the Gulf of Lions (Cortina et al., 2015). In a preliminary analysis of the three curves, the percentage of bioturbation shows changes not easily correlated with the SST at both locations, but similar trends appear regarding the presence of more bioturbated sediments toward the end of the main glacial periods around 130 kyr and 20 kyr. These preliminary results support the usefulness of the proposed method in sedimentary geology, opening a new way to evaluate the relationship of ichnological features with environmental and global changes.

Although the method presented here was applied to the percentage of bioturbation to test and illustrate its usefulness, the process can deal with greater complexity, as it depends on the type of data involved and the resolution required. In the case of other parameters such as ichnodiversity, ichnotaxa can be classified by a palate of colours in an RGB image, or in successive grey bands in a TIFF archive, thus allowing for the presence of both the original image in the RGB band and the "ichnology" bands to be measured and merged. Future ideas and developments will heighten the value of this methodology for palaeoecological studies. The possibility of generating multiple datasets as needed by the researcher is a road entailing great promise.

V.5. Conclusions

The use of Python in ichnological research makes it possible to conduct semiautomatic analyses of great volumes of data in a fast and easy manner. It will simplify work in applied ichnology, especially when dealing with long cores. This approach with no doubt proves to be of interest

to scientists involved in sedimentary geology or reservoir exploration, among other interests/disciplines.

Python scripts have demonstrated their usefulness in automatising ichnofabric analysis in marine core images, focusing on the percentage of bioturbation. The fact that continuous data can be obtained is one clear advantage concerning the commonly applied methodologies. Moreover, the Bioturbation Index and ichnofabric indices are commonly based on (subjective) naked eye recognition, whereas the proposed semiautomatic method is much more objective as it uses the real percentage without any bias. The proposed methodology allowed for a fast, semiautomatic evaluation of the percentage of bioturbated surfaces, based on an automated analysis. A similar procedure, yet based on traditional ichnofabric analysis, would have been far more time-consuming.

Further definition and improvement of scripting in the framework of ichnological research can lead to improvement in the integration and correlation of continuous ichnological information with other proxies.

The Python code is readily available and easy to use. This new tool, therefore, awaits future applications, to be developed in open platforms —for instance, project development platforms like GitHub— so that scientists can share their respective contributions. Scientific collaboration should always be encouraged and facilitated. Our proposal, having demonstrated its utility for the analysis of a quantitative ichnological property, holds great potential for the worldwide technological and social network of the research community.

V.6. Code availability

The code of the script used to produce the figures can be found in the Zenodo database see https://zenodo.org/record/3518837 (Casanova-Arenillas, 2019), with the name IchAnTool-Project. The code used was the console version being available also an older interface version. To run this code, it is necessary to have Python 3.7 on the computer and the modules Pillow and NumPy. The method was developed by Santiago Casanova Arenillas in 2019.

V.7. Availability of supporting data

The scripts used to produce the figures can be found in the Zenodo database see Casanova-Arenillas, 2019 with the name IchAnTool Project.

PART 3
RESULTS AND DISCUSSION

Chapter VI

Ichnological analysis as a tool for assessing deep-sea circulation in the Westernmost Mediterranean over The Last Glacial Cycle

Palaeogeography, Palaeoclimatology, Palaeoecology 562 (2021) 110082

Contents lists available at ScienceDirect

Palaeogeography, Palaeoclimatology, Palaeoecology

journal homepage: www.elsevier.com/locate/palaeo

https://doi.org/10.1016/j.palaeo.2020.110082

S. Casanova-Arenillas [a], F.J. Rodríguez-Tovar [a], F. Martínez-Ruiz [b]

[a] Departamento de Estratigrafía y Paleontología, Universidad de Granada, Campus Fuentenueva s/n, 18002, Granada, Spain

[b] Instituto Andaluz de Ciencias de la Tierra (IACT), Consejo Superior de Investigaciones Científicas-Universidad de Granada (CSIC-UGR), Avda. de las Palmeras 4, 18100, Armilla, Granada, Spain

Abstract

During the Last Glacial Cycle (last ~130 kyr) climatically induced changes in the ocean dynamics affected the tracemaker habitat in the Alboran Sea Basin (westernmost Mediterranean), as observed in sediment records from ODP Leg 161 Sites 976 and 977. The trace fossil assemblage present is assigned to the *Zoophycos* ichnofacies and is of low/moderate diversity and comprises common *Planolites, Chondrites and Thalassinoides*, with occasional *Scolicia* and *Zoophycos*. Ichnodiversity, size of biogenic structures and percentage of bioturbational sedimentary structures clearly correlate. Fluctuations in ichnological features evidence a well-developed short-term cyclic pattern that could be related to environmental changes such as export production and oxygenation at the seafloor. The percentage of bioturbational sedimentary structures correlates well with sea-surface temperature (SST) records obtained for the Alboran Sea and Gulf of Lions, as well as with the $\delta^{18}O$ profiles of Greenland ice cores. Correlation is seen for both the long-term (over the Last Glacial Cycle) and short-term changes, the latter comprising climate oscillations such as Heinrich Events, Younger Dryas, and periods of organic-rich layer deposition. Ichnological data also allow for a reconstruction of climatically induced changes in the ocean dynamics, which have a major incidence in the Western Mediterranean Deep Water that, in turn, affects deep-sea environmental conditions.

VI.1. Introduction

The Mediterranean Sea (Fig. VI.1) has been particularly sensitive to palaeoenvironmental changes due to its semi-enclosed nature, with limited connection with the Atlantic Ocean through the Strait of Gibraltar. It has also proven to be an exceptional natural laboratory for Earth Sciences research (Bethoux et al., 1999; Krijgsman, 2002; Durrieu de Madron et al., 2011). Regarding climate conditions, its location is unique, affected by northern and mid-latitudes as well as tropical climate systems (e.g., Lionello, 2012). Due to short water residence times, climatically induced changes significantly affect the Mediterranean in relatively short periods (Durrieu de Madron et al., 2011), including the deep parts of the basin. Furthermore, the Mediterranean water dynamics also affect and modify the Atlantic Ocean Overturning Circulation (AMOC) in different ways contributing to the global oceanic circulation (e.g., Rogerson et al., 2012; Bahr et al., 2015).

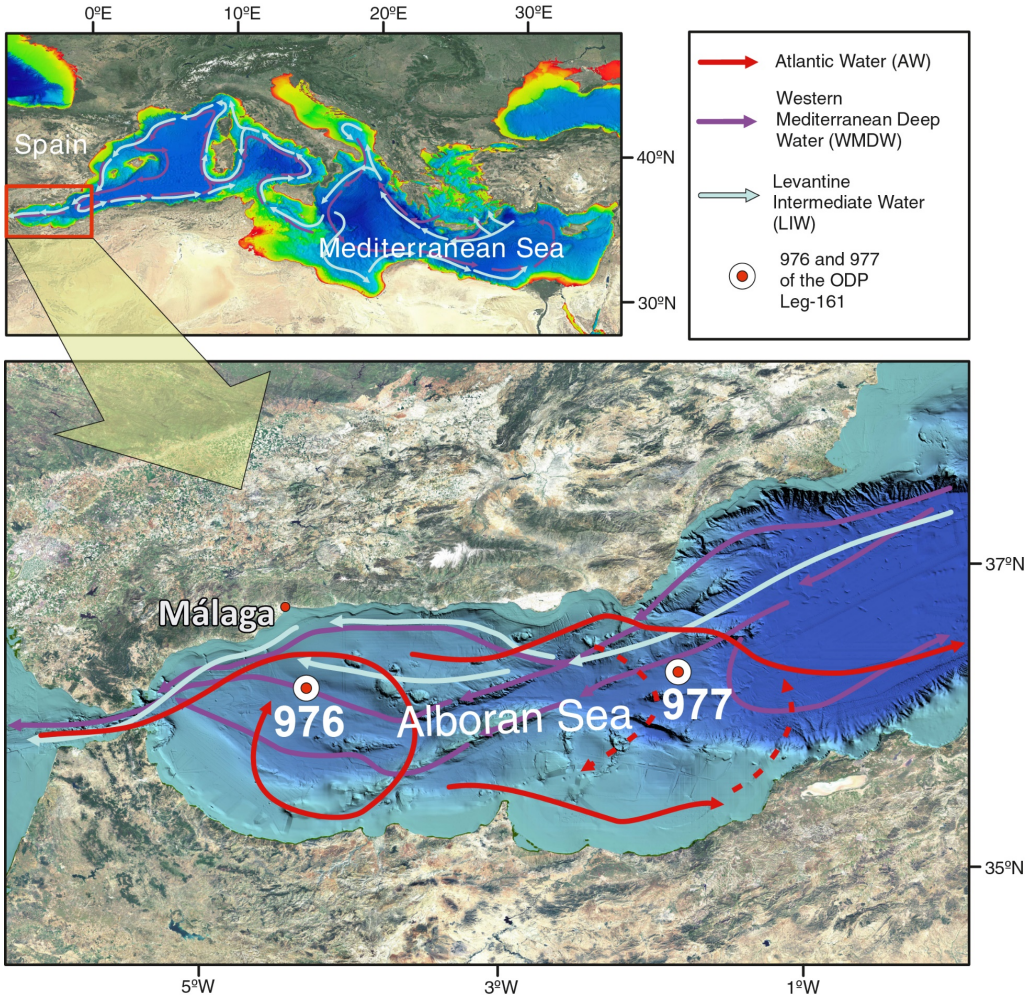

Figure VI.1. Location and oceanographic setting of cores 976 and 977 of ODP Leg-161 in the Alboran Sea Basin, Western Mediterranean, including simplified horizontal paths of the main water masses of the Mediterranean Sea.

At present, the Mediterranean Sea is subdivided into two main sub-basins separated by the shallow Sicily Channel: The Eastern Mediterranean (EMED) and the Western Mediterranean (WMED) (Fig. VI.2). In general terms, the Mediterranean Sea experiences anti-estuarine circulation (e.g., Millot, 1999; Millot and Taupier-Letage, 2005). Various water masses are distinguished (Fig. VI.2): a) At the surface, Atlantic Water (AW) enters as an inflow jet from the Atlantic through the Gibraltar Strait (e.g., Perkins et al., 1990; Millot, 1999; Macias et al., 2016). The AW flows to the East at shallow depth and is affected by mesoscale circulation that comprises two surface water gyres in the western and eastern Alboran area (Fig. VI.1) (e.g., Send et al., 1999; Pinardi et al., 2015); b) the Levantine Intermediate Water (LIW; Bethoux et al., 1999; Millot, 1999; Millot and Taupier-Letage, 2005; Pinardi et al., 2015) flows to the West in an anticlockwise pattern and modulates and contributes to the Mediterranean's Outflow Water (MOW) to the Atlantic Ocean, (Millot, 1999; Naranjo et al., 2012, 2015); c) in the deepest parts of the basins, trapped by the different sills, the Western Mediterranean

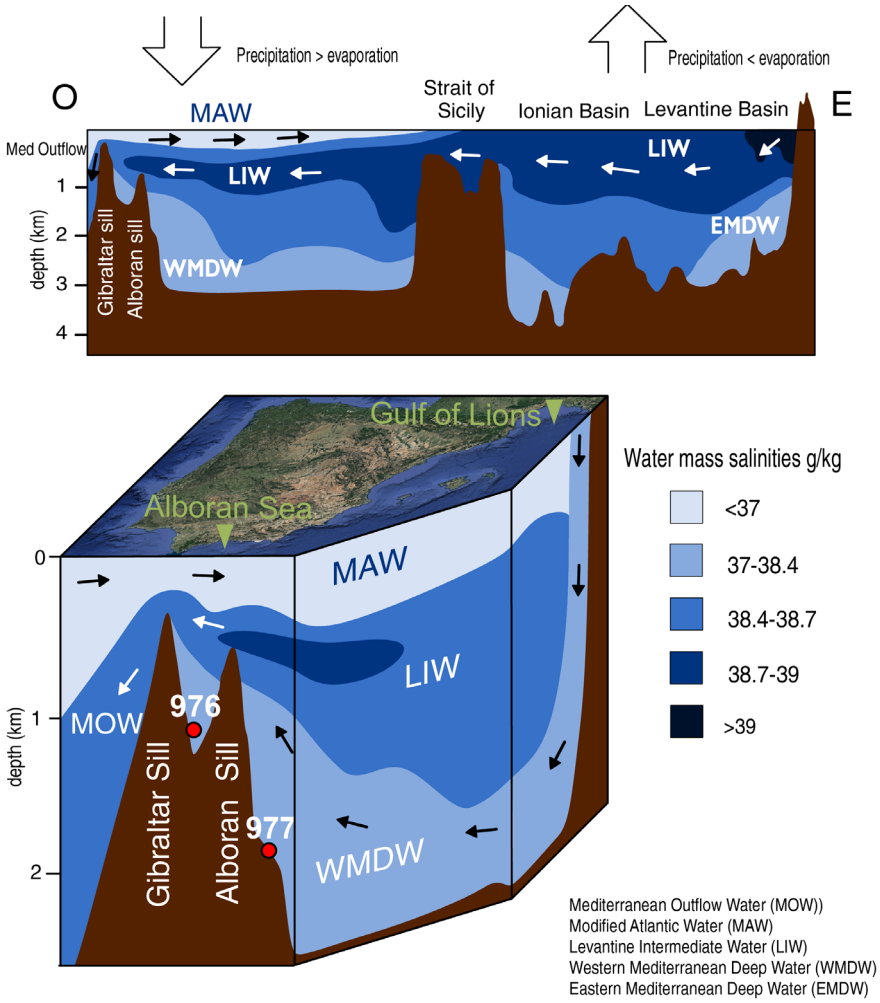

Figure VI.2. Vertical configuration of the main paths and currents in the Mediterranean and Alboran Sea Basins, along with Western Mediterranean Deep Water (WMDW) formation in the Gulf of Lions and simplified paths (modified from Cramp and O'Sullivan, 1999; Cacho et al., 2006).

Deep Water (WMDW) and Eastern Mediterranean Deep Water (EMDW) occur. They develop seasonally during winter in northern regions of the basins due to low temperature and evaporation inducing the production of deep convection, open-sea deep convection and cascading (Medoc Group et al., 1970; Gascard, 1978; Durrieu de Madron et al., 2013), because of the loss of buoyancy of surface waters caused by cold and dry N-NW winds from the continent (Medoc Group et al., 1970; Millot, 1999; Durrieu de Madron et al., 2013; Cisneros et al., 2019). In the Western Mediterranean Sea, the deep water mostly derives from the loss of buoyancy and sinking of more superficial water, both surface water and LIW, in the Gulf of Lions (Millot, 1999; Rhein, 1995) during winters. Thus, the WMDW overturning has been closely linked with climatic conditions in the northern hemisphere and Atlantic climate influence (Cacho et al., 2000; Sierro et al., 2005).

Over time, this circulation pattern has significantly changed in response to climate forcing. In particular, during the Last Glacial Cycle (last ~130 kyr; Dansgaard et al., 1993), the

Mediterranean Sea experienced rapid fluctuations in hydrographic conditions as the result of abrupt climatic changes in the Northern Hemisphere, which resulted from millennial-scale fluctuations between the penultimate and the current interglacials (Blunier and Brook, 2001; Siddall et al., 2003), that is, between Termination II (˜130 ka) and Termination I (˜11.7 ka) (Fischer et al., 1999; Hughes et al., 2013). Among them, Heinrich Events (H events), Dansgaard-Oeschger Stadials (D-O) (cold) and Interstadials (warm) (Heinrich, 1988; Dansgaard et al., 1993; Cacho et al., 2002) are the most prominent changes. The H events resulted from oceanic cooling and increasing ocean ice cover extension over the North Atlantic, which subsequently resulted in distinctive layers of ice-rafted debris in the northern Atlantic (Hemming, 2004). In this regard, the Alboran Sea basin offers an exceptional record for reconstructing deep-sea circulation oscillations, which are in turn linked to sea surface temperature (SST) and atmospheric temperature variations (Martrat et al., 2004; Pérez-Folgado et al., 2004; Martrat et al., 2007, 2014). In terms of deposition, these oscillations are linked to a recurrent accumulation of organic-rich sediments known as sapropels and organic-rich layers (ORLs) in the Eastern and Western Mediterranean, respectively. Sapropels have formed in the eastern basins cyclically over the last 13.5 million years (Rohling et al., 2015). Even though their origin has been a topic of intense debate, it is now widely accepted that productivity played a major role in their deposition, with enhanced organic matter fluxes (e.g., Calvert and Fontugne, 2001) and reduced oxygen levels promoted by stagnation and low ventilation of the deep water (Wüst, 1961; Cramp and O'Sullivan, 1999; Emis and Weissert, 2009; Rohling et al., 2015).

In the Western Mediterranean, the ORLs are still poorly investigated, and they do not correlate with warm insolation maxima periods like the eastern sapropels (von Grafenstein et al., 1999); yet, they could likewise be linked to low oxygenation during deglaciation periods and changes in productivity (Rogerson et al., 2008). Overall, freshwater input, deep-water ventilation and primary productivity are the main factors to be considered for ORL and sapropel formation (e.g., Cramp and O'Sullivan, 1999; Martínez-Ruiz et al., 2000; Rogerson et al., 2008; Rohling et al., 2015; Grant et al., 2016).

In the particular case of the Alboran Sea basin, high sedimentation rates (˜3±2m/kyr) allow an exceptional high-resolution analysis for palaeoceanographic reconstructions (e.g., Cacho et al., 2000; Martrat et al., 2007; Cacho et al., 2006; Rodrigo-Gámiz et al., 2011; Martínez-Ruiz et al., 2015). Furthermore, this basin is largely affected by the Atlantic inflow through the Gibraltar Strait (Naranjo et al., 2015). In turn, the MOW influences the AMOC (e.g., Hernández-Molina et al., 2014; Ivanovic et al., 2014; Jiménez-Espejo et al., 2015). Hence, the relationships between water mass exchange, circulation patterns, and climatic conditions hold keys for reconstructing deep-sea environmental parameters such as salinity, benthic food availability and, especially, oxygenation.

Among the diverse proxies that serve for reconstructing environmental conditions, ichnological analysis has proven particularly useful. Trace fossils record the behaviour of tracemakers in response to the environment and provide valuable information regarding the depositional and

environmental conditions. Ecological and depositional parameters affecting the marine realm (i.e., oxygenation, nutrients, hydrodynamic energy, rate of sedimentation, etc.) can be addressed through a detailed ichnological analysis (i.e., Wetzel, 1983; Savrda and Bottjer, 1986, 1987, 1989; Savrda, 2007; Rodríguez-Tovar and Uchman, 2010; Wetzel, 2010; Buatois and Mángano, 2011; Uchman and Wetzel, 2011, 2012; Wetzel and Uchman, 2012). Thus, ichnological information reveals as a key proxy for environmental conditions, particularly, when it is applied in sediment core records for palaeoclimatic and palaeoceanographic studies (Wetzel, 1991; Savrda, 1995; Rodríguez-Tovar et al., 2015). Notably, ichnological information has been incorporated in several multiproxy studies to investigate, for instance, glacial/interglacial transitions, Heinrich Events, and diverse Marine Isotope Stages (MIS) (Baas et al., 1997, 1998; Löwemark et al., 2004, 2006; Löwemark, 2012; Rodríguez-Tovar et al., 2015; Dorador et al., 2016; Hodell et al., 2017; Sánchez Goñi et al., 2019; Evangelinos et al., 2020; Pérez-Asensio et al., 2020; Rodríguez-Tovar et al., 2020a). Besides, the ichnofabric approach, as a paradigm, addresses ichnological features such as the amount of bioturbational sedimentary structures, their size and penetration depth, to assess environmental parameters including oxygenation and benthic food availability (Ekdale and Bromley, 1983; Bromley and Ekdale, 1986; Ekdale and Bromley, 1991; Taylor and Goldring, 1993; Ekdale et al., 2012; Savrda, 2016).

However, ichnological research in cores entails particular limitations due to features such as the narrow-exposed surface, two-dimensional core slabs, or the usual absence of complete structures, making the characterization of trace fossils and ichnofabrics more complicated (e.g., Dorador and Rodríguez-Tovar, 2014b; Knaust, 2017). The ichnotaxonomical classification of bioturbational structures may be further impeded by scarce information on diagnostic criteria or ichnotaxobases (Bromley et al., 1996; Bertling et al., 2006; Knaust, 2017) so that a precise ichnotaxonomical classification at the ichnospecies level is often impossible (usually conducted at the ichnogenus level; Bromley et al., 1996). Ichnological research in cores from modern marine deposits is particularly difficult when the material is unconsolidated, and the visual differences between biogenic structures and host sediment are weak (Dorador and Rodríguez-Tovar, 2015). To improve trace fossil visualization and the analysis of ichnological attributes in marine cores from modern deposits, a new high-resolution image treatment has emerged (see Dorador and Rodríguez-Tovar, 2018 for a recent review of the methodology). This novel method has proven to be a powerful tool for the ichnofacies model (Dorador and Rodríguez-Tovar, 2015) and ichnofabric approach (e.g., Rodríguez-Tovar and Dorador, 2014, 2015), and its usefulness has been demonstrated in numerous studies involving palaeoenvironmental reconstructions, ocean-atmosphere dynamics and sedimentary basin analysis (e.g., Rodríguez-Tovar and Dorador, 2015; Dorador and Rodríguez-Tovar, 2016a; Hodell et al., 2017; Dorador and Rodríguez-Tovar, 2018).

Within this context, a detailed ichnological analysis was conducted on sediment cores from the Alboran Sea Basin to evaluate the impact of environmental variations in deep-sea settings and the tracemaker habitat over the Last Glacial Cycle, to reconstruct oxygen conditions and deep-

sea circulation patterns. Such study aims to contribute to our understanding of the deep-sea dynamics in the westernmost Mediterranean Sea by adding detailed ichnological data to the currently available knowledge as well as describing the tracemaker community variations and correlating them with palaeoclimate and palaeoceanographic changes.

VI.2. Geological setting and studied sediment records

This study focuses on two sediment records from the westernmost Mediterranean, Sites 976 and 977, drilled in the Alboran Sea Basin during the Ocean Drilling Program (ODP) Leg 161 (Fig. VI.1). The Alboran Sea Basin is a marine back-arc basin covering 54,000 km2 and its seafloor exhibits a pronounced relief due to structuring by numerous grabens and half-grabens formed during Miocene rifting stages (Comas et al., 1992; Martínez-García et al., 2011). Miocene volcanism created seamounts and ridges in the basin (Alvarez-Marron, 1999), which in turn affect the circulation pattern of bottom currents as well as the depositional conditions (e.g., Ercilla et al., 2019; López-González et al., 2019).

The main sediment inputs to this basin are derived from river outputs and the aeolian dust coming from the African margin (e.g., Moreno et al., 2002). Despite lower rates during short periods, the sedimentation rates have been particularly high in the Alboran Sea Basin (Masqué et al., 2003) and considerably much higher than in the eastern Mediterranean Sea (Dominik and Mangini, 1979), as an example, sediment accumulation rates have ranged from 0.014 to 0.182 g cm^{-2} yr^{-1} over the last 100 years (Masqué et al., 2003). Over the Last Glacial Cycle, the sedimentation rates have significantly varied, between 0.1 and 0.6 cm/yr at Site 976, and between 0.01 and 0.3 cm/yr at Site 977 (Martrat et al., 2014). These high rates are due to the location of the basin between two continental margins, whose colliding plates represent a tectonically active regime (Comas et al., 1999), as a result, the south of the Iberian Peninsula and the north of the African continent present mountain ranges that are subjected to intensive erosion.

Site 976 (36° 12.318′N, 4°18.800′ W; 1108 m below sea level) is located in the West Alboran Sea Basin, on top of a basement horst 60 km off the southern Spanish coast. Site 977 (36° 1.907′ N, 1° 57.319′ W; 1984 m below sea level) is located in the East Alboran Sea Basin, south of the Al-Mansour Seamount (Fig. VI.1). Sediments drilled at these sites range from the Miocene to the present in age, and intervals spanning the Last Glacial Cycle have been selected for this study. These intervals are encountered within the upper 44 mcd (meters composite depth) at Site 976 and 25 mbsf (meters below seafloor) at Site 977. The sediments are generally hemipelagic mud with low sand content (Fig. VI.3).

At Site 976, five holes (A-E) were drilled. The splice of these cores was used in this study, it was elaborated using magnetic properties obtained by the shipboard scientific party, and the best-recovered sections were used to construct a continuous record. The upper 44 mcd consists of calcareous and clay sediments showing gradational alternations of burrowed and structureless mud (Shipboard Scientific Party, 1996b). Hemipelagic facies mainly consist of nannofossil-bearing clay containing 50% to 97% $CaCO_3$ (average 81%). The carbonate fraction is mostly composed of nannofossils (Shipboard Scientific Party, 1996b). There are 3 ORL types described by Shipboard Scientific Party, 1996a, 1996b: I, II and III differentiated by their TOC (Total Organic Carbon) values. The studied upper 44 mcd harbour eight ORL, with TOC ranging from 0.8 to 2% and thus, they are assigned to types II (1–2% TOC) and III (0–8-1% TOC) (Fig. 6.3) (Shipboard Scientific Party, 1996b).

At Site 977, hemipelagic facies are dominated by nannofossil clay and calcareous silty clay containing 30% to 50% $CaCO_3$. The carbonate component is dominated by nannofossils (70%), followed by micrite (20%), bioclasts (6%), and foraminifers (4%) (Fig. VI.3) (Shipboard Scientific Party, 1996a). The non-carbonate sand and silt components correspond to quartz, feldspars, mica, diatoms, sponge spicules, organic matter, and accessory minerals. The studied upper 25 mbsf harbour eight ORLs classified given the TOC values (Fig. 6.3), 3 types were differentiated by Shipboard Scientific Party, 1996a, 1996b (Fig. VI.3). TOC in site 976 ranges from 1.13% to 0.87%. Thus, ORLs from types II (0–8-1% TOC) and III (1–2% TOC) are present (Shipboard Scientific Party, 1996a).

The photographs used for this work are obtained directly from the ODP repository; they come from the digitalization of original core images taken during the expedition. The resolution is close to 80 ppi, with only slight variations.

The age model used in this study for both records (sites 976 and 977) is based on work from Martrat et al., 2004, and Martrat et al., 2014. Age models were used to derive age versus depth relations as well as sedimentation rates by means of linear interpolation. However, because the age model used for Site 976 (Martrat et al., 2014) does not include data points for the intermediate part of the studied interval, the interpolation and the ages obtained are approximate. The TOC data from both records (Shipboard Scientific Party, 1996b) was used in conjunction with colour and other lithological features to determine the ORL depths (Shipboard Scientific Party, 1996b, 1996a; Murat, 1999).

Image treatment served to analyse the ichnological features of the studied cores (Magwood and Ekdale, 1994; Dorador and Rodríguez-Tovar, 2014c, 2015, 2016a, 2018). This technique was applied, with minor modifications, in the initial steps of this study (Fig. VI.4). Besides, we overprinted the original colour on the image after treatment (as the process alters the natural colour) using a "colour" layer from the Adobe Photoshop® package. It changes only the hue value of the pixel but restores the natural colour of the image and maintains the changes in contrast and brightening that allows for better recognition of structural features (Fig. VI.5).

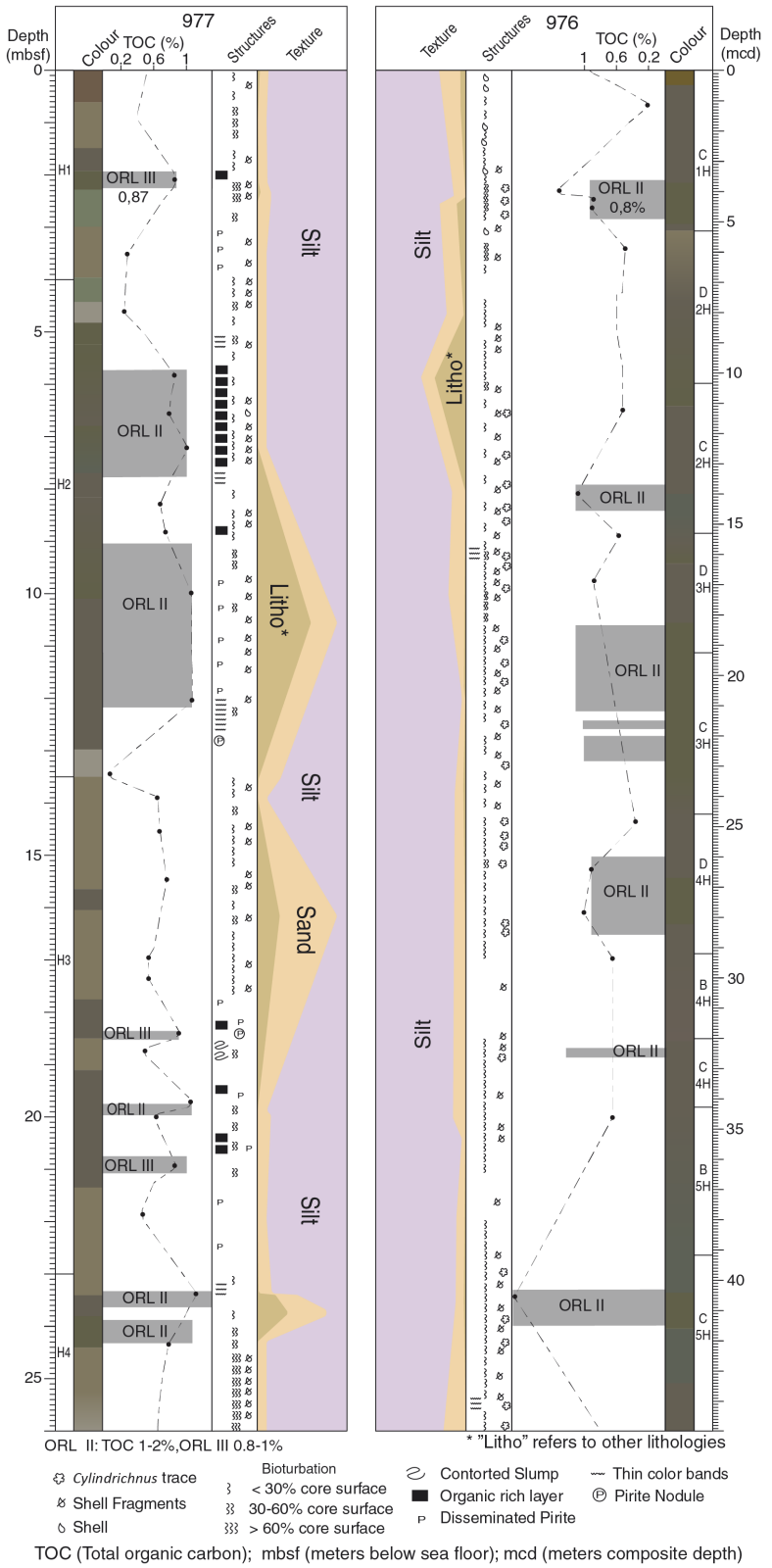

Figure VI.3. Sedimentological characteristics of cores 977 and 976 according to data from the Shipboard Scientific Party, 1996b, 1996a. Colour was determined using Munsell Soil Colour Charts (1975).

VI.3. Methods

The original images of cores at Site 976 have less quality than those of Site 977, meaning high-resolution image treatment affords better results for the latter. Even so, after treatment, some sections of the cores show comparatively poor visibility of the ichnological features; to be as conservative as possible, these sections were not considered in our study (Fig. VI.6, and indicated as "not used data" in Fig. VI.7). Among the bioturbational sedimentary structures, we distinguished between discrete traces fossils (with sharp outlines and a characteristic recurrent geometry) and mottled background (biodeformational structures with no distinct outlines and no recurrent geometry) (i.e., Wetzel, 1991; Rodríguez-Tovar and Dorador, 2015). Trace fossils were characterized at the ichnogenus level, mainly based on shape, size and infilling material. Further ichnological features include ichnogenera richness, and the percentage of area occupied by bioturbational sedimentary structures on the core surface are considered.

The percentage of bioturbational sedimentary structures was calculated following the method recently proposed by Casanova-Arenillas et al. (2020), which relies on a script for automatic pixel count to create continuous plots of the percentage of bioturbational sedimentary structures based on our previous interpretation. The functioning of the script is exemplified in Fig. VI.4. It combines a manual and semiautomatic selection of the bioturbational sedimentary structures on the core surface and then creates a continuous plot of the percentage of core surface area occupied by them. The obtained values can be correlated with the Bioturbation Index (BI; Taylor and Goldring, 1993, slightly modified from Reineck, 1963). Two plots were differentiated (Fig. VI.7, A and B), one showing exclusively the discrete traces, the other the percentage area occupied by all bioturbational sedimentary structures, including the mottled background. The resolution of the plots was 100 pixels for 977 and 200 for 976, roughly equal to 3.1 cm per data point for Site 977 and 6.1 cm per data point for Site 976, but it can change slightly from one photograph to another due to resolution changes.

Analysis of trace size involved the ImageJ program (Schindelin et al., 2012; Miguez-Salas et al., 2019). The data represents the size, as the occupied area in mm^2, of the individual traces throughout the core (Fig. VI.6); every plotted value is the area in millimetres of one of the differentiated traces on the core surface. Owing to size variability and the dominance of small traces such as *Chondrites*, we used a logarithmic scale for the vertical axis of the graphics to provide better visibility of the registered variations.

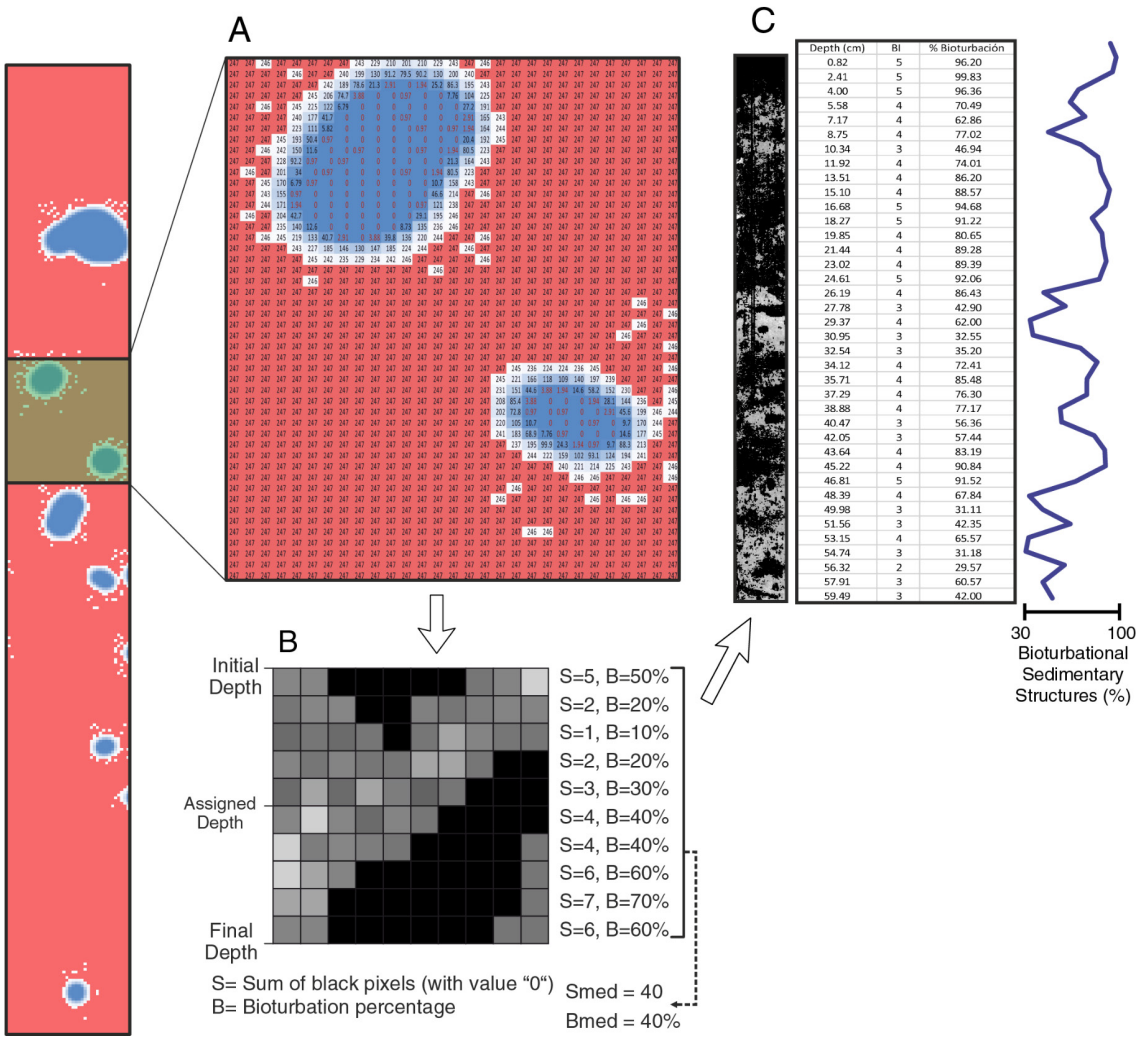

Figure VI.4. Flowchart of the script used to obtain the bioturbation plots. Modified from Casanova-Arenillas et al., 2020. Workflow: from an image (A), we obtain a matrix of the pixel values (B); the program then plots these data in depth (C) as "discrete bioturbation" or "biodeformational features".

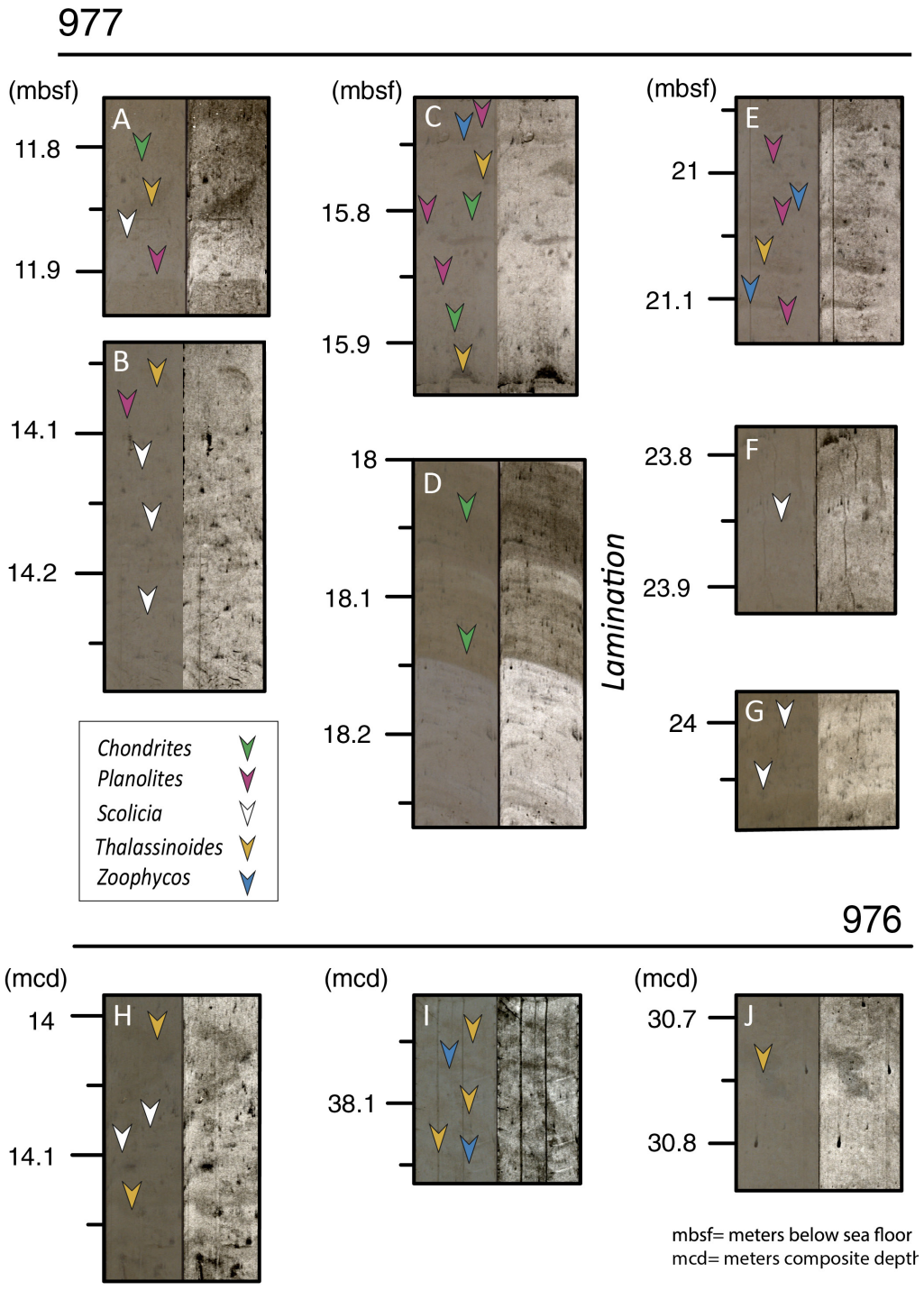

Figure VI.5. Examples of the main differentiated ichnotaxa in the studied cores, 977 and 976, in the original (left) and treated (right) images.

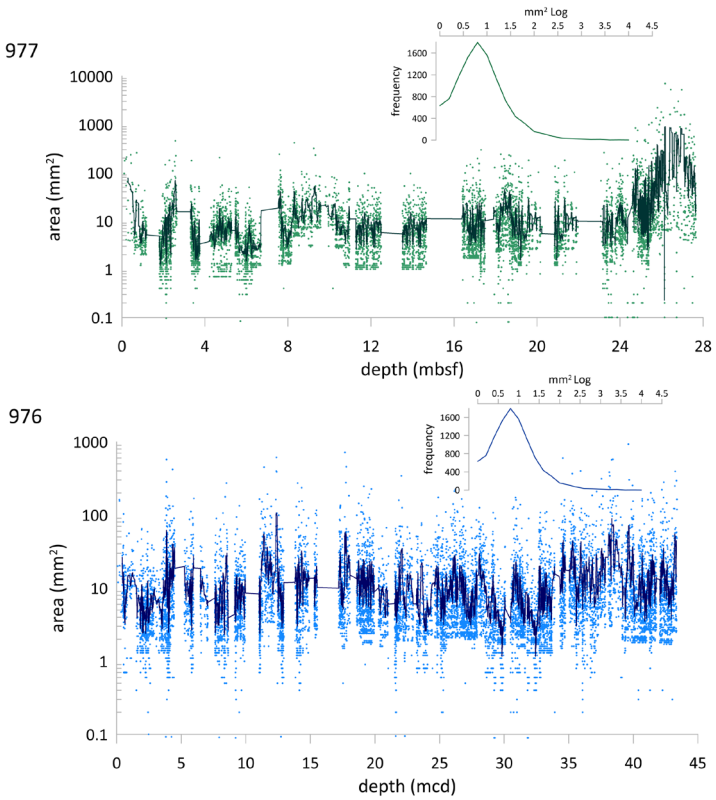

Figure VI.6. Area in millimetres of the studied discrete traces along cores 977 and 976. Every point represents a single differentiated trace, its depth and area.

VI.4. Results

VI.4.1. Trace fossil assemblage

The trace fossil assemblage is largely similar in the two cores. It is low to moderately diverse, consisting of *Chondrites*, *Planolites*, *Thalassinoides*, *Scolicia* and *Zoophycos* (Fig. VI.5). In some cases, mainly corresponding to ORL, millimetric-scale lamination is seen in the absence of discrete traces (Fig. VI.5 D). In both cores, *Planolites* and *Chondrites* are the most abundant ichnotaxa, whereas *Thalassinoides* are frequent but disseminated. *Scolicia* occurs locally in some short intervals of both cores. *Zoophycos* is the least abundant trace, appearing in just a few intervals, sometimes without conclusive identification.

Concerning the ichnological composition, biodeformational structures and discrete trace fossils have been differentiated. Biodeformational structures, showing undifferentiated outlines and the absence of a defined geometry (Wetzel, 1991; Wetzel and Uchman, 2012), is characterized by a mottled background. Discrete trace fossils are well recognized in most cases, showing a characteristic shape, and are not diffuse. Ichnotaxonomic identification is mainly based on ichnological observations achieved from cores (Knaust, 2017).

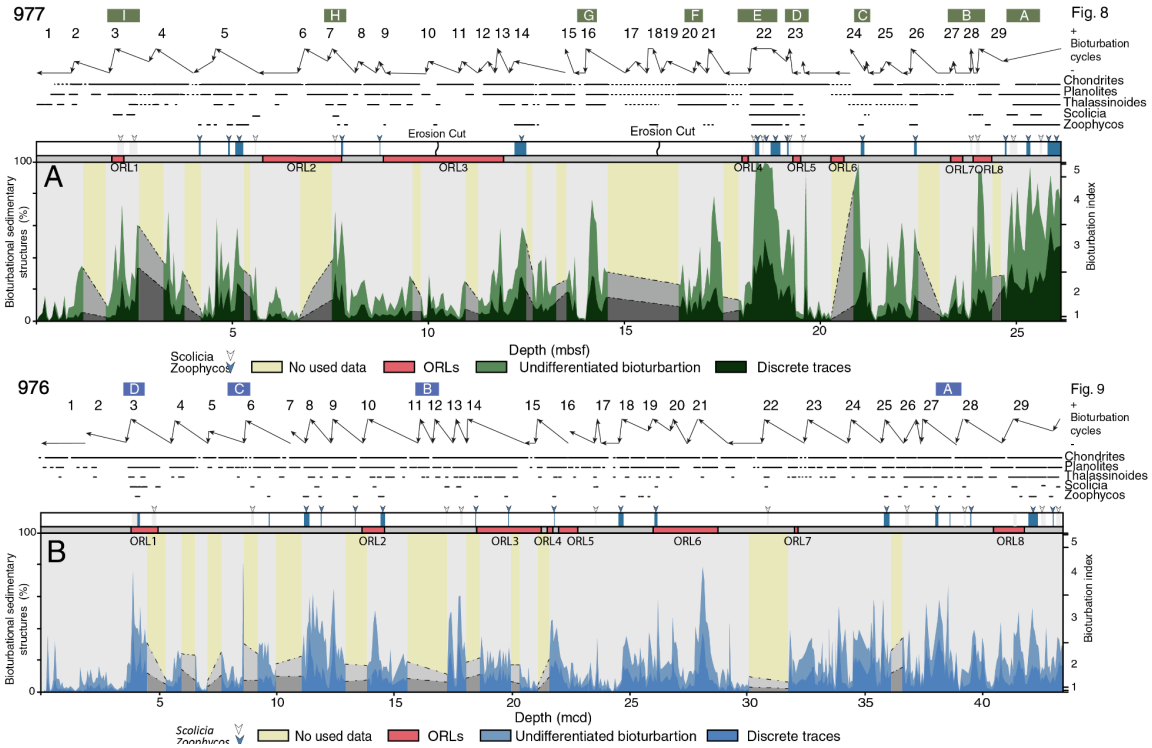

Figure VI.7. Ichnological features throughout cores 977 and 976, including differentiated ichnotaxa (with the highlighted position of Zoophycos and Scolicia), and percentage of bioturbational sedimentary structures and Bioturbation Index. Organic rich layer (ORL) positions are indicated. The main cycles of bioturbation distinguished by visual analysis of the core surface appear over the two plots. Note: A to me in core 977, and A to D in core 976, correspond to examples respectively illustrated in Fig. VI.8, and Fig. VI.9. Unused sections refer to ichnological information not included because of scarce visibility/poor quality of the original images and thus not reliable enough for interpretations.

Chondrites (von Sternberg, 1833) are characterized by clusters of small, millimetric, circular to subcircular sections widely distributed throughout the cores. Occasionally *Chondrites* crosscuts or overprints other traces (e.g., *Thalassinoides*). The producer of *Chondrites* is unknown. Ethological interpretations to date mostly infer feeding activities (e.g., Seilacher, 1990; Bromley et al., 1996; Hertweck et al., 2007; Knaust, 2017). The trace is interpreted as a deep tier structure, reflecting the activity up to some tens of centimetres into the substrate, in some cases related to chemo-symbiotic organisms tolerant of low-oxygen conditions (Seilacher, 1990; Rodríguez-Tovar et al., 2009, 2011; see recent revision in Baucon et al., 2020).

Planolites (Nicholson, 1873) appears as circular or subcircular, unlined burrow less than 1 cm in size. The fill is structureless and its colour is generally darker than the surrounding sediment. *Planolites*, abundant in the studied cores, appear throughout most of the core without significant changes in abundance. *Planolites* are usually present in upper tiers, corresponding to the shallowest sediments at or just below the seafloor, representing the activity of shallow (below the boundary surface), vagile deposit-feeders. This trace is thought to be produced by an active deposit feeder, attributed to a broad number of mainly worm-like organisms (e.g., Pemberton and Frey, 1982; Keighley and Pickerill, 1995; Rodríguez-Tovar et al., 2009),

although other possible producers, including arthropods or molluscs, have been proposed (Knaust, 2017).

Thalassinoides (Ehrenberg, 1944), consist of large circular, subcircular or elongated sections of burrows, usually >1 cm in size, allowing for their differentiation from *Planolites*. The trace is interpreted as a middle-tier structure, corresponding to the activity occurring a few centimetres deep into the substrate. *Thalassinoides* is usually interpreted as a dwelling and feeding structure (domichnia, fodinichnia) produced by crustaceans, particularly *callianassids* (Frey et al., 1984; Nickell and Atkinson, 1995; Schlirf, 2000; Ekdale and Bromley, 2003; Knaust, 2017). It has been associated with oxygenated environments in soft but cohesive substrates (Rodríguez-Tovar et al., 2008, 2017), but also settings experiencing lowered oxygenation (Wetzel, 1991).

Scolicia (Quatrefages, 1849) is observed as large, cm thick, oval cross-sections showing a central ridge, or in 10-40 cm thick bioturbated intervals as a series of indistinct lamellar back-fill structures. Their identification in recent soft sediments is demanding because of the weak contrast between the trace and the surrounding sediment (Fu and Werner, 2000). Thus, the presence of *Bichordites* cannot be discarded, because differentiation from *Scolicia* is difficult in the studied cores. This trace is produced by irregular echinoids as a result of deposit-feeding behaviour (Carmona et al., 2020). It is a common trace in deep-marine environments containing a considerable proportion of silt-sized material (Wetzel, 1991), the size of *Scolicia* being related to the quality of benthic food (Wetzel, 2008).

Zoophycos (Massalongo, 1855) are scarce in the studied cores and appear as a set of 2 or 3 horizontal to subhorizontal parallel burrows. Occasionally a weak internal spreite was observed. The trace tends to be darker than the surrounding sediment. Many organisms have been considered as probable *Zoophycos* producers, considering various behaviours in terms of feeding activity or dwelling, e.g., deposit feeding (domichnia and pascichnia) and farming or gardening microorganisms (agrichnia) (Bromley et al., 1999; Knaust, 2009; Rodríguez-Tovar et al., 2009; Kotake, 2014; Löwemark, 2015; Dorador et al., 2016; Łaska et al., 2017). This trace forms part of the *Zoophycos* and *Nereites* ichnofacies, appearing both in continental slopes and deep abyssal plain deposits, thus never found shallower than 1000 m in modern oceans (e.g., Löwemark, 2012). Its record is related to cyclic changes in the climate system that, in turn, may condition organic matter availability (Rodríguez-Tovar et al., 2011).

VI.4.2. Ichnological features

Ichnological features like the surface area of the discrete trace fossils (Fig. VI.6) and the percentage of bioturbational sedimentary structures vary across both studied cores, in agreement with observed changes in the trace fossil assemblage (Fig. VI.6, VI.7).

At Site 977, the percentage of bioturbational sedimentary structures shows a clear general trend from bottom to top. High percentages appear in the lower part of the core (from 26 to 23 mbsf), followed by a decreasing trend in the middle and upper parts (from 23 mbsf) (Fig.

VI.7A). Superimposed on this general trend, a cyclic pattern can be detected: 29 minor-order cycles of variable shape (smooth to sharp peaks) are recognized by visual analysis of the core images. Their correlation with the trace fossil assemblage is noteworthy. There is a clear correlation between ichnodiversity and the percentage of bioturbational sedimentary structures, with increased ichnodiversity being linked to higher percentages of bioturbational sedimentary structures. Accordingly, low-diverse ichnoassemblages, *Planolites* and occasional *Chondrites* are linked to lower percentages of bioturbational sedimentary structures. More diverse assemblages, with *Chondrites*, *Planolites*, *Thalassinoides, Zoophycos* and *Scolicia*, are registered when the percentage of bioturbational sedimentary structures increases (Fig. VI.7A).

The size of the traces evidences a trend similar to that observed for the percentage of bioturbational sedimentary structures. Larger sizes are registered in the bottom meters of core 977, then smaller values for the rest of the core, with minor cyclic variations (Fig. VI.6).

At Site 976, the percentage of bioturbational sedimentary structures (unlike Site 977) shows no significant general trend but is quite uniform. Still, as in the Site 977 record, a minor-order cyclic pattern evidences a total of 29 cycles (Fig. VI.7B). A close correlation is seen between ichnodiversity, percentage of bioturbational sedimentary structures, and size of traces. Low-diverse ichnoassemblages of small-size traces like occasional *Planolites* and probably some *Chondrites* are registered in little-bioturbated intervals, whereas intervals with higher percentages of bioturbational sedimentary structures exhibit an increased ichnodiversity (*Thalassinoides*, *Zoophycos*, *Scolicia*) and larger burrows (Figs. VI.6 and VI.7B). Size distribution is roughly uniform throughout the core, making it difficult to discern tendencies; yet cycles of increased size coincide with a greater percentage of bioturbational sedimentary structures in some intervals: 30 to 26 mcd, or 14 to 12 mcd (Figs. VI.6).

VI.5. Discussion

VI.5.1. Ichnology and palaeoenvironmental conditions at the studied sites

A comparison of the records at Sites 977 and 976 reveals a minor-order cyclic pattern, with a total of 29 cycles, as well as a correlation between ichnodiversity, percentage of bioturbational sedimentary structures, and size of burrows. However, the percentage of bioturbational sedimentary structures is significantly lower at Site 976 records than at Site 977. This is particularly evident for the lower part, with the absence of a clear trend.

The trace fossil assemblage in the studied records can be assigned to the *Zoophycos* ichnofacies, typical of the deep-sea environment (MacEachern et al., 1999; Buatois and Mángano, 2011; MacEachern et al., 2012; Rodríguez-Tovar et al., 2015). In these settings, organic matter

availability, sedimentation rate and oxygenation appear as the major limiting factors for tracemakers (Wetzel, 1983; Giannetti and McCann, 2010; Wetzel, 2010; Uchman and Wetzel, 2011; Wetzel and Uchman, 2012).

The studied deposits represent hemipelagic mud, with terrigenous and probably bottom current transported material (Ercilla et al., 2016). As no turbidites are recognized in the studied intervals, a relatively constant sedimentation rate is assumed, which is supported by the absence of major observable disruptions except for two erosion scars in core 977 (Fig. VI.7B). Thus, changes in the bioturbation features within each particular interval can be interpreted as a response to changes in oxygenation and organic matter content at the deep-sea bottom, although interrelation between the two parameters is variable (see Wetzel and Uchman, 2012; for a review).

The obtained ichnological information about ichnodiversity, percentage of bioturbational sedimentary structures, and size of trace fossils can be used as a tool to interpret variations in oxygen and organic matter content in the studied interval. In hemipelagic depositional environments, unaffected by turbiditic currents, the abundance of bioturbational structures and burrow size is known to decrease during de-oxygenation; the opposite occurs when oxygen content increases (e.g., Savrda and Bottjer, 1986, 1987, 1989, 1991; Savrda, 2007). Moreover, organic matter availability induces variations in ichnological features as it controls the amount of benthic food available and in combination with sedimentation rates can affect the amount of benthic food buried and the conservation of the traces (Uchman and Wetzel, 2011). Certain trace fossils like *Scolicia* may indicate the amount and the quality of benthic food (Wetzel, 2008), and *Zoophycos* has been associated with periods characterized by high seasonal primary production (Dorador et al., 2016).

VI.5.1.1. Palaeoenvironmental conditions in the East Alboran Basin (Site 977)

In light of the ichnological features expounded above, three main intervals can be discerned at Site 977 and correlated with variations in oxygen and organic matter content (Figs. VI.6 and VI.7):

a) The basal part from 26 to 23.8 mbsf shows higher values for ichnodiversity (*Chondrites*, *Planolites*, *Thalassinoides*, *Zoophycos*, and local sections with high *Scolicia* abundance), size (the highest area in mm2), and percentage of bioturbational sedimentary structures (> 40% to ~100%; BI 3 to 6) (Figs. VI.6, VI.7 and VI.8A). The abundance of discrete traces gradually decreases towards 23 mbsf, below ORL 8 (low bioturbated) and ORL 7 (laminated) (Fig. VI.7, VI.8B). Ichnological features support favourable environmental conditions concerning oxygen (aerobic) and organic matter availability at the seafloor and deep within the sediment, implying a well-developed macrobenthic tracemaker community. However, a gradual decrease in oxygenation can also be envisaged, probably associated with a period of accumulating organic

matter, as revealed by the ORL record. The presence of *Scolicia* in the upper part of ORL 8 (Fig VI.7) is interpreted as later bioturbation of organic-rich horizons from above when oxygenation had improved.

b) The middle part, from 23.5 mbsf to ~18.5 mbsf, shows an increase in ichnodiversity, size and percentage of bioturbational sedimentary structures, as the mottled background is well developed locally (Fig. VI.7, VI.8C). This increase is not smooth but shows substantial variations, the lowest values corresponding to ORL 6 and ORL 5 (Fig. VI.7, VI.8D). For instance, the laminated ORL 5 at 19.5 mbsf (Fig. VI.8C) is preceded by non-bioturbated sediment having neither lamination nor distinctive dark colour, evidencing low-oxygen conditions unfavourable for tracemakers (e.g., Wetzel et al., 2011). Above the ORL 5, a sharp increase in ichnological features is observed, eventually reaching (at the end) values similar to those observed at the beginning of the first interval (Fig 6.7, Fig. VI.8E), and documenting a rapid re-establishment of favourable environmental conditions at the deep-sea bottom.

c) The upper part of the record, from ~18.5 mbsf to the top, is characterized by successive fluctuations in ichnodiversity, size, and abundance of traces, but always generally shows lower values than the middle and basal parts (Fig. VI.7, VI.8F, G, H). This part contains the two most extended ORLs (3 and 2). The record suggests unfavourable conditions at the seafloor in terms of oxygen availability for a long time, followed by a slow re-establishment, determining the low values for ichnological features. These two ORLs are not laminated, but bioturbated (Fig. VI.8H), evidencing a comparatively low-oxygenated environment. At the top (~2.5 mbsf), the noteworthy abundance of *Scolicia* indicates that high amounts of benthic food were available. Bioturbation of ORL 1 (Fig. VI.8I) probably reflects a short period of oxygenation after deposition of the ORL and subsequent rapid bioturbation by the *Scolicia* tracemaker.

VI.5.1.2. Palaeoenvironmental conditions in the West Alboran Basin (Site 976)

Ichnological features throughout Site 976 record mark rapid fluctuations accentuating a broader uniform trend. For instance, ichnodiversity ranges from 2 to 5 ichnotaxa, BI ranges from 1 to 3, and the size (area in mm2) between 1 and 100 (Figs. VI.6 and VI.7). Clear differentiation of sections by ichnological features, as in the Site 977 record, is challenging. In comparison with Site 977, the generally lower values of the ichnological features at Site 976 point to less favourable environmental conditions (i.e., oxygenation, organic matter availability). This could be related to the higher sedimentation rate at Site 976 (between 0.1 and 0.6 cm/yr) compared to Site 977 (between 0.01 and 0.3 cm/yr). Although less favourable, these conditions were sufficient to maintain a well-developed tracemaker community, with a continuous record of *Chondrites* and *Planolites*, and even of *Thalassinoides*, implying fluctuating aerobic/dysaerobic conditions and benthic food availability (Figs. VI.7 and VI.9). The presence of *Zoophycos* and *Scolicia* throughout the studied intervals (Figs. VI.7 and VI.9) indicates the recurrent supply of organic matter. A relative scarcity of laminated intervals, attributed to the absence of oxygenation and thus, of track-making organisms, supports their continuous activity and only short-term/locally anoxic deep-sea bottom.

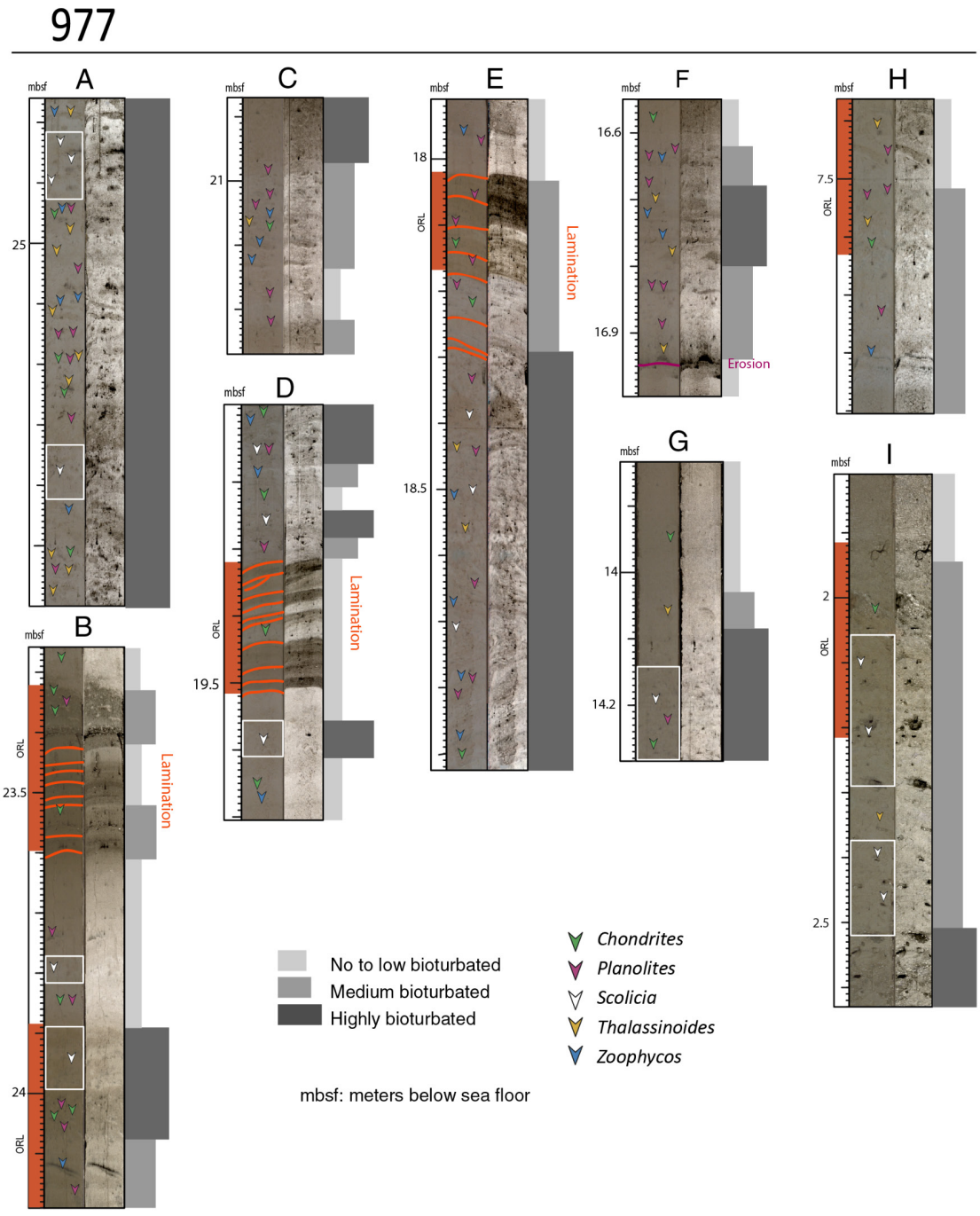

Figure VI.8. Ichnological features from core 977 selected to highlight relationships with ORLs. Locations of the examples are indicated in Fig. VI.7, and Fig. VI.10.

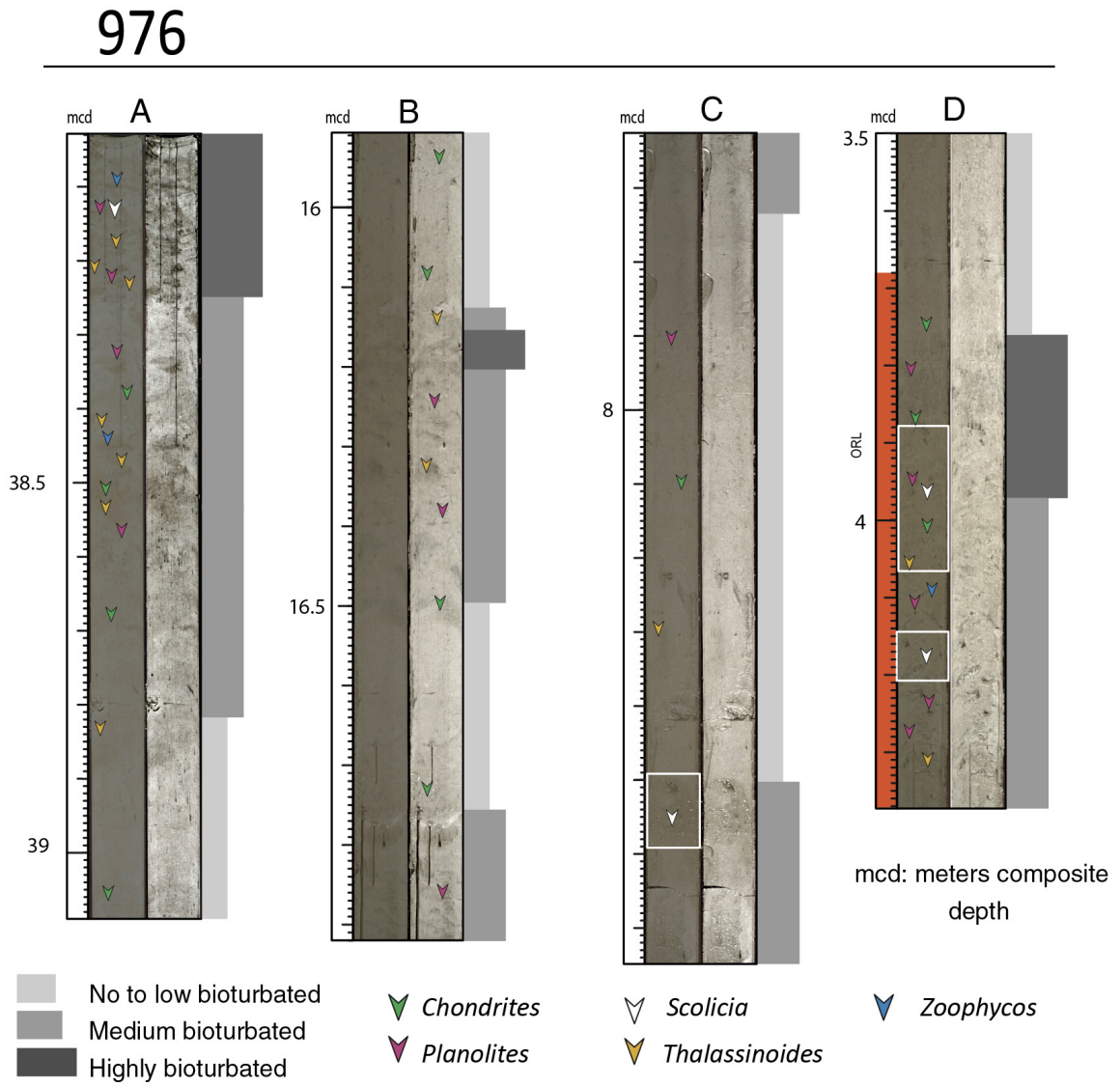

Figure VI.9. Examples of ichnological details from core 976 selected to highlight relationships with ORLs. Locations of the examples are indicated in Fig. VI.7, and Fig. VI.10.

VI.5.2. Last Glacial Cycle at the Alboran Basin, ichnological features and climatic proxies

Abrupt climate changes during the Last Glacial Cycle entailed rapid warming and cooling periods (e.g., Dansgaard et al., 1993; Martrat et al., 2004; Mauffrey et al., 2015) that affected the deep-water formation (WMDW and EMD) and the ventilation of the deep Mediterranean Basinss (Millot, 1990; Rogerson et al., 2008; Schroeder et al., 2012), directly affecting the macrobenthic habitat. Subsequently, climatically induced variations in environmental features at the sea bottom, with changes in oxygenation and organic matter availability, had an impact on the size and behaviour of the tracemakers that are expressed in the ichnological features.

Accordingly, the sedimentological and ichnological record at Sites 976 and 977 sheds light on the environmental conditions and variations during the Last Glacial Cycle. As shown in Fig. VI.10, changes in the ichnological features correlate with proxy records SST and Greenland ice records, used as a reference for the resolution and accuracy of the Pliocene/Holocene climate variations. The SST records are based on alkenones from the Alboran Sea basin (Martrat et al., 2004) and Gulf of Lions (Cortina et al., 2015), and the Greenland ice $\delta^{18}O$ profiles (Johnsen, 1999). Climatic events including the Marine Isotope Stages (MIS 1 to 6), Heinrich Events (HE 1 to HE 6), and Younger Dryas (YD) are also indicated (Ivy-Ochs et al., 2008). Ichnological data (Figs. VI.6 and VI.7) are plotted versus age (Fig. VI.10) by applying this approach.

Löwemark et al., 2008, and Löwemark, 2012 studied the variability of bioturbation during glacial-interglacial intervals concerning changes in primary and export productivity and bottom-water oxygenation. During interglacial warmer periods enhanced benthic food and productivity due to increases in dissolved inorganic compounds (nutrients), rather than changes in deep water ventilation, determining a strong increase in the abundance and diversity of tracemakers. Whereas, during glacial intervals limited primary and export productivity would lead to an impoverished ichnofauna, dominated by small, deeply penetrating trace fossils (Löwemark, 2012).

In the studied records, the presence of a moderately diverse and abundant trace fossil assemblage, together with the relatively constant sedimentation rates showing no abrupt changes (Martrat et al., 2004, 2014), points to relatively oxic bottom water and eutrophic conditions in the Alboran Sea Basin during most of the Last Glacial Cycle interval; However, these are interrupted by the episodes of low oxygenation (Pérez-Asensio et al., 2020), characterized by shallow trace penetration, small size, the low presence or even the lack of distinct burrows.

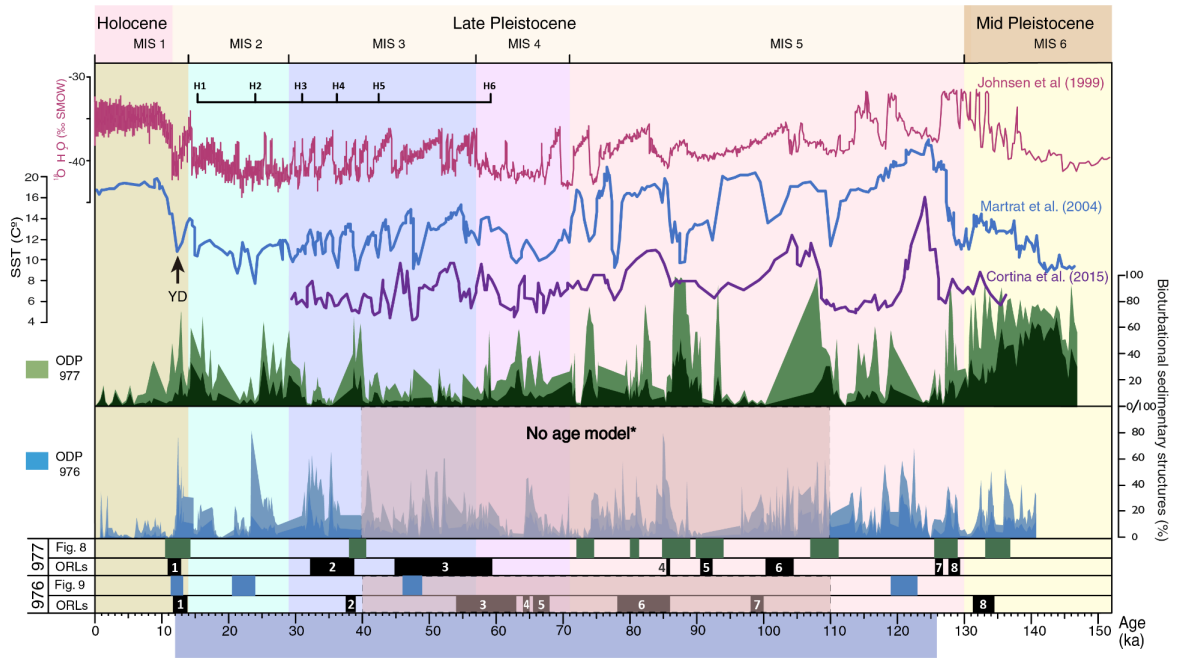

Figure VI.10. Correlation (in age) of the percentage of bioturbational sedimentary structures in cores 976 and 977 with sea surface temperature (SST) from Alboran (Martrat et al., 2004), and Gulf of Lions (Cortina et al., 2015), as well as δ18O data from Greenland (Johnsen, 1999), during the Last Glacial Cycle. Indication of the Marine Isotope Stages (MIS), Heinrich Events (H) and Younger Dryas (YD), plus position of the ORL. Note the location of selected examples in cores 977 (A to I) and 976 (A to D) in Fig. 6.8, and Fig. 6.9, respectively. Trace fossil information has also been compared with other proxy records (like geochemical, isotopes and micropalaeontological) in previous works to investigate glacial/interglacial transitions, Heinrich Events, and various MIS (Baas et al., 1998, 1997; Löwemark et al., 2004, 2006, 2008; Löwemark, 2012; Rodríguez-Tovar et al., 2015; Dorador et al., 2016; Hodell et al., 2017; Rodríguez-Tovar et al., 2019a; Sánchez Goñi et al., 2019; Pérez-Asensio et al., 2020).

This general pattern of favourable environmental conditions for the macrobenthic tracemaker community is punctuated by periods of lowered benthic food availability and dysoxia, determining a decrease in the ichnological parameters of ichnodiversity, size, abundance or even a local absence of bioturbation. The favourable habitat for the macrobenthic tracemaker community during the Last Glacial Cycle can be tied to the major impact of the deep-water circulation in the Alboran Sea (Figs. VI.1 and VI.2). The deep-water formation in the Western Mediterranean was particularly intense at certain periods, such as the cold periods. These are related to cold winters that increased the formation of oxygenated deep water (Millot, 1999) due to the sinking of the colder and denser water masses in the Gulf of Lions (Lacombe and Tchernia, 1974; Millot, 1990, 1999; Send et al., 1999; Cacho et al., 2006). As previously outlined, WMDW overturning has been closely linked with the climatic conditions in the northern hemisphere and Atlantic influence (Cacho et al., 2000; Sierro et al., 2005). The incidence of WMDW may be further sustained by the relationship between the ichnological features and SST records from the Alboran Sea (Martrat et al., 2004) and the Gulf of Lions (Cortina et al., 2015).

Given the three parts differentiated at Site 977, three scenarios are envisaged:

a) The basal part of the record (from 26 to 23.8 mbsf; ~147–125 ka), showing high values of ichnodiversity, size, and percentage of bioturbational sedimentary structures, correlates in most cases with colder SST values during the MIS 6, before the onset of the Last Glacial Cycle (Fig. 6.10). Changes in deep-water circulation and the incidence of colder water during this MIS 6 could regulate the availability of oxygen (oxic) and organic matter at the seafloor and in the sediments. WMDW formation has been associated with the strengthening of the north-westerly winds on the Gulf of Lions during glacial stages (Frigola et al., 2008) represented by low SST values, as the deep water formation occurs during winters and is associated with the strength of north winds producing buoyancy loss of the superficial water. The WMDW formation allows oxygenation of deep parts of the basin, favouring a well-developed macrobenthic tracemaker community. The transition between the end of the MIS 6 and the beginning of the Last Glacial Cycle is marked by a significant rise in the SST, which correlates with a decreasing trend in ichnological features, in particular, the presence of *Scolicia*, coinciding with the ORLs formation. This could indicate enhanced organic matter flux and decreasing oxygenation during a short warmer period in Termination II.

b) The increase in ichnodiversity, size and percentage of bioturbational sedimentary structures registered in the middle interval (from 23.5 mbsf to ~18.5 mbsf; ~125–85 ka), corresponds with most of the MIS 5 and reflects long-term fluctuations in SST values recorded during the first part of the Last Glacial Cycle (Fig. VI.10). The fluctuations can be tied to the repetitive influence of colder, oxygenated deep bottom water as well as sufficient organic matter to sustain the macrobenthic community.

c) The upper part of the core (from ~18.5 mbsf to the top, ~last 85 ka) includes a first interval comprising the youngest part of the MIS 5 along with MIS 4, MIS 3, and MIS 2. This correlates with the "cooling" period of the Last Glacial Cycle. A second interval, corresponding to the MS1 and mainly spanning the Holocene (at ~12–0 ka), fits with Termination I (Pérez-Folgado et al., 2004) (Fig. VI.10). The glacial interval shows fluctuations in, size, and abundance of traces, generally exhibiting lower values than those registered in the middle and basal parts of this record. This suggests an increased influence of cold deep waters, hence decreasing bottom-water oxygenation. This interpretation is supported by the formation of ORLs. The second "warmer" interval exhibits a significant decrease in the percentage of bioturbational sedimentary structures and thus, supports a relationship between low bioturbation and warmer waters.

Our preliminary data confirm the link between the percentage of bioturbational sedimentary structures and the long-term SST trend registered for the Last Glacial Cycle, which is also observed for the short-term scale changes. Thus, high percentages of bioturbation ($> 60\%$, even ~100%) registered at the end last penultima glacial (~145 - ~127 ka), during the glacial period (~108 ka, ~86 ka, ~73 ka, ~40 ka and ~ 15 ka) and the Younger Dryas, coincide with low SST values and rapid cooling. A similar pattern, though less evident due to lower bioturbation

values is seen at ~63 ka, a little bit displaced, also at ~55 ka, ~48 ka, ~44 ka, ~42 ka, and ~33 ka we can see similar trends.

These preliminary results underline the impact of cold water and associated deep water conditions on the macrobenthic habitat, improving environmental conditions, in particular, oxygen and benthic food availability and hence, favouring bioturbation. The correlation between a large area occupied by bioturbational sedimentary structures and low temperature is more clearly recognized in the SST record from the Alboran Sea (Martrat et al., 2004) than in the Gulf of Lions (Cortina et al., 2015). In the context of short-term changes, our data evidence a variable relationship between the features of the ORLs and the ichnological record, from dark laminated ORLs without or with scarce bioturbation (ORL4, Fig. VI.8D and ORL5, Fig. VI.8E), to partially or to bioturbated ORLs (ORL3, Fig. VI.8H). This change highlights the complexity of ORL formation in terms of organic matter content and oxygen availability, and the effects on the benthic habitats.

Discerning a relationship between the percentage of bioturbational sedimentary structures and SST in Site 976 is not so straightforward. Fluctuations in the ichnological features are less evident and the age model available is incomplete, making the correlation very tentative. Moreover, the influence of a different palaeoceanographic setting in the West Alboran Basin (Fig. VI.1) cannot be discarded. In particular Site 976 was less affected by the influence of the WMDW, being at a shallower depth, with minor influence on the deep-sea bottom and therefore on the macrobenthic tracemaker community.

VI.6. Conclusions

Ichnological analysis of sediment records recovered at ODP Sites 976 and 977 in the Alboran Basin, spanning the Last Glacial Cycle (last ~130 kyr) and Holocene, reveals a low/moderate diverse trace fossil assemblage consisting of common *Planolites*, *Chondrites* and *Thalassinoides*, and local *Scolicia* and *Zoophycos*, belonging to the *Zoophycos* ichnofacies.

Ichnological features such as ichnodiversity, size of biogenic structures and percentage of bioturbational sedimentary structures show clear correlation. Lowly diverse ichnoassemblages with smaller traces of *Planolites* and occasional *Chondrites* feature lower percentages of bioturbation. In turn, more diverse assemblages with larger *Planolites*, *Chondrites*, *Thalassinoides*, *Zoophycos* and *Scolicia* are registered when the percentage of bioturbational sedimentary structures increases.

These ichnological features vary throughout the studied time interval, evidencing a well-developed short-term cyclic pattern, mainly related to environmental changes in oxygenation and organic matter availability at the deep-sea bottom.

Correlation of the percentage of bioturbational sedimentary structures with other climate proxies, like alkenones SST records from the Alboran Sea and Gulf of Lions, and the Greenland

$\delta^{18}O$ profile, reveals a close relationship at both the long-term scale, over the Last Glacial Cycle, and the short-term, with fluctuations including the Heinrich Events, Younger Dryas and intervals of ORL formation. Climatically induced changes and fluctuations in the ocean dynamics, which have a major incidence in the Western Mediterranean Deep Water, caused changes in environmental conditions at the deep-sea bottom and affected the macrobenthic tracemaker community. However, all these relationships are complex and further studies should be directed to understand processes affecting benthic food availability in the basin.

Chapter VII

Ichnological evidence for bottom water oxygenation during organic-rich layer deposition in the Westernmost Mediterranean over the Last Glacial Cycle

Marine Geology 443 (2022) 106673

Contents lists available at ScienceDirect

Marine Geology

journal homepage: www.elsevier.com/locate/margo

https://doi.org/10.1016/j.margeo.2021.106673

S. Casanova-Arenillas, F.J. Rodríguez-Tovar. F. Martínez-Ruiz

[a] Departamento de Estratigrafía y Paleontología, Universidad de Granada, Campus Fuentenueva s/n, 18002, Granada, Spain

[b] Instituto Andaluz de Ciencias de la Tierra (IACT), Consejo Superior de Investigaciones Científicas-Universidad de Granada (CSIC-UGR), Avda. de las Palmeras 4, 18100, Armilla, Granada, Spain

Abstract

Organic rich layers (ORLs), deposited in the westernmost Mediterranean over the Last Glacial Cycle, have been studied integrating sedimentological and ichnological information from sediment records recovered at Ocean Drilling Program Leg 161 Sites 976 and 977. The conducted study has served to redefine the ORLs initially differentiated in sediment records from Sites 977 and 976, with seven new ORLs recognized, as well as extensions and subtraction of some parts in the ORLs previously defined. In addition, three different ORL types are distinguished according to sedimentological and ichnological features. Type 1 with intermediate thickness is highly bioturbated, mainly consisting of abundant *Scolicia* and *Planolites*, frequent *Chondrites*, and possible *Thalassinoides* in the base, which are interpreted as supporting dysoxic conditions during deposition. Type 2, corresponding to thicker intervals, shows alternance of highly to moderately bioturbated parts, revealing variable oxygen conditions — from moderate to extreme dysoxic or even suboxic. Type 3 consists of short, laminated intervals characterized by the absence of bioturbation, indicating anoxic or suboxic conditions and determining unfavourable macro benthic habitat. The amended ORLs show a correlation between the Sea Surface Temperatures and established climatic events over the Last Glacial Cycle in the Western Mediterranean.

VII.1. Introduction

The present study is centred on the cyclic deposition of organic carbon rich sediments from the Alboran Sea Basin over the Last Glacial Cycle. We have analysed two sediment records at the East and at the West of the Alboran Sea Basin (Fig. VII.1), which come from two drilling sites from Leg 161 of the Ocean Drilling Program (ODP).

These organic-rich sediments deposited in the Western Mediterranean are normally called organic-rich layers (ORLs) differentiating them from the Eastern Mediterranean "Sapropels". The studied time interval in the Mediterranean spans from the beginning of the penultimate interglacial and Marine Isotope Stage 5, ~130 ka, until the end of the Würn Glaciation over the northern hemisphere, ~11 ka (e.g., Dansgaard et al., 1993). Despite ORLs being layers enriched in Total Organic Carbon (TOC) and cyclically deposited like the sapropels, they are not equivalent layers, probably entailing a more complex set of conditions behind their deposition. ORLs are not always synchronic with sapropels and do not seem to follow the insolation maxima as sapropels do (von Grafenstein et al., 1999; Cacho et al., 2002; Rogerson et al., 2008; Rohling et al., 2015). Whereas sapropels have been extensively studied (among many others, Kidd et al., 1978; Sigl et al., 1978; Rohling and Hilgen, 1991; Rohling, 1994; Cramp and O'Sullivan, 1999; Grimm et al., 2015; Rohling et al., 2015; Grant et al., 2016; Wu et al., 2018), ORLs from the Western Mediterranean are largely unexplored, with the exception

of the most recent one, the ORL 1 (Bárcena et al., 2001; Cacho et al., 2002; Rogerson et al., 2008; Rodrigo-Gámiz et al., 2011; Jiménez-Espejo et al., 2015; Martínez-Ruiz et al., 2015; Pérez-Asensio et al., 2020). However, ORLs also represent important organic carbon accumulations and record the response of the Mediterranean to palaeoceanographic and climate variability.

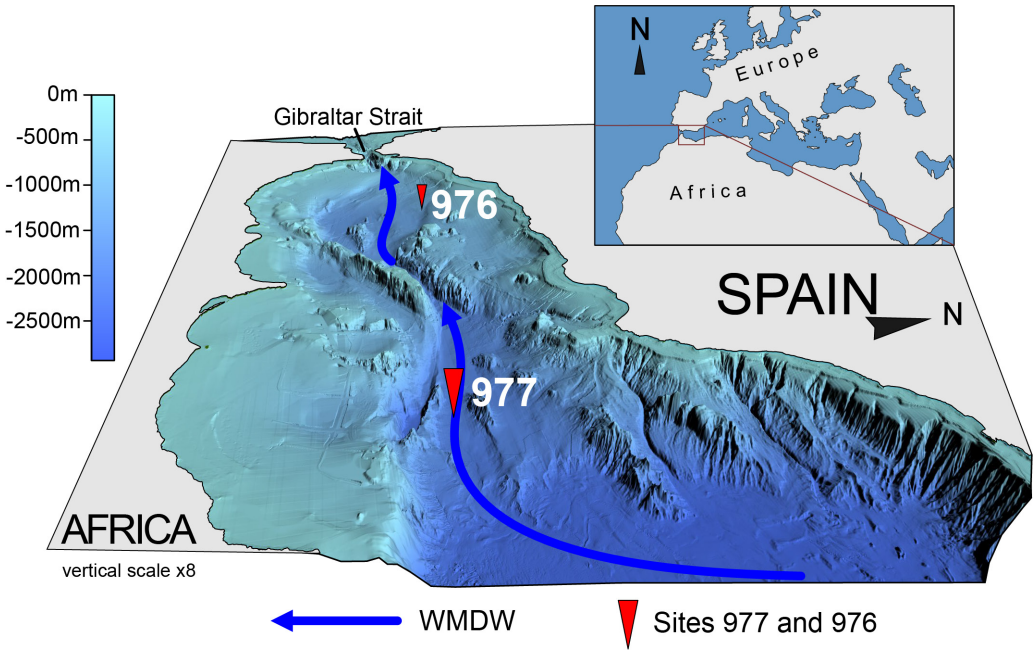

Figure VII.1. Location of the ODP Sites used for the study (Sites 977 and 976). The blue arrow shows the main circulation pattern of the Western Mediterranean Deep Water towards the Gibraltar Strait (For interpretation of the references to colour in this figure legend, the reader is referred to the web version of this article).

In general, most organic matter (OM) in the marine environment is mineralized either from primary productivity or from continental input before its burial; but when production exceeds degradation part of it is preserved in the sediment (e.g., Middelburg et al., 1999; Berner, 2003). The dominant factor in OM preservation has been intensively debated for decades (e.g., Calvert, 1987; Pedersen and Calvert, 1990; Hedges and Keil, 1995; Hedges et al., 1997; Moodley et al., 2005; Arndt et al., 2013; LaRowe et al., 2020) particularly because of the high variability observed over space and time in the deep ocean (Canfield, 1994; Berner, 2003; Blair and Aller, 2012; Arndt et al., 2013). For instance, past oceans have had generalized O_2-depleted zones in which considerable amounts of OM accumulated and were preserved in the geological records (Jenkyns, 2010). Yet in modern oceans, the presence of large oxygen-depleted areas is limited to very few places —e.g., the isolated basins of the Black Sea or the Baltic Sea— or the oxygen minimum zones derived from biological productivity that appear in some upwelling continental margins like Namibia or Peru. The amount of OM preserved depends on an interlaced combination of factors, such as the quantity of OM reaching the bottom due to productivity (Emeis et al., 2000), and the velocity of degradation, in turn, related to oxygenation and burial velocity, hence sedimentation rate. Other factors that can affect the degradation of OM include

composition, electron acceptor availability, benthic microbial community, physical properties, and macrobenthic activity (e.g., LaRowe et al., 2020). Because the relative importance of these factors varies over time and space, OM-rich intervals in the geological record could point to very diverse signatures (e.g., Aller, 1982; Middelburg, 1989, 2018; Mollenhauer et al., 2007; Zonneveld et al., 2010; Arndt et al., 2013; LaRowe et al., 2020). TOC values in the Western Mediterranean can reach values of 2.27%, as registered in the Balear Basin, 2% in the Alboran Sea Basin, or even values over 6% in the Ionian Sea (Murat, 1999). During ODP Leg 161, the Shipboard scientific party established a limit of 0.8% TOC to define ORLs, contrasting with the values of 2% used during leg 160 of the ODP in the Eastern Mediterranean to define sapropels (Kidd et al., 1978; Murat, 1999; Emeis et al., 2000). Background TOC values found in the Western Mediterranean are also higher than those of the Eastern Basin.

In the Eastern Mediterranean Sea, the simultaneous occurrence of high productivity along with low oxygenation in the bottom waters is held to be the main factor behind sapropel deposition (e.g., Rohling et al., 2015). In the Western Mediterranean, previous work has evidenced that the main factors controlling ORL deposition are productivity and bottom water oxygenation, based on foraminifera, biomarker, and geochemical analysis (Casford et al., 2003; Meyers and Arnaboldi, 2005; Pérez-Asensio et al., 2020 among others). Debate persists about which causes are predominant, or if all events could have the same set of conditions (Rohling et al., 2015). Recent studies in the Western Mediterranean propose that productivity alone cannot produce the low oxygen conditions necessary for ORL deposition, for which reason decreasing deep-water ventilation would also be required (Rogerson et al., 2008; Rodrigo-Gámiz et al., 2011; Pérez-Asensio et al., 2020). The sedimentation rate also influences TOC content and its dilution in the sediment (e.g., Tyson, 2001); however, the fact that it remains high in the Alboran Sea Basin in the studied time would mean it is not a main controlling factor for ORL deposition in this setting.

The deep-water stagnation that leads to ORL deposition has been proposed to be produced by a combination of low aspiration over the Gibraltar Strait (Rogerson et al., 2008; Rohling et al., 2015; Pérez-Asensio et al., 2020) and a decrease in the rate of deep-water sinking over the Gulf of Lion related to buoyancy changes (Millot, 1999; Cacho et al., 2002; Frigola et al., 2008; Rogerson et al., 2008; Pérez-Asensio et al., 2020). Changes in the precipitation-evaporation balance can moreover induce salinization of the superficial waters during certain periods —not necessarily the colder periods— inducing buoyancy variations that could enhance deepwater sinking during warmer phases (Cisneros et al., 2019). Variations in deep-water ventilation are also related to climatic swifts over the northern hemisphere, for example, the ones resulting in Dansgaard-Oeschger and Heinrich Events (Sierro et al., 2005; Frigola et al., 2008; Rohling et al., 2015). Despite a reported decrease in ventilation during Heinrich Events due to the freshening and decreased density of superficial waters (Sierro et al., 2005; Rogerson et al., 2008; Rohling et al., 2015), which may precondition posterior low oxygenation events, its effect alone would hardly suffice to promote ORL deposition. ORL 1 does not show a clear correlation with these events (Rogerson et al., 2008). Variations in the Levantine Intermediate Water have also

been invoked to explain the absence of influence of Heinrich Events in the ORLs, due to compensation of its possible effects (Rogerson et al., 2008). Still, further investigation is required for reconstructing the palaeoceanographic conditions leading to ORL deposition elsewhere than the ORL1 (14.5 - 8.5 ka), which has been more profusely studied (Pérez-Folgado et al., 2004; Rogerson et al., 2008; Bazzicalupo et al., 2018; Pérez-Asensio et al., 2020).

One important open question surrounds the precise oxygen conditions during deposition. Ichnological analyses of deep-sea sediments have proven to be valuable for constraining oxygen conditions and OM preservation. At the time of deposition in deep-sea environments, depositional and ecological conditions at the sediment and in bottom waters — such as benthic food availability, oxygenation, hydrodynamic energy, and sedimentation rates — have a major impact on the macrobenthic trace maker community, hence on ichnological features as ichnodiversity, bioturbation degree and size of the traces, among others (i.e., Savrda and Bottjer, 1989, 1987, 1986, 2007; Savrda, 2007; Wetzel, 2010; Buatois and Mángano, 2011; Uchman and Wetzel, 2011, 2012; Rodríguez-Tovar, 2021). For this reason, ichnological features are reliable proxies when reconstructing bottom- and pore-waters conditions and for palaeoceanographic interpretations (Löwemark, 2012; Löwemark et al., 2006; Rodríguez-Tovar and Dorador, 2015; Rodríguez-Tovar et al., 2018, 2019b, 2020a; Hodell et al., 2017; Sánchez Goñi et al., 2019). In the wake of a general ichnological study of sediment records from the Alboran Sea Basin, looking at the relationship between the abundance of bioturbation and climate changes during the Last Glacial Cycle (Casanova-Arenillas et al., 2020, 2021), the present study offers a detailed analysis of the westernmost ORLs distinguished over this time interval, to reconstruct palaeoceanographic dynamics. Our main aim is therefore to characterize the ORLs in terms of ichnology and sedimentology, beyond previous results, and typify ORLs based on such characterization. ORL types can then be related to variable palaeoenvironmental conditions, particularly oxygen content and ocean dynamics.

VII.2. Regional setting

Over the decades, diverse studies explored ventilation and circulation in the Mediterranean using models, direct observations or proxies (e.g., Wüst, 1961; Millot, 1999; Pinardi and Masetti, 2000; Millot and Taupier-Letage, 2005; Sierro et al., 2005; Rogerson et al., 2008; Frigola et al., 2008; Naranjo et al., 2012; Pinardi et al., 2015; Bazzicalupo et al., 2018; Pérez-Asensio et al., 2020). The insights they provide for palaeocirculation reconstructions have changed over time, from the early stationary models to current models based on dynamic changes and sub-basin switching circulation patterns. The general and simplified oceanographic setting of the water masses in the Mediterranean includes three masses that extend over the Eastern and Western Mediterranean, in turn, are divided into multiple sub-basins. Mediterranean circulation shows an anti-estuarine pattern (Millot, 1999; Millot and Taupier-Letage, 2005) with a less saline water mass — the Atlantic Water (AW)— entering through

the Gibraltar Strait and circulating superficially, dominated by winds towards the Eastern Mediterranean. Then, when it reaches the eastern part of the Mediterranean, due to excessive evaporation in the Levantine Basin, it gains salinity and density; in conjunction with northern dry winds, it suffers cyclonic sinking, thereby generating the Levantine Intermediate Water (LIW) (Bethoux and Gentili, 1999; Millot and Taupier-Letage, 2005; Pinardi et al., 2015). The LIW circulates towards the west at the middle depths and finally leaves the Mediterranean over the Gibraltar Strait, contributing to Atlantic circulation (Baringer and Price, 1999; Jiménez-Espejo et al., 2015; Naranjo et al., 2015). Two other water masses, the Western and Eastern Mediterranean Deep Water (WMDW and EMDW) flow in the deep parts of the two basins, resulting from the seasonal sinking of LIW and surface waters in the northern parts of the two sub-basins owing to open sea convention and cascading that is favoured by cold winds coming from the continent during winters (e.g., Medoc Group et al., 1970; Millot, 1999; Millot and Taupier-Letage, 2005; Schroeder et al., 2008, 2012; Durrieu de Madron et al., 2013; Naranjo et al., 2015; Somot et al., 2018; Cisneros et al., 2019). The WMDW, the water mass located at the bottom of the Western Mediterranean, is formed in the Gulf of Lions in winter by the above process of cyclonic sinking (e.g., Rhein, 1995) and is also important for Mediterranean outflow, mixing with the LIW and directly contributing by means of Bernoulli Aspiration (Rogerson et al., 2008; Millot, 2014).

The Alboran Sea Basin (Fig. VII.1), the westernmost Mediterranean Basin, it is of particular interest for palaeoenvironmental reconstructions for two reasons: 1) its high sedimentation rates allow for exceptional high-resolution studies of past oceanic conditions (e.g., Cacho et al., 2000, 2006; Martrat et al., 2007; Rodrigo-Gámiz et al., 2011, 2014), and 2) its location between the Atlantic and the Mediterranean climate regimes, being influenced by both, and hence a key region for reconstructing the Atlantic influx and the Mediterranean Outflow as well as the Mediterranean water masses dynamics (e.g., Heburn and La Violette, 1990; Naranjo et al., 2015). The entry of AW through the Gibraltar Strait affects productivity in the Alboran Sea Basin, as the anticyclonic gyres and Atlantic Jet cause upwelling in the northern parts of the Basin (Sarhan, 2000)The Mediterranean water coming out from the Gibraltar Strait —the Mediterranean Outflow Water— influences the Atlantic overturning circulation, AMOC (Hernández-Molina et al., 2014; Bahr et al., 2015; Jiménez-Espejo et al., 2015). The Alboran Sea also receives the influence of water masses coming from the eastern basins, the LIW, and the WMDW.

The study sites are found at depths of 1984 mbsl and 1108 mbsl, under the influence of the WMDW (Bethoux et al., 1999). The varying conditions influencing deep water sinking in the northern sector of the basin may have influenced ORL deposition in this setting. Decreasing WMDW formation could have promoted dysoxic bottom waters over time, given that the dissolved oxygen in the Western Mediterranean Deep Water has been correlated (among other factors) to the deepwater removal influenced by climatic shifts (e.g., Rogerson et al., 2008; Mavropoulou et al., 2020).

The records studied entail an initial identification of ORLs and sediment characteristics established during ODP Leg 161. Afterwards, for many years, diverse work focused on the foraminiferal record and environmental and palaeoclimatological reconstructions have been published (e.g., Martrat et al., 2004, 2014; Pérez-Folgado et al., 2004; Combourieu Nebout et al., 2009). Notwithstanding, most of these studies focus on the Holocene and the most recent ORL. Research into the older ORLs is nearly absent and stands as a challenge for better understanding the origin of these organic-rich layers.

VII.3. Materials and methods

The studied sediment record corresponds to Sites 977 and 976 from Leg 161 of the ODP, and its general sedimentology and characteristics were described during the ODP cruise (i.e., Shipboard Scientific Party, 1996a, 1996b), and subsequent analyses strove to identify and define ORLs present in the record Shipboard Scientific Party, 1996a, 1996b; Murat, 1999). Both Sites are in the Alboran Sea Basin (Fig. VII.1): Site 977 deeper, at 1984 m, at the east of the Alboran Ridge; and Site 976 lies at 1108 m depth in the western Alboran Sea Basin. The sediments of the selected time interval (Last Glacial Cycle) correspond to open marine hemipelagic facies (Fig. VII.2) consisting of nannofossil-rich silty clay with an average clay content of 81% in Site 977 (Shipboard Scientific Party, 1996a) along with nannofossil rich clay, calcareous silty clay, and clay having 30–50% of carbonate content at Site 976 (Shipboard Scientific Party, 1996b).

The age models for these records were obtained from Martrat et al., 2004, and Martrat et al., 2014, and linear interpolation was used to correlate our depth data with age.

Ichnological analysis of the selected record was based on core images obtained from the ODP database. At Site 976, images were gathered from four available holes, drilled next to each other, to arrive at a more precise ichnological characterization (Fig. VII.2). Here, ichnological analysis entailed the application of high-resolution digital image treatment using Photoshop™ Software (Magwood and Ekdale, 1994; Dorador and Rodríguez-Tovar, 2014a, 2014b, 2016a, 2018; Rodríguez-Tovar and Dorador, 2014, 2015). This method increases the visibility of biogenic structures, providing particularly successful results with modern sediment cores, where the visibility of the traces due to low lithification is very limited.

The main ORLs for ichnological analysis were distinguished according to the depths reported previously in ODP studies and published in the ODP Leg 161 Initial Reports (Shipboard Scientific Party, 1996a, 1996b), being based on TOC values, magnetic susceptibility and colour.

A greyscale analysis was performed in view of average vertical grey values using ImageJ® software (e.g., Schindelin et al., 2012). The average grey value for the pixels in the horizontal lines of the images is obtained, after which a plot is made to represent the vertical grey value variation. Greyscale analysis has proven useful to visualize colour changes throughout sediment

cores, and in particular, changes in reflectance. By identifying "darkness" and thus possible ORL intervals, these greyscale plots can mark the location of OM-enriched intervals in the sediments. Several thin horizons along the cores were excluded from this study since changes in grey values detected were at times due to artefacts such as variations in the position of the camera, or cracks and surface imperfections produced during the treatment of the core sections. The greyscale analysis was conducted only at Site 977. The available images from Site 976 were of comparatively poor quality —sediment colour is much more homogeneous than in Site 977, the only visible colour variations being a consequence of the incidence of light when photographed. Thus, the greyscale data served for a detailed analysis of the ORLs originally defined by the Shipboard Scientific Party, as well as for the addition of new ones.

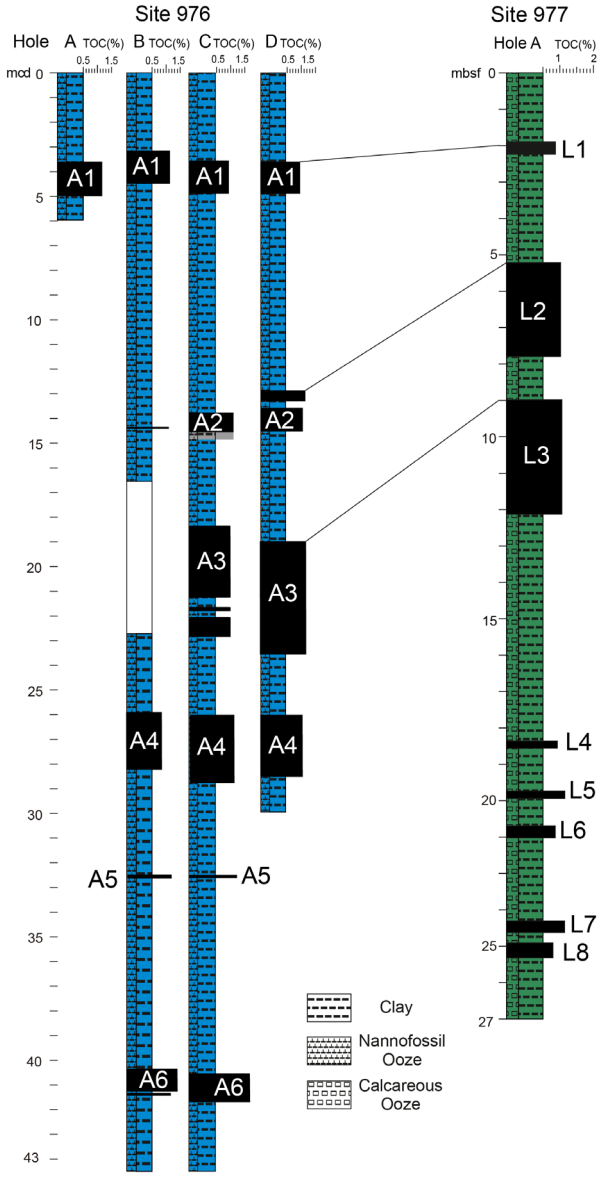

Fig. VII.2. General lithological logs of the studied holes from Sites 977 and 976 with the position of the ORLs (L1 to L8 in Site 977 and A1 to A6 in Site 976) and the corresponding TOC values (Shipboard Scientific Party, 1996a, Shipboard Scientific Party, 1996b). In site 977 only one hole was drilled, the 977A. 4 holes that were drilled in Site 976 indicated from A to D.

VII.4. Results

VII.4.1. Greyscale analysis in Site 977

The grey value plot presents a pattern of clear variations that correlate well with the interval and the internal variation of the previously defined ORLs (Fig. VII.3). Yet it also shows variations not directly correlated with the ORLs identified on ODP Leg 161 (Shipboard Scientific Party, 1996a, 1996b). Overall, the ORLs have a characteristic decrease in grey values (contrast of 20 to 30 points with respect to the surrounding sediment), especially L4, L5, L7 and L8. Internal variability is observed in L2 and L3, however, as well as in L1, which presents an extended range of variability, having a peak beyond the range of the layer as defined in the Initial Report.

During ODP Leg 161, at least 40 ORLs were described in the first 417 m of the holes drilled in the basin. At Site 977, eight of them are located in the upper 26 m corresponding to the Last Glacial Cycle. The obtained greyscale values improve the original ORL differentiation. Original ORLs (L1 to L8) were therefore characterized in greater detail, and new ORL intervals could be identified.

In view of the ORLs initially defined, the newly conducted analysis on ORL L1 reveals a grey value increase that extends further than the original interval (Shipboard Scientific Party, 1996a, 1996b). The ORLs L4, L5, L7 and L8 (L6 is not visible) present a clear peak in grey value that is well-correlated with the darker laminated or bioturbated layers observed in the core images, supporting the original characterization (presented in Fig. VII.3).

In sum, the more recently conducted research allows for a tentative definition of new ORL intervals not considered in the original ORL based on fluctuations in greyscale values.

Accordingly, a total of seven new ORL intervals are defined here (a to g, blue colour bands, in Fig. VII.3), and previous ORLs, originally defined during the ODP campaign, intervals have been modified, through extensions or subtractions (green and red colour bands, respectively, in Fig. VII.3). Moreover, ORLs L2 and L3 should be reconsidered, by the subtraction of some parts, as a possible succession of different events. The new colour bands are differentiated by contrast in the greyscale (reported contrast of between 12 and 24). The TOC values measured during the ODP campaign in the new layers go from 0.4% to 0.8%, below the established limit, but these data should be taken with caution and are of low resolution. The thickness of the new layers goes from 10 cm for layer a to 40 cm for layer g, for instance, the largest one observed.

VII.4.2. Trace fossil assemblage

Trace fossil assemblages from the studied records at Sites 977 and 976 present a low-to-moderate diversity, consisting of *Chondrites*, *Planolites*, *Thalassinoides*, *Scolicia* and less frequent *Zoophycos* (Casanova-Arenillas et al., 2021) (Table VII.1). Concerning the ORLs intervals, *Chondrites*, *Planolites*, and *Scolicia* are the most abundant ichnotaxa.

VII.4.3. Ichnological features in the organic-rich layers

The ichnological analysis of the ORLs reveals significant variability mostly related to the presence/absence of traces, degree of bioturbation, ichnodiversity, and distribution.

VII.4.3.1. Bioturbation in the originally defined ORLs from Site 977

The eight ORLs (L1 to L8) identified in Site 977 during ODP Leg 161 (Shipboard Scientific Party, 1996b, 1996a) range from highly bioturbated to non-bioturbated and laminated sediments (Fig. VII.4; Table VII.2).

ORL L1 (~9 ka- ~14 ka) is about 30 cm thick, presenting a mottled background with locally identifiable discrete traces. The bottom of ORL L1 presents abundant bioturbation, in particular *Planolites*, *Scolicia* and *Thalassinoides*, and potential *Chondrites*. The size of the traces decreases upward. ORL L2 (~32 ka- ~39 ka) corresponds to a thicker interval of 220 cm. A mottled background is locally observed. The trace fossil assemblage consists of *Chondrites*, *Planolites*, *Scolicia* and *Thalassinoides* at the base. The abundance and size of biogenic structures are lower than in ORL L1, but also show a variable record throughout both ORLs, in association with colour variation in the sediment. ORL L3 (~46 ka- ~62 ka) is similar in thickness to ORL L2, around 310 cm, and shares the assemblage of *Chondrites*, *Planolites*, *Scolicia* and *Thalassinoides* at its base, but is less bioturbated. Like ORL L2, it shows variations in the trace fossil assemblage and the sediment colour through the ORL. In turn, ORL L4 (~85.5 ka- ~86.3 ka) is a thin layer, 30 cm, characterized by clear horizontal lamination and colour banding, and a generalized absence of bioturbation. Only occasionally in the lighter parts, small and dispersed *Chondrites* can be tentatively identified. ORL L5 (~91 ka- ~93 ka) is 20 cm thick, being very similar to ORL L4. ORL L6 (~105.8- ~110 ka) is between two core sections and its characteristics are not at all clear in the available images. ORL L7 (~125.5 ka- ~126.6 ka) is 25 cm-thick and resembles ORLs L5 and L4, except that at the top of this layer, a massive and sandy interval appears in which discrete traces attributable to *Planolites* of less than 1 cm can be observed. ORL L8 (~127.6 ka- ~129.3 ka) is a bioturbated layer, 40 cm thick, very similar to ORL L1. The trace fossil assemblage consists of *Chondrites*, *Planolites*, and *Scolicia* with an upward increase in the trace size and bioturbation percentage.

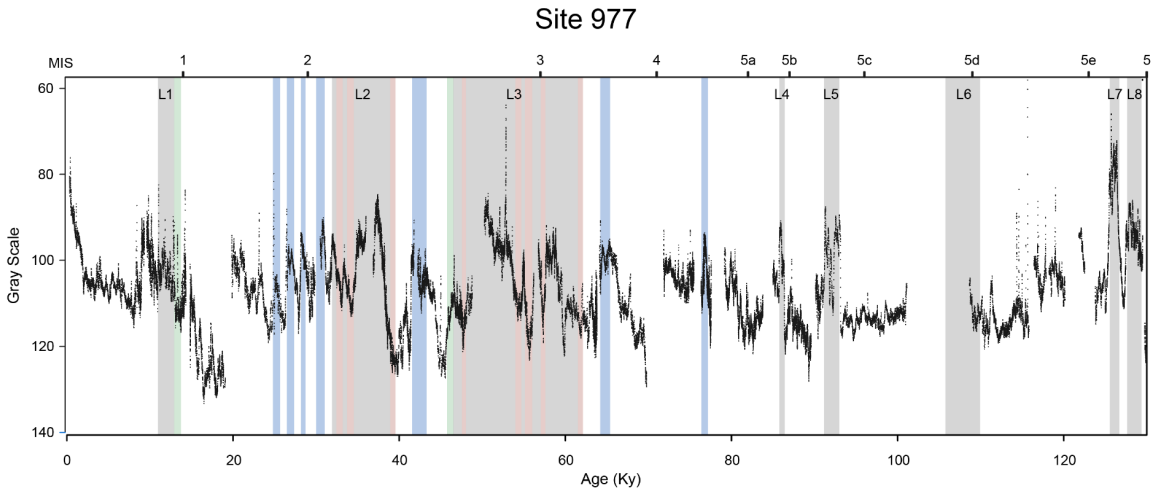

Figure VII.3. Grey value plot in age with the location of the 8 ORLs (L1-L8) from site 977, hole A.

VII.4.3.2. Bioturbation in the ORLs from Site 976

The six ORLs (A1 to A6) from records at Site 976 differentiated during ODP Leg 161 (Shipboard Scientific Party, 1996a, 1996b) are characterized by the presence of bioturbation and the absence of lamination (Fig. VII.5; Table VII.3). The ORLs from Site 976 present an incomplete chrono-stratigraphy and cannot be directly correlated in age or appearance with the ones from Site 977. Still, detailed characterization is interesting to discern lateral variations within the Basin and during ORL deposition.

ORL A1 has a similar appearance in the four drilled holes (Fig. VII.2, Fig. VII.5), corresponding to a 90 cm bioturbated section and showing a mottled background. The trace fossil assemblage comprises *Chondrites*, *Planolites*, *Thalassinoides*, and *Scolicia*, the last especially abundant in the lower part. A decrease in the degree of bioturbation, abundance and size of trace fossils is observed upward. ORL A2 presents features similar to those of ORL A1, with *Chondrites*, *Planolites* and *Thalassinoides*, and *Scolicia* in the lower part. A reduction in size and abundance of the discrete traces is observed upward. Locally, a weak banding could be differentiated in the middle part, associated with the darker sediments. ORL A3 appears as a long, 320 cm, not always well-preserved layer. Bioturbation is moderate, with local increases in abundance in the middle and upper parts. Some darker intervals lack trace fossils, but banding/lamination is likewise absent. The trace fossil assemblage mainly comprises *Chondrites*, *Planolites* and *Thalassinoides*, with occasional *Scolicia*. Tentatively, some structures could be assigned to *Zoophycos*. ORL A4 refers to a 150–170 cm thick section with low and sparsely distributed bioturbation, though higher abundance is noted upward. The trace fossil assemblage consists of *Chondrites*, *Planolites* and *Thalassinoides*, with *Scolicia* mainly in the upper part. Tentatively, like in ORL A3, some structure(s) could be assigned to *Zoophycos*. ORL A5 is a thin, 2 to 10-cm thick, bioturbated layer with *Chondrites* and *Planolites*, and probably *Scolicia*. Locally, weak banding is envisaged. ORL A6, about 60–70 cm thick, is moderately bioturbated, with an assemblage of *Chondrites*, *Planolites*, *Scolicia* and *Thalassinoides*.

Table 7.1. Different ichnogenus differentiated.

Ichnogenus	Ichnological features	Relationship with ORL intervals	Interpretations	References
Chondrites	A cluster of millimetric size circular to ovalate burrows	Disseminated, low abundance. Can crosscut other traces	Deep tier structure. Feeding activities of chemo-symbiotic organisms. Tolerant to low oxygen conditions	von Sternberg (1833), Hertweck et al. (2007), Rodríguez-Tovar et al. (2009); Rodríguez-Tovar and Uchman (2011), Bromley (1996), Knaust (2017), Baucon et al. (2020)
Planolites	Circular to subcircular small burrows (less than 0.5 cm). Fill colour different from that of the host sediment	Mainly registered at the bottom or top in ORLs, showing multiple changes in colour and bioturbation. Occasionally in the middle parts for unchanged ORLs	Produced by active deposit feeders, usually attributed to worm-like organisms, though other means of production like molluscs and arthropods cannot be discarded	Nicholson (1873), Pemberton and Frey (1982), Keighley and Pickerill (1995), Rodríguez-Tovar et al. (2009)
Thalassinoides	Large burrows, of over 1 cm in diameter. Fill darker than the surrounding sediment.	At the bottom and top of the ORL intervals in both cores, and rarely in the middle part	Middle-tier structure representing the action of organisms inhabiting galleries for dwelling and feeding activities at a few centimetres below the sediment surface. The producer is usually interpreted as a crustacean, particularly the callasinoids	Ehrenberg (1944), Frey et al. (1984), Nickell and Atkinson (1995), Schlirf (2000), Ekdale and Bromley (2003), Knaust (2017)
Scolicia	Large burrows, usually exceeding 1 cm, show a cross-section where a small dot of darker sediment appears in the centre of a lighter subcircular burrow, or as a lamellar-filled structure representing the displacement of the producer	This trace has been identified in several parts of the ORLs, determining significant bioturbation	Produced by deposit-feeding echinoids and can be found in silt-sized sediments. Its presence is associated with the abundance and quality of benthic food	Quatrefages (1849), Wetzel, 1991, Wetzel, 2008, Carmona et al. (2020)
Zoophycos	Horizontal spreiten burrow darker than the surrounding sediment.	Scarce, only registered at the top of some ORLs from core 976.	Unknown producer, being assigned to variable behaviour but mainly to feeding activities.	Massalongo (1855), Bromley et al. (1999), Rodríguez-Tovar et al. (2009) Hunter et al. (2012)Löwemark (2012); Kotake (2014), Löwemark (2015), Dorador et al. (2016), Łaska et al. (2017)

Table VII.2. ORLs are defined by the ODP scientific time in Site 977. Type as defined in this paper, sedimentary features, ichnological features", grey values and TOC measurements from the Initial Reports.

ORL	Type	Sedimentary features	Ichnological features	grey values	TOC
977					
L1	Type 1	30 to 40 cm sections with no sedimentary structures	Abundant *Scolicia* and presence of *Planolites*, *Chondrites* and *Thalassinoides* at the base of the layer. The size and abundance of the traces decrease from the bottom to the top of the section	105–95	0.87
L2	Type 2	220 cm section with high cyclical variability in colour	Highly bioturbated in the base with *Thalassinoides*, *Planolites* and *Chondrites*. A gradual decrease in size and abundance of the discrete traces	113–88	1.02 to 0.79
L3	Type 2	310 cm section with cyclical variability in colour and sedimentological features. Higher values in greyscale towards the top of the section	Bioturbated in the base with *Chondrites*, *Thalassinoides* and *Scolicia*	123–87	1.07 to 0.87
L4	Type 3	30 cm short section with lamination and two greyscale levels, higher values in the top middle section	Low bioturbated to no bioturbated, with only *Chondrites* as a possible discrete trace. Abrupt decrease of bioturbation at the beginning of the ORL	119–106	0.93
L5	Type 3	20 cm short section with lamination. Abrupt changes in the greyscale values alternating between darker and lighter sediments	Low to no-bioturbated, with only *Chondrites* as possible discrete trace	115–110	1.13
L6	Type 3*	Not studied in detail due to core limitations		116–92*	0.79
L7	Type 3	40 cm laminated section, with alternating changes in greyscale value. The top presents a sand intrusion followed by non-laminated sediment	From the base to the sand intrusion, no to low bioturbation with only *Chondrites* as a possible trace. The top of the layer presents a dark-coloured interval with abundant *Planolites*	90–72	0.98,1.13
L8	Type 1	40 cm section with no lamination. Greyscale variations with two intervals, with lighter sediment in the base	Abundant *Scolicia*, presence of *Planolites* and *Chondrites*. The abundance and size of the *Scolicia* are higher at the top of the layer, making the colour of the sediment lighter	103–86	1.00, 1.26

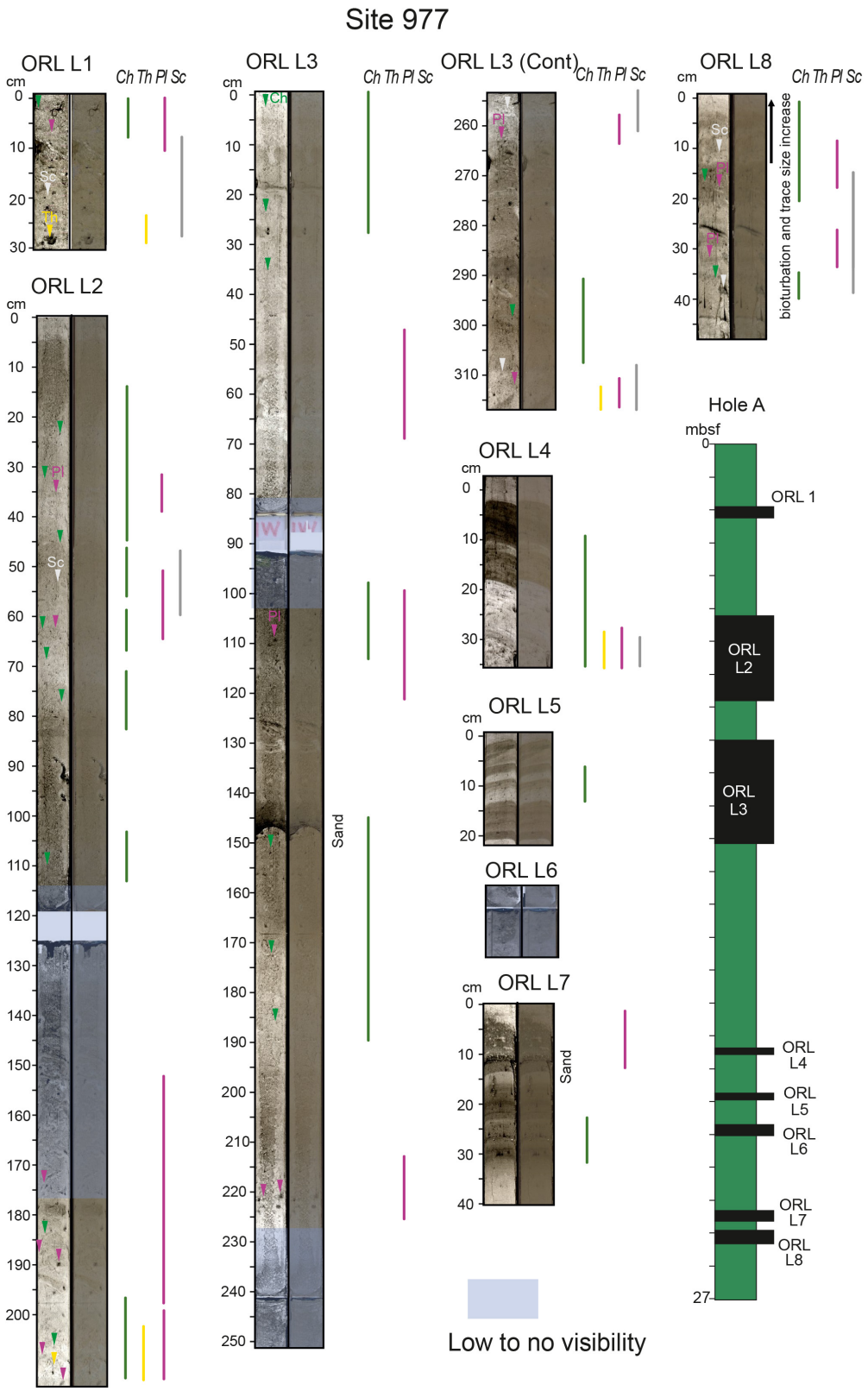

Figure VII.4. ORLs differentiated in Site 977 with the indication of the trace fossil distribution. Ch = Chondrites, Pl = Planolites, Sc = Scolicia, Th = Thalassinoides.

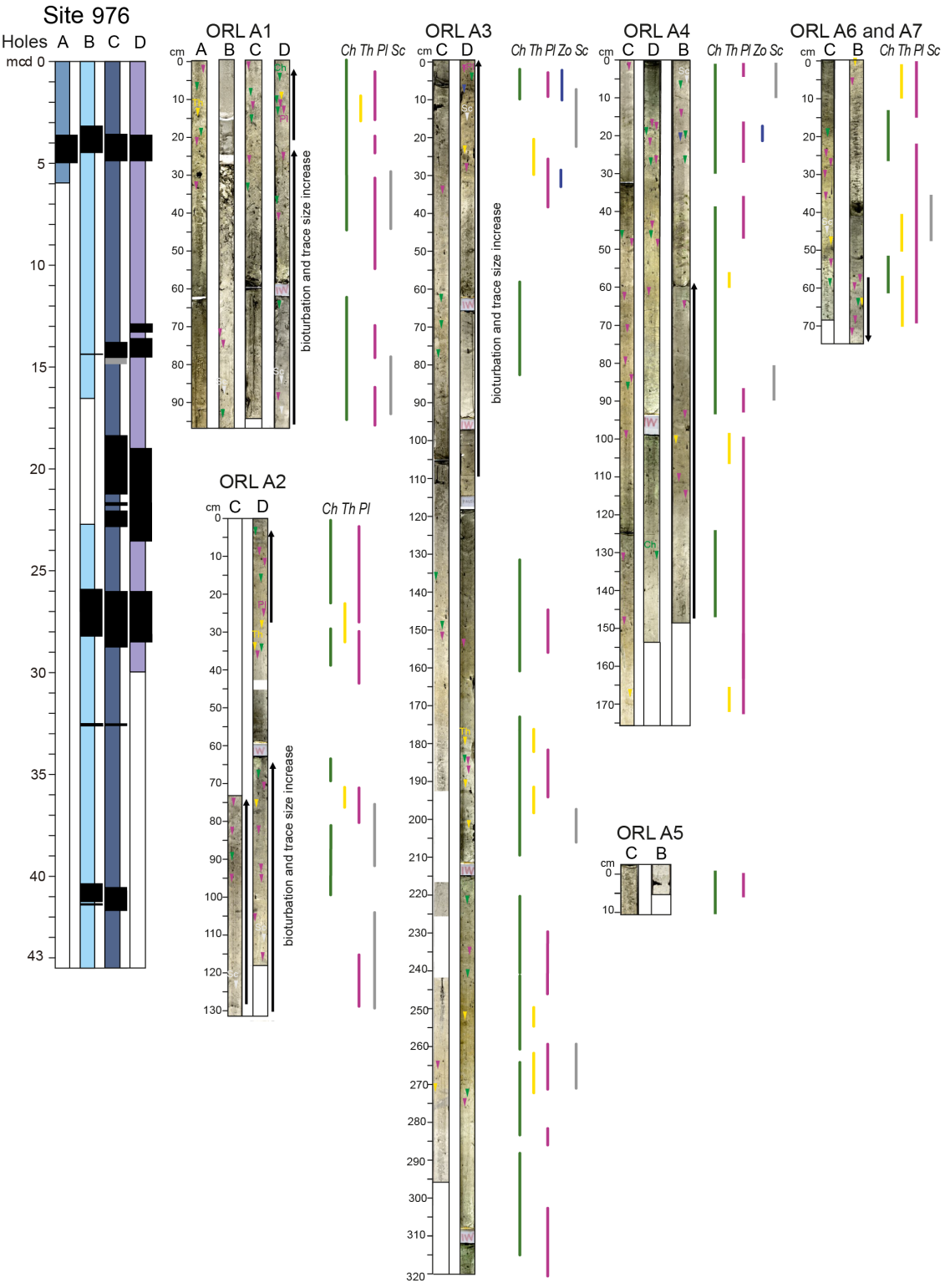

Figure VII.5. ORLs differentiated in Site 976 with the indication of the trace fossil distribution. *Ch* = *Chondrites*, *Pl* = *Planolites*, *Sc* = *Scolicia*, Th = *Thalassinoides*. The 4 holes that were drilled in Site 976 are indicated from A to D.

Table VII.3. ORLs are defined by the ODP scientific time in Site 976. Type as defined in this paper, sedimentary features, ichnological features and TOC measurements from the Initial Reports.

ORL	Type	Sedimentary features	Ichnological features	TOC
976				
A1	Type 1	100 cm layer without identifiable sedimentary structures	Highly bioturbated with *Chondrites*, *Planolites* and *Thalassinoides*. *Scolicia* is abundant in the base and probably present in the middle part of the interval. Burrow sizes increase from the bottom to the middle (30 cm) and then decrease to the top	1.13. 0.8, 0.95, 0.93
A2	Type 1	110 to 50 cm layer without identifiable sedimentary structures. A colour change appears, with lighter sediment at the base and darker at the top	Presence of *Scolicia* in the base. *Chondrites*, *Planolites* and *Thalassinoides* can be identified in the rest of the interval. The abundance and size of the burrows increase from the bottom to the top of the layer (especially seen in hole C), with a decrease from the middle part (60 cm) in hole D	1.09, 1.1,
A3	Type 2	A long section of up to 320 cm. Variation in grey value with several colour cycles	Presence of *Chondrites*, *Planolites* and *Thalassinoides* in the bottom, middle and top of the section. *Zoophycos* appear at the top of the layer. The size and abundance of the burrows are low, increasing in the middle (190–210 cm) and top of the ORL section	0.97, 1.08, 0.75, 0.560
A4	Type 2	Length up to 170 cm in a section without identifiable sedimentary structures	Presence of *Chondrites*, *Planolites* and *Thalassinoides*. Increase in size and abundance of burrows from the bottom to 50 cm, and then decrease to the top. The possible presence of *Scolicia* in the middle and top of the layer. *Zoophycos* at the top	0.82, 1.1, 0.97,0.92, 1.01
A5	–	Short 10–5 cm layer with no structures	Highly bioturbated with *Chondrites* and *Planolites*	1.19,
A6	Type 1	50–60 cm long with greyscale variations from dark to lighter sediment	*Chondrites*, *Planolites* and *Thalassinoides*. *Scolicia* over the beginning of the layer. The trace size and abundance decrease from the bottom to the top of the layer	1.42, 1.85

VII.4.4. Ichnological and sedimentological features: Types of ORLs

Ichnological (ichnotaxonomy, distribution, size, and abundance of the traces) and sedimentological features —including the thickness of the ORL intervals and grey values in the studied records— allowed us to characterize different ORL types beyond the ones originally described at Sites 976 and 977 (Shipboard Scientific Party, 1996a, 1996b). Differentiation was more feasible for Site 977, as the images and data were more detailed, whereas for Site 976 merely general discernment was attempted. Only the originally described ORLs from ODP are included in this analysis to detail palaeoenvironmental interpretations previously proposed. The differentiated types are as follows (Fig. VII.6):

Type 1: Characterized by a thickness ranging from 30 to 40 cm in Site 977 and up to 120 cm in 976. Bioturbation is generalized, with the presence of a mottled background, and with trace fossils registered throughout the entire ORL, but showing differences from bottom to top. At the base, burrows are abundant and range from 5 cm to a few millimetres. The size and abundance gradually decrease upward. Trace fossil assemblage consists of abundant *Scolicia* and *Planolites*, frequent *Chondrites*, and possible *Thalassinoides* in the base. ORL L1 and ORL L8 of Site 977 (Table VII.2), and ORLs A1, A2 and A6 from Site 976 (Table VII.3) are assigned to this type.

Type 2: Characterized by thick intervals, up to 310 cm, and cyclic changes in colour and bioturbation features, as well as a clear greyscale internal fluctuation. In Site 977, they correspond to the ORLs L2 and L3 (Table VII.2), and in Site 976, they could be assigned to the ORLs A3 and A4 (Table VII.3). Given their thickness and features, an evident differentiation from other parts of the cores, not associated with ORLs, is unclear. Even though a transition from non-ORL bioturbated sediment with big traces to an ORL having unbioturbated or low-bioturbated sediments is recognized. Type 2 also includes heavily to moderately bioturbated intervals.

Type 3: It is characterized by well-developed laminations and absence of bioturbation, as well as an evident peak in the inverted greyscale, and magnetic susceptibility reduction, determining a good differentiation from the surrounding sediments. This type is assigned to ORLs L4, L5 and L7 of Site 977, corresponding to intervals about 20 to 30 cm thick, registered from the end of the penultimate glacial maximum to present (Table VII.2). It cannot be discarded that ORL L6 could also correspond to type 3, but the location between two coring sections makes a conclusive assignation difficult. At Site 976, these laminated ORLs are not present (Table VII.3).

VII.5. Discussion

During ODP Leg 161, other than the classical definition of ORLs based on TOC values (Murat, 1999), the shipboard party relied on further characteristics, e.g., colour and magnetic susceptibility. In the Alboran Sea Basin, significantly higher sedimentation rates than in the eastern basins led to dilution and lower TOC content in ORLs and higher background values. Thus, the ORL definition was based on a 0.8% minimum TOC together with colour contrast and magnetic susceptibility (Murat, 1999). In addition to this, as mentioned, the greyscale was used to extend information based on the observed ichnological features, even though not all the original ORLs present a clear differentiation when the core surface is observed.

VII.5.1. Ichnological features in the ORLs and environmental implications: The role of anoxia

In general, the ichnological information has proven to be a very useful proxy for the characterization of past anoxic events such as the Faraoni Event (upper Hauterivian; Rodríguez-Tovar and Uchman, 2017), the Bonarelli Event (Cenomanian-Turonian boundary; Uchman et al., 2008, 2013a, 2013b; Rodríguez-Tovar et al., 2009, 2020b; Rodríguez-Tovar and Uchman, 2011; Monaco et al., 2012, 2016) and the Toarcian Oceanic Anoxic Event (Early Toarcian; i.e., Rodríguez-Tovar and Uchman, 2010; Reolid et al., 2014; Miguez-Salas et al., 2017, 2018; Rodríguez-Tovar et al., 2017, 2019c). For further information, see the recent review on the Toarcian Oceanic Anoxic Event revealing the variable oxygenation and the absence of global and generalized anoxia (Rodríguez-Tovar, 2021).

The ichnological characteristics of more recent sediments such as the ORLs have been poorly studied, however. Scarce and undetailed references to bioturbation were originally included in ORLs descriptions in the ODP Leg 161 Initial Reports (Shipboard Scientific Party, 1996b), and just recently more detailed ichnological analyses were undertaken (Pérez-Asensio et al., 2020).

The occurrence of ORLs involves complex processes that may depend on such factors as primary productivity, anoxic conditions, and sedimentation rate, which play a variable role according to different authors (Müller and Suess, 1979; Pedersen and Calvert, 1990; Kuypers et al., 2002; Rohling et al., 2015). Again, not only is the increase in the OM flux determinant for the formation of these layers; in fact, oxygen restriction without enhanced productivity might not result in ORLs deposition (Rogerson et al., 2008).

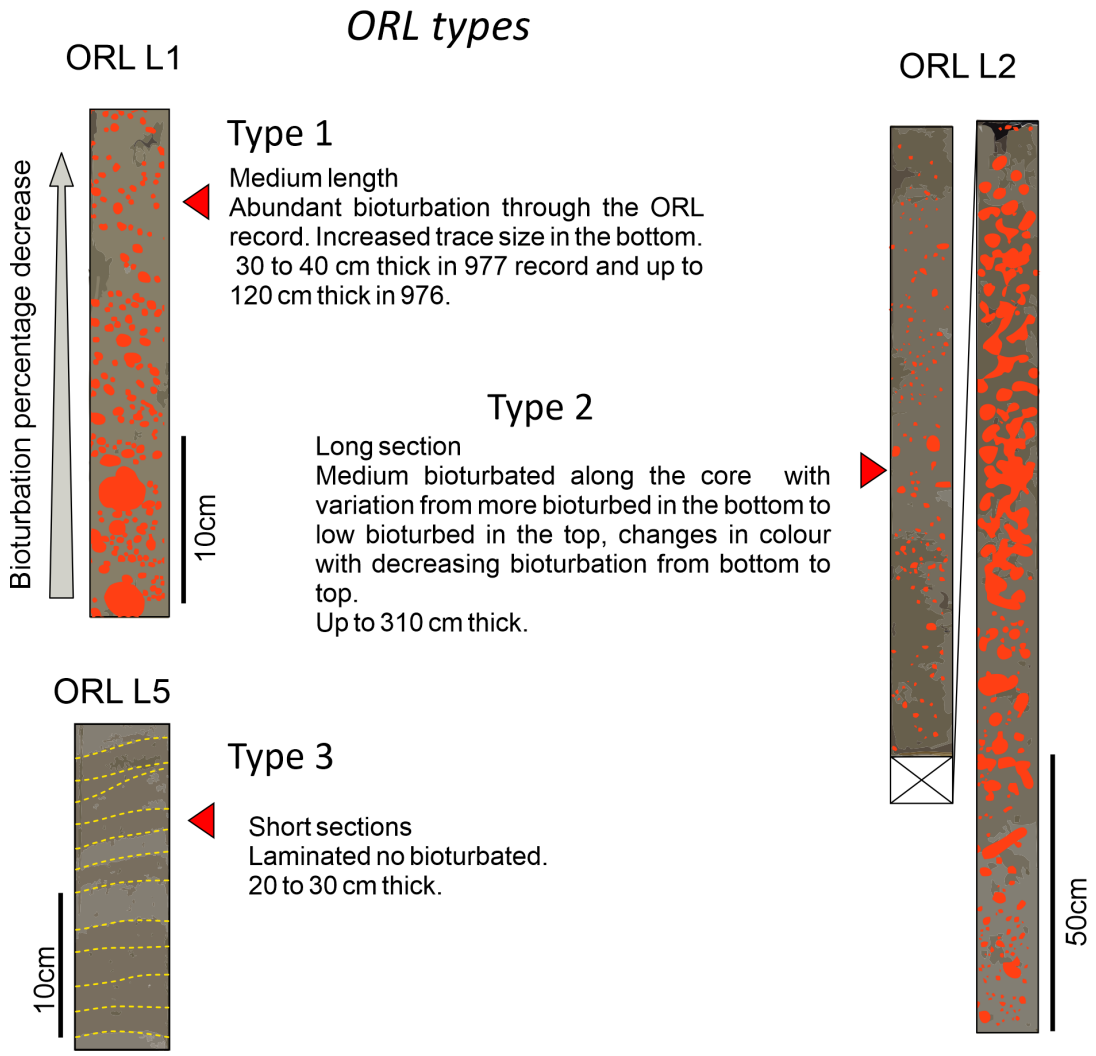

Figure VII.6. Examples of differentiated ORL types with description and schematization.

According to the obtained data, some of the ORLs registered during the Last Glacial Cycle in the Alboran Sea Basin at Sites 977 and 966 support dysoxic (2.0–0.2 ml/l O2) to suboxic (0.2–0.0 ml/l O_2) and anoxic conditions (0.0 ml/l O_2), following values from Tyson and Pearson, 1991 as indicated by variability in the ichnological features and the local presence of lamination. In oxic conditions with a steady flux of benthic food, light sediments (corresponding to non-ORLs) with TOC values below 0.8% are observed, and a well-developed trace maker community determines a variable number of discrete traces imposed upon a mottled background (Fig. VII.7A).

The ichnological assemblage associated with such conditions features the presence of more or less abundant *Thalassinoides* and *Planolites*, with punctual *Scolicia* and *Zoophycos*. Oxygen levels are maintained above the dysoxic threshold with certain fluctuations, which produced the variations evident in the trace fossil assemblage and abundance.

During deposition of the Type 1 ORL, generalized dysoxic conditions with abundant benthic food gave rise to discrete traces, and a mottled background, in combination with darkly

coloured sediments and high TOC values of 0.8 to 1.2% (Fig. VII.7B). Dysoxic conditions impeded a well-developed trace maker community. Upward, decreases in both the abundance and size of biogenic structures reveal the deterioration of palaeoenvironmental conditions during ORL deposition. In Type 2 ORL, variations in colour, TOC, and trace fossil assemblage are observed, with lighter sediment presenting moderately abundant traces and darker intervals presenting low or absent bioturbation. This suggests variable oxygen conditions during the ORL deposition, from moderately to extremely dysoxic (Fig. VII.7C).

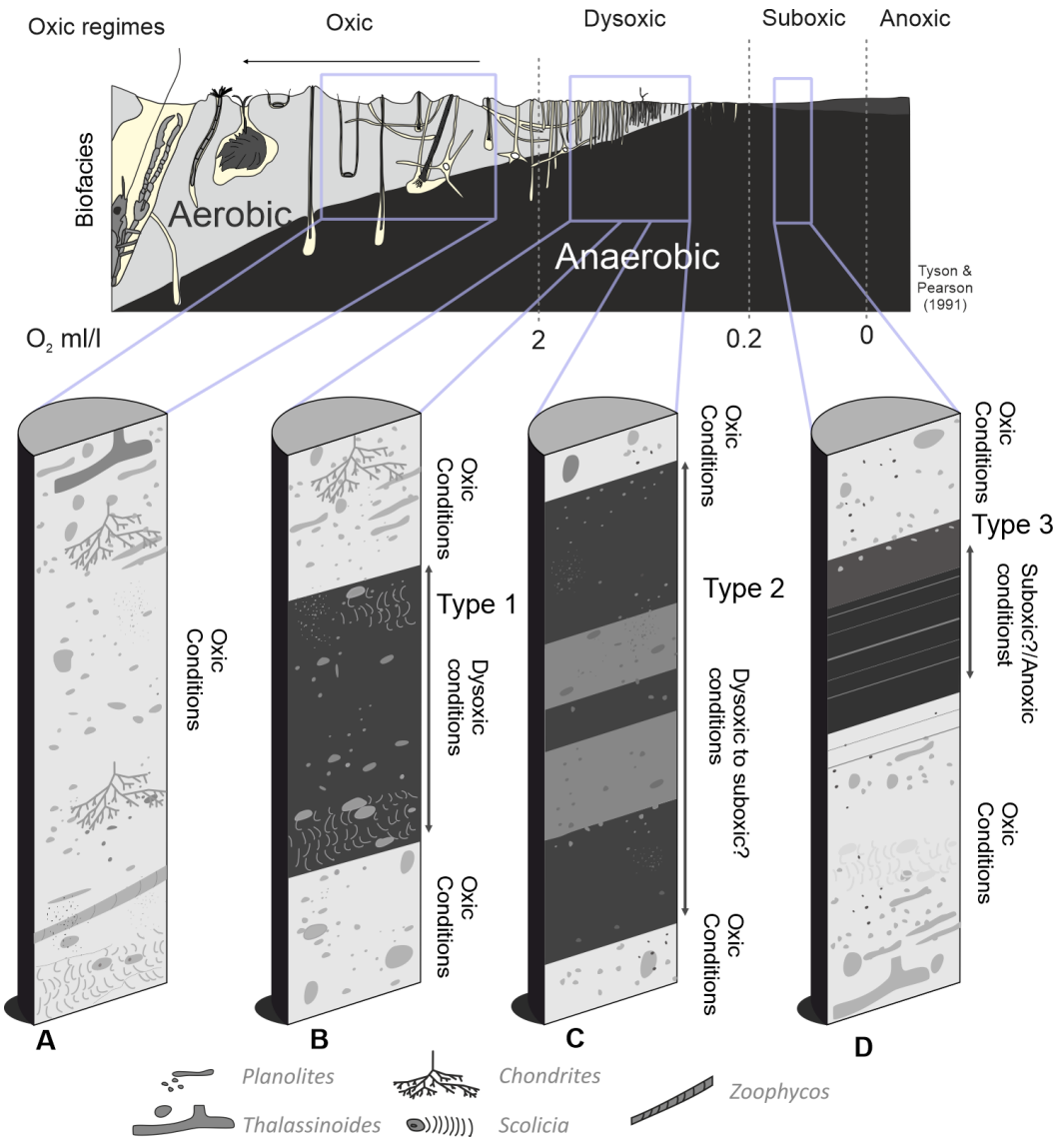

Figure VII.7. Top: Schematization of the oxic regimes and tiering according to Tyson and Pearson (1991). Bottom: Scenarios for oxygen conditions according to the ORL types proposed (see text for explanation).

Type 3 ORL corresponds to laminated and non-bioturbated short intervals, indicating an inhabitable macrobenthic environment. The absence of a macrobenthic tracemaker community supports suboxic or anoxic conditions (Fig. VII.7D).

According to the above, even though ORLs has been commonly related to periods of deep-water stagnation and oxygen depletion (e.g., Rogerson et al., 2008; Rohling et al., 2015; Pérez-Asensio et al., 2020), and largely associated with laminated, non-bioturbated, or only scarcely bioturbated sediments, our results are indicative of significant variability in palaeoenvironmental conditions. All the originally proposed ORLs at Site 976 and most of those at Site 977 —corresponding to ORLs types 1 and 2— are bioturbated, including a mottled background and discrete traces. This fact supports the absence of generalized anoxic conditions during some of the ORLintervals in the Alboran Sea Basin, but rather oxygenated conditions favouring the development of a macrobenthic trace maker community and, in turn, bioturbation. Only ORLs assigned to Type 3, showing lamination and absence/scarce bioturbation, could be indicative of such anoxic conditions.

VII.5.2. ORL position, fact or artefact?

Traditionally ORLs are defined by increased TOC values concerning surrounding sediments. Nonetheless, post-depositional modifications can lead to a drop in TOC percentages —the presence of "ghost" layers only detectable by geochemical data, as observed in other basins (Jung et al., 1997; Larrasoaña et al., 2006; Löwemark et al., 2006). Thus, colour and ichnological information evidencing variations in oxygen conditions even when TOC enrichment has been lost could be used to recognize ORL intervals irrespective of TOC values. Based on this possibility, we tentatively propose the existence of new intervals, including some that could have TOC contents below the 0.8% TOC threshold.

In Fig. VII.8 these new intervals are presented, including some images that serve to visualize variations in the core surface. The intervals are thin and tend to correlate with the fluctuations observed in the $[Ca^{+2}]$ plot and the Sea Surface Temperature (SST) (Fig. VII.8). Such good correlation evidence that colour variations respond to climate changes taking place in the Northern Hemisphere and over the Alboran Sea.

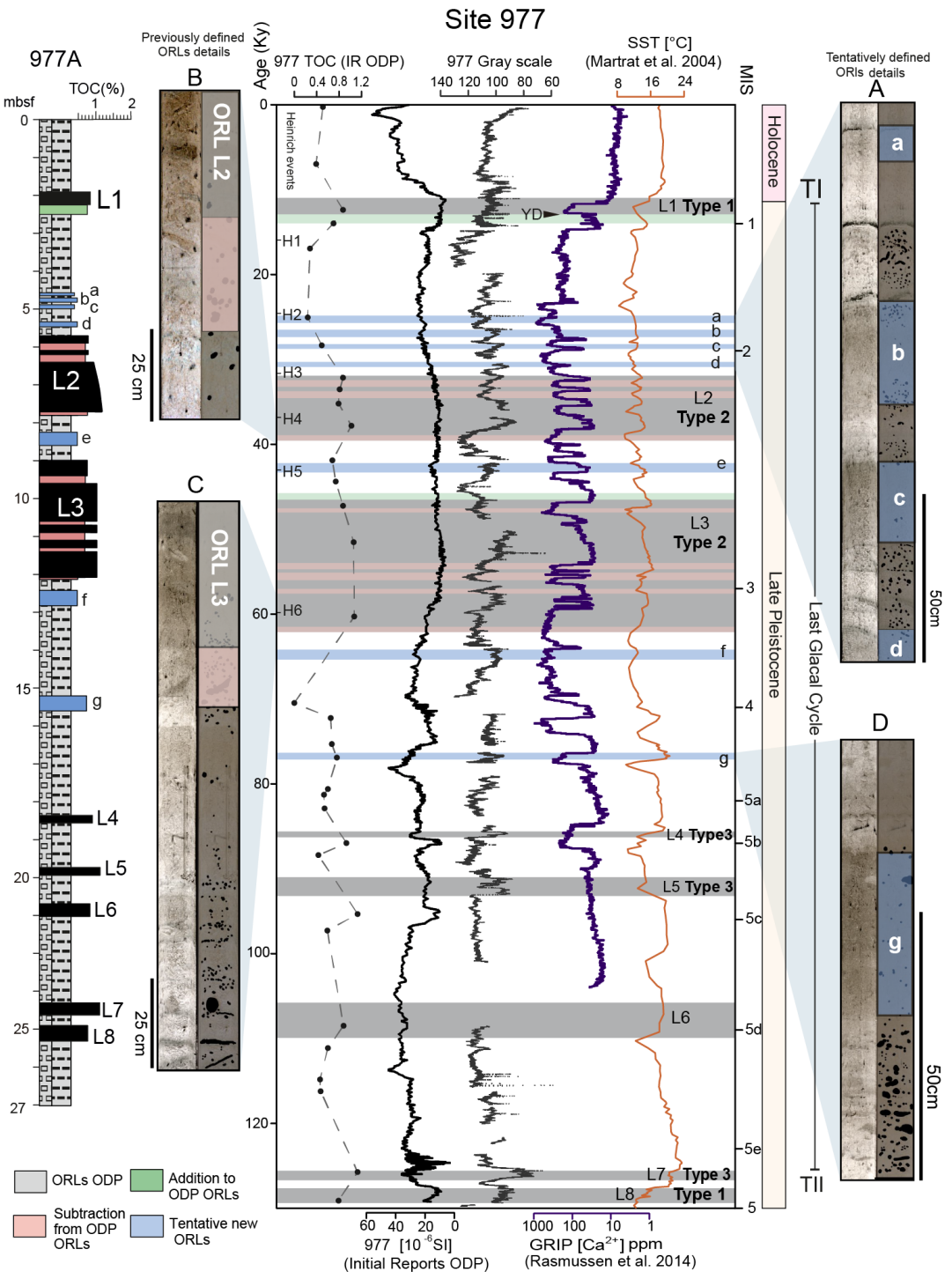

Figure VII.8. Correlation between the greyscale and colour values, TOC, magnetic susceptibility, and sea surface temperature (SST) for Site 977. The position of the ORLs is indicated, with differentiation between the original proposal from the initial reports (grey), the added parts (green) and the removed parts (red), and the newly defined ORLs (a to g; blue). MIS: Marine Isotope Stage. The 6 Heinrich Events are indicated in the left part of the figure. In addition, 4 details of the core surface of both newly defined ORLs and changes in the previously defined ORLs are added indicated with the letters A, B, C and D. $[Ca^{+2}]$ here is a proxy for stadial in the northern hemisphere, as it records the dust concentration over Greenland, indicative of changes in regional and hemispheric circulation changes. (For interpretation of the references to colour in this figure legend, the reader is referred to the web version of this article).

As mentioned before, in addition to the new ORL intervals proposed, some of the original ORLs have been modified by extensions or subtractions of certain parts. One clear example is ORL 1, profusely studied, with a well-known position and age. According to the greyscale analysis, its position with respect to the ODP initial reports must be modified, by extension in the lower part, suggesting that this layer is probably thicker than originally indicated. This proposal is concordant with the age obtained in studies of the ORL 1 in other records in the Mediterranean Sea (Cacho et al., 2002; Rogerson et al., 2008; Rodrigo-Gámiz et al., 2011; Martínez-Ruiz et al., 2015). Furthermore, the extension is in consonance with the proposed ages of ORL L1 in the Alboran Sea (Jiménez-Espejo et al., 2015; Pérez-Asensio et al., 2020), since when converting the depth data to age using the Martrat et al. (2004) age model, the ORL L1 extends from 14 ka to 8 ka. The opposite occurs with ORLs L2 and L3, where colour changes might evidence an overestimation of the thickness of ORL L2 and L3 originally considered.

According to the above, the originally proposed ORL position, number, thickness and age in the Alboran Sea Basin could be different in some cases. Variations in the colour and ichnological features within thicker ORLs could, moreover, be indicative of changes in palaeoenvironmental conditions during the ORLs deposition, revealing interruptions during ORL deposition or the existence of multiple shorter ORL events that were combined in the original description.

VII.5.3. Palaeoenvironmental and palaeoceanographic implications

It must be stressed that ORLs cannot be correlated with the eastern sapropels (Rohling et al., 2015): a major difference, apart from lower carbon content, resides in chronology, since ORLs were not always deposited during the same time intervals. As stated by Rogerson et al., 2008, ORLs do not occur during pluvial maxima every time; and the origin cannot, therefore, be directly related to the irruption of freshwater. In the Eastern Mediterranean sapropel origin is described as a result of an increase in precipitation and subsequent freshening of the surface layer that produces buoyancy increase and deep-water stagnation, in combination with productivity blooms produced by the nutrients reaching the sea within the rivers (Rohling et al., 2015): It is possible, however, that the irruption of freshwater from continental ice not coincident with pluvial maximum, especially from the Alps, could induce the buoyancy increase decoupled from pluvial maxima during deglaciation events (Rogerson et al., 2008).

Recent works, focused on the same ODP Sites from the Alboran Sea Basin, demonstrate that there is a correlation between the ichnological features variations and palaeoceanographic conditions, especially in terms of changes in ventilation and benthic food availability (Casanova-Arenillas et al., 2021). Thus, the integration of ichnological information with other sedimentological characteristics is one key to understanding the palaeoenvironment associated with the different types of ORLs over the Last Glacial Cycle. The occurrence of the ORLs —

whether previously defined or tentatively proposed here— is coherent with restricted ventilation during some of the warming periods over the last interglacial, and at least partial oxygenation occurring between these depositional events (Fig. VII.8). The significance of these restriction events in combination with factors including the LIW characteristics could have led to the differences among the different ORLs, or even stand as the main cause behind these differences, as LIW composition can affect the sinking and composition of the WMDW (Incarbona and Sprovieri, 2020). Notably, during Heinrich Events, low saline water coming from the polar iceberg melting entered through the Gibraltar Strait, impacting circulation in the Mediterranean (Cacho et al., 2002; Sierro et al., 2005), notwithstanding, it did not produce substantial deep-water restriction (Sierro et al., 2005), which is coherent with the apparent absence of any relation between the Heinrich Events and either the greyscale of the bioturbational features in the studied record. Over the Last Glacial Cycle, intense variation in atmospheric conditions resulted in rapid changes in climate conditions over the Western Mediterranean (Martrat et al., 2004; Bazzicalupo et al., 2018), hence in the atmosphere/ocean dynamics, affecting deep-water masses and their ventilation (Cacho et al., 2002). In particular, the Last Glacial Maximum is associated with cold and arid conditions (Lionello, 2012) that affected oceanographic conditions driving ORL formation. Still, the correlation of ORLs with climate events is not fully understood. Comparison of the three differentiated types of ORLs at Site 977 with the SST record (Martrat et al., 2004) in conjunction with the use of calcium ion concentration data ([Ca^{2+}]) for better visualization of the stadial/interstadial variation in the northern hemisphere (Rasmussen et al., 2014), and the magnetic susceptibility and TOC contents (Shipboard Scientific Party, 1996b), would evidence diverse environmental conditions for these ORL types (Fig. VII.8). Meanwhile, [Ca^{2+}] in the ice cores is an excellent proxy for stadial in the northern hemisphere, as it records the dust concentration, which is indicative of changes in regional and hemispheric circulation (Fischer et al., 2007; Rasmussen et al., 2014).

Type 1, as the most bioturbated one, appears in both Terminations I and II (TI and TII), in agreement with the onset of warmer conditions and thus less deep-water sinking. Type 1, taking in ORL L1 from Site 977 and probably A1 from Site 976, is defined as the basin-wide ORL 1 (Rogerson et al., 2008; Pérez-Asensio et al., 2020). Under Type 1 the ORL L8 can also be included, having formed towards the end of the penultimate glacial period warming phase, and having ended following the interglacial post-glacial warm period. As type 1 ORLs present abundant bioturbation, it can be interpreted as revealing generalized oxic/dysoxic conditions that occurred at least partially during parts of the deposition of this layer. Therefore, extended suboxic/anoxic conditions were not reached during the TI and TII in this Basin, and the dysoxic conditions were not constant. ORL type 1 is accordingly suggested to be mostly related to productivity variations rather than to a strictly anoxic environment. The fact that both type 1 ORLs (ORLs L1 and L8) appear during a similar climatic trend, at the beginning of Terminations I and II (Fig. VII.8), further supports the idea that similar events occurred at the end of the penultimate and last glacial periods, even though the two deglaciations show differences —for example, the absence of a cold spell like the younger dryads in the TII (Martrat

et al., 2014). A similar ORL appearing in the deglaciation event might signal enhanced productivity events with no strong deep-water restriction, allowing for a diverse trace-maker community. At the end of the Last Glacial Period, enhanced primary productivity has been linked to Atlantic inflow in the Alboran Basin because of the wind and jet-induced upwellings (Ausín et al., 2015a, 2015b) during the end terminations and Younger Dryas; a similar context could be envisaged for the TII.

Type 2, including thicker ORL intervals with internal cyclic changes in bioturbation and colour than when plotted with SST and [Ca^{+2}], shows a correlation with the DO interstadial-stadial cycles. Assuming a direct correlation between the climate changes in the Mediterranean and the deep-sea bottom conditions (e.g., Martrat et al., 2004; Frigola et al., 2008), these cyclic variations suggest oxygenation changes throughout the entire Alboran Basin during the period of deposition of these thicker layers.

Type 3 ORL correlates with warm periods, except for ORL L4, which is associated with a cold phase. Type 3 is interpreted to be related to suboxic/anoxic conditions based on the absence of bioturbation and a well-developed lamination. When considering climate conditions, the relation to warming phases is recognized but points to highly variable correlation; at different phases of a warm interstadial, at the beginning and the end of the warming phase, and the peak of the interstadial (Fig. VII.8). Interestingly, some of the Type 3 ORL ages coincide with the low $\delta^{18}O$ values in Soreq Cave speleothems (Bar-Matthews et al., 2000) from the Eastern Mediterranean related to sapropel formation: ORL L4 (~85.5- ~86.3 ka) could match low $\delta^{18}O$ (~85- ~ 79 ka) related to S3 formation (83 ka; Rossignol-Strick and Paterne, 1999), while ORL L7 (~125.5- ~126.6 ka) fits with the low $\delta^{18}O$ (~124- ~ 119 ka) related to S5 formation (124.2 ± 2 ka; Rossignol-Strick and Paterne, 1999). Even though we cannot assign a type to ORL L6, due to visibility issues, it is dated at ~105.8- ~110 ka, and could coincide with the $\delta^{18}O$ (~108- ~ 100 ka) related to S4 (103.3 ± 3.4 ka, Rossignol-Strick and Paterne, 1999). This means that not all the ORLs are decoupled from the sapropel events in the East and that the conditions producing sapropels likewise bear an impact on ORL formation at certain points of the geological record, and interestingly this coincidence is with the best-defined, bioturbation lacking, suboxic/anoxic ORLs from the Alboran Sea Basin.

Considering the subtractions and additions of the Original ORLs (Fig. VII.8) and the new, tentatively defined ORLs (a, b, d, e, f, g in Fig. VII.8), a clear coincidence can be seen in many cases with the climatic variations of the northern hemisphere. The fact that some of them appear in the middle of warm periods or during warming phases agrees with the theoretical model of deep-water renewal being controlled by winter's cold north winds, and the entry of freshwater from continental ice melting; altogether, they induce buoyancy changes that inhibit water sinking, and imply reduced Bernoulli Ventilation due to sea level increase (Cacho et al., 2002; Frigola et al., 2008; Rogerson et al., 2008). This correlation supports the connection of the deep environments in the Western Mediterranean with the Westerlies and the AMOC

variations during climatic changes. Such a correlation is not always observed, however, and some ORLs (newly or previously defined) may not appear during warming phases or might even be coincident with minimum SST values (e.g., ORLs "a", or "L1" Fig. VII.8). In sum, there is a complicate combination of multiple factors controlling the events, not producing an always coincident response to the same climatic variations, implying there is a need for much further exploration of the different ORLs of the Mediterranean, beyond the ORL 1, and extending to previous glacial cycles.

VII.6. Conclusions

A detailed sedimentological and ichnological analysis of the ORLs deposited over the Last Glacial Cycle in the Alboran Sea Basin and recorded at ODP Sites 977 and 976, reveals the presence of different types of ORLs and supports variable environmental conditions over this time interval resulting in ORL deposition. Three ORL types (1, 2 and 3) are recognized according to variable palaeoenvironmental parameters, and main variations in oxygen conditions. Type 1, with an intermediate thickness (30 to 40 cm), corresponds to high to moderate bioturbated intervals. The trace fossil assemblage consists of abundant *Scolicia* and *Planolites*, frequent *Chondrites*, and possible *Thalassinoides* in the base, supporting dysoxic conditions during deposition, which prevented a well-developed trace maker community. Type 2 corresponds to thicker intervals (up to 310 cm), showing an alternance of highly to moderately bioturbated intervals, revealing variable oxygen conditions from moderate to extremely dysoxic or even suboxic ones. Type 3 consists of thin (20 to 30 cm), laminated intervals characterized by an absence of bioturbation, indicating anoxic or suboxic conditions and determining an unfavourable macrobenthic habitat.

Ichnological and colour analyses made it possible to refine the original ORLs characterization, by adding new ones, or extending or subtracting parts of the initially described ORLs. Seven new intervals have been tentatively added (a, b, c, d, e, f, g) to the originally proposed ORLs at Site 977. The amended ORLs show a correlation between the Sea Surface Temperatures and the recognized climatic events over the Last Glacial Cycle in the Alboran Sea Basin.

The conducted integrative research improves the original definition of the ORLs based exclusively on colour contrast, magnetic susceptibility, and TOC, thus providing new insights to advance our understanding of ORL deposition in the Western Mediterranean.

Chapter VIII

Reconstructing deep-sea palaeoenvironments in the Western Alboran Sea Basin over the end of the Last Glacial Period and the Holocene: Insights from a multiproxy approach

***Submitted to Palaeogeography, Palaeoclimatology, Palaeoecology in 2023**

S. Casanova-Arenillas[1], F. Martínez-Ruiz[2], F. J. Rodríguez-Tovar[1], J. N. Pérez-Asensio[1], R. Monedero-Contreras[2], V. Villasante-Marcos[3]

[1] Departamento de Estratigrafía y Paleontología, Universidad de Granada, Avda. Fuente Nueva s/n, 18071, Granada, Spain

[2] Instituto Andaluz de Ciencias de la Tierra (CSIC-UGR), Avenida de las Palmeras 4, 18100, Armilla, Granada, Spain

[3] Laboratorio de Magnetismo de Materiales y Magnetismo Ambiental (L-MAGNA), Instituto Geográfico Nacional, Real Observatorio de Madrid, C/Alfonso XII, 3, 29014, Madrid, Spain

Abstract

A deep-sea sediment record from the Western Alboran Basin has been analysed using a multiproxy approach, integrating sedimentological features (i.e., sediment colour), magnetic susceptibility, elemental ratios, benthic foraminiferal assemblages, and ichnological characteristics to gain new insights into how deep-sea environments and palaeoceanographic conditions have responded to climate change over the last 37 kyr. Furthermore, the combination of proxies made it possible to recognize diagenetic signals and interpret new low-frequency events in the deep basin. Significant fluctuating oxygenation is recognized in the Western Alboran Basin. Short-term periodic low-oxygen events are recorded, especially during Heinrich Stadials 2 and 3 (HS 2 and HS 3) and Glacial interstadials 8 and 5 (GI 8 to GI 5), where the presence of a discontinuous previously described Organic Rich Layer 2 (ORL 2) is inferred. From the Last Glacial Maximum (LGM) to the present day, the basin reached its minimum oxygenation between 16 kyr before the present (BP) and 8 kyr BP, which corresponds to a period that includes the end of the Heinrich Stadial 1 (HS 1) and the Organic Rich Layer 1 (ORL 1). During this period, a number of events can be linked to changes in oxygen conditions: i) the inception of low oxygen conditions during the first stage of the HS1; ii) a reoxygenation that occurred during the pre-ORL 1, between the demise of Heinrich Event 1.1 (HE 1.1) and the inception of the Bølling-Allerød (BA); iii) the ORL 1 inception during the BA, the onset of low oxygenation conditions involving punctual short duration reoxygenation events that are indicated by several proxies; iv) a partial discontinuous reoxygenation during the Younger Dryas (YD); v) the return to low-oxygen conditions at the end of ORL 1; and vi) a rapid reoxygenation at 8 kyr BP along with the demise of the ORL 1.

VIII.1. Introduction

The Mediterranean Sea (Fig. VIII.1) has proven to be an exceptional setting for palaeoclimatic reconstructions, offering significant potential for scientific research while also being crucial for forecasting the consequences of current climate change (Stanley, 1972; Giorgi, 2006; Lionello et al., 2006; Durrieu de Madron et al., 2011; Xoplaki et al., 2012; Martínez-Ruiz et al., 2015; Rohling et al., 2015; Borreggine et al., 2017). The basin's unique features —particularly its semi-enclosed nature and short residence times— make it highly sensitive to climate variability (Stanley, 1972; Durrieu de Madron et al., 2011). The Mediterranean Sea also features an excellent availability of high-resolution records with which to study past climate change (Lionello et al., 2006). In addition, the Mediterranean has recorded the evolution of northern and middle-latitude climates, making it an exceptional site for discerning global interconnections among regional and global climate systems (Lionello et al., 2006). Among its subbasins, the Alboran Basin (Fig. VIII.1) is particularly interesting. Its high sedimentation rates enable high-resolution studies, and its proximity to the Strait of Gibraltar sheds light on

the interconnections between the Atlantic and Mediterranean (Rogerson et al., 2012; Martínez-Ruiz et al., 2015).

Recent studies have explored palaeocirculation, palaeoclimate, and past environmental changes in the context of the Mediterranean Sea, as well as the sedimentology and oceanographic dynamics of the Alboran Sea (Allen et al., 1999; Cacho et al., 1999; Moreno et al., 2002; Sierro et al., 2005; Martrat et al., 2007; Frigola et al., 2008; Lejeusne et al., 2010; Martínez-Ruiz et al., 2015; Rohling et al., 2015; Pérez-Asensio et al., 2020; Sierro et al., 2020; Casanova-Arenillas et al., 2021, among others). Still, many uncertainties persist regarding past environmental conditions and ocean-atmosphere interactions in the Western Mediterranean. For instance, the triggering processes behind the oxygen restriction events that produced the Organic Rich Layers (ORLs) deposition in the Western Mediterranean are intriguing and poorly understood (e.g., Rogerson et al., 2008; Rohling et al., 2015). Remarkably, there is a lack of studies about ORLs older than the more recent ORL1, associated with the last Deglaciation, with many interpretations about the mechanisms of formation being dragged only from this more recent layer (ORL 1).

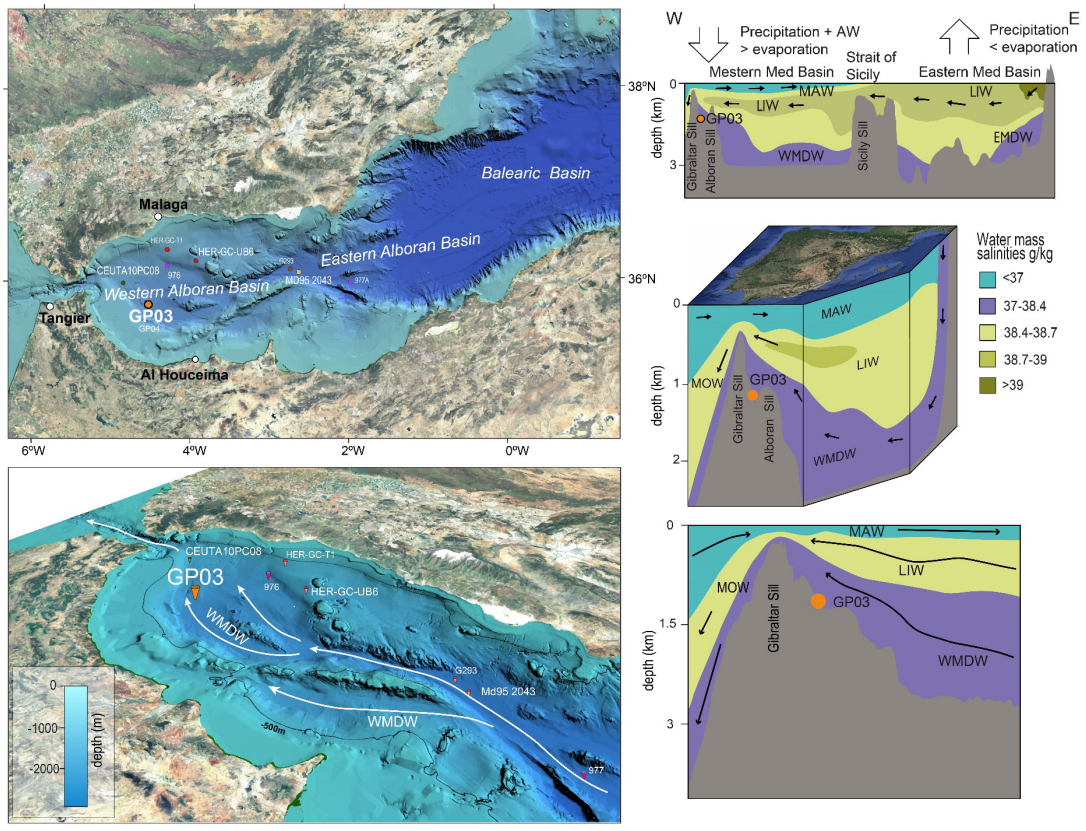

Figure VIII.1. Location of the studied GP03 core in the Western Alboran Basin (Western Mediterranean) and other surrounding cores (GP04, 976, 977, G293, Md95 2043, HER-GC-T1, HER-GC-UB6, and CEUTA 10PC08) added for reference. Water masses from the Mediterranean are represented at different depths, and their circulation is represented. EMDW: Eastern Mediterranean Deep Water, LIW: Levantine Intermediate Water, MAW: Modified Atlantic Water, WMDW: Western Mediterranean Deep Water.

Throughout the past 37 kyr, the Northern Hemisphere has experienced significant climate variability. The Last Glacial Period is characterized by rapid warmings followed by slow returns to colder conditions, known as DO cycles (Dansgaard et al., 1982; Johnsen et al., 1992; Bond et al., 1993, 1997; Dansgaard et al., 1993; Rasmussen et al., 2014). In addition, periodic events of ice sheet rupture and iceberg migration occurred during the Last Glaciation; they are known as the Heinrich Events (HE), and the associated cold periods as the Heinrich Stadial (HS; Heinrich, 1988; Bond et al., 1992; Andrews and Voelker, 2018). The melting of these icebergs on their way southward changed the surface water salinity over the Atlantic and the Mediterranean, with significant consequences for both ocean systems (Sierro et al., 2005). The causes and mechanisms of these intra-glacial climate changes are still under debate, although more recent advances correlate them to the ice sheet-ocean-atmosphere system, to astronomical changes, and to consequential episodic calving of ice sheets (e.g., Boers et al., 2018; Li and Born, 2019; Rousseau et al., 2022). Rapid climate variability stands as an intriguing example of abrupt climate change having no consistent relationship with external astronomical forcing.

The impact of DO warming on the Earth's system has been extensively studied, as it implies changes of 10 °C to 12 °C and a vast reorganization of marine and atmospheric configurations (Kindler et al., 2014; Boers et al., 2018) in very short periods: less than 100 years on average (Wolff et al., 2010). Such rapid climate shifts are suitable analogues for understanding current climate change. Their possible impact on environmental conditions in the Mediterranean Sea is especially interesting because of the correlation with low oxygenation in the deep basin over geological timescales (Frigola et al., 2008) and substantial reconfigurations in oceanographic conditions and ecological variations in continental regions (Cacho et al., 1999; Moreno et al., 2002; Sánchez Goñi et al., 2002; Martrat et al., 2004; Malanotte-Rizzoli et al., 2014).

In this study, a multiproxy approach that combines sedimentological, palaeontological, geochemical, and magnetic proxies was applied to reconstruct the impact of climate variability on deep basin redox conditions. The obtained data allowed us to decipher environmental conditions in the deep Western Alboran Basin and its response to rapid climate variations. New insights into this scenario likewise prove useful to envisage possible future responses to rapid anthropogenic climate change.

VIII.2. The Alboran Basin: A multiproxy approach

VII.2.1. The Western Alboran Basin setting

The studied site, GP03, is located in the westernmost Mediterranean Sea, the Alboran Basin, which is separated from the Atlantic Ocean by the Strait of Gibraltar. It opens eastward to the Balearic Basin, reaching a depth of 3000 m below the seafloor (mbsf) (Fig. VIII.1). From the Balearic Basin, the water depth decreases gradually across the Alboran Basin on a gentle slope towards the Strait of Gibraltar with a minimum depth of approximately 300 mbsf in the Camarinal Sill. The Western Alboran Basin has a maximum depth of around 1300 m and is located between the Strait of Gibraltar and the Alboran Sill (Fig. VIII.1), for which reason it is significantly affected by the Atlantic-Mediterranean exchange.

The studied time interval (ca. 37 kyr) encompasses the end of the Last Glaciation, the last deglaciation, and the Holocene (Lowe et al., 2008). The DO climatic variability is recognized in Greenland ice cores (Rasmussen et al., 2014) and is therefore referred to as Glacial Stadials (GS) for the cold intra-glacial periods and Glacial Interstadials (GI) for the warm intra-glacial periods. Cold and dry conditions characterize stadial phases in the Western Mediterranean region, while warm and humid conditions characterize the interstadials, as pollen records also suggest (Sánchez Goñi et al., 2002; Moreno et al., 2005; Camuera et al., 2019). Other important climatic events took place during the studied period. For instance, the African Humid Period (AHP) occurred between 5.5 kyr BP and 14 kyr BP (Tierney et al., 2017), resulting in a substantial increase in precipitation over northern Africa and the expansion of vegetation cover over the Sahara, which entailed severe impacts on sediment input and runoff to the Mediterranean Basins (Wu et al., 2016, 2018; Tierney et al., 2017; Duhamel et al., 2020; Crocker et al., 2022).

Oceanic circulation in the Mediterranean Sea can be described as anti-estuarine, meaning evaporation exceeds the basin's runoff. There is a constant input of Atlantic water through the Strait of Gibraltar to compensate for this, while a highly saline and dense water flux leaves the basin flowing in the reverse direction (towards the Atlantic Ocean) at higher depths (Wüst, 1961; Millot, 1999; Millot and Taupier-Letage, 2005; Schroeder et al., 2012; Pinardi et al., 2019). Upon entering the Atlantic, this dense water forms the Mediterranean Outflow Water (MOW), influencing Atlantic circulation overall and, in particular, the Atlantic Meridional Overturning Circulation (AMOC; Voelker et al., 2006; Rogerson et al., 2012; Sierro et al., 2020). The Mediterranean water masses are grouped into three primary ones having different salinities and temperatures: Modified Atlantic Water (MAW), Levantine Intermediate Water (LIW), and Mediterranean Deep Water (MDW). The MDW is further subdivided into Eastern

and Western Mediterranean Deep Water (EMDW and WMDW), respectively occupying the depths of the Eastern and Western Mediterranean basins and separated by the Sicily Sill (Fig. VIII.1; Wüst, 1961; Millot, 1999; Millot and Taupier-Letage, 2005; Schroeder et al., 2012). The GP03 site lies under the influence of the WMDW (Fig. VIII.1). Variations in the circulation and renewal of this water mass have a direct influence on the environmental conditions there and, in turn, are correlated with its formation in the Gulf of Lions, its aspiration through the Gibraltar Strait, and local ventilation due to mixing inside different basins (Medoc Group et al., 1970; Lacombe et al., 1985; Millot, 1999; Millot and Taupier-Letage, 2005; Rogerson et al., 2008; Schroeder et al., 2012).

The unique geographic location of the Western Alboran Basin, situated between Africa and the Iberian Peninsula, determines the sediment characteristics in the area, with a predominance of fine mud. The primary source is riverine sediments transported by contourites along-slope, and gravity flows from the shelf to the deep basin, primarily from the Iberian margin and, to a lesser extent, from the African margin (Fabres et al., 2002). These processes are the primary controllers of terrigenous sediment in areas closer to the slope (Ercilla et al., 2019). However, the fine particles may reach the central Alboran Basin setting by means of hypopycnal flows, end member turbidites, and lateral advection by relatively slow bottom currents (Juan et al., 2020). Saharan regions are some of the largest dust sources in the world (Washington et al., 2009) and are undoubtedly a main source of lithogenic particles in this area, greatly influencing the sedimentology of the Alboran Basin (Moreno et al., 2002).

Carbonate biogenic particles from primary phytoplankton producers also significantly contribute to the sediments. This contribution, whether from biogenic carbonate synthesis in the water column above or due to particle advection from other areas, is much higher in the Western than in the Eastern Alboran Basin because of its higher productivity associated with south-Iberian upwelling generated by the Atlantic jet (Masqué et al., 2003). Thus, the general composition at present is influenced by several factors, including river inputs, marine carbonate synthesis in shallow waters, biogenic production in surface waters, and the movement of water masses (Masqué et al., 2003).

One noteworthy feature of the Western Mediterranean is the occurrence of organic-rich layers (ORL; Sigl et al., 1978; Cramp and O'Sullivan, 1999; Murat, 1999; Emeis et al., 2000; Rohling et al., 2015). ORLs share certain features with their Eastern Mediterranean counterparts, the sapropels, and they are generated mainly by the reduced ventilation of the WMDW. The reduction in ventilation, usually tied to an increase in primary production, may be considered a primary cause of the deposition of ORLs (Rogerson et al., 2008; Martínez-Ruiz et al., 2015; Rohling et al., 2015).

VIII.2.2. Multiproxy approach to palaeoenvironmental studies

When studying a sediment record, multiple information can be obtained through different types of approaches, such as chemical and mineral composition, palaeontological features, magnetic properties, and sediment colour. As a result, applying a multiproxy approach utilizing a range of independent proxies from the same environmental changes can lower the uncertainty of the interpretations made. Such a multiproxy approach has been increasingly used in different areas and with varying combinations of proxies (e.g., Nieto-Moreno et al., 2011; Martínez-Ruiz et al., 2015; Bazzicalupo et al., 2022; among many others). Thus, the present study relies on a selection of very different proxies. Another advantage is that the perturbations of diagenetic signals can be discerned, obtaining not only the environmental conditions of the deposition but also some early diagenetic conditions associated with post-depositional changes.

Mineral composition and diagenetic processes influence colour variations. Among other factors, colour can respond to changes in mineral composition, e.g., the presence of mafic minerals with darker shades or increased carbonate appearing lighter in colour. Another critical consideration is the presence of preserved organic matter (OM), which induces the darkening of the sediment and is valuable for detecting organic-rich layers (Thomson et al., 1995; Casanova-Arenillas et al., 2022). It is the main factor controlling colour variation in the studied record.

Magnetic susceptibility has been widely used for decades as a proxy for palaeoenvironmental and palaeoclimatic variations (Thompson and Oldfield, 1986; Maher and Thompson, 1999; Evans and Heller, 200; Liu et al., 2012; Kodama and Hinnov, 2014). Susceptibility reflects contributions from all the minerals present in a sample, either ferromagnetic (high and positive susceptibility, e.g., titanomagnetite, magnetite, greigite, pyrrhotine, goethite, hematite), paramagnetic (low and positive, e.g., Fe-containing clays, pyrite) or diamagnetic (very low and negative, e.g., calcite, quartz). It can be influenced by such processes as variations in terrigenous versus biogenic fractions (e.g., Dinarès-Turell et al., 2003), aeolian versus fluvial terrigenous input (e.g., Larrasoaña et al., 2008), sediment provenance (e.g., Lyons et al., 2012; Oldfield et al., 2014; Hällberg et al., 2020) and early diagenetic remobilization and precipitation of Fe-phases (Liu et al., 2012b). In particular, because iron is very sensitive to redox conditions, the diagenetic alteration of iron oxides and oxyhydroxides makes magnetic susceptibility suitable for studying the post-depositional oxygenation evolution of sediments (e.g., Riedinger et al., 2005; Shin et al., 2018).

VIII.2.2.1 Palaeontological proxies

Ichnological features have proven helpful in studying changes in the environmental conditions of sedimentary basins (Knaust and Bromley, 2012). They are especially valuable for deep marine environments, allowing for interpretation of palaeoenvironmental conditions such as

pore- and bottom-water oxygenation, sedimentation rate, benthic fluxes, and substrate features (e.g., Löwemark et al., 2006; Rodríguez-Tovar et al., 2018; Miguez-Salas et al., 2019; Rodríguez-Tovar, 2021, 2022; Casanova-Arenillas et al., 2022).

Benthic foraminiferal assemblages are also helpful for reconstructing palaeoenvironmental conditions (Caralp, 1988; Murray, 2006; Jorissen et al., 2007; Pérez-Asensio et al., 2020). The key environmental parameters determining benthic foraminiferal assemblages would be organic flux to the ocean floor and bottom water oxygenation, as well as water depth, temperature, and salinity (Morigi et al., 2005; Murray, 2006; Jorissen et al., 2007; Pérez-Asensio and Aguirre, 2010; Pérez-Asensio, 2021).

VIII.2.2.2. Geochemical proxies

Bulk sediment chemical composition is a valuable proxy for palaeoenvironmental reconstructions because it reflects a variety of factors, including riverine and aeolian dust terrigenous input to the basin, environmental conditions at the time of deposition, and post-depositional diagenetic processes (e.g., Calvert and Pedersen, 1993; Tribovillard et al., 2006; Martínez-Ruiz et al., 2015).

Thus, terrigenous input can be reconstructed from various elemental ratios that are commonly used to indicate sediment sources and sedimentological processes (Tribovillard et al., 2006; Calvert and Pedersen, 2007; Algeo and Tribovillard, 2009). Precipitation and wind strength determine variability over the source areas and the atmospheric configuration over the Atlantic, African, and Mediterranean regions (Martínez-Ruiz et al., 2015; Rodrigo-Gámiz et al., 2015; Mesa-Fernández et al., 2022).

The titanium enrichment against Ca (Ti/Ca ratio) evaluates the relative variations between the terrigenous and carbonate fractions and is commonly used as a proxy for increased continental runoff and sediment transport. The value of the Ti/Ca ratio will increase when the terrigenous fraction increases its contribution to the total sediment weight (Arz et al., 1998; Bahr et al., 2005; Calvert and Pedersen, 2007; Jaeschke et al., 2007; Litt et al., 2009; Pierau et al., 2010; Govin et al., 2012; Stuut et al., 2014; Rothwell and Croudace, 2015). The Ti/Ca ratio has recently been used as a proxy for current intensity in the Western Mediterranean due to the potential detrital transport with fine grain winnowing of the currents in the deep basin (Mesa-Fernández et al., 2022). Another important ratio is potassium enrichment (K/Al ratio), used as a proxy for fluvial input in the Alboran Basin, reflecting the illite content variations, a mineral mainly presents in clays derived from the river runoff (Martínez-Ruiz et al., 2015). A high K/Al ratio is usually correlated with humid periods, and given the significant transport capacity of rivers, with an increase in the terrigenous fraction against the carbonate fraction (Jiménez-Espejo et al., 2007; Martínez-Ruiz et al., 2015). Additionally, the Zr/Al ratio can be used to reconstruct past fluctuations in aeolian input (Calvert and Pedersen, 2007; Martínez-Ruiz et al., 2015).

Oxygenation variations in the water column and sediments can be reconstructed from trace metal ratios (e.g., Calvert and Pedersen, 1993; Jones and Manning, 1994; McLennan, 2001; Algeo and Lyons, 2006; Tribovillard et al., 2006; Algeo and Tribovillard, 2009; Algeo and Li, 2020). The authigenic enrichment of molybdenum and uranium is particularly interesting for palaeo-redox studies (Tribovillard et al., 2006; Bennett and Canfield, 2020). Uranium and molybdenum enrichment factors (U EF, Mo EF) are valuable proxies for oxygen content in the sediment, as these elements are stable and non-reactive; they are dissolved in seawater under oxic conditions but authigenically precipitate under low oxygen conditions (Calvert and Pedersen, 1993; Algeo and Tribovillard, 2009). U and Mo are less influenced by changes in the terrigenous fraction, as they tend to have an authigenic origin. They also have short residence times and low content in the upper crust, precipitating directly from the water column owing to changes in environmental factors (Algeo and Tribovillard, 2009; Tribovillard et al., 2012).

Other trace metal proxies can be used to describe redox conditions; here, we also present the Fe/Al ratio using the total Fe. This ratio has been used as a proxy for low oxygen conditions in the water column or for diagenetic processes in ancient sediments (Lyons and Severmann, 2006) associated with iron enrichment due to pyritization in the presence of HS_2. Its enrichment is usually associated with remobilization processes (e.g., dissolution and diffusion) in the sediment column. The downward diffusion can cause its authigenic precipitation (mainly as pyrite) when it reaches euxinic conditions in the underlying sediments (Nijenhuis et al., 2001; Lyons and Severmann, 2006; Clarkson et al., 2014).

Bromine is usually enriched in marine OM. Thus, the enrichment of these elements generally characterizes organic-rich layers and sapropels (Rothwell and Croudace, 2015). Bromine content, or Br/Al and Br/Cl ratios, can serve as proxies for estimating OMin marine sediments and productivity (e.g., Mayer et al., 2007; Ziegler et al., 2008, 2010). In addition, because terrestrial OM is somewhat deficient in bromine, it has also been used to differentiate between OM sources (Mayer et al., 2007; McHugh et al., 2008).

VIII.3. Materials and Methods

VIII.3.1. Lithology and age model

The GP03PC core was obtained during the Gasalb oceanographic cruise onboard the R/V Pelagia in November 2011 in the Western Alboran Sea at latitude 35.7871° N, longitude 4.5343° W, and water depth of 1306.5 mbsl (Fig. VIII.1). The core lithology is homogeneous, with no evident colour changes. It is dominated by dark greenish hemipelagic mud clays with some foraminifera and shell fragments. To obtain the age model for GP03PC, the Ba record was correlated with a twin record, the GP04PC, which was well-dated using mass spectrometry ^{14}C dates on ten sediment intervals and tie points with other records in the Alboran Sea (Morcillo-

Montalbá et al., 2021). The peaks in the Ba/Al and Ba/Ti ratio plots obtained from XRF-analysed samples and X-ray fluorescence (XRF) core scanners, available for both cores, were used to establish a total of 14 tie points, obtaining a reasonably good correlation between the Ba records of both cores (A to N in Fig. VIII.2).

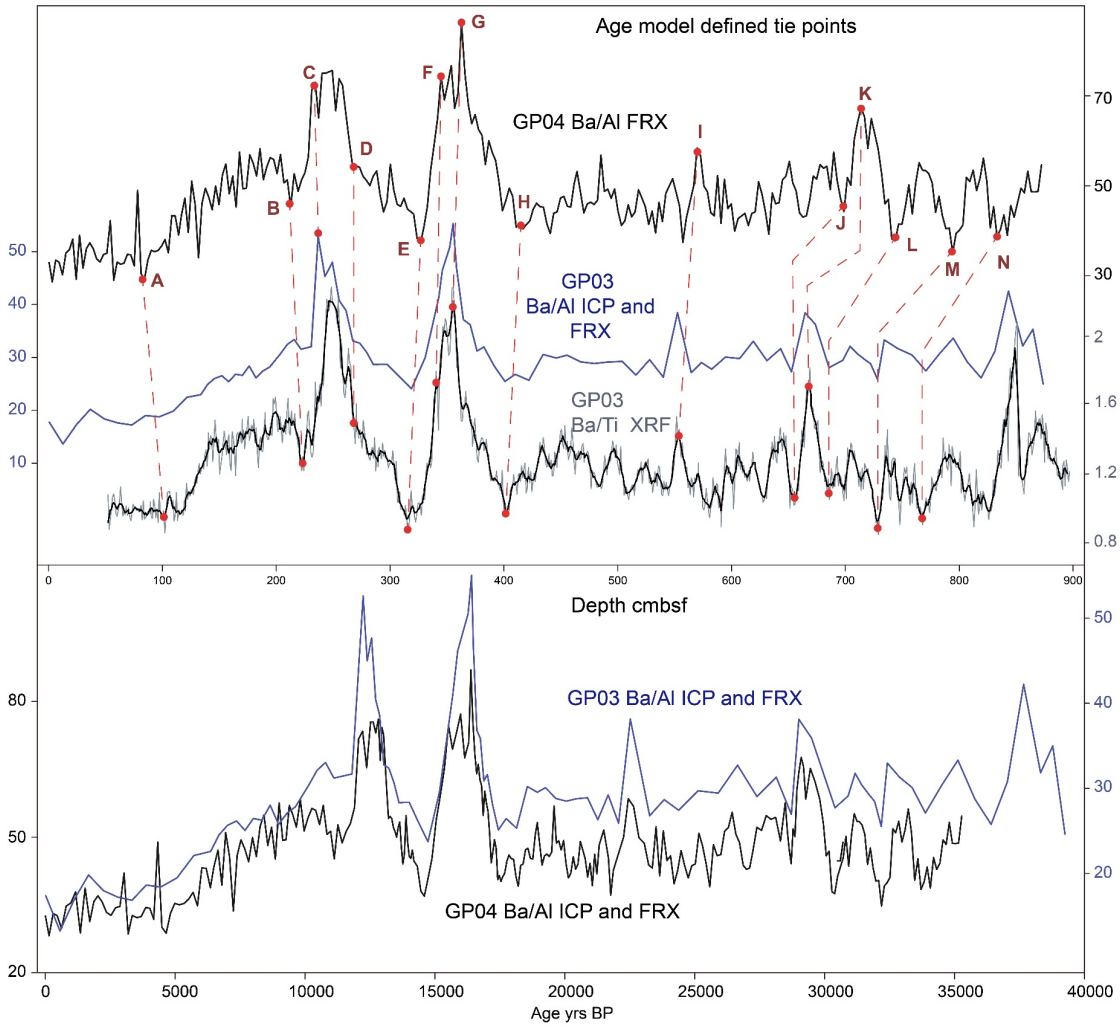

Figure VIII.2. Tie points used for the age model in the Ba plot of GP03 and GP04 (a twin core to the studied GP03), and correlation between the plots from the two cores after being projected by age. cmbsf: centimetres below the sea floor

VIII.3.1. Colour and magnetic properties analyses

Colour analysis of the core sediments was conducted using ImageJ software on high-resolution images. After obtaining the average of the grey values from the RGB spectra, the plot was cleaned of outlier data (Fig. VIII.3). In our case. The colour data was unsuitable for comparing distant core sections, as slight lighting variations between the photographs could introduce changes in the grey value. Still, it is helpful to examine colour changes between consecutive intervals.

After drying at 40° C, the magnetic susceptibility was obtained from discrete samples every 2.5 cm along the core at the Material and Environmental Magnetism Laboratory (*Laboratorio de Magnetismo de Materiales y Magnetismo Ambiental, Instituto Geográ/co Nacional*). Low-frequency (LF, 0.465 kHz) magnetic susceptibility was measured ten times for each sample using Bartington MS3/MS2B dual-frequency equipment. The average mass-normalized values and standard deviations were calculated and plotted (Fig. VIII.3).

VIII.3.3. Palaeontological analysis

VIII.3.3.1. Ichnological features

Ichnological analysis was performed using high-resolution images treated for better visibility of traces (Dorador and Rodríguez-Tovar, 2014b, 2016a, 2018; Casanova-Arenillas et al., 2020). Despite the core sedimentological homogeneity, a general characterization of the ichnological features was possible by differentiating between low and high bioturbated intervals. Thus, intervals without clear bioturbation were not considered in the analysis (Fig. VIII.3).

VIII.3.3.2. Benthic foraminifera

We selected 32 diverse samples to cover the main climatic and palaeoenvironmental events from the Last Glacial Maximum (LGM) and the end of the middle Holocene, around 4 kyr BP, ORL1, and the first half of the Holocene. At least 100 benthic foraminifera were counted and identified in these samples at the species level from the size fraction >125 µm. Raw benthic foraminiferal counts were grouped into three benthic foraminiferal species groups to calculate the relative abundance (%) of these ecological groups, indicative of different oxygen conditions (Schmiedl et al., 2003) (Fig. VIII.4, Fig. VIII.S5; see supplementary material for the list of species belonging to each group and their abundances):

A: Low-oxygen benthic taxa: Species and genera that prefer a low-oxygen environment, including deep infaunal taxa.

B: *Gyroidina* spp. are opportunistic high-oxygen species that appear in the transition from anoxic/suboxic to oxic conditions.

C: High-oxygen benthic taxa: Species and genera that prefer high-oxygen conditions, including epifaunal taxa, miliolids and other oxic species.

Furthermore, *Hyalinea balthica* might be used as a proxy for deep water temperature (Murray, 1973; Van Morkhoven et al., 1986; Hermelin, 1991) since it is a cold water species commonly found in the North Atlantic and in the Mediterranean.

Along the studied interval, relative abundance (%) changes among these three benthic foraminiferal species groups and *H. balthica* reveal variations in environmental conditions.

VIII.3.4. Elemental analysis

Bulk elemental variations were obtained from high-resolution X-ray fluorescence (XRF) core scanner analysis, performed using an Avaatech III Core Scanner system (Serial No. 21) at the CORE LAB laboratory of the University of Barcelona. The scan was performed on the surface of the split core (at 10 mm resolution), which was previously smoothed to remove irregularities and roughness. To prevent contamination, desiccation, and air contact between the sediment surface and the analyser prism, a four mm thick Ultralene layer was applied to the sediment surface. Elemental composition was examined in three independent runs using voltages of 10 kV, 30 kV (Pd-thick filter), and 50 kV (Cu filter), with 2.0 mA and excitation periods of 10, 25, and 35s. Iterative Least Square software (WIN AXIL) from Canberra Eurisys was used to handle the raw data to investigate the X-ray spectra.

Several intervals were selected for discrete sample geochemical analysis involving the previously obtained core scanner analysis, the known age model, and the core surface photographs. The samples were taken every 3 to 6 cm, depending on the interest of the interval. For this study, major elements were determined at the Andalusian Earth Science Institute (IACT) by XRF using a Wavelength Dispersive Spectrometry (WDXRF) Bruker AXS Pioneer S4. Trace elements were measured using inductively coupled plasma mass spectrometry (ICP-MS; Perkin Elmer Sciex Elan 5000) at the Centre of Scientific Instrumentation of the University of Granada (CIC, UGR). The samples were digested with HNO3 and HF. The internal standards for Rh and Re were used in this study. The instrument error was ±2% for an elemental concentration of 50 ppm.

Different ratios were calculated from both analyses (Fig. VIII.5), and the data from the core scanner were compared with the ICP-MS and discrete sample XRF, corroborating and correcting the results of the core scanner.

When studying the lithogenous phase, the elemental data obtained are usually normalized, which can be accomplished using elements with conservative behaviour during weathering, such as aluminium or titanium (Calvert and Pedersen, 2007). Another normalization method that allows comparison with other records is using the enrichment factors (EF) obtained by dividing the normalized values by the average crustal ratio:

$$X_{EF} = [(X/Al)_{sample}/(X/Al)_{PAAS}]$$

Where $(X/Al)_{sample}$ ratio is the concentration in our sample and $(X/Al)_{PAAS}$ is the concentration ratio of the same element in the Post Archean Australian Shale (McLennan, 2001). usually performed with trace metals, as enrichment factors are recommended over bimetal factors as redox proxies (Algeo and Liu, 2020; Bennett and Canfield, 2020). This study presents most results as ratios against Al or Ti, while Mo, U, and Ba data from discrete sample analysis are presented as enrichment factors (EF) for comparison.

VIII.4. Results

VIII.4.1. Sediment properties

The studied record has a homogeneous composition with no evident variations in lithology. Greyscale_analysis (Fig. VIII.3) reveals sudden and distinct shifts in the average grey value of the sediments, suggesting significant changes in their composition. For instance, Greyscale shows an evident diminution during the interval that encompasses the initiation of the second stage of HS1 (approximately 17 kyr BP, Hodell et al., 2017) and the end of ORL1 in the basin (defined around 8 kyr BP; Cacho et al., 2002; Jiménez-Espejo et al., 2008; Rodrigo-Gámiz et al., 2011). The Greyscale value change is associated with OM content, with low values indicating darker sediment with more OM content, and it shows variation in other core sections, having a good correlation with the warm phases between GI9 and GI5 (Fig VIII.3) and rapid variability from HS3 to the inception of ORL1.

The magnetic susceptibility of the sediments presented low but steadily increasing values from 38 kyr BP until the end of the H1 event (between 1.4 and $2.5 \cdot 10^{-7}$ m^3kg^{-1}). Some low periodicity fluctuation accompanies this general trend, showing alternating relative maxima and minima with periods between 1.1 and 2.1 kyr BP until reaching a peak of $2.1 \cdot 10^{-7}$ m^3kg^{-1} at the beginning of the LGM. Afterwards, no further fluctuations are observed; following the low at the LGM, a general increasing trend continues, peaking at $2.5 \cdot 10^{-7}$ m^3kg-1 before HE. After H1, a decrease occurs; there is a low at early ORL1, followed by an increase during the early BA, and finally, a decrease to the end of the BA. The Younger Dryas (YD) is marked by a robust and steep reduction in susceptibility, with an almost symmetrical funnel shape centred at the middle of the YD, reaching values as low as $0.9 \cdot 10^{-7}$ m^3kg^{-1}. After the YD, susceptibility steadily increased, showing minor fluctuations until reaching more stable values of approximately $3 \cdot 10^{-7}$ m^3kg^{-1} in the mid-Holocene. Small peaks were observed before and after 4 kyr BP, followed by a minor decrease, then a substantial increase to a peak of $4.5 \cdot 10^{-7}$ m^3kg^{-1}, a relative minimum of $3.6 \cdot 10^{-7}$ m^3kg^{-1}, another peak of $4.5 \cdot 10^{-7}$ m^3kg-1 and finally a substantial increase up to $6.2 \cdot 10^{-7}$ m^3kg^{-1} in the topmost centimetres of the core. These late Holocene strong fluctuations correlate well with dry/cold (high susceptibility; Late Bronze Age-Iron Age, Dark Ages, and Little Ice Age) and humid/warm (low susceptibility; Roman Humid Period and Medieval Climate Anomaly) climatic periods. A generalized continuous increase in magnetic susceptibility values is recorded throughout the studied interval (Fig. VIII.3). The values oscillated between $10^{-7}m^3/kg$ and more than 5x $10^{-7}m^3/kg$ in the top part of the core.

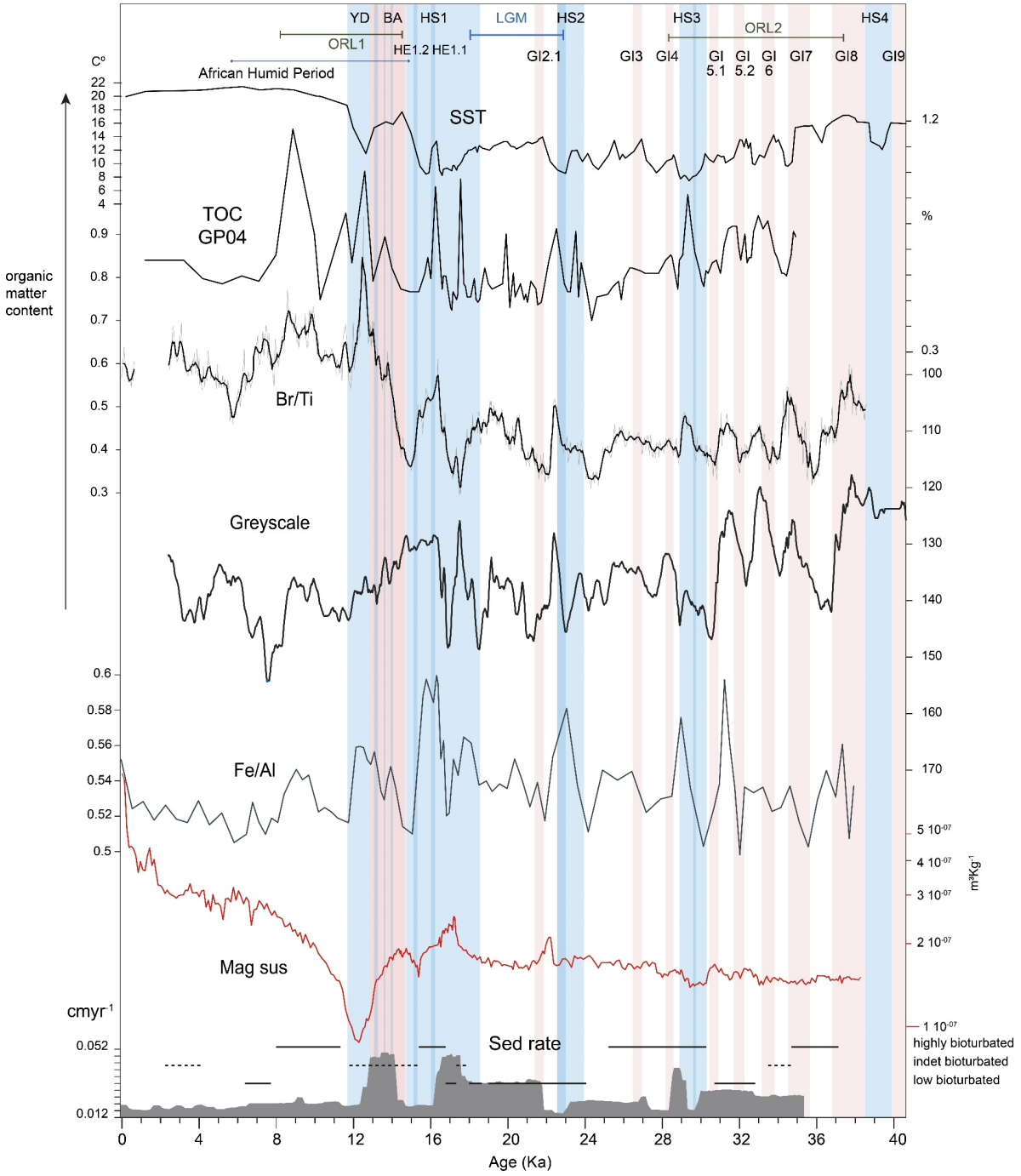

Figure VIII.3. Magnetic susceptibility, Fe/Al (iron enrichment), Br/Ti (OM), greyscale values, bioturbation, and sedimentation rate of the core GP03, and total organic carbon (TOC) of record GP04 (Morcillo-Montalbán et al., 2021). GI (Glacial interstadial) are represented by describing the cold-warm oscillation during the Last Glacial Cycle event locations based on the SST and Morcillo-Montalbán et al. (2021), as well as the ages of the Glacial stages and interglacial proposed in the literature (see Supplementary information). YD: Younger Dryas, HE: Heinrich Event, HS: Heinrich Stadial, ORL: Organic Rich Layer, TOC: Total organic Carbon.

VIII.4.2. Palaeontological proxy record

VIII.4.2.1. Ichnological features recognized in the core surface

Highly to low bioturbated intervals were recognized in the core. There is an important event of bioturbation at the end of HS3 and in the period before HS2. Bioturbation was also observed during HS1 and at the end of ORL1. Although there are points where bioturbation could not be well recognized, there is an indication that the complete ORL1 interval was bioturbated at some point.

VIII.4.2.2. Benthic foraminiferal data of the last 20 kyr

The foraminiferal low-oxygen benthic taxa group (Fig. VIII.4 A) indicates changes in bottom-water ventilation in the basin. The temporal evolution of this group shows three main phases:

In the first phase (Fig. VIII.4 A I), the relative abundance (%) of this group rapidly increased, coinciding with the dates of ORL 1 inception around 15 kyr BP as defined in the literature (Cacho et al., 2002; Jiménez-Espejo et al., 2008; Rodrigo-Gámiz et al., 2011). It reached a maximum value of approximately 40% at the beginning of the Bølling-Allerød (BA) period (14.6 kyr BP, Rasmussen et al., 2014).

In the second phase (Fig. VIII.4 A II), the percentage decreased from its maximum values until reaching minimum values for the ORL interval at the beginning of the Holocene, around 11 kyr BP.

The last phase (Fig. VIII.4 A III) showed a slight recovery towards the end of ORL 1, ending with an abrupt decrease at 8 kyr BP towards minimum values that continue for the rest of the record.

In addition to this general pattern of three phases, a second-order variation indicates a decrease in the low-oxygen taxa at several points of the ORL (Fig VIII.4 A, f, h, and j); these variations correlate with the internal climatic variability of the BA period and the YD. In addition, there was a slight increase in the low-oxygen taxa during HE 1.1 (Fig VIII..4 A c) and the recorded LGM (Fig. VIII.4 A a).

Gyroidina spp., an opportunistic high-oxygen benthic species, increased from the end of the YD (Fig. VIII.4 B), peaked at the end of ORL 1, and diminished after during the early Holocene.

The benthic foraminifer Hyalinea balthica, preferring cold waters, appears during the YD, showing its highest relative abundance. With lower relative abundances, this species also occurs in the GI 1d and GI 1b cold phases (Fig. VIII.4 C).

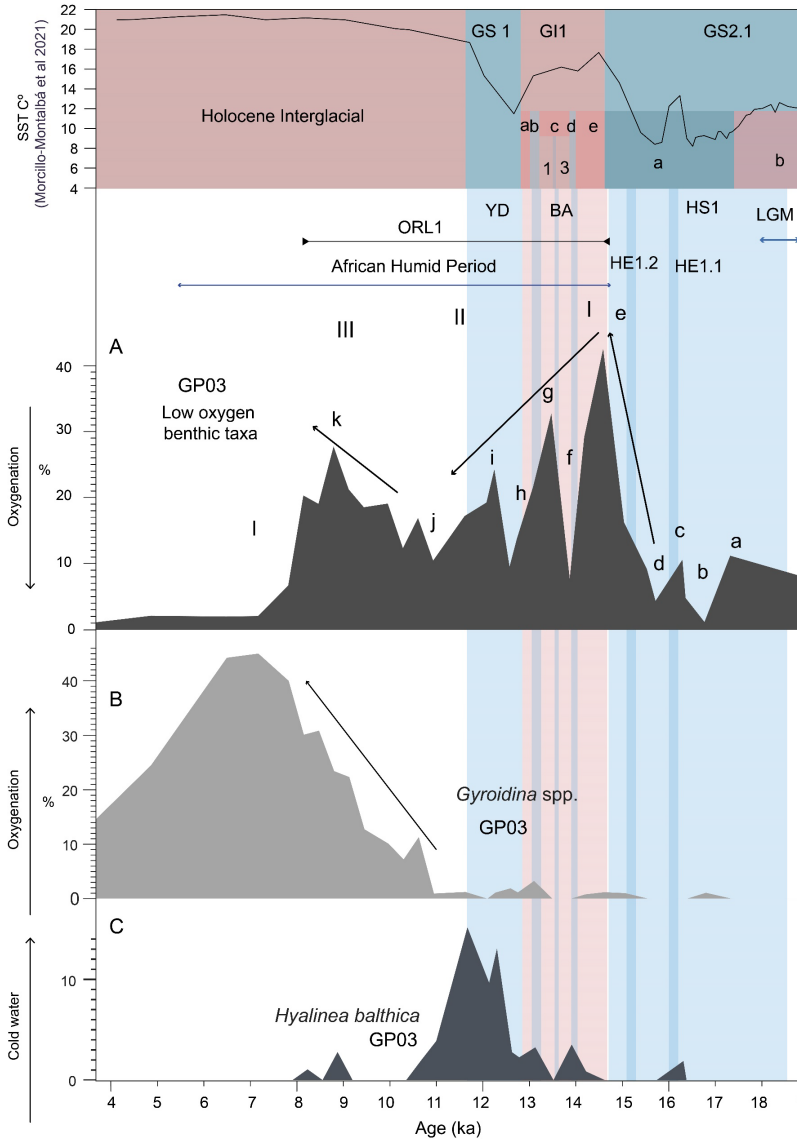

Figure VIII.4. Benthic foraminiferal data (low oxygen benthic taxa (A), *Gyroidina* spp. (B), and *Haylinea balthica*) for core GP03. See Fig. 8.3 for abbreviations. I: The first section of ORL1 with lower oxygenation. II: YD ventilation, III: return to less oxygenation after YD. "b" and "d" (moments of maximum oxidation in the pre-ORL period. "a" and "c" minimum oxygenation periods during the pre-ORL. e, g and k maximum in low oxygenation during ORL. f, h, and j points of reoxygenation during ORL1.

VIII.4.3. Chemical composition

VIII.4.3.1. Variations in the terrigenous fraction

Geochemical data show two main patterns of variation in the terrigenous fraction, one being described by the K/Al and Ti/Ca ratios — supporting an increase in fluvial discharge and a terrigenous fraction increase (Martínez-Ruiz et al., 2015) — and one described by the Zr/Ti ratio aeolian proxy. These two patterns are complementary and contrary. K/Al and Ti/Ca ratios show several positive peaks, which broadly coincide with warming interstadial phases seen in the sea surface temperature (SST) record until the LGM, when the correlation is lost (Fig. VIII.5). For instance, positive peaks occurred immediately after HS2 onset, two times during HS1 first stage and on the BA onset (Fig. VIII.5). During the early Holocene, the Ti/Ca ratio had low values but presented a rapid recuperation to the present. The Zr/Al ratio has several peaks showing rapid variability following the climatic changes of the Last Glacial Cycle; at the BA onset, it underwent a prominent decrease followed by a prominent positive peak during the BA. During the Holocene, the proxy shows a decreasing trend toward the minimum value reached at present.

VIII.4.3.2. Redox conditions, productivity, and organic matter preservation

The MoEF and UEF (Fig. VIII.5) proxies were selected for reconstructing palaeoredox conditions. These two ratios show very similar patterns, the main difference being that the oldest section of core UEF presents an enrichment while the MoEF remains low. The Br/Ti ratio (Figs. VIII.3 and VIII.6) records OM preservation and is well correlated with the Mo and U records (Figs. VIII.3, 8.5 and VIII.6); Br/Ti ratio also correlates with sediment colour, especially for GI5 to GI8. The Total Organic Carbon (TOC) from the GP04 record (Morcillo-Montalbá et al., 2021) correlates well with the Br/Ti ratio, greyscale (Fig VIII.3), and other redox proxies. The Fe/Al ratio may also indicate redox conditions. It correlates with other redox proxies like U and Mo (Fig. VIII.5). The main periods of oscillations in redox conditions in the basin are HS1 and ORL1 (14.7–8 kyr BP); less abrupt events of redox trace metal enrichment appear over the HS2 and HS3, and the GI5 to GI8, especially during the GI8, coinciding with the predicted onset of the ORL2 (Murat, 1999).

The Ba/Ti ratio (XRF core scanner) determines the excess Ba content. The ratio reveals two significant peaks, at HE1.1, around 16 kyr BP, and during YD (Fig. VIII.5). There are three minor peaks in GI8, HS3–GI4, and HS2–GI2, as well as a low-frequency cyclicity between HS3 and HS4, with peaks at GI8, GI7, GI6, and GI5. The Ba/Ti ratio decreased gradually from YD to the present, with values below the LGM.

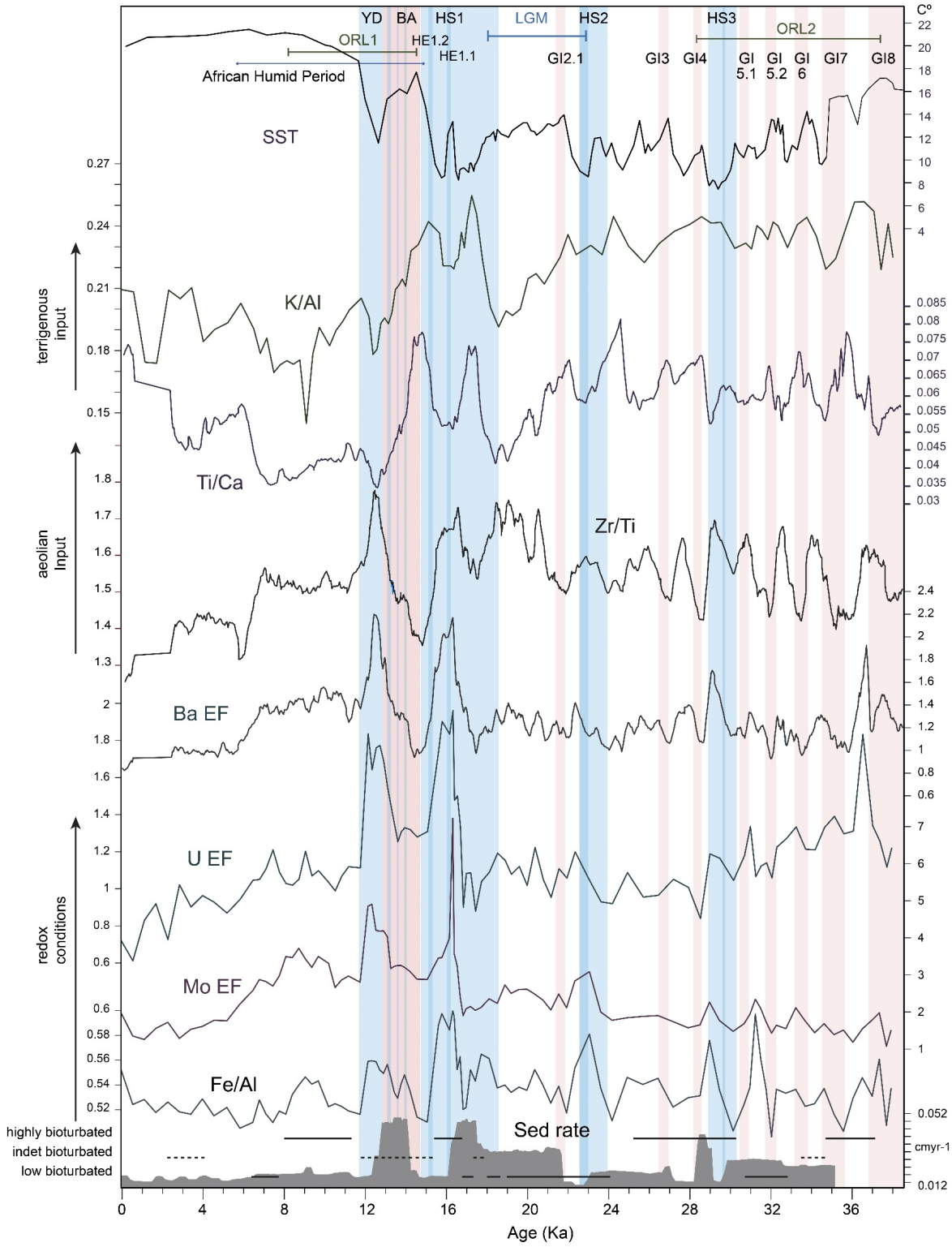

Figure VIII.5. Elemental ratios of selected trace metals for core GP03, grouped according to redox, aeolian and terrigenous. See Fig. VIII.3 for abbreviations.

VIII.5. Discussion

VIII.5.1. Variable response of the redox proxies

Redox proxies, which include chemical, physical, and palaeontological indicators, typically provide a cohesive signal of the environmental events that have occurred. However, differences between the peaks indicated by benthic foraminiferal and geochemical data in certain parts of the record, such as H1 and ORL1, suggest that the redox conditions can also be influenced by factors such as diagenetic displacements and erasures of the syndepositional signal or differential enrichment depths inside the sediment.

VIII.5.1.1. Benthic foraminifera

Benthic foraminifera accurately records bottom water conditions with a minimal age error related to the depth they inhabit (Buzas et al., 1993; Jorissen et al., 2007); moreover, benthic foraminifera live in the first millimetres or centimetres, the majority around 20 mm below the seafloor (mmbsf) (Buzas et al., 1993). Under low oxic conditions and high benthic flux of OM, benthic foraminifera live closer to the sediment surface (Van der Zwaan et al., 1999) and more accurately reflect the age of events. Benthic foraminiferal assemblages do not suffer from diagenetic remobilization and are not altered by the return to high oxygen conditions, so they conserve the original signals that might be displaced in other proxies. In our record, we assumed the benthic foraminifera to be a reliable indicator of oxygen conditions during ORL. Even though the peaks of U and Mo occur during HE1.1 and YD (Fig. VIII.5), we interpret that the points of maximum basin oxygen depletion occurred during BA and early Holocene (Fig. VIII.4).

VIII.5.1.2. Trace metals

Several important factors should be considered when interpreting trace metal enrichment. Authigenic enrichment of trace metals, such as U and Mo, does not necessarily occur on the surface of the sediment but at a certain depth below it (Zheng et al., 2002; McManus et al., 2005; Tribovillard et al., 2006). The depth of authigenic enrichment is detected as a peak in the vertical record; as it occurs after the deposition of the sediments, it can overprint previous signals, creating a temporal lag that must be considered. For instance, it has been observed that precipitation from porewaters can occur several cm within the sediment in the transition between the low-oxygenated and the anoxic pore water; this is common in environments with relatively high oxygen content in the bottom waters and can be further favoured if there is an increased accumulation of organic matter in a level below the sediment surface (e.g., King et al., 2000; McManus et al., 2005; Costa et al., 2018, 2023; Jacobel et al., 2020).

The sedimentation rate also plays a significant role in the preservation of redox elements signatures. Lower sedimentation rates have been associated with lower oxygenation enrichment (Costa et al., 2018; Liu and Algeo, 2020); as there is more time for the oxygen to penetrate the sediment, the redox trace metals can be diffused out of the sediment (Costa et al., 2018). This effect is even more significant if there is bioturbation (Zheng et al., 2002; Costa et al., 2018). Sudden sedimentation rate changes can, therefore, induce redox metal enrichment variations unrelated to bottom water environmental changes.

Another crucial point to be considered when interpreting authigenic enrichment is the early diagenesis mobilization of redox elements. After the low oxygen conditions that produced the authigenic enrichment have finished, there could be penetration in the sediment of high oxygenated water; under these new conditions inside the sediment, redox metals bearing authigenic minerals can dissolve again. Once dissolved, they may diffuse upward to the water column or downward to the still-reducing and still-not-oxygenated sediment, where they reprecipitate (Colley and Thomson, 1985; Thomson et al., 1993, 1995, 1999; Van Santvoort et al., 1997; Douglas and Adeney, 2000; Mangini et al., 2001; Morford et al., 2009a, 2009b; Jacobel et al., 2017, 2020). Re-oxygenation displacement in U enrichment peaks has been observed in other settings, reaching more than 50 cm below the sea floor and able to displace the peak below the original stratigraphic level where redox conditions started (Jacobel et al., 2017, 2020). In addition, these remobilization processes can be facilitated by bioturbation-induced irrigation (e.g., Morford et al., 2009a). Two prominent peaks of U and Mo have been recognized. The one occurring in the YD level was probably affected by these processes further enriched during diagenesis; it would indicate a certain depth of enrichment in the redoxcline during the last interval of the ORL1 more than a process occurred in YD. This will be further discussed below in the context of ORL accumulation processes.

In sum, the observed trace metal peaks should be interpreted in conjunction with other proxies and environmental factors; they indicate the transition between redox and oxic conditions but are not necessarily situated in the stratigraphic level that temporarily corresponds to that event. The discussed factors mean the peaks could appear imprinted in sediments deposited several centuries before low oxygenation conditions occurred in the basin. All these processes should be considered for a correct palaeo-redox interpretation of the sediment record. For this reason, a multiproxy For this reason, a multi-proxy approach is needed to accurately interpret past oxygen conditions (Jacobel et al., 2020).

One interesting approach for understanding all the processes involved when there are diverse data available with no apparent correlation is the use of machine learning prediction models like neural networks. We explored this possibility, as seen in the annexed material. Known points of the core that are easily ascribed to specific target conditions —an ORL or NO ORL in our case— can be used to train a machine learning model (Neural network or Bayes Naïve), and then these models serve to classify the rest of the record, an example being found in Figures VIII.S1, VIII.S2, VIII.S3 in the supplementary material.

VII.5.1.3. The magnetic signal as a proxy of diagenetic alteration

Redox conditions can alter the primary magnetic signal from detrital magnetite. This can happen by dissolution in the sections reaching redox conditions or diffusion and precipitation of Fe minerals in the oxidation fronts of organic-rich sediments (Larrasoaña et al., 2008). Such an alteration destroys the primary palaeoenvironmental signal and imprints it with an altered signal of dissolution (Liu et al., 2012). Alteration of these signals depends on many factors and can produce a destruction of the magnetic signal by precipitation of amorphous minerals and pyritization or its increase through the production of magnetic oxides (Larrasoaña et al., 2008; Liu et al., 2012; Qian et al., 2021). The pronounced susceptibility minimum in the YD sediments (Fig. VIII.3) is interpreted as evidence of Fe reduction and dissolution of the original detritic highly magnetic ferromagnetic minerals. The dissolution was followed by diffusion and possibly reprecipitation in the form of authigenic minerals, either as amorphous or cryptocrystalline low-susceptibility Fe oxy-hydroxides precipitated where the upward diffusion of Fe^{2+} reached oxygen or as paramagnetic low-susceptibility pyrite, where downwards diffusion of Fe^{2+} encountered sulfidic conditions. In any case, magnetic signal destruction is promoted and evident. A similar interpretation of the susceptibility minimum after HE1 would be more tentative, as its magnitude and stratigraphic extension are much lower. It can also fall between the expected values due to variations in terrigenous input without invoking dissolution effects.

VIII.5.2. Integrative analysis of oxygen conditions and response to climate and oceanographic forcings

VIII.5.2.1. Main events and drivers of the ventilation and organic matter preservation

Considering all the studied proxies, the oxygen variations in the basin and how they correlate with climate changes and palaeoceanographic conditions can be interpreted. Higher U and Mo enrichment values indicate low oxygen conditions within the sediment associated with less ventilation. Lower greyscale values, higher Br/Ti ratio, and higher TOC are interpreted as proxies for higher accumulation of OM and are generally also associated with low oxygen conditions inside the sediment. Hence, OM preservation because of both low deep-water oxygenation and increased sedimentation rates is inferred. However, a clear relationship with productivity changes that occurred during warm interstadials, as inferred from other records in the basin, is not clearly observed (Ausín et al., 2015a; Bazzicalupo et al., 2018; Fig. VIII.S4), so the oxygen depletion is apparently not related to an excess of OM from productivity, but rather a probable depletion of oxygen in the bottom waters.

The Fe/Al ratio can be considered as a pyritization proxy (Lyons and Severmann, 2006), but it is clearly influenced by the detrital fraction. Thus, we interpret it in combination with the magnetic signal because increases in the Fe/Al ratio associated with decreases in magnetic susceptibility could indicate amorphous Fe minerals like pyrite formation. Finally, as discussed previously, benthic foraminifera accurately indicates changes in the oxygen conditions of the basin seafloor, and magnetic susceptibility can account for strong redox diagenetic alterations.

The changes in oxygenation in the deep Alboran Basin respond to variations in the WMDW formation in the Gulf of Lions (Millot, 1999; Cacho et al., 2000; Frigola et al., 2008). Deep-water renewal has shown annual to decadal variations in oceanographic observations over the last few decades, responding to climate conditions during fall and winter and the preconditioning of water masses (Somot et al., 2018; Cisneros et al., 2019). In the deep Western Alboran Basin, a rapid response of geochemical redox proxies to ventilation changes is observed, indicating oxygen depletion several times during the end of the Last Glacial and Early Holocene. The main slowing down of the WMDW would occur during GI8, GI7, GI6, and GI5, the HEs, and the last deglaciation (Figs. VIII.3, VIII.5, VIII.6, VIII.7 and VIII.8). The trigger of this WMDW slowdown is inferred to not be the same for the HE as for the GI; the GI is warm and more humid, with a change in the westerlies strength and the increased riverine inputs causing the stop in deep water generation. In contrast, the HE occurred during dry and cold glacials that are usually associated with more ventilation (Frigola et al. 2008), although during HE, iceberg melting induced an increase in buoyancy that impacted the deep-water generation (Sierro et al., 2005).

VIII.5.2.2. DO events and missing ORL2

The 40 kyr record has the GI8, GI7, GI6, and GI5 (5.1 and 5.2) as the oldest interstadials. During the first period of the record, there was an alternation between lower oxygen conditions of the deep basin during the warm phases and more oxygenation during the cold stages (Fig. VIII.3, 8.5 and VIII.8), as also reported in the Eastern Alboran Basin (Cacho et al., 2000), implying a substantial reduction of the WMDW renewal during these four interstadials. The period that includes these four interstadials (plus some period outside this time span) has been interpreted broadly as the time when the ORL2 was deposited (Murat, 1999) and described as having several cycles of fluctuating oxygen conditions (Casanova-Arenillas et al., 2022). It is consistent with higher TOC values in the Eastern Alboran core MD95-2043 (Cacho et al., 2000). Neuronal network analysis results further support ORL2 deposition at the studied GP03 Site (Fig. VIII.S2).

Overall, results confirm that this period was characterized by cyclical oxygen decrease in the basin influenced by the DO warm phases. Interestingly, this period also coincides with a maximum of insolation in the northern hemisphere (Hughes et al., 2013). During this insolation maxima, increased fluvial discharge from North Africa was observed, but it has been argued that it was insufficient to form sapropels in the Eastern Basin (Blanchet et al., 2021). Still, the increased fluvial discharges and the decreased north winds during warm interstadials would

create favourable preconditioning to reduce WMDW formation, generating ORL-like sediment intervals. In addition, this phase is characterized by high sedimentation rates, which further contribute to the conservation of the redox signal and OM during the ORL2.

VII.5.2.3. End of the glacial period, Heinrich stadials 3 and 2 (HS3 and HS2)

After GI5, the record characteristics changed associated with the LGM interval of shorter interstadials and more prevalent glacial conditions. The proposed redox and productivity records did not show any significant variations in ventilation during the stadials. The most important feature acknowledged would be the low oxygen conditions inferred for HS2 and HS3 (Fig. VIII.6 and VIII.7). The HEs are expected to present WMDW reduced production as a response to the buoyancy gain related to less saline water entering the basin from the Atlantic iceberg migration and melting (Sierro et al., 2005).

HS3 is characterized by a colder interval occurring at the middle of the glacial stage (W. J. Fletcher et al., 2010), which is the moment when the HE occurred; this is supported in the record of Br/Ti ratio and U and MoEF (Fig. VIII.6 and VIII.7). Susceptibility decreased during this period without correlation with detrital inputs, suggesting that reductive conditions stabilized in the sediment during the HE interval in the middle of HS3 (Fig. VIII.7). The top part of the interval shows an increase in the sedimentation rate, favouring the preservation of the low oxygenation signal.

During HS2, the HE occurred in the final part of the stage. Again, it is supported by the Br/Ti, MoEF and U EF (Fig. VIII.6). In addition, there is an increase in magnetic susceptibility values at the top (Fig. VIII.7); increases in magnetic susceptibility at the top of the high TOC sapropels have been correlated in the Eastern Mediterranean with biogenic magnetite precipitated by certain bacteria during oxidation of the top part of a sapropel (Qian et al., 2021). Oxidation at the topmost part of the interval can be inferred, indicating that GI4 could still be a low-oxygenated interval with the signal lost due to post-depositional processes.

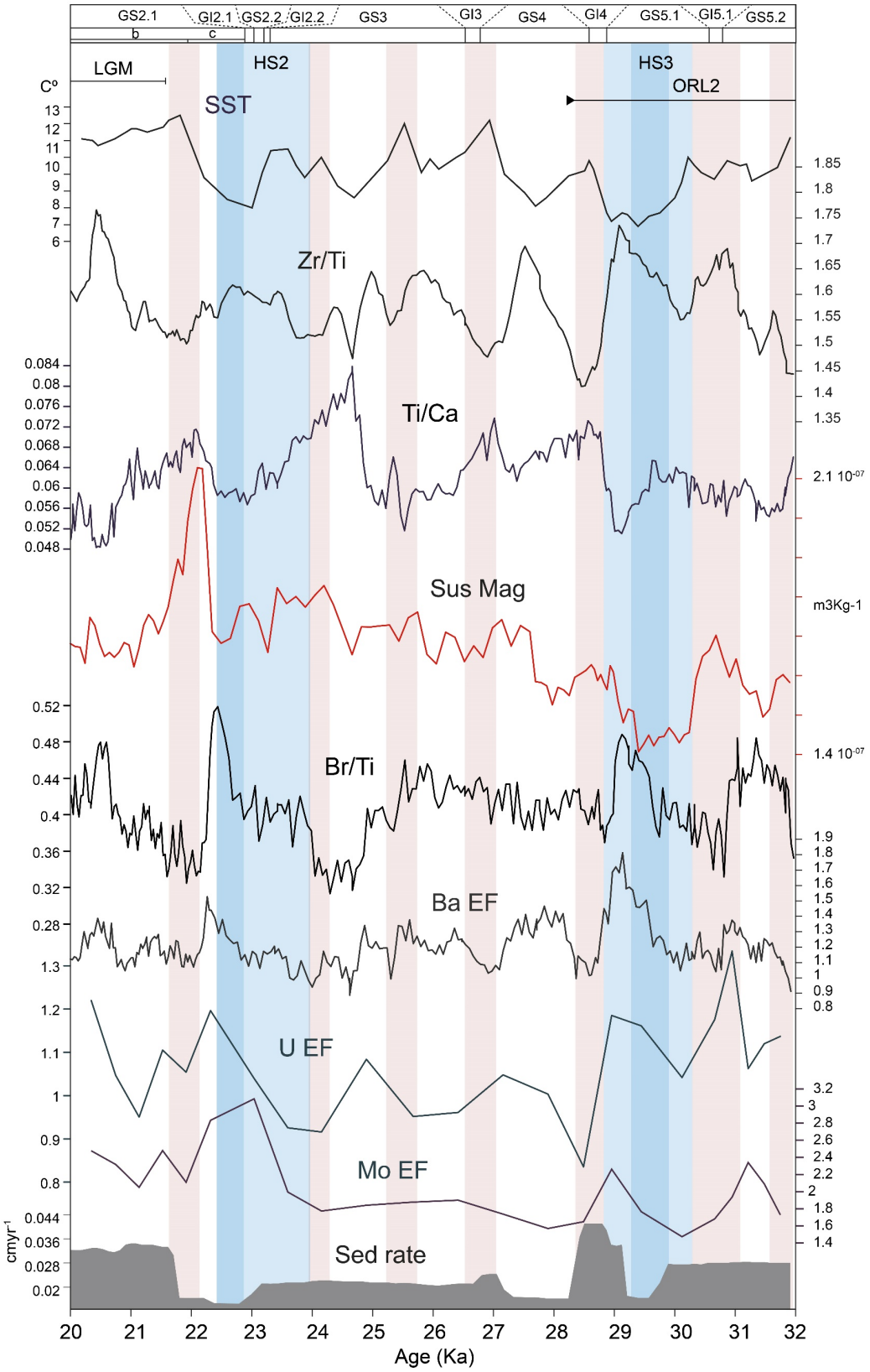

Figure VIII.6. Geochemical and magnetic evolution during Heinrich stadials 2 and 3 for core GP03.

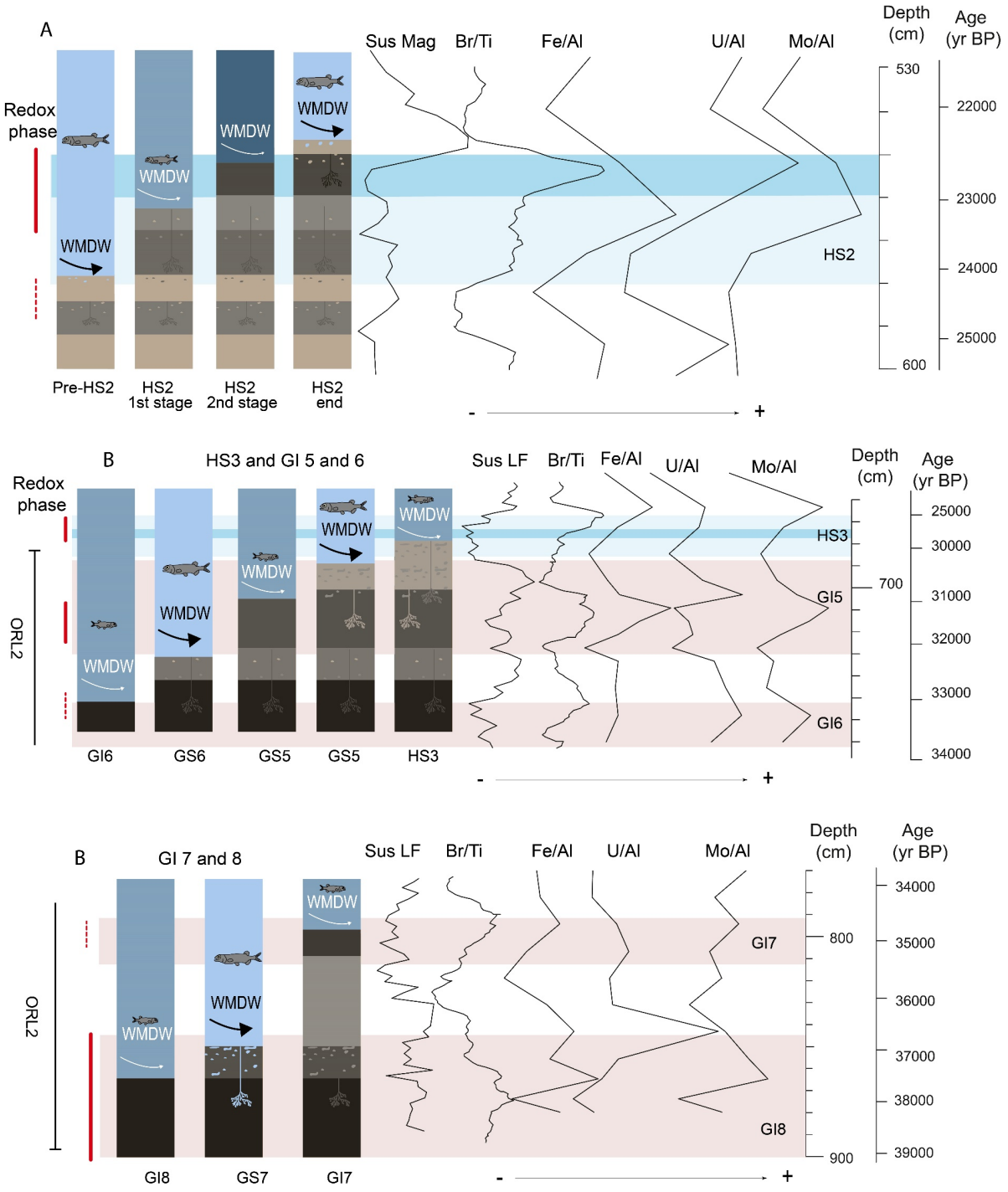

Figure VIII.7. A: Schematic model of the HS2, B: HS3, and C: GI 8 to 5 deposition events; every column represents one of the three primary states, pre-HS, early HS, and HE

VIII.5.2.4. Henrich Stadial 1

HS1 (18 – 14.9 kyr BP) was the result of the southward shift of the polar front in response to a weakened AMOC (Bond and Lotti, 1995; Barker et al., 2015; Hodell et al., 2017) triggered by meltwater discharge that occurred during the recession of the European North American ice sheets (Zaragosi et al., 2006; Stríkis et al., 2015; Toucanne et al., 2015). During HS1, two stages have been distinguished (Broecker and Putnam, 2012). The first stage, occurring between 18 and 16.2 kyr BP (Broecker and Putnam, 2012; Sierro et al., 2020), is associated with the weakening of the AMOC, which was triggered by melting water from the Laurentide and Eurasian ice sheets (McManus et al., 2004; Peck et al., 2007; Hodell et al., 2017). A colder second stage occurred between 16.1 and 14.7 kyr BP (Sierro et al., 2020), triggered by additional freshwater coming from the Laurentide ice sheet due to the large surge of icebergs (Hodell et al., 2017). The second collapse was stronger and caused HE 1.1 (around 16 kyr BP); another event, HE1.2 (around 15 kyr BP), took place later. However, HE1.1 was more significant and even reached the Portuguese margin (Zahn et al., 1997; Schönfeld et al., 2003; Plaza-Morlote et al., 2017). In the continent, HS1 shows 3 phases: HS1a (18.4–17.2 kyr BP), characterized by generally arid (cold) conditions; HS1b (17.2–16.9 kyr BP), more humid (warm); and HS1c (16.9–15.7 kyr BP), with arid (cold) conditions (Camuera et al., 2021).

In the studied record, the MoEF and UEF recorded a significant event of low oxygenation (Fig. VIII.5) during HE1.1 and HE.1.2, considering that MoEF and UEF peaks occur a few centimetres below the sediment surface during the enrichment. This event happened during a period of increased SST. Likewise, TOC, greyscale values, and Br indicate that this period recorded an increase in OM preservation. The event coincides with increased aridity, as suggested by Zr/Ti, Ti/Ca, and K/Al ratios, supporting that this oxygen decrease event responded to oceanographic conditions (entrance of fresh water from the Atlantic) and not to riverine input freshening.

During HS1, benthic foraminiferal species groups showed no evident increase in low-oxygen species. A small peak that coincides with the inferred low oxygenation event at 16 kyr BP can be interpreted as low oxygen conditions occurring during a short time, unaffecting benthic foraminiferal community. From 15 kyr BP and including the HE1.2, the benthic foraminifera indicate the onset of oxygen depletion related to ORL1 (Figs. VIII.4 and VIII.8).

At the end of HS1, the WMDW showed a strengthening in other Alboran records (Alonso et al., 2021), pointing to increased aspiration in the Alboran and the arrival of more oxygenated waters from the Balearic Basin. The WMDW strengthening can be observed here in the Western Alboran Basin record, which shows a rapid decrease in trace metal enrichment and a decrease in low-oxygen benthic species at the end of HS1, indicating prevalent high oxygenation during this phase (Figs. VIII.3, VIII.5 and VIII.8). The return to colder and drier conditions during the HS1, plus the buoyancy of the top layer returning to normal after the HEs, most likely produced a reactivation of the WMDW formation and can explain the proxy record observed. Ventilation of the basin would also affect the trace metal signal of the previous

interval. Oxygen penetration appeared to have reached HE1.1, where high contents in organic matter favoured the reducing environment, concentrating redox metals in the redox-oxic transition. Moreover, from 16 kyr BP to approximately 15 kyr BP, the drop in sedimentation rate would cause a decrease in TOC and trace metal enrichment due to more extended penetration of oxygen in the sediment and increased OM oxidation.

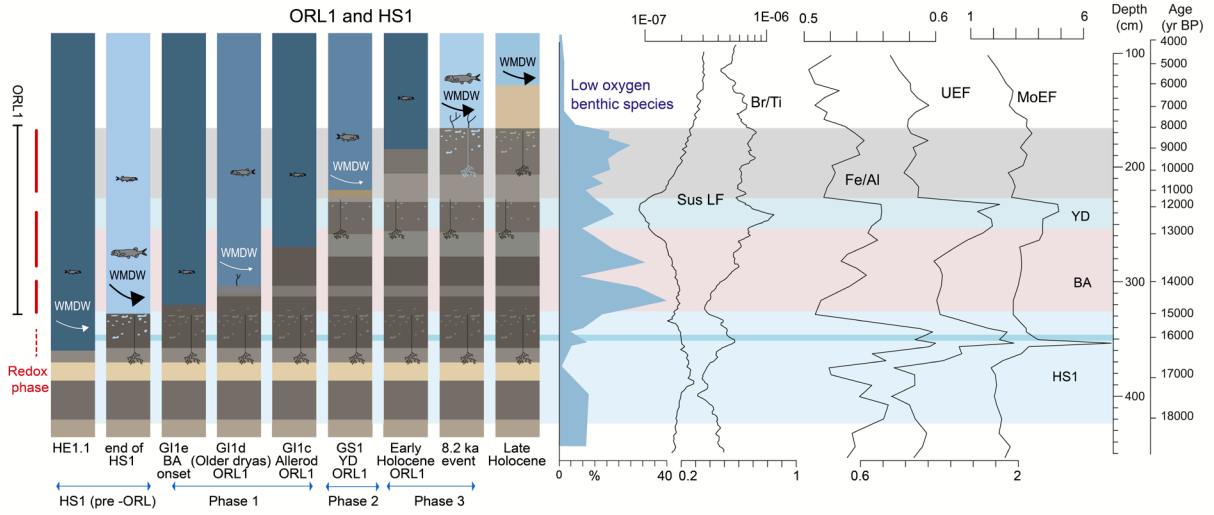

Figure VIII.8. In the schematic model of the OR1 and HS1 event depositions, every column represents the sediment column's state at deposition.

VIII.5.2.5. Organic Rich Layer 1

We distinguish three phases in view of the environmental changes observed for the ORL1.

VIII.5.2.5.1 Phase I Bølling–Allerød

BA occurs during GI1 and has been defined as a warm period punctuated by several cold periods (Broecker, 1992; Rasmussen et al., 2014). Given the rapid temperature and sea level increase, the basin became severely restricted with the onset of the ORL1 between 14.5-8.5 kyr BP (e.g., Murat, 1999; Cacho et al., 2002; Jiménez-Espejo et al., 2007; Pérez-Asensio et al., 2020; Casanova-Arenillas et al., 2022; Mesa-Fernández et al., 2022). In our record, low oxygen benthic foraminifera defined the onset of ORL1, and the beginning of the BA showed the most significant increase in the low benthic taxa ecological group during the study period (Fig. 8.3).

The benthic foraminiferal records evidence a distinct variability in oxygen conditions during the BA, especially the GI1d colder phase, showing higher bottom water ventilation. The ventilation events observed in the BA period explain the changes in the non-preservation of TOC and Br signals during the HS1 end and the BA onset. Sedimentation rates could also account for these changes without needing a burndown to explain the differential conservation of TOC in the interval. However, the enriched values of MoEF and UEF indicate that low oxygen conditions were probably dominant since H1.1, despite short ventilation events and

changes in the sedimentation rate that produced the observed rearrangement and differential response of proxies.

VIII.5.2.5.2. Phase II YD

Cold and dry conditions established during the YD are expected to increase WMDW formation, as observed in the Western Mediterranean (e.g., Mesa-Fernández et al., 2022). Compared to BA, the relatively low oxygen benthic foraminifera values support partial reoxygenation during the YD. In addition, the relative abundance of the cold-water species *Hyalinea balthica* increased, indicating the entry of colder waters into the deep basin. This further supports the fact that higher ventilation occurred during the YD and the introduction of cold Atlantic waters into the system.

During this phase, Mo and EF rapidly diminished after a sharp peak at the beginning of the period. This peak indicates a significant alteration in the redox conditions in the sediment related to changes in the bottom water oxygenation. The diffusion of U and Mo probably increased the strength of these peaks. As for benthic foraminifera, they show an event of bottom water ventilation at the beginning of the YD, with a fluctuation towards the end of the YD towards less oxygenation and another event of ventilation after YD.

Nevertheless, this event was discontinuous and reflected a return to low-oxygen conditions during the middle of the YD. The deep basin could thus reflect the internal variation of the YD —warmer and wetter to the end due to the gradual reactivation of the Atlantic overturning circulation (Bartolomé et al., 2015). This internal warm and wet interval could explain the fluctuations observed in the low-oxygen benthic foraminifera (Fig. VIII.4).

Ventilation of WMDW during YD could be linked to climate changes, allowing for colder and drier conditions that favoured ventilation. An acceleration of the LIW and MOW during these phases has also been observed, ventilating shallower Mediterranean depths (Trias-Navarro et al., 2023), which could have favoured ventilation of shallower layers of the WMDW.

Evidence of redox dissolution of magnetic minerals can be interpreted from the magnetic susceptibility in the YD sediment interval. Accordingly, this indicates that euxinic conditions were reached at some point within the sediment in this interval. However, it may be argued that euxinic conditions were not reached temporarily during the YD but rather later on, during the second and lower oxygenated part of ORL1 (Fig. 8.4), with the precipitation of the authigenic trace metals occurring below the sediment-water interface. The observed magnetic signal alteration reflects the depth below the sediment surface where these conditions were reached, the higher sedimentation rates allowing for a greater amount of OM to be buried during the end of the BA and the YD (Fig. 8.3).

VIII.5.2.5.3. Phase III Early Holocene

After the reoxygenation period, there was a return to lower oxygen conditions, which peaked again at the end of ORL 1 (Fig. VIII.8). A slowing down of the WMDW is inferred from the

benthic foraminifera and reached a maximum at around 8.5 kyr BP, just before the reoxygenation occurring at the end of ORL 1 in relation with the 8.2 kyr BP cold events (Fig. VIII.8). The rapid return to oxygenated conditions proposed after the ORL 1 in the basin favoured the opportunistic repopulation of *Gyroidina* spp. (Fig. VIII.4), interpreted as an opportunistic species in post-sapropelic conditions and appearing in the Alboran record (Caralp, 1988; Pérez-Asensio et al., 2020). *Gyroidina* rapidly occupies the empty ecological niche left by the low-oxygen taxa, further indicating that this is the main event of reoxygenation and the end of ORL 1 for the Western Alboran Basin. During reoxygenation, trace makers colonize the uppermost portion of ORL 1, penetrating several centimetres (Fig. VIII.8). This bioturbation facilitates the infiltration of oxygenated water into the sediment, resulting in the downward diffusion of redox elements.

The lower sedimentation rates can moreover explain the absence of U or OM enrichments in the final part of the ORL, as proposed in some studies; low sedimentation along with reoxygenation can erase the original signal, leading to possible misinterpretations of the duration of the events (Costa et al., 2018), which can be avoided due to the other proxies used here.

Given the record of ORL 1 and the inferred ORL 2 (see VIII.5.2.2), considerable differences exist between both intervals concerning the preservation of TOC and the general environment and the potential triggers of these events. While ORL 1 shows a much more continuous and evident record of low ventilation and TOC accumulation, the record of ORL 2 is fragmented and interrupted by reventilating events that could erase the signal of many low-oxygen proxies. These differences can result from fundamental variations in the triggers and climate configurations that produce these layers.

VIII.5.2.6. Basin-wide Alboran Sea environment comparison during the last 20 kyr

Comparison of obtained low-oxygen benthic foraminiferal data from the last deglaciation with other low-oxygen benthic foraminiferal records inside the Alboran Basin (Fig. VIII.9; Pérez-Asensio et al., 2020) reveals the local record of the oxygenation changes in the GP03 Site; the interpreted events of reoxygenation inside the basin related to short-term climatic changes during the BA and YD had not been previously observed in other settings. This underlines the high sensitivity of benthic foraminifera to short-term ventilation changes at around 1300 m water depth in the Western Alboran Sea.

At the deep Western Alboran Basin (i.e., GP03 Site), a re-ventilation event during the YD is indicated by relatively lower low-oxygen benthic taxa values than in the BA. Such re-ventilation is also evident in the much shallower site HER-GC-UB6 (Pérez-Asensio et al., 2020) but does not show the temporary decrease in ventilation recorded during the warmer and wetter mid-YD (Fig. VIII.9). Furthermore, the shallower site HER-GC-UB6 maintained the better-ventilated conditions during the remaining ORL 1 interval (early Holocene). In contrast, the

deep site GP03 records a decrease in ventilation during this part of the ORL 1, related to the arrival of well-ventilated intermediate waters at the shallower site HER-GC-UB6 (Pérez-Asensio et al., 2020).

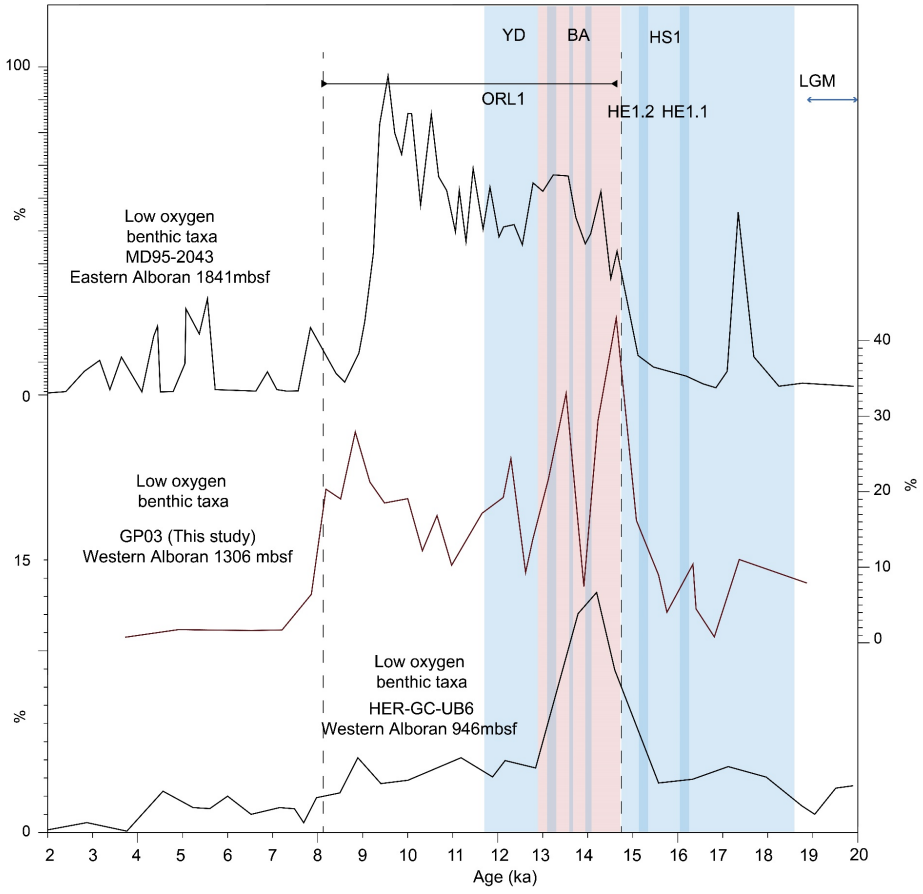

Figure VIII.9. Evolution of low oxygen benthic taxa in GP03 compared with other core records (MD95- 2043 and HER-GC-UB6) in the Alboran Basin (Pérez-Asensio et al., 2020).

The Eastern Alboran MD95 2043 record (Pérez-Asensio et al., 2020) also shows a re-ventilation during the YD and low-ventilated conditions during the early Holocene part of the ORL 1, as for the western Alboran GP03 site. Both deep parts of the Western and Eastern Alboran Basin, therefore, maintained lower oxygenation during the last part of the ORL 1, and the ventilation of the YD did not continue during the early Holocene at deeper settings, most likely because of the stratification of the WMDW and the newly formed Deep Water flowing above the denser stagnant water (Rogerson et al., 2008).

The end of the ORL 1 appears to have occurred earlier in the Eastern Alboran Basin than in the Western Alboran Basin (ca. 8.9 ka vs. ca. 8.2 ka), which indicates that the Western Alboran Basin continued to be restricted longer.

ORL 1 in the Mediterranean Basins is subdivided into two phases based on U and Mo values; the first (15–11.7 kyr BP) is more euxinic, and the second (11.7–9 kyr BP) is more suboxic-

ferruginous but maintains high carbon content due to increased sedimentation rates (Mesa-Fernández et al., 2022).

VIII.6. Conclusions

A multidisciplinary and integrative sedimentological, geochemical, and palaeontological analysis of the GP03 record in the Western Alboran Basin (Westernmost Mediterranean), spanning the last 37 kyr BP, allows for a detailed interpretation of significant changes in deep-sea oceanographic conditions, with special attention to bottom waters and pore-water oxygenation, in response to climate changes, thus providing new insights into environmental changes over the Last Glacial Period and Holocene. This approach has made it possible to differentiate short oxygenation events not previously recognised and describe diagenetic and syndepositional events that would have otherwise been overlooked.

Attending to the terrigenous geochemistry, the last 37 kyr can be divided into two main phases that respond to continental humidity and sea level, such as the period of the glacial conditions before the Last Glacial Maximum and the phase of deglaciation and Holocene.

During the glacial phase, several events of substantial environmental variability are interpreted based on the geochemical proxies and neural network classification of the complete data set (including geochemical, magnetic and colour proxies). Glacial Interstadial 8 to Glacial Interstadial 5 (GI8 and GI5) show cyclical decreases in oxygen levels due to reduced deep water renewal during warm phases and increased sedimentation rates. This cyclical variation — especially GI8— coincides with the supposed position of Organic Rich Layer 2 (ORL 2), probably consisting of various discontinuous events of low oxygenation coinciding with warm phases that would also affect the preservation of redox proxies and Total Organic Carbon. Heinrich Events 3 and 2 (HE3 and HE2) show low oxygen conditions, possibly due to reduced Western Mediterranean Deep Water production in response to fresher water from melting the Atlantic iceberg.

After the Last Glacial Maximum, benthic foraminifera allows precise reconstruction of redox conditions. Three main phases in the temporal evolution of the low-oxygen benthic taxa group are identified, indicating changes in bottom-water ventilation. Maximum basin oxygen depletion points occurred during Bølling–Allerød (BA) warming and the early Holocene, coinciding with the ORL 1 deposition. However, the peak of U and Mo occurs during HE 1.1 and Younger Dryas (YD). In addition, the oxygen decrease event preceded ORL 1 at the end of Heinrich Stadial 1, with a period of full reoxygenation between HE 1.1 and ORL 1 initiation.

Differences between the peaks indicated by benthic foraminiferal and geochemical data suggest that diagenetic displacements and erasures of the syndepositional signal or differential enrichment depths inside the sediment can influence the interpretation of redox conditions. Foraminifera information allows the interpretation of oxygen conditions in the bottom waters

during deposition, whereas post-depositional remobilisation can also affect the geochemical trace metal proxies.

During deposition of ORL 1 —between 15 kyr BP and 8 kyr BP—climatically driven short reoxygenation events occurred, allowing endobenthic bioturbation and trace metal remobilization in some parts of the record. During the BA, at least one reoxygenation event occurred during the GI 1d cold phase, evidenced by an alteration in the redox trace metal signals below it and the changes in the foraminifera assemblage. Moreover, there was a significant reoxygenation phase during the YD.

VIII.7. Supplementary Material

VIII.7.1 Event timing in the literature

Table VIII.S1. Age of Heinrich Stadials. Based on Be dating in continental settings

Event	Onset (yr BP)	End (yr BP)	References	Conditions
HS1	18.6	14.7	Hodell et al. (2017), Allard et al. (2021)	Cold
HE1.1	16.2		Hodell et al. (2017)	
HE1.2	15.1		Hodell et al. (2017)	
HS1a	18.4	17.2	Camuera et al. (2021)	Cold, generally arid
HS1b	17.2	16.8	Camuera et al. (2021)	Increased precipitation and temperature
HS1c	16.9	15.7	Camuera et al. (2021)	Cold, dry conditions
HS2	24	22.4	Morcillo-Montalbá et al. (2021) based on SST	Cold, dry
HS3	28.9	30.3	Morcillo-Montalbá et al. (2021) based on SST	Cold, dry
HS4	40.2	38.3	Rasmussen et al. (2006),; Allard et al. (2021)	Cold, dry

Table VIII.S2. Age control of events.

Event	Onset (yr BP)	End (yr BP)	References	Conditions
African Humid Period	14800	5500	COHMAP Members (1988); Roberts (1998), deMenocal et al. (2000)	Humid
Timescale datum (8.2 kyr cold event)	8186		Alley et al. (1997)	Cold
Organic rich layer 1 (ORL1)	14500	8200/8900	Cacho et al. (2002); Jiménez-Espejo et al. (2008), Rodrigo-Gámiz et al. (2011)	Humid
Last Glacial Maximum (LGM)/GS-2b	18000	23000	CLIMAP project members (1976), CLIMAP project (1981)	Cold Dry
Organic rich layer 2 (ORL2)	28300	37200	Cramp and O'Sullivan (1999), Pérez-Folgado et al. (2004)	Humid

Table 8.S3 Age of Glacial Stadials and Interstadials (GS and GI) from Rasmussen et al., 2014

Event	Onset (yr BP)	End (yr BP)	References	Conditions
Younger Dryas (YD)/GS1	12846	11653	Rasmussen et al. (2006); Steffensen et al. (2008)	Cold, Dry
GI-1a (Allerød)	13049	12846	Björck et al. (1998)	Humid, Warm, warmer
GI-1b	13261	13049	Björck et al. (1998)	Humid, Warm, colder
GI-1c1	13550	13261	Rasmussen et al. (2014)	Humid, Warm, warmer
GI-1c2	13610	13550	Rasmussen et al. (2014)	Humid, Warm, warmer, colder
GI-1c3	13904	13610	Björck et al. (1998)	Humid, Warm, warmer
GI-1d	14025	13904	Rasmussen et al. (2014)	Humid, Warm, colder
GI-1e (Bölling)	14642	14025	Rasmussen et al. (2006), Steffensen et al. (2008)	Humid, Warm, warmer
GS-2.1a (oldest dryas)	17430	14642	Rasmussen et al. (2014)	Dry, Cold
GS-2.1b	20850	17430	Lowe et al. (2008), Rasmussen et al. (2014)	Cold, warmer
GS-2.1c	22850	20850	Lowe et al. (2008), Rasmussen et al. (2014)	Cold
GI-2.1	22970	22850	Rasmussen et al. (2014)	Warm
GS-2.2	23170	22970	Rasmussen et al. (2014)	Cold
GI-2.2	23290	23170	Andersen et al. (2006), Lowe et al. (2008), Rasmussen et al. (2014)	Warm
GS-3	27490	23290	Lowe et al. (2008), Rasmussen et al. (2014)	Cold
GI-3	27730	27490	Andersen et al. (2006), Lowe et al. (2008), Rasmussen et al. (2014)	Warm
GS-4	28550	27730	Lowe et al., (2008), Rasmussen et al. (2014)	Cold
GI-4	28850	28550	Andersen et al. (2006), Lowe et al. (2008), Rasmussen et al., 2014	Warm
GS-5.1	30550	28850	Rasmussen et al. (2014)	Cold
GI-5.1	30790	30550	Rasmussen et al. (2014)	Warm

GS-5.2	31990	30790	Blockley et al. (2012), Rasmussen et al. (2014)	Cold
GI-5.2	32450	31990	Svensson et al. (2008), Rasmussen et al. (2014)	Warm
GS-6	33310	32450	Blockley et al. (2012), Rasmussen et al. (2014)	Cold
GI-6	33690	33310	Svensson et al. (2008), Rasmussen et al. (2014)	Warm
GS-7	34690	33690	Blockley et al. (2012), Rasmussen et al. (2014)	Cold
GI-7a	34830	34690	Rasmussen et al. (2014)	Warm
GI-7b	34970	34830	Rasmussen et al. (2014)	Warm, colder
GI-7c	35430	34970	Svensson et al. (2008), Rasmussen et al. (2014)	Warm
GS-8	36530	35430	Blockley et al. (2012), Rasmussen et al. (2014)	Cold
GI-8a	36810	36530	Rasmussen et al. (2014)	Warm
GI-8b	37070	36810	Rasmussen et al. (2014)	Warm, colder
GI-8c	38170	37070	Svensson et al. (2008), Rasmussen et al. (2014)	Warm
GS-9	39850	38170	Blockley et al. (2012), Rasmussen et al. (2014)	Cold
GI-9	40110	39850	Svensson et al. (2008), Rasmussen et al. (2014)	Warm

VIII.2 Modelling the ORL position

Naïve Bayesian classification and neural networks

Machine learning algorithms can classify complex data and recognize patterns in a reclassified training set.

To look for the hidden pattern in the data set, we used a Naïve Bayesian classification and a neural network classification. Both were obtained using the software "OrangeTM", which runs in Python and uses the “Scikit-learn: machine learning in Python,” 2023.

In the Naïve Bayesian, a Bayesian network is used to classify data; each random variable X is represented as a node in these networks. A directed edge between two nodes indicates a probabilistic influence (dependency) between the parent and child variables (Sahami et al., 1998). Hence, the network's topology reflects that each node X is conditionally independent of its non-descendants, given its parents (Sahami et al., 1998). To build a probability distribution satisfying these conditions, each node X in the network has to be paired with a conditional probability table that defines the distribution over X, giving any plausible assignment of values to its parents. This statistical technique can be used to train an algorithm with a specific set of data, a training set, and then apply the trained algorithm to other unclassified data; the algorithm will then give a probability of these new data being ascribed to one of the classes (Sahami et al., 1998).

On the other hand, McCulloch and Pitts (1943) introduced the neural network (NN); this method also classifies a data set after being trained with a previously classified sub-data set).

In Figure VIII.S1, we applied a neural network with 8 points of the data set to recognize ORL and NO ORL from the foraminifera data. The results show that the beginning of the HS 1 interval is classified as ORL, which indicates that the foraminiferal composition, even beyond the selected Species, indicates similarities with those of the ORL, concordant with the observed low oxygenation assumed for this interval from other proxies.

In Figures VIII.S1 and VIII.S2, we applied a neural network (Fig. VIII.S1) and Naive Bayes model (Fig. VIII.S2) to predict the ORL-like layer's position. They were made using a known categorized set of points as ORL and NO ORL, known thanks to the benthic foraminifera data and their data for the Magnetic susceptibility, the Ba XRF area. The greyscale, S XRF area, Br/Ti, UEF, MoEF, sedimentation rate, and TOC. All data were interpolated to 50 kyr time intervals to allow the comparison.

Interestingly, the Models predict the position of ORL-like intervals based on the values of its ten analysed features, showing that conditions of oxygen depletion happened in the basin during the Heinrich Stadial 1 second stage, end of HS 2 and 3, and during the 37-32 kyr BP period, coinciding with the approximate location of the ORL (Murat, 1999; Casanova-Arenillas et al., 2022) and with correlation with the warm periods associated with the GI 6, 7 and 8.

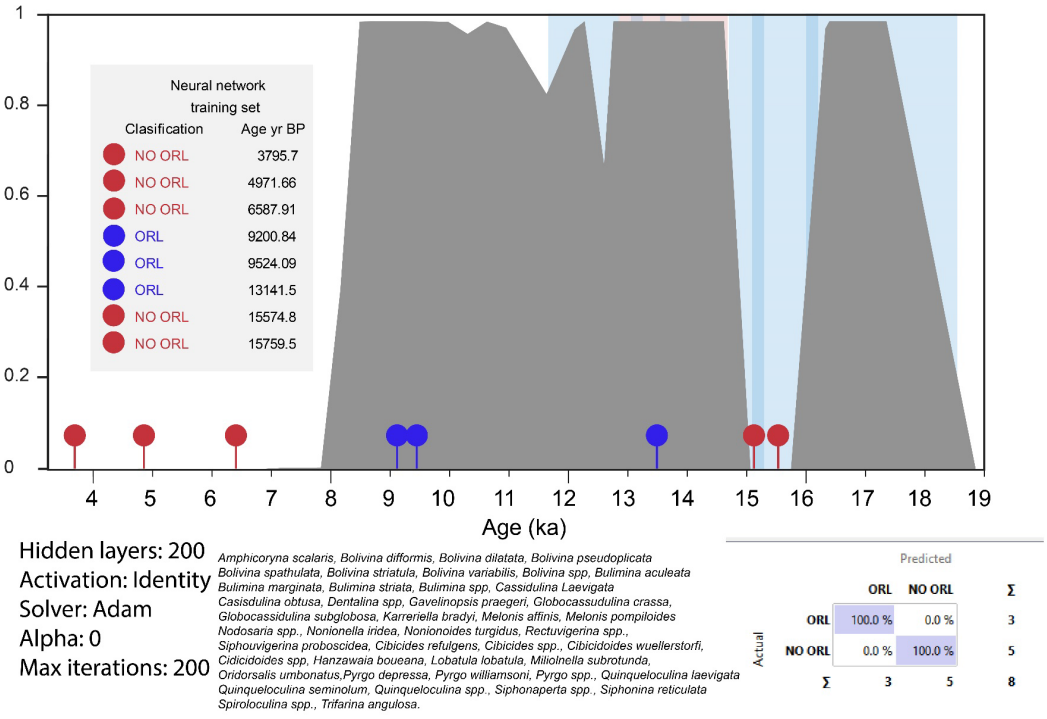

Figure VIII.S1. Neural network analysis results from the foraminiferal species. The model training was done using some known core sections, assigning them to ORL or no ORL; later, the model was used in the whole core, detecting multiple sections that presented characteristics similar to those of the ORL.

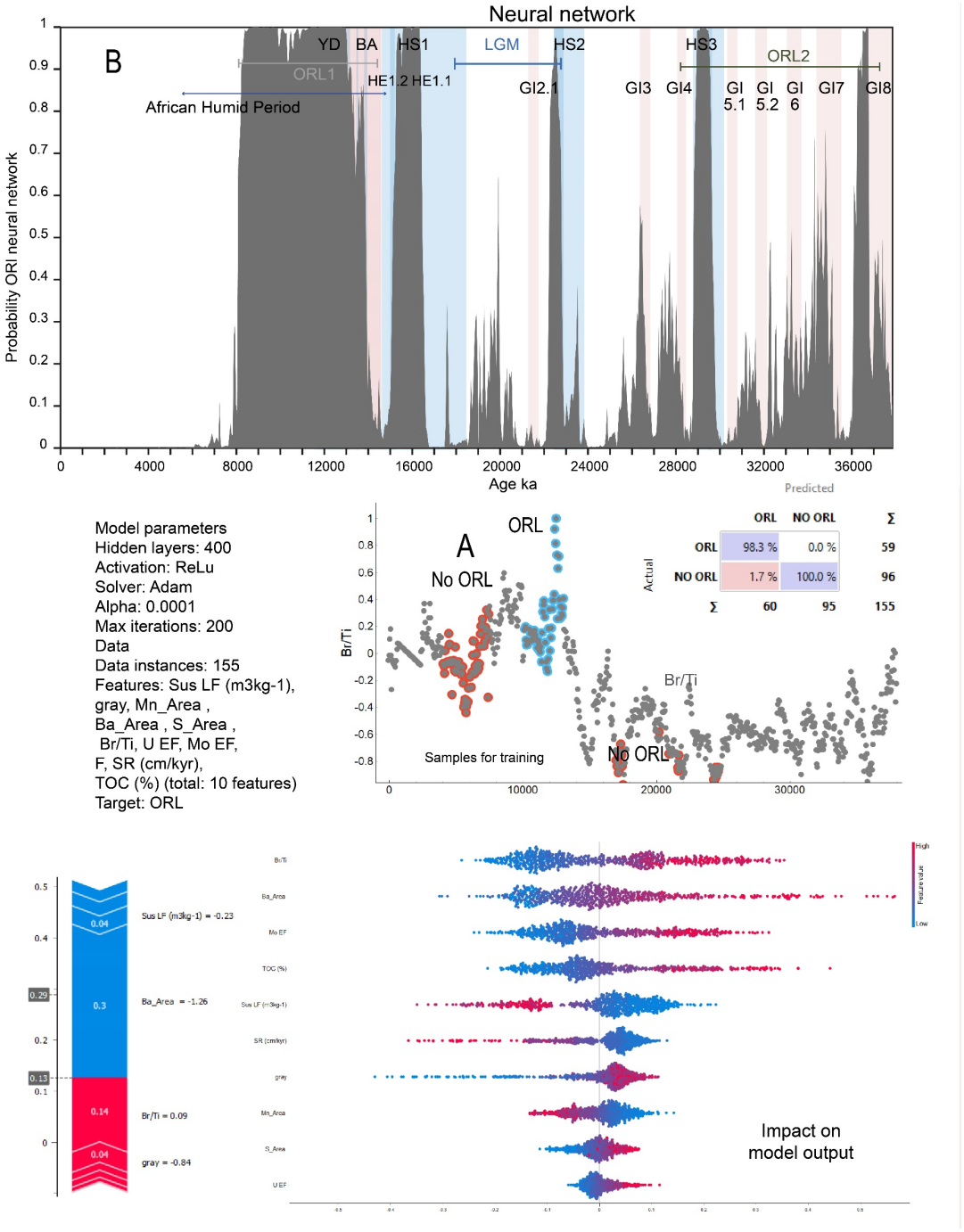

Figure VIII.S2. Neural network analysis results. The model training was done using some known sections of the core, assigning them to ORL or no ORL; later, the model was used in the whole core, detecting multiple sections that presented characteristics similar to those of the ORL.

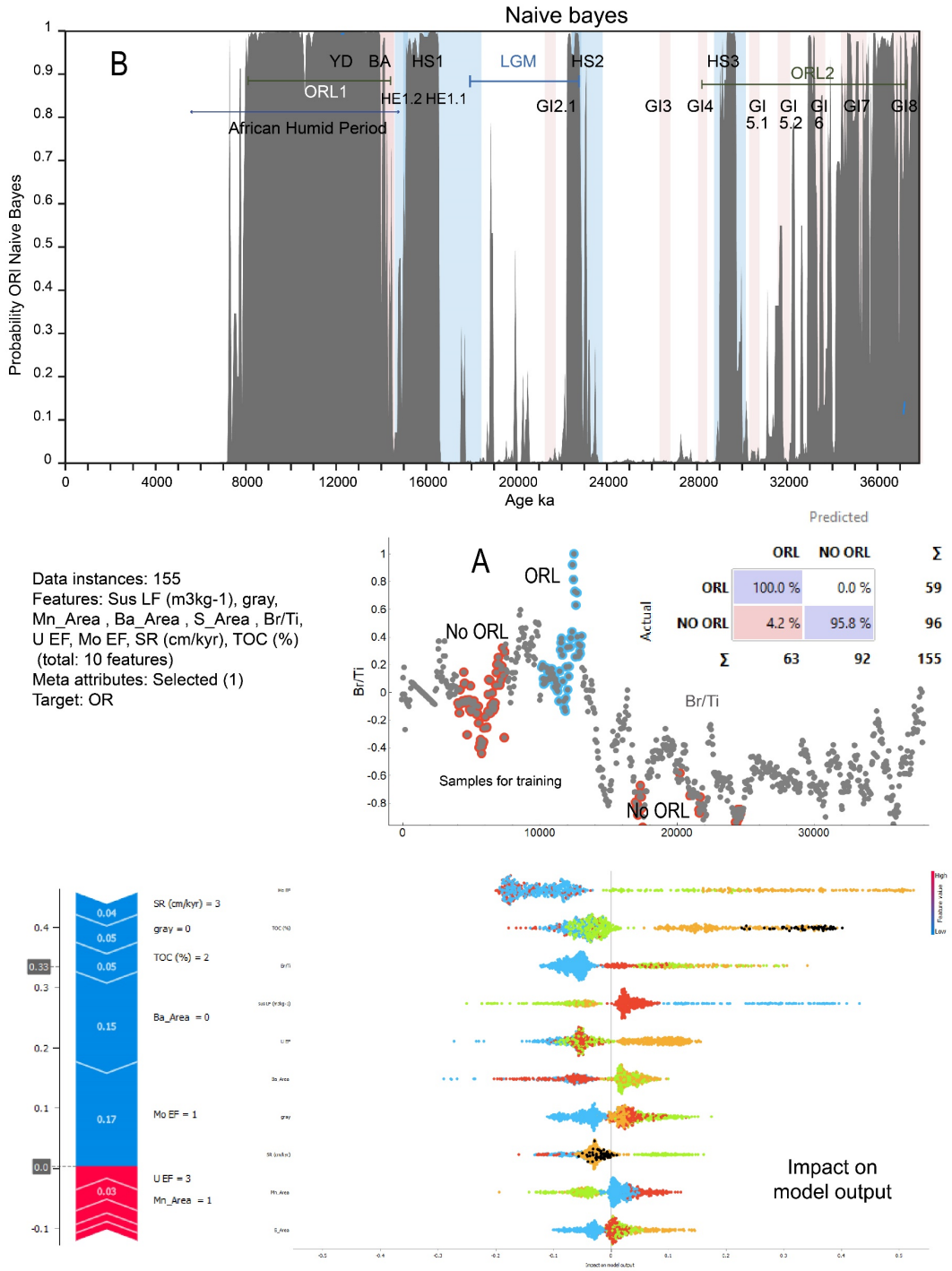

Figure VIII.S3. Naïve Bayes model analysis. The model training was done using some known core sections, assigning them to ORL or no ORL; later, the Model was used in the whole core, detecting multiple sections that present characteristics like that of the ORL.

VIII.3 Productivity in the basin over the last glacial

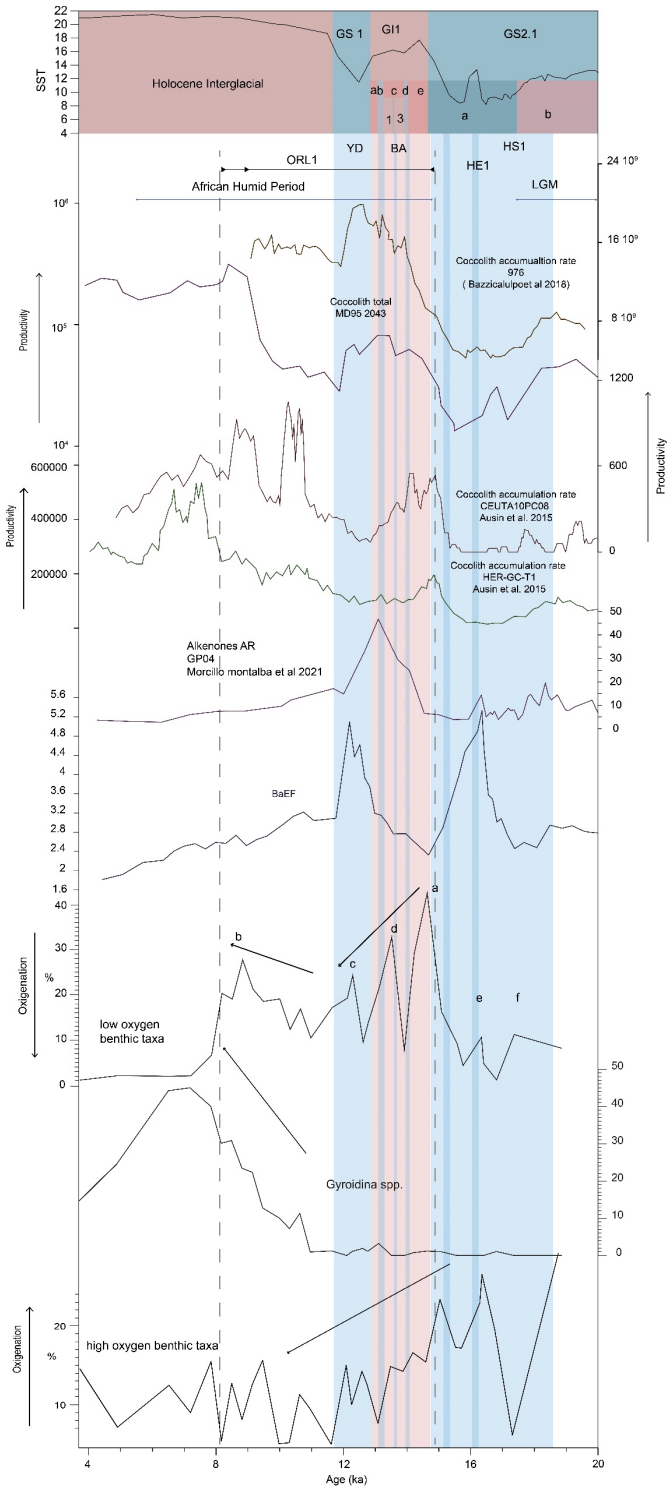

Figure VIII.S4. Benthic foraminiferal data (low oxygen benthic taxa, *Gyroidina* spp., and high oxygen benthic taxa) from GP03, comparing with coccolith total abundance in core MD95 2043 and coccolith accumulation rate in cores 976, CEUTA10PC08 and HER-CG-T1, from the Alboran Basin. Alquenones from Core GP04 (Montalba et al., 2021) and Ba EF from this study are also presented.

VIII.4 Principal component analysis of the data set

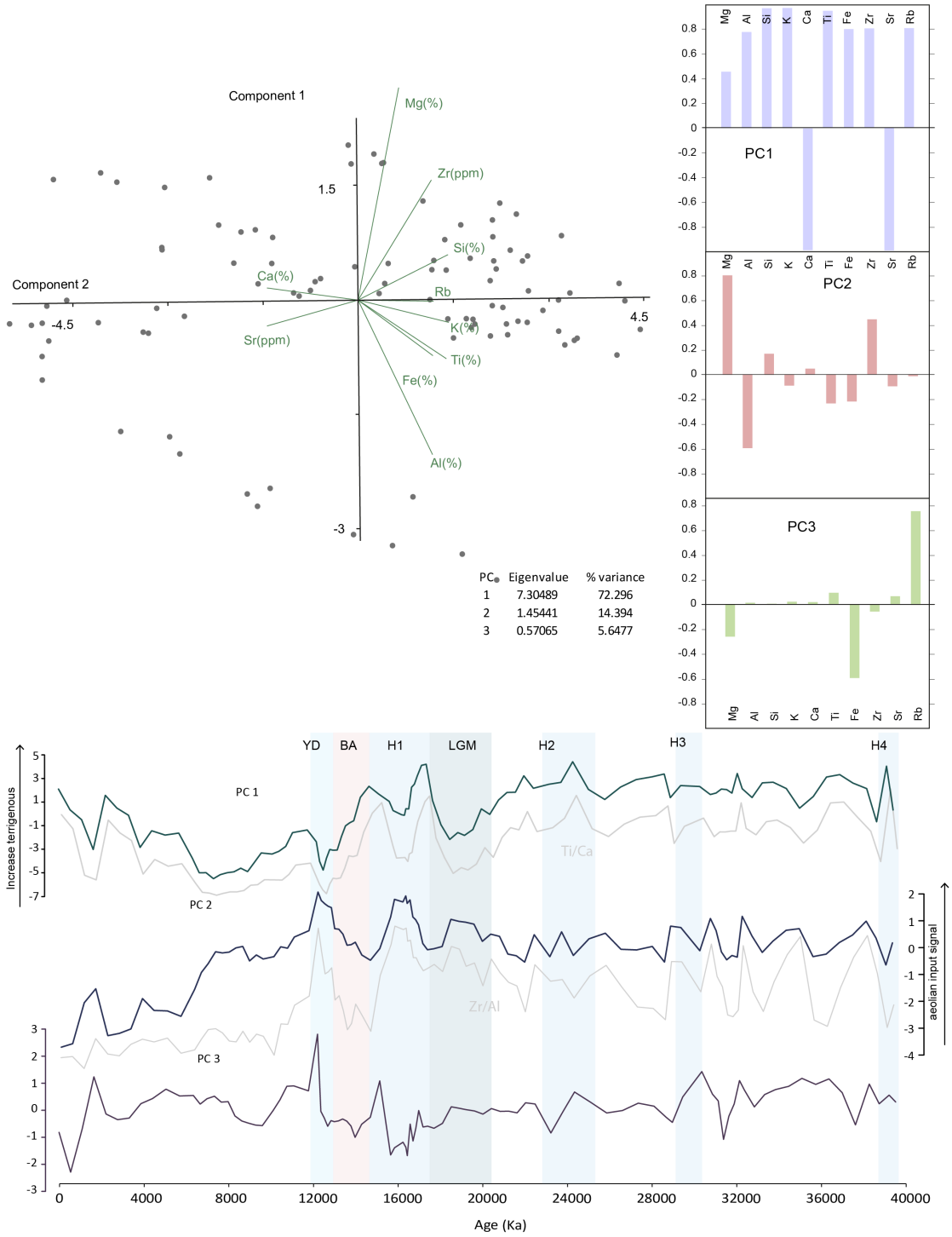

Figure VIII.S5. PCA analysis using only detrital fraction elements. Terrigenous fraction variation associated with fluvial inputs is the central control of the variation in the data set (PC1). Aeolian input controls the PC2; finally, grain size associated with Rb/K seems to be the main factor influencing the PC3.

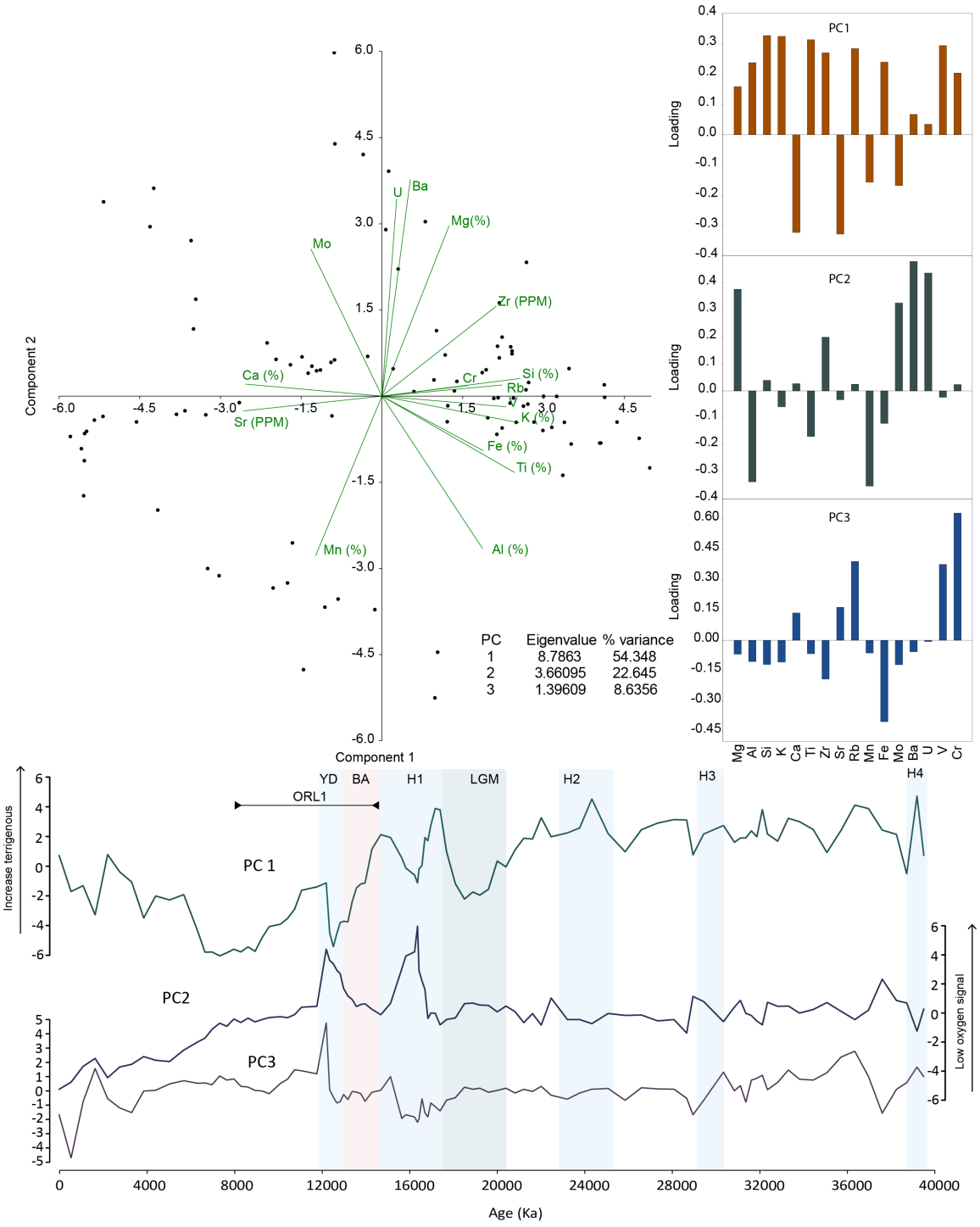

Figure VIII.S6. PCA analysis, including redox elements. The main factor controlling the variation here is the detrital fraction against carbonate variation (PC1); PC2 is governed by the redox conditions associated with U and Mo. Finally, PC2 seems controlled by Rb, Cr, and Fe so that it could be related to redox remobilization or grain size.

Chapter IX

Eastern Mediterranean deep environment during the Last Glacial Cycle

IX.1. Introduction

IX.1.1. The study of the Eastern Mediterranean Basin

The Eastern Mediterranean region has attracted particular attention in the fields of palaeoceanography, palaeoclimatology, and sedimentology, given the high sensitivity of this region to climate change. During its recent geological history, the region has been subjected to significant changes in bottom water conditions, particularly in terms of oxygenation of the bottom waters when an especially profound alteration in the thermohaline circulation has occurred, leading to the cyclic deposition of layers of enhanced carbon content (Kidd et al., 1978; Rossignol-Strick et al., 1982; Cramp and O'Sullivan, 1999; Emeis et al., 2000; Rohling et al., 2015, among many others). As previously stated in this thesis's introduction, these layers are called sapropels in the Eastern Mediterranean Basin; they differ from the ORLs in the Western Mediterranean Basin and have been more intensively studied as they are better developed.

To complement the conducted research on ORLs from the Western Mediterranean, a record from the Eastern Mediterranean near the Sicily Channel and the Gulf of Sirte was studied (LC10, Fig. IX.1). This region is of special interest regarding the dynamic Eastern Mediterranean water masses. It is an excellent location to study the exchanges between the Eastern and Western Mediterranean basins, the humidity and climate fluctuations in adjacent areas, and the Eastern basin's oxygenation at middle to deep depths (Dinarès-Turell et al., 2003; Incarbona and Sprovieri, 2020). It has also been observed that the reactivation of the fluvial systems in North Africa during the African Humid Periods (AHP) leads to imprints in

the composition of the sediments deposited in the area (e.g., Wu et al., 2018; Blanchet et al., 2021). In addition, the area is far enough from the Nile to receive less influence from its sediments (Wu et al., 2018), which allows for better observation of the Libyan fluvial system evolution over time.

This chapter approaches a preliminary reconstruction of the deep-sea environment in the Eastern Mediterranean Basin over the Last Glacial Cycle. This objective is accomplished by integrating geochemical and ichnological proxies using techniques developed in previous chapters. The results enhance our comprehension of environmental changes in the deep basin in response to climate variation at the time of sapropel deposition, which is also of great interest for comparison with the related ORLs in the Western Mediterranean Basin and further understanding of the interconnection between both regions.

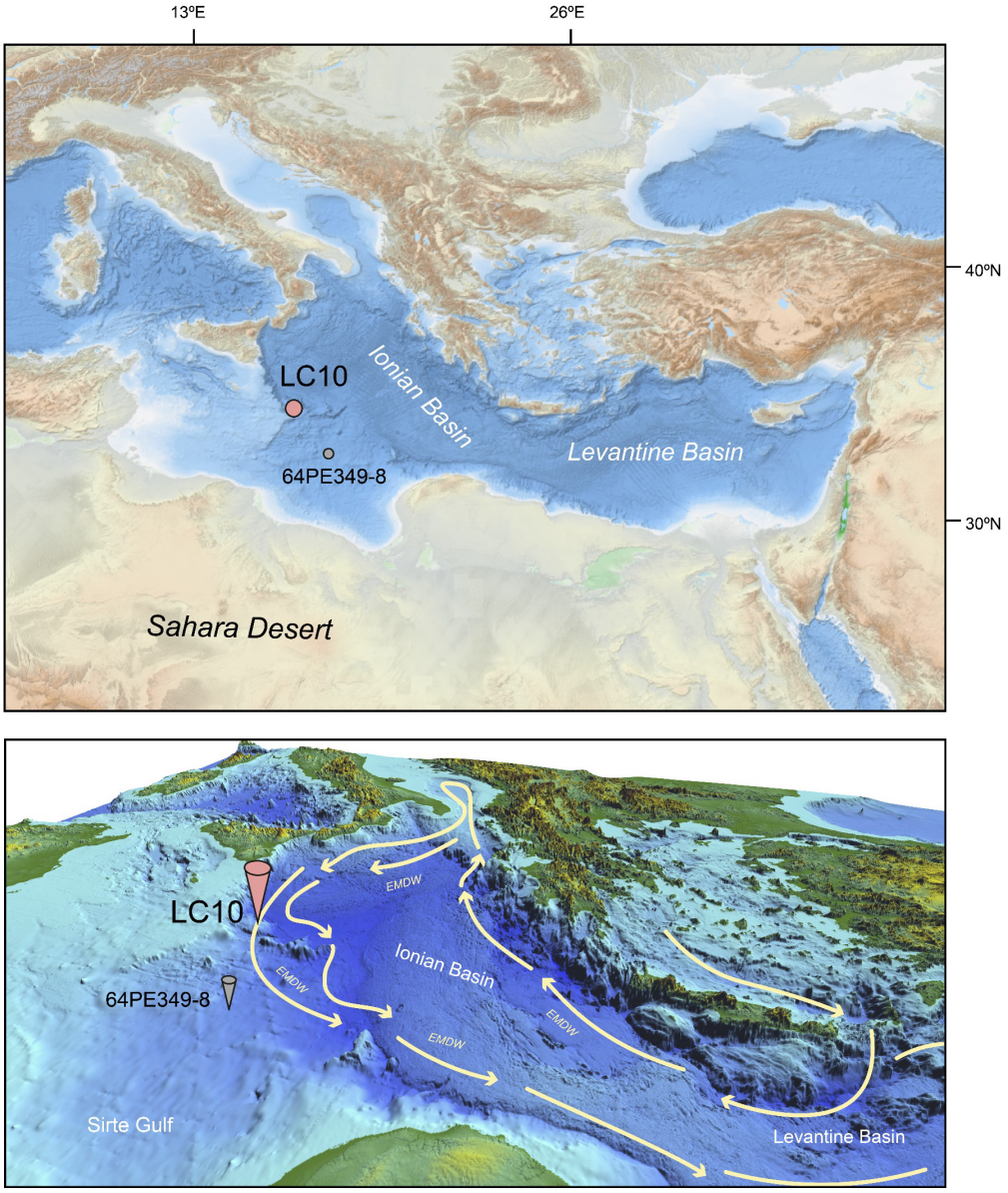

Figure IX.1. Location of the studied core LC10 and other selected cores in the Eastern Mediterranean Basin.

IX.1.2 Climatic forcings on the Sirte Gulf sediment composition

Oscillation in the humidity over an area —represented as the amount of rain that discharges over the continental area— varies over time, meaning changes in the sediment composition, specifically in the terrigenous fraction. These changes reflect the variable relative contribution of aeolian and riverine inputs. Thus, such palaeoclimatic variations are one of the main controls of the composition of the terrigenous fraction in the Eastern Mediterranean (Wu et al., 2016, 2018; Blanchet et al., 2021; Crocker et al., 2022). The interpretation of these signals for palaeoclimatic studies is complex as, for example, the dust of the aeolian fraction can have faraway provenance areas reacting to climatic changes occurring in those regions, while fluvial signals depend on close riverine discharges. The interpretation of these signals for palaeoclimate reconstructions should consider these factors.

The climate over the provenance area of the studied core in Northern Africa has undergone important changes over the Last Glacial Cycle. During precession minima, higher summer insolation in the Northern Hemisphere increases monsoon intensity over North Africa. For example, the AHP resulted in significant changes in the region's aridity, increased fluvial discharge by river reactivation, and even greening of North Africa (e.g., Rossignol-Strick, 1983; Ziegler et al., 2010; Wang et al., 2017). These humidity oscillations were the main mechanism triggering the sapropel deposition in the Eastern Mediterranean (Rossignol-Strick et al., 1982; Bar-Matthews et al., 2000; Rohling et al., 2015; Grant et al., 2016; Blanchet et al., 2021).

The incision of the African Monsoon over Northern Africa also has important implications for the terrigenous fraction, as recorded in the dust and riverine input variations in the deep basins (Ehrmann et al., 2013; Wu et al., 2016, 2018; Ehrmann and Schmiedl, 2021). In the studied setting, the main changes in the detrital fraction composition result from these variations in the humidity over the different Sahara and sub-Saharan regions. As has been said, the enhanced precipitation led to the reactivation of the North African fluvial systems, increasing fluvial inputs; also, the greening of the sub-Saharan area led to a subsequent decrease in aeolian input coming from this area (e.g., Bar-Matthews et al., 2000). However, there were certain periods when the dust input derived from palaeolakes and alluvial deposits in Subsaharan Africa was impaired by the advance of the Intertropical Convergence Zone (ITCZ) towards the north, while at the same time, the reactivation of fluvial systems in the north of Africa had not yet occurred (Bakker et al., 2019).

Blanchet et al. (2021) demonstrated that river discharge occurred during warm interglacial phases of MIS 1 and 5 when an increase in the summer and autumn rainfall over the entire catchment areas —forced by the insolation maxima and the displacement of the African Monsoon north— fed river systems and intermittent coastal streams in the Libyan region that are desiccated at present. In contrast, during glacial phases MIS 3 and 4, shorter-lasting and

less intense humid events triggered by Mediterranean storms were associated with autumn and winter precipitation over the Libyan coastal regions. MIS 5 and MIS 1 were relatively humid in the Mediterranean (e.g., Blanchet et al., 2021; Camuera et al., 2022), and increased precipitation involved the deposition of sapropel layers S4, S3 and S1 (Ehrmann et al., 2013; Ehrmann and Schmiedl, 2021).

IX.2. Material and methods

IX.2.1. Materials

LC10 is a piston core of 19.86 m recovered at 1322 mbsf in the Ionian Basin, at a bank north of Heron Valley in the East of Sicily Strait (Fig. IX.2; 35° 12.77 N, 16° 34.88' E). The core was recovered during the Marion Dufresne Cruise 81 in 1995 under the MAST II PALAEOFLUX Programme. It was sampled and analysed at Southampton's British Ocean Sediment Core Research Facility (BOSCORF). Sections 21 to 15, covering the Last Glacial Cycle, were selected for this study. Lithology corresponds to greyish-yellow to olive-grey foraminifer-rich mud and nannofossil ooze slightly to strongly bioturbated. Thin probable ash layers are also recognized, one identified in the studied interval at 472 cmbsf.

IX.2.2. Analytical methods

Core images were obtained using Geotek MSCL-CIS (Core Imaging System), and core radiographs were obtained using a GeoTek ScoutXcan X-Ray Imaging Scanner, both at the British Ocean Sediment Core Research Facility (BOSCORF) in Southampton.

ITRAX analysis for the cores was conducted using COX Analytical Systems ITRAX X-ray Fluorescence Core Scanner (XRF-CS) with a point every 0.2 cm at BOSCORF. From the initial XRF-CS analysis, 72 samples were selected for discrete sample analysis. Major elements for 72 selected samples were determined at the Andalusian Earth Science Institute using XRF and WDXRF Bruker AXS Pioneer S4. $\delta^{18}O$ and $\delta^{13}C$ were measured for the 72 samples on a GC connected to a MAT 253 isotope ratio mass spectrometer via a GC-III combustion interface at Leibniz Laboratory, Kiel, with a precision of $< \pm 0.08$ ‰ for $\delta^{18}O$ and of $< \pm 0.05$ ‰ for $\delta^{13}C$ on carbonates and calibrated to the V-PDB scale.

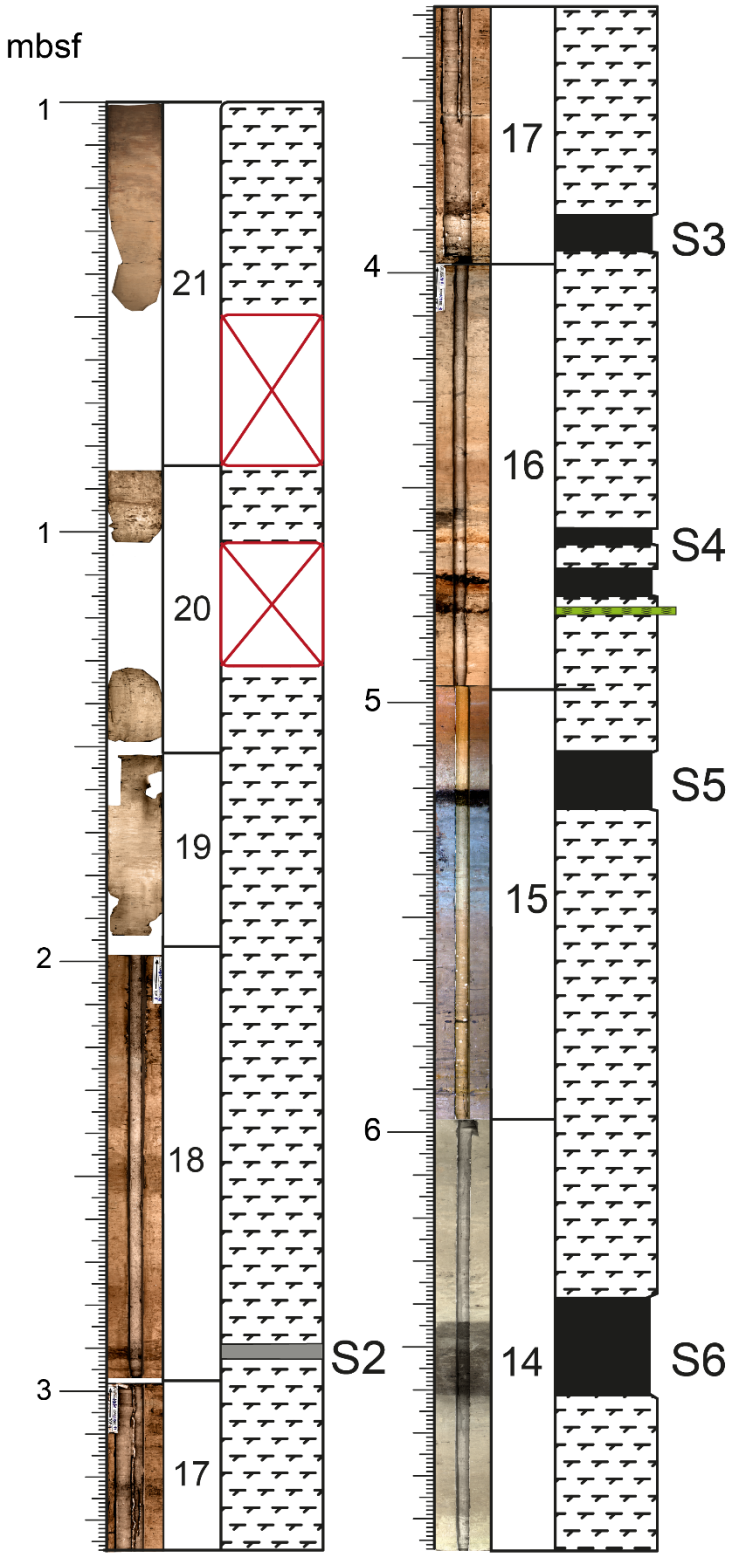

Figure IX.2. LC10 core log of the studied section, showing the position of sapropels 2 to 6. The numbers indicate the core splits.

IX.2.3. Element normalization and calibration

XRF core scanner data were normalized using the counts per second (CPS), the measurement time and the X-ray scattering from the ITRAX (Gregory et al., 2019). Elemental ratios were obtained for diverse palaeoenvironmental information, primarily Ti and Ca data from XRF Core scanner data, and Al and Ca concentration in discrete samples obtained from XRF and ICP-MS analyses served as conservative elements for obtaining informative ratios to evaluate carbonate and terrigenous input. This methodology ensures a more accurate reflection of the actual variation in the concentration of the target element of interest against the fraction to which it belongs (Weltje et al., 2015; Gregory et al., 2019). Some element ratios from ITRAX analysis were calibrated using discrete sample analysis with a direct linear transformation (Fig X.3; Weltje et al., 2015; Gregory et al., 2019), making it possible to derive the real values from the counts and thus a calibrated high-resolution record. For this method, it is advisable to use logarithms of the XRF ratios, as they can usually be converted linearly, with less error, to the composition results obtained from the XRF in discrete samples (Weltje et al., 2015; Gregory et al., 2019).

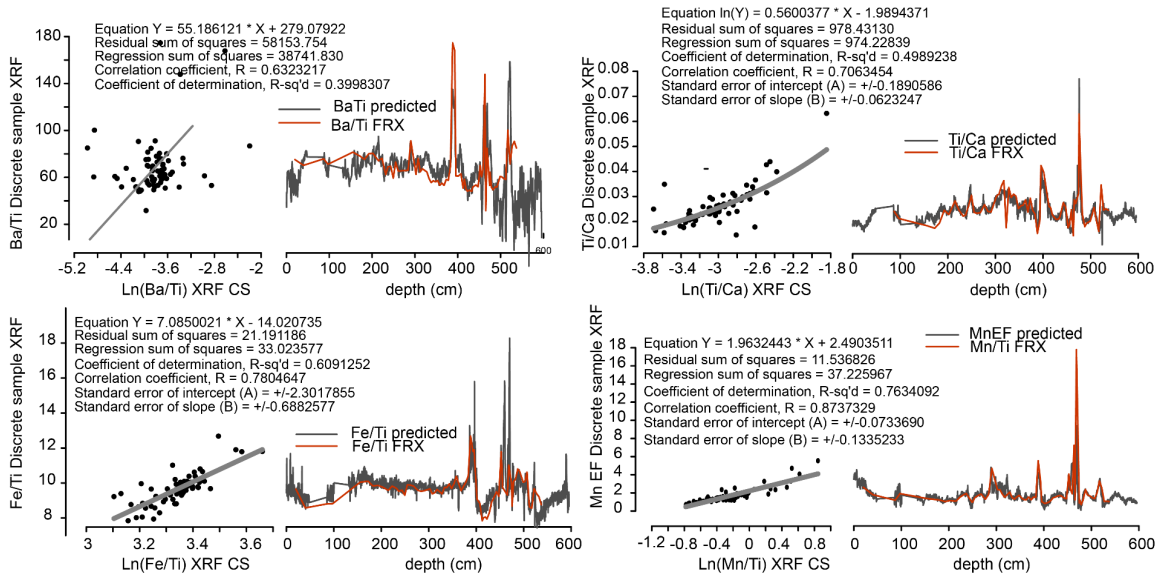

Figure IX.3. Calibration of Ti/Ca XRF core scanner plot by an exponential regression line or a linear regression using the composition results from FRX analysis in discrete samples.

IX.2.4. Age model

The age model was obtained using a combination of $\delta^{18}O$ profile tie points and the position of the sapropels based on geochemical and visual analysis (Table IX.1, Fig. IX.4). Linear interpolation was used to create the age model. The age of the top of the core was estimated to be 5000 years. BP using the average sedimentation rate of the available intervals. Piston cores tend to show differential compaction during recovery; hence, a reduction of sedimentation rate with depth is expected as an artefact, being observed in the age-depth plot resulting from our age model.

Table IX.1 Tie points used for the age model.

Event	Age (kyr) bot	Age (kyr) top	Depth (cm) bot	Depth (cm) top	insolation cycle	References
MIS1 Middle		10		20		Konijnendijk et al. (2015)
MIS2 end		20		97		Konijnendijk et al-(2016)
Sapropel 2	52	55	294	288	6	Muerdter et al. (1983); Bar-Matthews et al. (1998)
MIS3 end		30		190		Blanchet et al. (2021)
Sapropel 3	80.8	85.8	397	385.5	8	Grant et al. (2016)
Sapropel 4	101.8	107.8	475	456	10	Grant et al. (2016)
S4 interruption	104	105.4	468.5	463	10	Grant et al. (2016)
tephra	108.4					Vogel et al. (2010)
MIS4peak		66.245		350		Blanchet et al. (2021)
Sapropel 5	121.5	128.3	527	510	12	Grant et al. (2016)
Sapropel 6	176	170	653	645	16	Emeis et al. (2003)

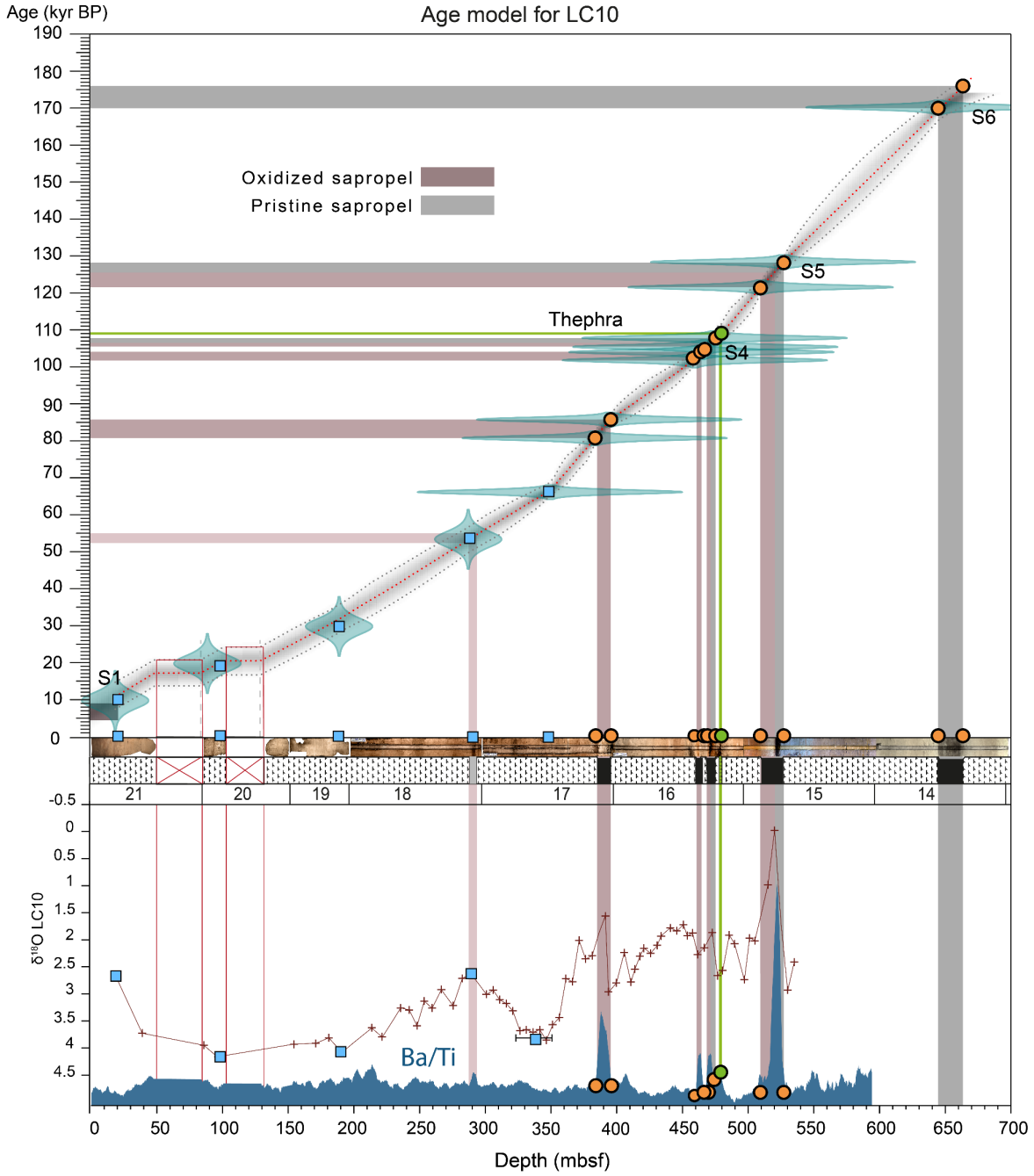

Figure IX.4. Age model of the LC10 core against selected events (sapropels 2, 3, 4, 5 and 6). Sapropel 1 does not appear represented in the core, but based on the projection of the sedimentation rate, it seems the core starts at 5000 mbsf. Green points indicate tephra layers, blue squares tie points against $\delta^{18}O$, and orange points indicate the limit of the sapropels used for dating.

IX.3. Results and discussion

IX.3.1. Geochemical proxies and climate changes

The $\delta^{18}O$ profiles in the Mediterranean correlate with the freshening of the surface layers in the Eastern Mediterranean; thus, it follows the humidity changes in the catchment areas (Bar-Matthews et al., 1997, 2000). The LC10 $\delta^{18}O$ increases during sapropels and during the MIS 2. The record shows a general decreasing trend over the Last Glacial Period, with the minimum close to the top of the record, which can be correlated with the LGM (Fig IX.5). Following this period, a rapid increase is observed, corresponding with the Early Holocene and the last AHP. The general decreasing trend of the LGM is not in a straight line but fluctuates, with 4 relative maxima. Correlations with the insolation eccentricity, tilt and precession (ETP) maxima, with the relative sea level (RSL; in this case in the Red Sea; Grant et al., 2016), and with other $\delta^{18}O$ records from the basin (Fig IX.5; Konijnendijk et al., 2015; Blanchet et al., 2021), reveal that the humid phases occur as expected during insolation maxima and that most humid phase occurred during sapropel 5, while the other sapropels developed during comparatively less humid phases.

The Ti/Ca ratio shows a significant decrease during S5 and S3 (Fig. IX.6). However, at the end of S4 and several times during MIS2 and MIS3, the ratio shows an increase in the carbonate fraction against the terrigenous fraction. These events could be associated with increased biogenic material reaching the sea floor, characterised by greater productivity; however, a decrease in the terrigenous fraction cannot be discarded. One possible mechanism for a decrease in the terrigenous fraction could be the reduced influence of the rivers on the setting during highstand conditions, as most fluvial input would have been trapped in the extensive continental platform of the Gulf of Sirte. Another option is that the observed abrupt changes in the Ti/Ca ratio at the site can likewise be associated with changes in the continental humidity over North Africa, with the reduction of terrigenous fraction during humid phases due to impaired dust input and trapped fluvial sediments in the platform. Following the last explanation, successive short-duration low-intensity humid periods could occur during MIS2 and MIS3 and even during MIS 4 (Fig IX.5 and IX.6). There is evidence of humid phases in the MIS2 and MIS4, which could leave the observed signal here. For example, at 58-49 ka, increases in precipitation over Africa have been observed in other settings (Almogi-Labin et al., 2009), and some of them can be associated here with the S2 formation around 55 ka (Lourens et al., 1996). Further humid phases are identified in some records, like around 38 kyr BP (Revel et al., 2010), determining reduced exchanges between the Eastern and Western basins (Di Donato et al., 2022). These other shorter humid episodes in the Mediterranean did not produce sapropels but impacted the oceanography and could be tentatively correlated with some of the variations in the Ti/Ca plot (Fig IX.6).

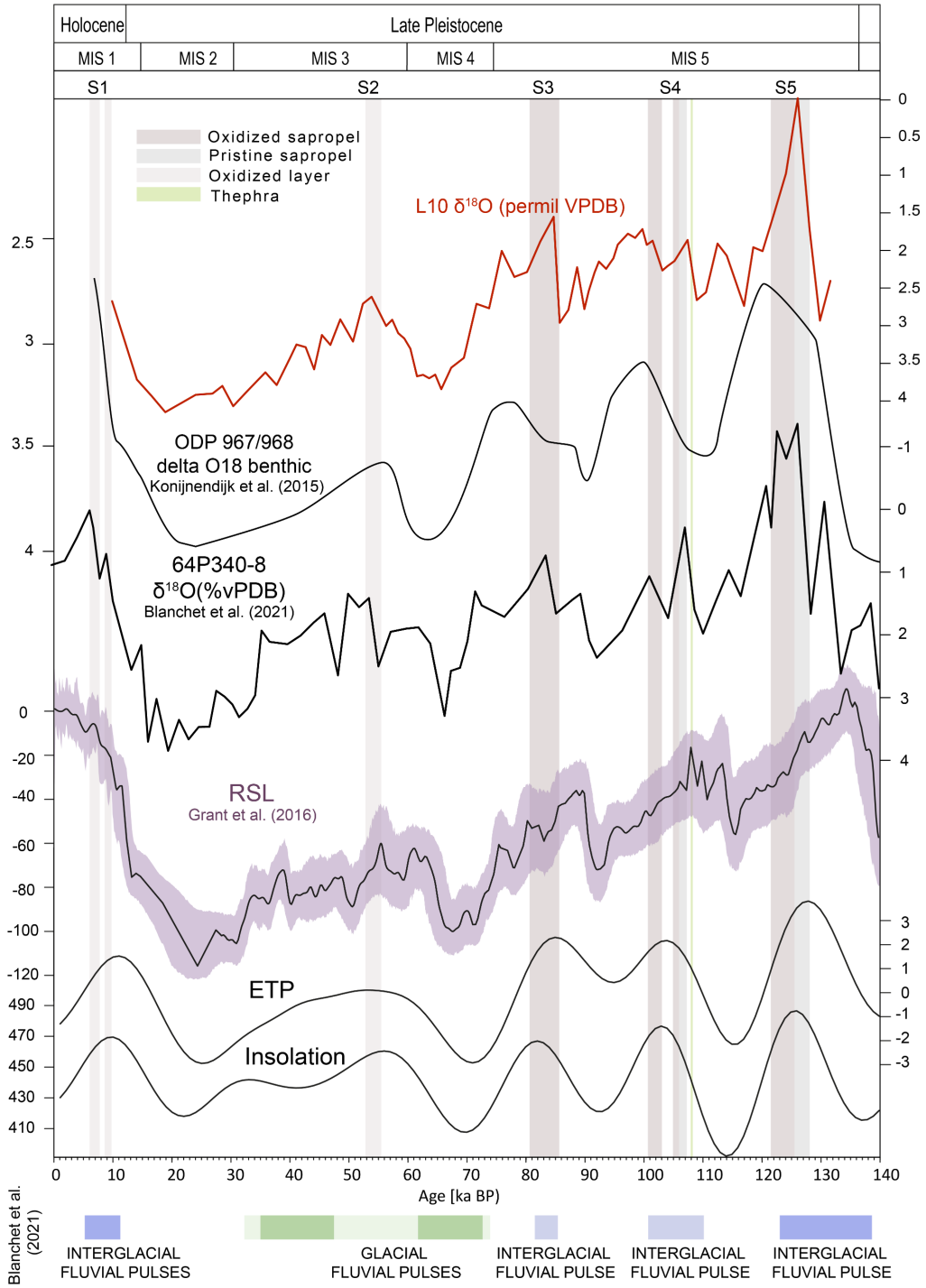

Figure IX.5. Comparison of LC10 $\delta^{18}O$ record with other records in the basin (see text for an explanation; Konijnendijk et al., 2015; Blanchet et al., 2021).

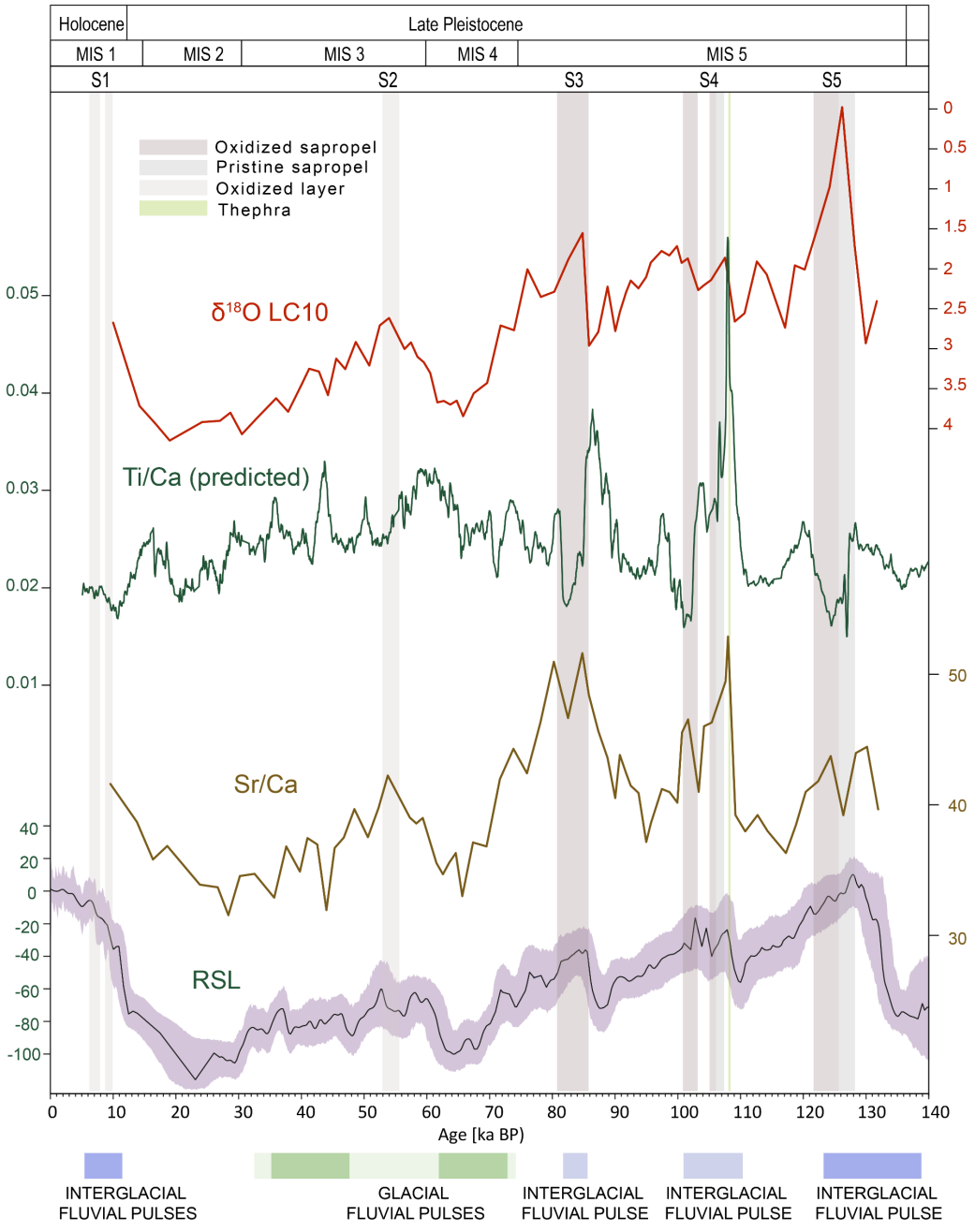

Figure IX.6. Geochemical proxies for detritic fraction variation. From top to bottom of the image LC10 $\delta^{18}O$, representing the age model's main climatic variations and the tie points. The Ti/Ca ratio plot represents the relative variations between the carbonate versus the terrigenous fraction. The Sr/Ca ratio represents the variations in the sea level, as explained in the text. At the bottom, the relative sea level (RSL) from Grant et al. (2013) was measured at the Red Sea. Below the age scale, there is a representation of the approximate duration of the fluvial pulses described recently for the north of Africa fluvial system by Blanchet et al. (2021).

Another interesting geochemical elemental ratio in this setting is the Sr/Ca ratio, which shows increased values during S3 and S4 and, less importantly, during S5, yet scarcely during MIS3 in the inferred position of S2 (Fig IX.6). The Sr/Ca ratio has been correlated with increased shallow source area carbonates reaching the basin (Reitz and De Lange, 2006), associated with bypassing shallow carbonates from the shelf typically occurring during sea level rises (e.g., Rothwell and Croudace, 2015). This association comes from the increased input of high Sr aragonite, which requires a shallow origin (e.g., Thomson et al., 2004; Rothwell et al., 2006; Rothwell and Croudace, 2015). The Sr/Ca ratio record from LC10 significantly correlates with sea level variations, particularly during sapropels. This suggests that the rise of sea level during these periods and the increment in the mobilization of sediments with carbonates formed in the shelf reaching deep basin most likely contributed to the enhancement in this ratio. Additionally, Sr/Ca could be indicative of high sea levels and higher remobilization of self-sediments to the basin tied to fluvial discharges. In that case, the Sr/Ca ratio of the LC10 record indicates the presence of the 55 ka humid event, even though evidence of S2 could have been removed from other proxy records. The correlation between increases in the Sr/Ca ratio and sapropels is stronger in S4 and S3 than in S5. S4 and S3 are interglacial sapropels characterized by lower sea levels, which could have facilitated the transport of shelf sediments to the basin more effectively than during interglacial highstand periods.

IX.3.2. Authigenic precipitation: the geochemical signature of sapropels and post-depositional processes

The Ba/Ti and Br/Ti ratios allow for precise identification of sapropels in the LC10 record, even if oxidized, and they are good proxies for the presence of OM and enhanced productivity (Tribovillard et al., 2006). These proxies showed no signals of post-depositional alteration (Fig. IX.7) and served here to locate the sapropel's original position. A special framework must be invoked in interpreting the position of S2, which does not present these signals.

Authigenic trace metal ratios like UEF, MoEF, Cu/Ti and Mn/Ti are mainly controlled by oxygenation conditions (e.g., Vine and Tourtelot, 1970; Calvert and Pedersen, 1993; Algeo and Maynard, 2004; Tribovillard et al., 2006; Algeo et al., 2020), but they appear to have suffered important remobilizations. Alteration of these metals' content is expected, especially in the sapropels, showing evident burnout. Continuous exposure to relatively high oxygen bottom waters with low sedimentation rates, specifically below 2 cm/kyr, could cause authigenic minerals to dissolve and permeate out of the sediment, removing any primary record (Mangini et al., 2001; Jacobel et al., 2017, 2020; Costa et al., 2018). The oxidation and diffusion of elements by oxygen penetration can continue for a considerable time, and when another sapropel layer deposits, it can protect from the oxidation of older sapropel (De Lange et al., 2008). Thus, from relatively close in-depth sapropels S2, S3, S4, and S5, the amount of oxidation is much more important as we descend in the record. This explains why S2, S3 and

S4 can be considered "ghost sapropels" in the studied setting, with S5 conserving an unoxidized interval, and why the remobilization of the redox elements is stronger in the shallower sapropels.

Mn, Fe and Cu enrichments serve to recognize oxidation fronts in sapropels and can be used to reveal the extension of the reoxygenation of previously anoxic sediments (De Lange et al., 1994, 2008; Löwemark et al., 2006). Accordingly, the studied record reveals that S3 and S4 were oxidized, while S5 was partially oxidized. The "ghost" S2 shows a complex Mn signal indicative of a composite reoxygenation process. The remobilization of Cu, Fe, and Mn occurred in distinct ways, with Cu showing more peaks and concentrating at different depths than the others; Mn and Fe have peaks at different depths. This diffusion pattern suggests a fractionation ladder in the precipitation of trace metals within the reoxygenation layer. This phenomenon appears because different trace metals undergo varying processes and pathways during reoxygenation, leading to differential redistribution within the sedimentary layers (Monedero et al., 2023b).

Pyritization processes are observable in the trace metal record and can be detected through the sulphur content (Thomson et al., 1995, 1999). Pyritization below the sapropel is known to be produced during diagenesis, generating a grey layer below sapropels that was mistaken in the past for preconditioning conditions (Thomson et al., 1995, 1999; Reed et al., 2011). In the LC10 record, extended parts under the sapropels were pyritized, as seen by the increasing sulphur indicated by Ln(S) (Fig IX.7). The reductive environment displaced the Fe by diffusion, as shown by the reduction in Fe/Ti ratios in the interval preceding the sapropel (Fig IX.7). Moreover, there is an increase in the Fe/Ti ratio in the oxidation zone of the sapropels, where the remobilised Fe precipitates as oxides (Morford et al., 2009a). In addition, the amount of S is related to the strength of the anoxia (Warning and Brumsack, 2000; Reed et al., 2011). Thus, S5 was comparatively the most anoxic event, followed by S3, whereas S4 does not appear to be excessively restricted.

Modern low-oxygen marine systems have Mo–U covariation patterns that can be attributed by elaborating empirical, conceptual models from modern settings to specific depositional system characteristics and processes (Algeo and Tribovillard, 2009; Algeo and Liu, 2020). Such techniques have been applied successfully in the Mediterranean Basin (Monedero-Contreras et al., 2023a). Although finding evidence of U and Mo enrichment during sapropel layers was anticipated, most of the enrichment occurs below sapropels except for S5, with a well-defined diffusion path, as seen in Figure IX.8.

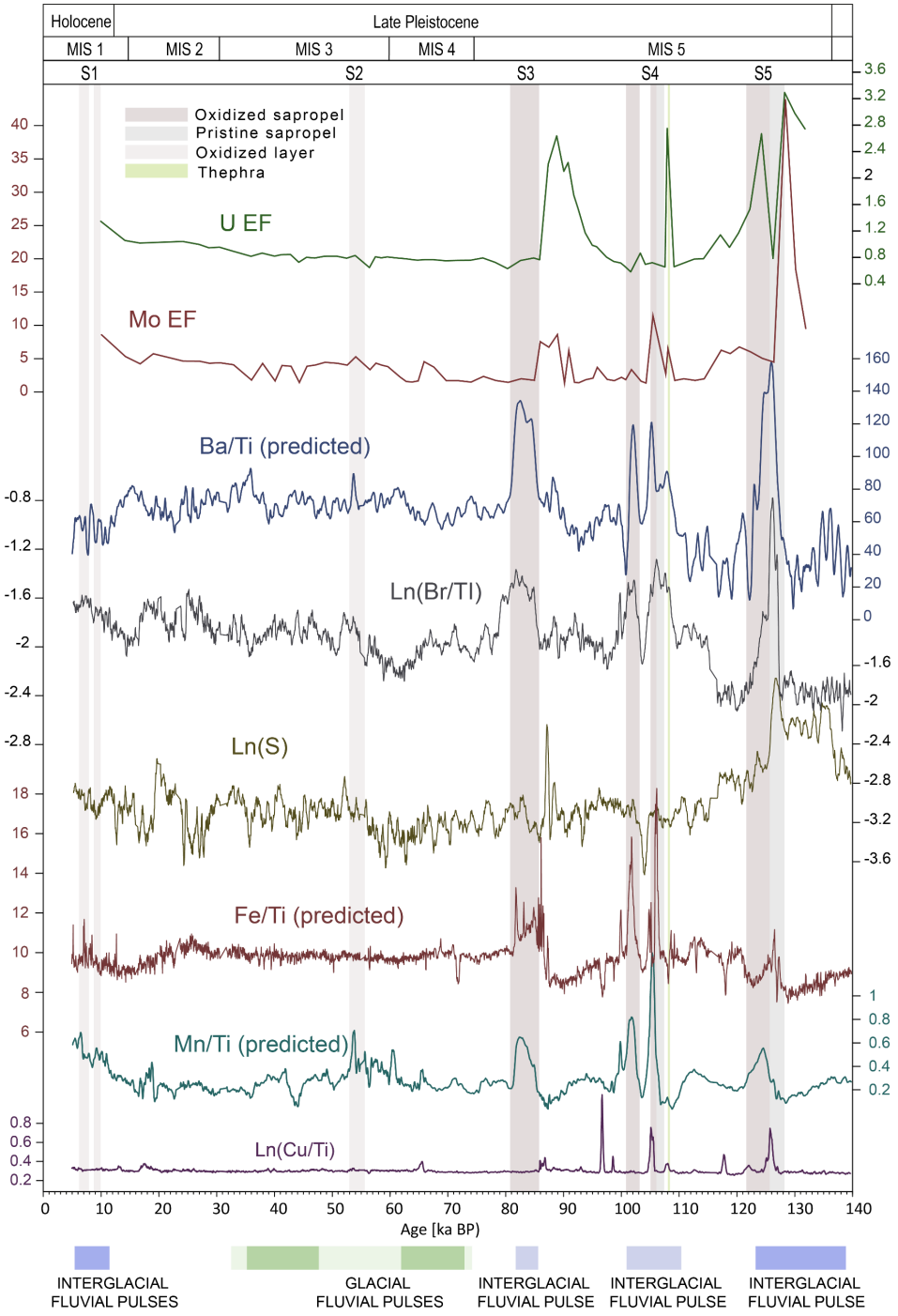

Figure IX.7. Evolution of geochemical trace metal proxies along the studied interval at the LC10 core.

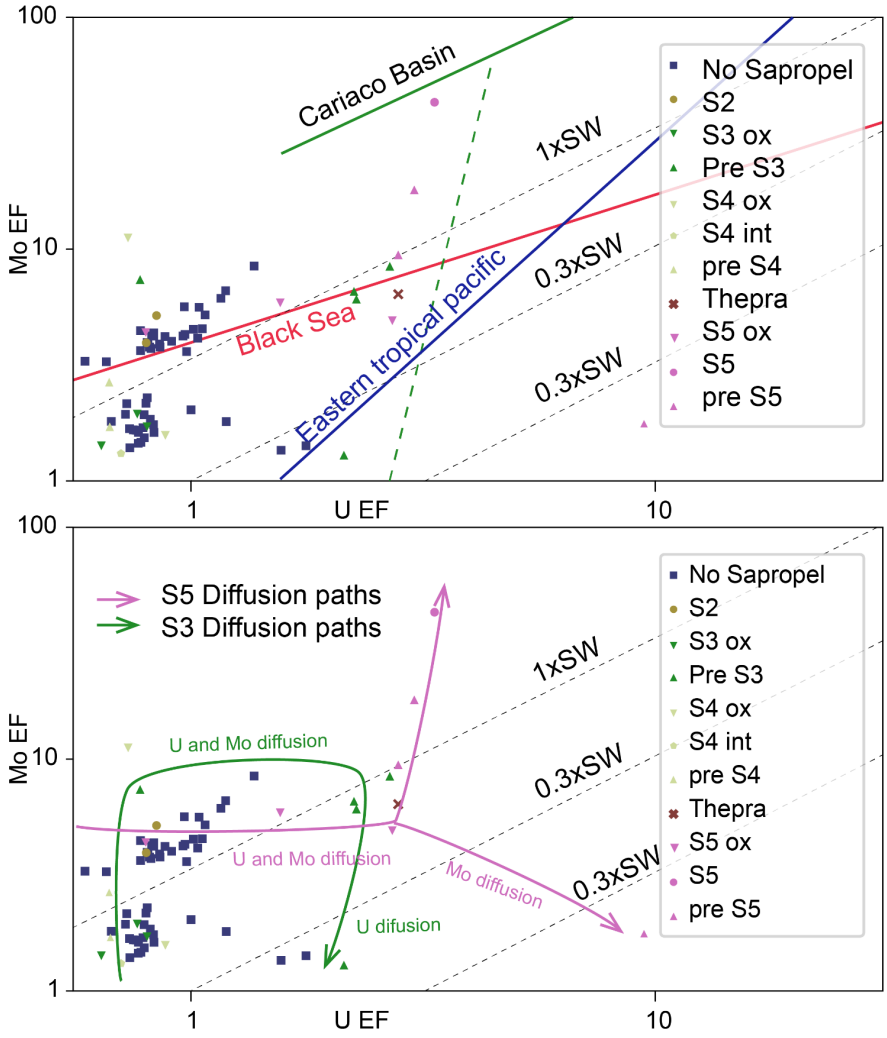

Figure IX.8. MoEF-UEF diagrams in LC10 core and comparison with known settings (Morford et al., 2009b). A displacement of the signals is observed, the sapropel points decoupling from the expected values, while the S5 points that have not undergone remobilization of Mo and U show the expected enrichment values.

The S2, S3, and S4 values are similar to the non-sapropel intervals. However, as mentioned before, in the studied record, S3 and S5 show an extensive relocation of U and Mo within the sediment column, transported below the sapropel layer in the reduction area, the pyrite formation aiding in the fixation of the trace metals in this interval (Monedero-Contreras 2023b); this explains why the pre-sapropel and post-sapropel intervals show the enrichment in U and Mo expected inside the sapropels (Figs IX.8). The absence of this diffusion and concentration of U and Mo in S4 could be attributed to the absence of favourable conditions for the concentration of trace metals below the layer with no pyrite enrichment. Furthermore, the absence of Mo and U diffusion downwards could be due to the bioturbation of the sediment layer following the deposition of S4 (see IX.3.3, Figs. IX.9, IX.10 and IX.11), influencing the direction of element diffusion. These elements would have, therefore, diffused upward into the water column in S4 and downward in S3 and S5. Hence, the interplay between euxinia,

bioturbation, and the timing of sedimentary processes would contribute to variations in the diffusion patterns of trace elements within the different sapropel layers.

S5 is the only sapropel that conserves part of the original signal, showing the enrichments expected of a restricted basin (like the Carioco Basin; Monedero-Contreras 2023a). However, a major part of the signal is defused downward, with a differential diffusion of Mo against U, likewise observed in S3, with U diffusing further downward (Fig. IX.7 and IX.8).

IX.3.2. Ichnological features, sapropels and environmental conditions

Detailed ichnological analysis of the LC10 record reveals the presence of *Chondrites, Planolites, Thalassinoides* and *Trichichnus*; also, *Scolicia* and *Zoophycos* are tentatively recognised. As explained in Chapters VI and VII, in a relatively stable deep marine environment, benthic food availability and bottom/pore water oxygenation are the main factors controlling the macrobenthic trace maker community and, then, ichnological features (e.g., Bromley et al., 1996).

Chondrites are related to lower levels of oxygen than other traces, especially when they appear alone, and thus are generally associated with suboxic/extreme dysoxic environments (Bromley and Ekdale, 1984; Bromley et al., 1996; Baucon et al., 2020; Vinn et al., 2020; Rodríguez-Tovar, 2021). The exclusive presence of *Chondrites* in sapropels (Fig. IX.10) could indicate minor improvement in oxygen conditions, allowing only the bioturbation of *Chondrites* trace makers. In the inter-sapropel layers, e.g., between S4 and S3 —starting some cm above S4 and after S5 (Fig. IX.10 and IX.11)— the scarcity of traces, with the only presence of some *Chondrites*, could indicate a major incidence of benthic food concerning oxygen conditions.

Zoophycos, tentatively recognized just below S3, could further support low oxygen conditions (Bromley and Ekdale, 1984; Ekdale and Lewis, 1991; Baucon et al., 2020). Nevertheless, *Zoophycos* was not observed in the other sapropel layers, highlighting some particularity of the S3 layer in case of its real presence. For instance, *Zoophycos* do indeed concentrate pyrite, as made evident by the Ln(S) record (Fig. IX.7), where important peaks in S in *Zoophycos* point to a role in the downward diffusion of euxinic conditions.

Certain core sections present intense mottling over imposed by discrete traces tentatively interpreted as *Scolicia* (Fig. IX.9). This is especially evident around 65 kyr BP. *Scolicia* are associated with the abundance and quality of benthic food (Kröncke, 2006; Wetzel, 2008; Carmona et al., 2020), and the feeding movement of recent echinoids (*Echinocrepis rostrata*) has been related to a small-scale distribution of seafloor phytodetritus coverage (Miguez-Salas et al., 2022). Hence, sections characterized by the presence of *Scolicia* can be linked to intervals of high productivity under well-oxygenated bottom water. *Scolicia* has also been associated with sandy intervals in the Mediterranean (Löwemark et al., 2006). The possibility that they

indicate periods of important variation in the terrigenous input can, therefore, not be discarded. In fact, they appear during periods of increased Ti/Ca ratio, which could indicate changes in substrate features.

Trichichnus "mycelia", corresponding to less than one mm wide tubular traces and up to several decimetres in the vertical dimension (Häntzschel, 1975), has been observed in recent sediment from the Mediterranean (Löwemark et al., 2006). Modern marine sediments are usually pyritized below 10 to 20 cm (Löwemark et al., 2006). Their abundance is tied to reduced bottom water (Thomsen and Vorren, 1984). In LC10, *Trichichnus* appears as a pyritized trace, only visible in the radiographs under sapropel layers S4 and S5. The diagenetic process enhances the visibility of *Trichichnus*, which might indicate the depth at which pyritization occurred during sapropel deposition, evidencing some degree of pyritization under S4 that was not evidenced by the geochemical proxies. This observation agrees with the colour change in the pre-S5, pre-S4, and pre-S3 intervals associated with these pyritization processes. (Figs. IX.10 and IX.12).

In LC10, *Thalassinoides* appears concentrated in a few sections of the record, mostly pre- and post-S3; it also appears at 58 ka, 65 ka, 99 ka and before and after S5 (Fig IX.9), indicating periods of good ventilation of the sea floor.

Planolites is an extremely facies-crossing form found in various facies and, therefore, less indicative of palaeoenvironmental conditions. Here, it often appears associated with the mottled background of heavily bioturbated sediments. Still, the absence of *Planolites* in layers S5 and S4b might indicate the maintenance of low oxygen conditions within the sediment after the end of sapropel deposition. Because abundant indeterminate bioturbation also appears in those intervals, any interpretation of the *Planolites* record should be made with care.

Some authors (i.e., Zirks et al., 2019) proposed differential ventilation in the Eastern Mediterranean, with middle layers that oxygenate only a portion of the water column. As LC10 is in the way of the Eastern Mediterranean Deep Water after it forms in the Adriatic Sea and lies at a relatively shallow depth and close to the continental shelf, it could explain the abundant bioturbation observed in the core, as well as the rapid oxidation of sapropels.

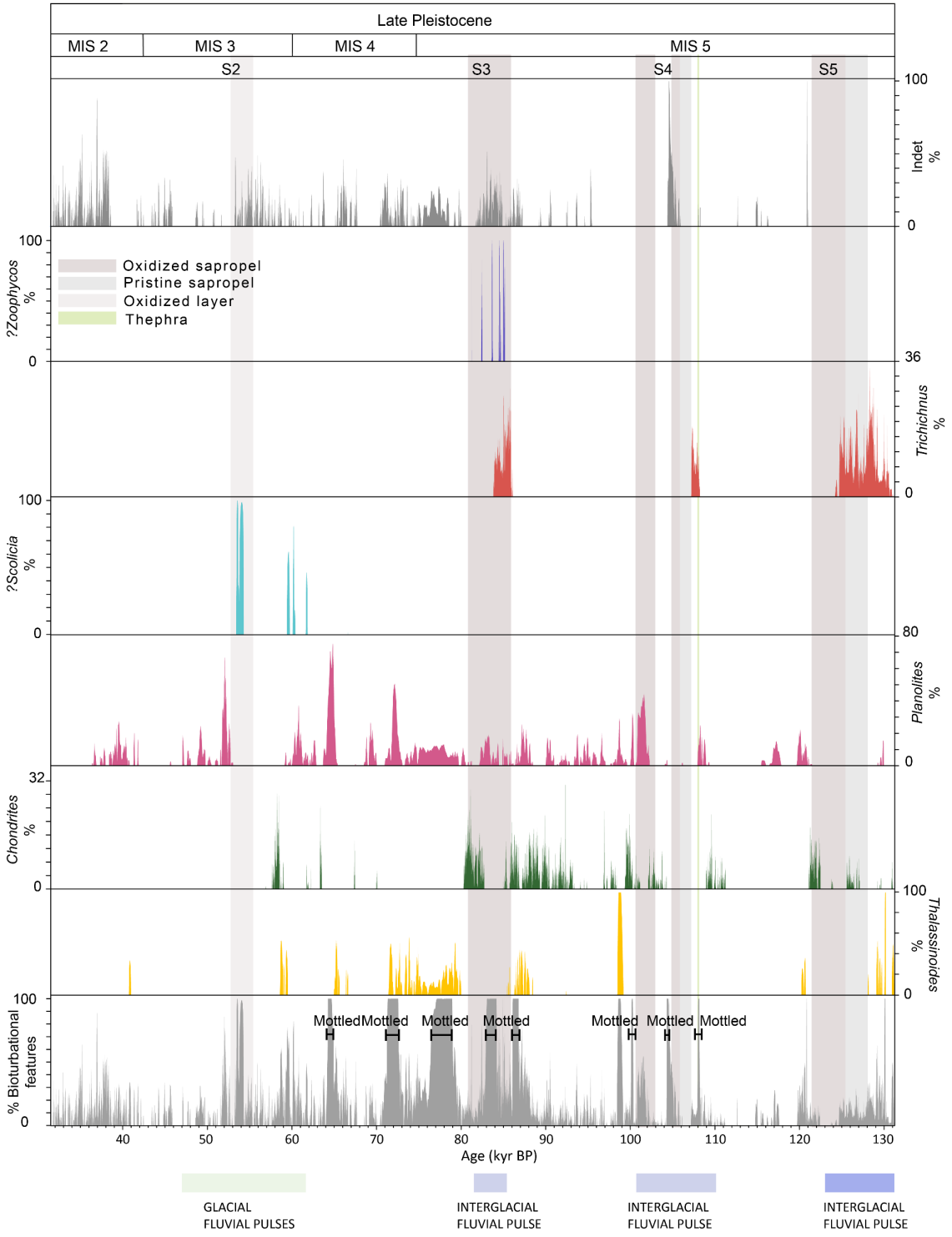

Figure IX.9. Distribution of the total amount of bioturbation and differentiated ichnogenera in the 40-145 ka interval. The percentage of area occupied by every individual ichnogenus is presented with a colour code that is maintained throughout the chapter. The total mottled bioturbation indicates the total % of the area occupied by traces and mottled ichnofabric.

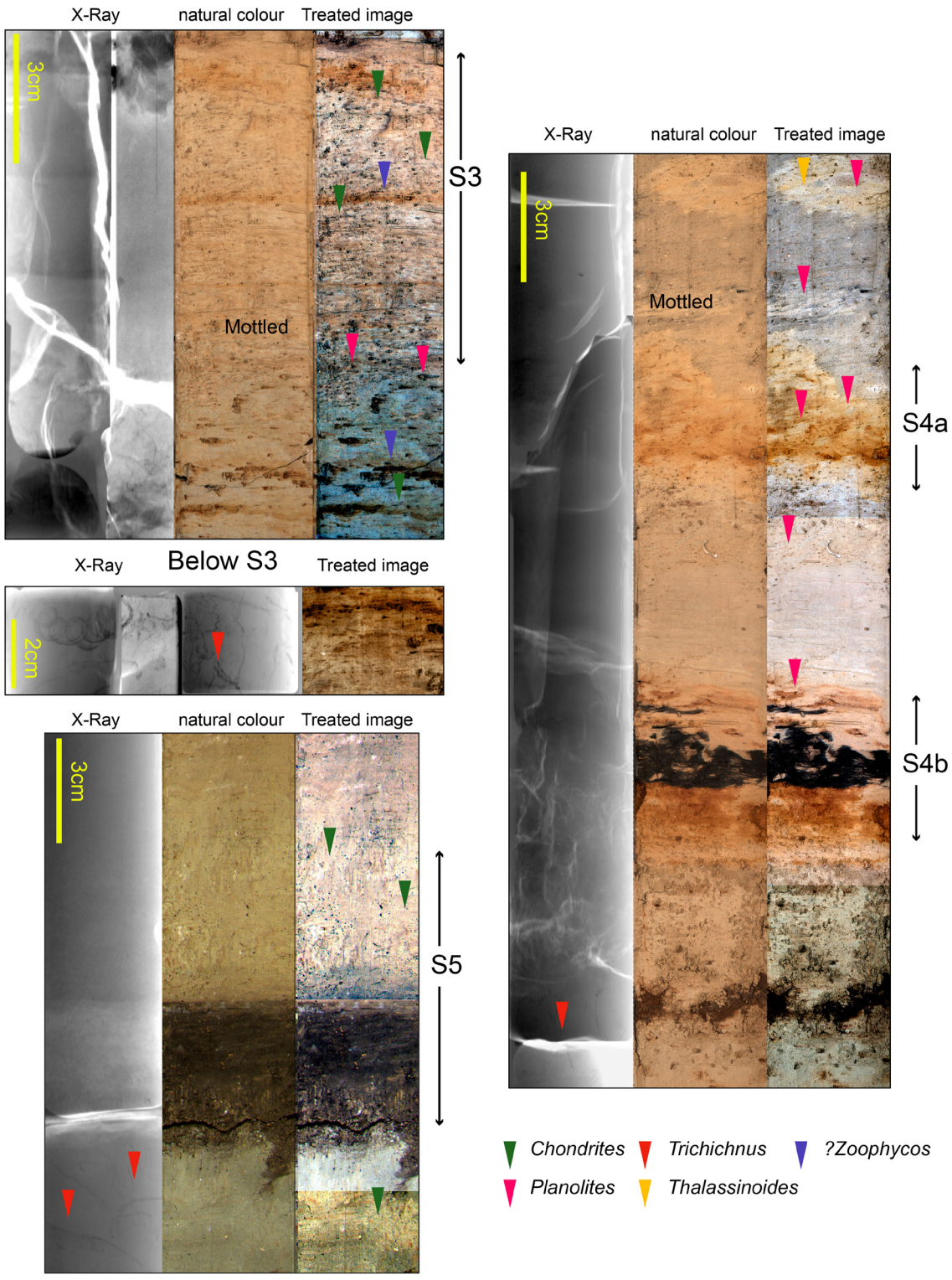

Figure IX.10. Close-up views (X-ray image, not treated natural colour image, treated image) of S5, S4 and S3 sapropels with observed ichnological features.

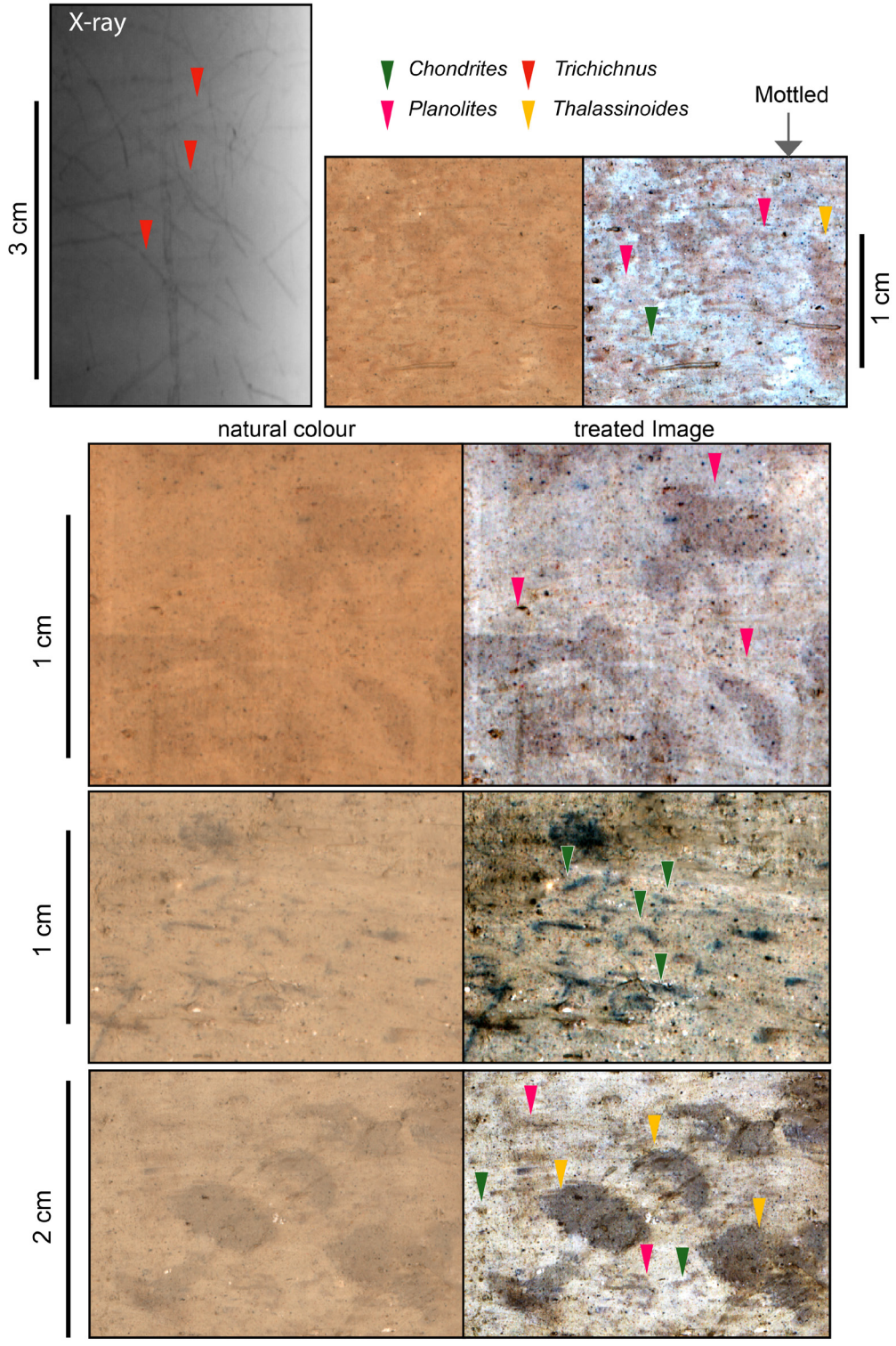

Figure IX.11. Details of the main identified ichnogenera: *Chondrites*, *Planolites, Thalassinoides* and *Trichichnus*, before (left) and after (right) image treatment.

IX.3.3 Temporal evolution and data integration

Integrating geochemical and ichnological information makes it possible to interpret oxygenation evolution throughout the studied interval, including S5, S4 and S3. Here, a preliminary interpretation of the possible oxygen evolution is proposed. Before S5, a relatively well-oxygenated environment can be interpreted based on the presence of *Thalassinoides* at 535 cmbsf (around 135 kyr BP). Sapropel S5 is characterized by the absence of discrete and large traces, with only some *Chondrites*, which agrees with the observed trace metal, indicating an establishment of suboxic conditions. In the layer interpreted as the postdepositional oxidised layer, between 510 and 520 cmbsf, *Planolites* and *Thalassinoides* traces occur, revealing a colonization post-reoxygenation of the top-most part of the sapropel, and the recovery of oxygen in the bottom water. The transition from sapropel-forming conditions to more oxygenated conditions is accompanied by a gradual reduction in the Ba signal and a total relocation of U and Mo upwards and downwards (Figs. IX.7 and IX.8). Thus, the conditions may have been gradually more oxygenated, the sapropel demise being progressive. Such observations agree with the significantly slower deepwater renewal rates that played an important role in forming sapropel S5, congruent with the proposed suppression of overturning during the last interglacial due to increased stratification from high riverine freshwater input under enhanced monsoon forcing (Rossignol-Strick et al., 1982; Rohling et al., 2015; Andersen et al., 2018).

The interval between S5 and S4 (~515-478 cmbsf) presents homogeneous composition and colour. It has no discrete traces, and the trace metal record is stable, which could reveal unfavourable conditions for the macrobenthic trace maker community, probably related to very low benthic food availability under a well-oxygenated environment, leaving only the full bioturbated sediment of the top layer without discrete traces indicative of lower tiers. Just below S4 (~478 cmbsf), there is a layer characterized by an altered texture and grain size, featuring a significant increase in the Ti/Ca ratio (Fig. IX.7) that could be interpreted as a thepra (as at 108.4 kyr BP in Vogel et al., 2010). The presence of this layer is not associated with any significant environmental change, and it may determine the first peak observed in UEF and MoEF values.

The onset of S4 is associated with the second important peak in Mo and U that follows the "thepra layer", coinciding with a change to a reddish colour (Fig. IX.12). S4 is divided into two parts, with a noticeable interruption in the middle, as observed in other parts of the basin (Grant et al., 2016).

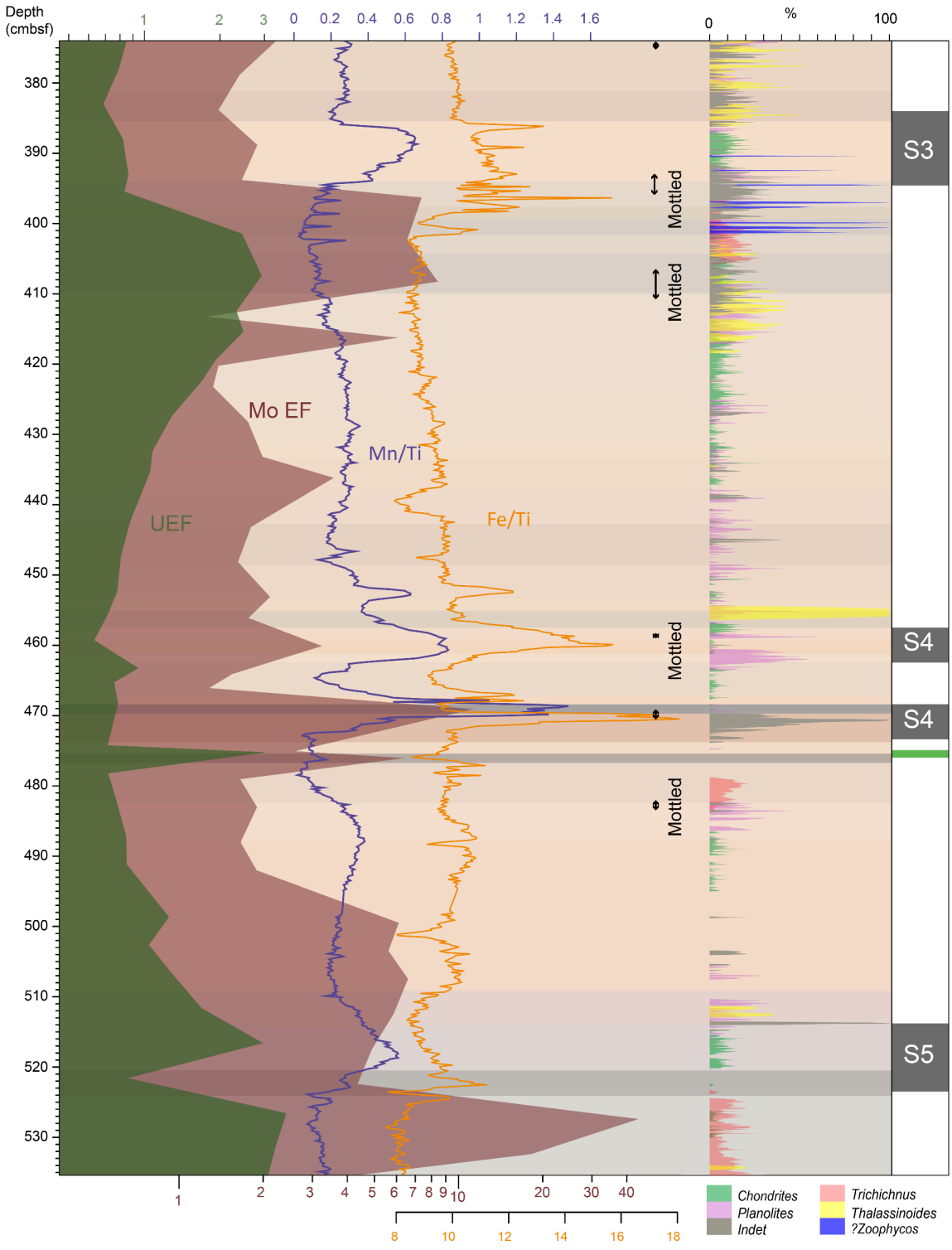

Figure IX.12. Depth plot of main trace metal records and ichnological features. The colour of the plot background represents the observed colour in the sediment, indicating changes in the RGB value.

The top of the first interval of S4 (S4b) shows a black colour, coinciding with an Mn peak and an important Mo enrichment. Geochemical evidence suggests it is part of the oxidation front; this atypical oxidation front is tentatively interpreted as having formed during the sapropel layer oxidation, the dissolved manganese encountering oxygen after migration from anoxic layers below, and Mo enrichment being due to the trapping of this element in the hydroxide-rich minerals (De Lange et al., 2008). Nonetheless, the very high Mn enrichment points towards the possibility of a very rich Mn source. The presence of the thepra below could explain the great amount of Mn in the S4 bottom layer, as the sapropel layer is rather thin, or else the migration of Mn from other sapropel layers like S5.

Further exploration and data acquisition are needed to answer this question. Thus, the first part of S4 is completely oxidized, and at the top of the black layer, frequent discrete traces appear to affect the black sediments or even enter inside them, although they have not been identified (indet. Figs IX.9 and IX.12), they could be described as *Planolites*. The interrupting interval of S4 presents no discrete traces, and no mottling is evident. Even if it seems to correspond to an oxygenated environment in light of the observations, no further interpretation of the environment is possible for this interval. Finally, interval S4a (the upper S4 interval) is preceded by abundant *Planolites*, defined by *Chondrites* and followed by abundant *Thalassinoides* that indicate a depth of reoxygenation at around 457cmbsf (Fig. IX.12) around 100 kyrs ago on the used age model.

Between S4 and S3, there is a clear gradation in both the bioturbational features and the trace metals, especially in U content, yet as explained above, the U gradation mostly corresponds to post-depositional migration. In any case, it is interesting that bioturbation appears to be a factor controlling this migration, relocating U to the more bioturbated sections. Bioturbation rapidly decreases a few cm above the S4 (˜100 kyr BP, ˜452 cmbf). Then, prior to the S3 inception, a gradual increase in bioturbation involving *Chondrites* (starting at ˜435 cmbsf, 93 kyr BP) to *Thalassinoides* (starting at ˜ 415cmbsf, ˜88 kyr BP, Figs. IX.9 and IX.10 and IX.12) would reveal the gradual establishment of a well-developed tiering community under favourable conditions at the end of this period. Before S3 deposition, the Ti/Ca ratio reveals a gradual rise in terrigenous input, indicating a progressive shift in sedimentation, with a reduced influx of carbonate into the basin and a greater contribution of the terrigenous fraction. This period is additionally marked by low precipitation, and the enhanced terrigenous flux derives from dust (Blanchet et al., 2021). However, it could be tentatively proposed that it was produced by current intensification —the Deep Eastern Mediterranean velocity increased during this period, as expressed by greater oxygen availability. The bioturbation gradually decreases toward the inception of S3 as the larger traces of *Thalassinoides* and *Planolites* disappear, probably indicating a gradual decline in oxygenation.

S3 is oxidised, and there is no colour indication of its presence, but the Ba/Ti ratio allows for its recognition. Abundant *Chondrites* and *Zoophycos* characterise the basal part and a few cm below, indicating a fairly intense deoxygenation event. These findings may be in agreement with those of Zwiep et al. (2018), who detected that during S3, the reducing conditions were

stronger than in the most recent sapropel (S1) deposited during the Holocene Interglacial and even similar to those of the well developed S5.

After S3, a period of rapid changes in sedimentation is reflected by the Ti/Ca ratio, and several layers of dark colour could indicate short-duration oxygen restriction events that did not generate sapropel layers. For instance, humid periods are described during the MIS2 and MIS3 in the Mediterranean (e.g., Blanchet et al., 2021; Camuera et al., 2022). Blanchet et al. (2021) pointed out that river runoff occurred in the area occupied today by Libya during the warm interglacial phases of MIS1 and MIS5, and that there were less intense and shorter events of riverine reactivation during MIS3 and MIS4, more related to winter storms from the Mediterranean. Langgut et al. (2018) reported that 56-44 kyr ago, increased precipitation in the Levant was correlated to human dispersion from Africa and associated with a local intensification of the monsoon system or increased winter precipitation. At least one of these layers could correspond to the S2 layer —here only slightly inferred— occurring during an insolation maximum (Fig. IX.6) in the Eastern Mediterranean, with local effects on productivity and deep oxygen conditions. In the LC10 record, several dark layers having no evident geochemical signals could also be associated with humid periods in North Africa (Revel et al., 2010). The other geochemical proxies do not indicate any redox signal surviving the diagenesis, except the Mn/Ti ratio, which has been used, for example, to locate the S2 tentative position and the oxidation zones of the other sapropels. *Chondrites* would indicate that some intervals around 60 ka presented oxygen depletion. Even if these interpretations cannot be affirmed with confidence, there is indeed some evidence of several rapid fluctuations during the MIS3 that may be correlated to the described glacial fluvial pulses, along with short duration events of oxygen depletion or increased productivity, some "short and less developed sapropels" that could resemble the ORL of the Western Mediterranean.

IX.4. Conclusions

The region comprising the Gulf of Sirte and Sicily channel in the Eastern Mediterranean was affected by abrupt oceanographic changes during sapropel deposition that significantly impacted bottom water oxygenation.

Sapropels 3, 4 and 5 (S3, S4 and S5) are recognized in the LC10 record. Nonetheless, the characteristics of each are very different, indicating different conditions during their deposition as well as variable reactions to post-depositional oxygenation and early diagenesis processes. S5 is well developed, being the best-preserved layer in the record. There is evidence of trace metal remobilization, intense pyritization beneath this layer, and bioturbation at the top part of the sapropel. S4 is divided into two events separated by an interruption. Both intervals underwent oxidation and bioturbation. Due to the oxidation processes, the bottom layer of S4 developed a high manganese enrichment, resulting in a distinctive geochemical record. S3 is also oxidised, though its presence is only detected by trace metals, its Ba record, and

ichnological features. While the S3 sapropel also shows intense bioturbation of *Chondrites,* no other traces are recognised. Even if slightly inferred, S2 was probably poorly developed and removed by post-depositional oxidation. Other restriction events inferred, given the Ti/Ca record and colour, are likely related to increased freshening in the basin, possibly linked to HEs 4, 5, and 6 or humid short-duration phases.

PART 4

INTEGRATED DISCUSSION AND CONCLUSIONS

Chapter X

Integrated Discussion

X.1. Ichnological features as a tool

X.1.1. Advances and perspectives

During the elaboration of this thesis, a quantitative technique was developed and tested, which is less time-consuming, efficient, and useful, refining previous research (e.g., Dorador and Rodríguez-Tovar, 2014a, 2014b, 2014c; Rodríguez-Tovar and Dorador, 2014; Dorador and Rodríguez-Tovar, 2016b; Dorador et al., 2016; Dorador and Rodríguez-Tovar, 2018; Miguez-Salas et al., 2019), improving ichnological analysis of marine cores and facilitating the integration of ichnology in marine palaeoenvironmental research.

The new technique employs a novel approach, utilizing variable complex scripts to analyse binary images. It has been successfully applied in diverse contexts, showcasing its versatility and applicability, clearly demonstrating its usefulness in integrating ichnological analysis in the research of marine cores. This methodology permits the comparison of ichnological data with continuous datasets comprising geochemical proxies, colour analysis, and/or magnetic susceptibility. Chapters VI and IX of this thesis evidence its application in various scenarios and demonstrate how the newly developed procedures can be effectively utilized in a number of contexts. It holds great promise for advancing future research endeavours.

In Chapter VI, the technique was applied to relatively old photographs that provided valuable insights despite their lower resolution, allowing for the incorporation of quantitative continuous ichnological analysis into older records studied previously using different proxies. New information and conclusions can be derived by contrasting the ichnological data obtained through this technique with already existing data.

In Chapter IX, the technique was implemented in a context of further complexity, aided by a more refined development of the method and better images. Characterizing the amount of

bioturbation by ichnogenera becomes particularly valuable when comparing and discussing the data alongside geochemical proxies.

X.1.2 Environmental analysis using continuous ichnological data

The ichnological data collected were used to assess variations in oxygen and organic matter concentration during the Last Glacial Cycle in the Mediterranean Basins. Parameters such as ichnodiversity, bioturbation percentage, and trace fossil size offer valuable insights into palaeoenvironmental conditions.

Chapter VI integrates ichnological data and correlates them with the known climate variability of the Mediterranean area, producing interesting results about the bioturbation and deep-sea conditions over the Last Glacial Cycle. A link was observed between the percentage of bioturbation and the long-term SST trend registered for the Last Glacial Cycle. The results revealed high percentages of bioturbation registered at the end of the Penultimate Glacial Cycle (~145 - ~127 ka), at points during the Glacial Period (at ~108 ka, ~86 ka, ~73 ka, ~40 ka and ~ 15 ka) and the YD during periods of low sea surface temperature. Further increases in bioturbation, but less important, are detected at ~63 ka or with some depth displacement at ~55 ka, ~48 ka, ~44 ka, ~42 ka, and ~33 ka (Fig. X.1). These findings confirm that cold water and deep-water renewal improve the macrobenthic tracemaker habitat, most likely due to oxygen availability combined with sufficient benthic food.

Chapter VII includes more detailed research on the different environmental conditions during ORL deposition, proving through sedimentological and ichnological features that these layers do not reflect similar events. The distinction between the 3 types of ORLs during the Last Glacial Cycle implies noteworthy heterogeneity in these layers. Some ORLs are intensively bioturbated, whereas others present a total absence of bioturbation and may even show lamination. However, these distinctions are mostly seen for the deep parts of the Alboran Sea Basin, the shallower parts (e.g., 976 and GP03 sites) being less prone to differentiations; this indicates an important spatial heterogeneity and suggests different layers in the deep waters. Ichnological and colour analyses moreover made it possible to refine the initial description of ORLs by adding new ones and extending or removing portions of previously described ORLs.

In the LC10 core situated in the Eastern Mediterranean Basin (Chapter IX), ichnogenus differentiation allowed for better characterization of the palaeoenvironmental variation. Different colonization phases tied to changes in benthic flux and deep-water ventilation were recognized. The characterization of bioturbational features before and after sapropel formation demonstrates how the oxygen and food variations correlated to climatic changes.

X.2. Last Glacial Cycle multi-basin comparison

The Last Glacial Cycle was a complex period with important climatic variability that impacted the deep basins' environmental conditions. Throughout the thesis, important changes indicated by the proxies, specifically referred to the oxygen content variation, have been observed. The Last Glacial Cycle was punctuated by rapid warmings observed as the main factor impacting the western Mediterranean area's deep-water circulation, while the monsoon cycle was much more important than these rapid variations in triggering sapropel-producing conditions.

The observations made during this thesis can be due to the ORLs being linked to the WMDW renewal, associated with cold winter conditions like the GS phases and impaired during GI warm phases —except during HE when a freshened AW entered the Mediterranean Basin through the Gibraltar Strait (Cacho et al., 2000; Sierro et al., 2005; Frigola et al., 2008). Widespread cold conditions over the North Hemisphere, such as those during GS, favour deep water formation today. The cold conditions are linked to positive sea-level pressure anomalies occurring west or northwest of the British Isles, and especially low pressure over the Mediterranean. Such configurations are thought to reflect conditions resembling those of an extreme phase of the recently established NAO (Maheras et al., 1999). In the past, during the GS, the AMOC slowdown led to conditions that may be seen as analogues of the NAO^+ situation, where the dipole between the Azores High and the Iceland low gets stronger, accelerating and deviating the westerlies northward. These colder, dryer and stronger winds were directed and accelerated towards the Mediterranean Sea area by orographic features and incised over areas such as the Gulf of Lions and the Ligurian Sea, inducing the WMDW and EMDW formation as proposed in multiple studies (e.g., Cacho et al., 1999; Frigola et al., 2008). At the same time, equivalent processes conditioned polar wind configuration in the Eastern Mediterranean Basin and its incision in the Aegean and Cretan Seas and the southern portion of the Turkish coast, determining an increase in evaporation rates (e.g., Medoc Group et al., 1970; Schott et al., 1996; Millot, 1999; Pinardi and Masetti, 2000; Schroeder et al., 2008; Josey et al., 2011; Pinardi et al., 2015). In contrast, during interstadial phases, the NAO^- like situation would favour storm track deviation towards the Mediterranean Sea, increasing both precipitations (e.g., Fletcher et al., 2010; Toucanne et al., 2015; Camuera et al., 2021) and sea temperature (Cacho et al., 1999, Martrat et al., 2004), while reducing wind intensity over the Northern Basin, inhibiting the development of deep and intermediate water in the Western Mediterranean by increasing buoyancy (Sierro et al., 2005; Frigola et al., 2008; Rohling et al., 2015).

The described process of deep-water variation over time is common in Western and Eastern basins. However, sapropel formation over the Eastern Basin is linked to different processes. Consensus exists that the formation of Mediterranean sapropels is closely related to the reduced deep-water ventilation that occurred by means of a freshening of surface waters and increased nutrient availability in surface waters of the Eastern Basin propitiated by the monsoon

influence over Northern Africa (Rossignol-Strick et al., 1982; Rohling, 1994; Revel et al., 2010; Box et al., 2011; Rohling et al., 2015; Castañeda et al., 2016; Grant et al., 2016, 2022; among many others). These postulations have been confirmed by models (e.g., Grimm et al., 2015; Vadsaria et al., 2019) and proxy records (e.g., Cornuault et al., 2016; Filippidi et al., 2016). In addition, several studies document the importance of stratification in these processes through neodymium isotopic composition in the biogenic fraction (Cornuault et al., 2018; Wu et al., 2019) or redox trace metal elemental composition (Jilbert et al., 2010; Tachikawa et al., 2015; Tesi et al., 2017).

During sapropel deposition, there is fluvial input intensification (Allen et al., 1999; Rohling et al., 2015; Filippidi et al., 2016) during the described GI phases. Sapropel formation is also linked to the northward migration of the ITCZ, determining the intensification and incision of the African Monsoon in the basin with the consequent increase in Nile discharge and reactivation of North African rivers. Monsoons mostly impacted the Eastern Mediterranean basins, the penetration being only up to 31°N in North Africa (Tierney et al., 2017; Sha et al., 2019), reactivating the Libyan riverine systems and increasing the Nile flux (Wu et al., 2017; Duhamel et al., 2020; Blanchet et al., 2021). When the monsoons retracted further south, the characteristic increase of wind-blown dust in the basin occurred and was registered, coinciding especially with the GS (Revel et al., 2010, 2014; Zhao et al., 2012).

Another important constituent of the Northern Hemisphere palaeoclimate and palaeoceanography to be acknowledged before further discussion of the drivers of ORL and sapropel formation is the HE and its impact on the basin (Sierro et al., 2005). HE impaired deep water formation during HS, mostly due to the important freshening of the AW that enters the Gibraltar Strait (e.g., Sierro et al., 2020).

Many open questions remain about the particularities that lead to the differences observed between ORLs and sapropels. They do not always occur synchronically, and their triggers vary in intensity and continuity over time. Many studies have contributed with observations, including those presented in this thesis, as seen in Figure 10.1. One explanation for the complexity observed may stem from the variable reactions of the different parts of the Mediterranean Sea area to the two main, non-coherent climate systems that acted during the Quaternary. On the one hand, the Glacial-Interglacial transition and its internal variability ultimately result from variations in the ice volume in the South and North Poles, driven by astronomical changes in the Earth's axis.

On the other hand, even if affected by ice volume and glacial transitions, monsoon variation is not dominated by them (Larrasoana et al., 2003; Lionello et al., 2023). The differences between ORLs and sapropels are not observed during GS, as the ice growth blocks the influence of the monsoon on the Mediterranean Basin. During interstadial phases, however, there were differential responses of the Mediterranean Basin depending on the monsoon, whose intensity or incision is controlled by the insolation cycle characteristics (e.g., Wang et al., 2017).

In the Eastern Mediterranean, only the interstadial events occurring during isolation maxima caused stagnation, while stadials occurring during insolation maxima caused a notable rise in Mediterranean ventilation that inhibited sapropel formation (Sierro et al., 2020). During MIS 5a, 5c, and 5e, summer insolation maxima occurred (Fig X.1), and consequently, the deposition of S3, S4 and S5 is observed in the Eastern Mediterranean. While S5 occurs during the beginning of the Emian Period — similar to what occurred for S1 during the beginning of the Holocene — the stagnation events associated with S3 and S4 were triggered by the abrupt warming of interstadial events —Glacial Interstadial 21.1 and 24.2— which likewise coincide with insolation maxima (Fig X.1; Sierro et al., 2020).

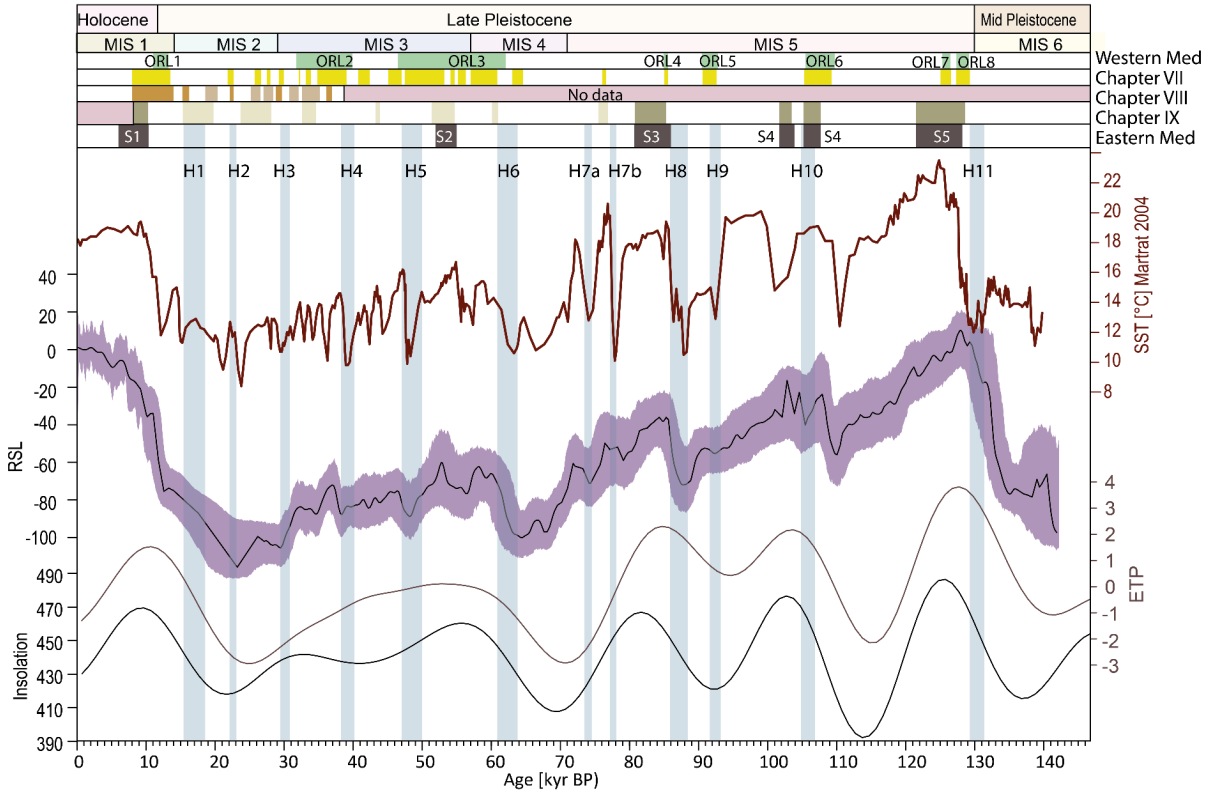

Figure X.1. Position of the ORLs and sapropels during the last 140 kyr. The SST in Alboran (Martart et al., 2004), the sea level in the Red Sea (Grant et al., 2013), the Insolation and ETP, and the Heinrich Events' position are compared. Chapter VII, VIII and IX refers to the results obtained during the correspondent chapters, thus the position of the ORLs and sapropels observed in the records studied in this thesis.

At the onset of the last two interglacials (Holocene and Eemian), and coinciding with insolation maxima, sapropel and ORLs were not correlated but rather occurred in different times or sequential with an ORL preceding the sapropel by several centuries or even millennia. For example, during the Holocene, the initial deposition of the ORL 1 was followed by the start of a sapropel deposition during the middle of the event, and the sapropel deposition continued after the Western Mediterranean Deep Basins returned to well-oxygenated conditions. Other

similar relations have been observed in this thesis, with the low oxygenated ORL 8 and anoxic ORL 7 (Type 1 and 3; Chapter VII; Casanova-Arenillas et al., 2022) that follow the HE11 in the Western Alboran Sea Basin preceding S5. However, ORL 7 is laminated and resembles sapropels from deep parts of the Levantine Basin; thus, the level of restriction of the Western Mediterranean that preceded the Eemian was higher than during the Holocene and could tentatively be considered a sapropel that extended throughout the whole Mediterranean Sea.

Similarly, the second most developed sapropel in the studied records, S3, corresponds to an anoxic and laminated ORL 4. Hence, the circumstances that led to preconditioning and the development of well-developed sapropels were preceded by similarly well-developed ORLs that tended to occur earlier and declined earlier. This correlation is coherent with other Mediterranean records.

In addition to the times of sapropel deposition, decreased deep ventilation appears in the Eastern Mediterranean during MIS 2 and MIS 3 and not only during sapropel S2 (Revel et al., 2010; Cornuault et al., 2016; Di Donato et al., 2022). These periods are punctuated in all the studied records of the Mediterranean by events where proxies indicate a decrease in the oxygenation of the deep basin (Fig 10.1). Thus, tentatively associated with humid periods during these intervals, rapid periodic insolation in the Eastern and Western Mediterranean deep basins possibly resulted in the formation of some of the ORLs, most notably 2 and 3, which could probably be described as a grouping of much shorter events associated with interstadial conditions and Heinrich Events. (See chapters VII, VIII and IX).

Against this background, four scenarios can be proposed for the ventilation of the deep water (Fig X.2A, B, C and D):

The first scenario that can be described is similar to the present-day situation (Fig X.2A), taking place in periods with enough sinking events to maintain both basins well-oxygenated.

Another two scenarios proposed (Fig X.2 B and C) reflect the restriction of deep water occurring in only one of the basins. This happens during most ORLs that do not coincide with monsoon maxima, as those occurring in MIS 2, 3, and 4, except for part of the ORL 3 that coincides with S2 (Fig X.1 and Fig X.2B). The other way around occurs during the second part of S1, S3, S4 and S5, as the ventilation is recovered in the Western Mediterranean Basin but not in the Eastern Basin (Fig 10.2A).

Finally, during strong insolation, monsoon activation, and GI warm conditions, ORLs and sapropels were deposited closer in time. In this case, some ORLs have sapropel-like features (Fig 10.1; 10.2D) produced during the early S5, the first phase of S4 and early S3. This scenario might also apply to the period after YD during S1 and ORL 1 (Fig 10.1). Less developed ORL 3 would coincide with S2 temporarily at the beginning of MIS 3 (Fig 10.1).

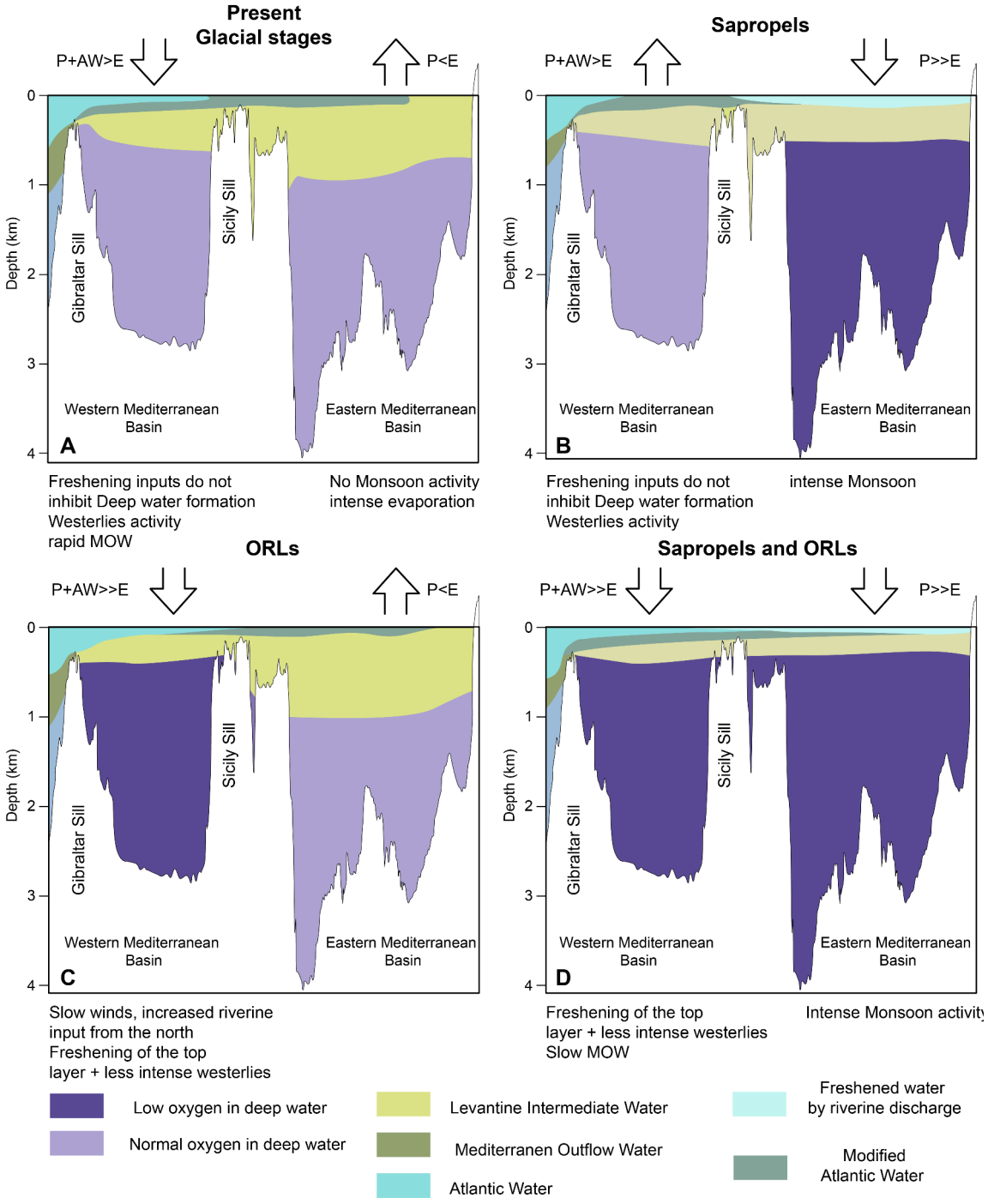

Figure X.2. Inferred Mediterranean water masses during different events of the Last Glacial Cycle. The figure presents four proposed scenarios for the configuration of the ventilation of the deep water in the Mediterranean. Each scenario is linked with one of the observed types of ORLs and correlated with climatic events (see text).

Chapter XI

Conclusions

Overall, this thesis has yielded significant results in two key topics: the application of novel methodologies that integrate multiple proxies and our understanding of Organic Rich Layer (ORL) formation and correlation with sapropels. The findings indicate that ORLs may result from varying environmental conditions and exhibit considerable variability in terms of the extent of bottom water oxygen depletion. This variability is observed both spatially and geographically. In contrast, sapropels would be more consistent events driven by monsoon activity and the subsequent freshening of the Eastern Basin, which increases nutrient availability. Well-defined events for ORL deposition do not appear to have equivalent counterparts, making their study more difficult.

The use of Python scripts and image analysis for automatic and semi-automatic ichnological analysis in well marine cores of recent sediments has great potential for improving palaeoenvironmental research, facilitating a deeper understanding of environmental dynamics and processes, and because of its compatibility with other proxies, it contributes to a more holistic interpretation of sedimentary records and their environmental implications. The methods and tools developed can improve ichnofabric analysis.

In sum, the multiproxy approach —integrating continuous ichnological features, geochemical composition, benthic foraminifera assemblage, sediment colour or magnetic properties— has emerged as a powerful tool to assess palaeoclimatic, oceanographic or environmental changes, allowing for a detailed redox reconstruction of marine deep basins.

The research conducted and described here made it possible to interpret environmental variability in bottom water conditions in the Mediterranean Sea basins during the Last Glacial Cycle. The results of this thesis have corroborated that the Last Glacial Cycle was a period characterised by important variations in environmental conditions in the deep basin of the Mediterranean Sea, indicated by significant changes in the used proxies. These variations were likely controlled by significant climatic observed in this period.

A robust correlation exists between ichnological information and other climate proxies in the Alboran Sea Basin, including alkenone SST records and $\delta^{18}O$ profiles. This correlation is observed not only during the Last Glacial Cycle but also in conjunction with shorter timescale events, such as Heinrich Events, Younger Dryas, and intervals of ORL formation. Cold stadials

are generally associated with increased deep-water ventilation, impacting the trace maker community.

Three types of ORLs are differentiated, reflecting variable palaeoenvironmental parameters and significant fluctuations in oxygen levels.

- Type 1, characterized by an intermediate thickness, corresponds to intervals with moderate to high levels of bioturbation, indicating oxygen availability, permitting a well-developed trace-maker community.
- Type 2 consists of thicker intervals, alternating from highly to moderately bioturbated sections, indicating fluctuations in oxygen conditions of moderate to extremely dysoxic or suboxic states.
- Type 3 is characterized by thin layers and displays a laminated structure without signs of bioturbation, associated with anoxic or suboxic conditions and an unfavourable macrobenthic habitat.

In addition, ichnological and colour analyses made it possible to refine the initial description of ORLs, highlighting the existence of many not previously described ORL-like layers in the Alboran Sea Basin, plus important internal variability in ORLs observed in previous studies. The revised ORL records demonstrate a better correlation between climatic variation, especially Dansgaard–Oeschger cycles and Heinrich Events, and ORL deposition during the Last Glacial Cycle.

The internal variability of ORLs was confirmed in ORL1, between 15 kya BP and 8 kya BP, with climatically driven brief reoxygenation events occurring during the period, allowing for bioturbation and trace metal remobilization. The reoxygenations are associated with the high-frequency cold-warm transition. During the Bølling–Allerød, at least one reoxygenation event occurred at the GI-1d cold phase, as indicated by a change in the redox trace metal signals and modifications in the foraminifera assemblage. During the Younger Dryas, there was a significant reoxygenation phase. Organic Rich Layers (i.e., ORL1, ORL2) were not periods of total anoxia, but important fluctuations are related to short-term climate changes.

In the Eastern Mediterranean Basin, specifically in the zones close to the Gulf of Sirte and Sicily channel, abrupt oceanographic changes impacted the environmental bottom water oxygen; they produced changes in ichnological features and geochemical composition and determined sapropel formation. Ichnological and geochemical variability between sapropels (S3, S4 and S5 being well developed, and S2 weakly registered) is observed, revealing both distinctive sapropel development and the re-establishment of oxygen conditions afterwards. Moreover, benthic food fluxes proved important for the reworking and survivability of the layers to burndown and signal displacement.

Comparison between the Eastern and Western Mediterranean demonstrates that the drivers of variability between the two basins can be partially correlated during some intervals. In the Western Mediterranean, ORLs are linked to the stadial-interstadial transitions and Heinrich

Events during the Last Glacial Cycle due to a reduced renewal of the Western Mediterranean Deep Water in a context of warming, freshening and westerlies displacement, modifying evaporation and buoyancy of the surface waters and the capacity of the deep water to sink. The Eastern Mediterranean experienced the influence of this climatic variability from the northern hemisphere, but it is strongly affected by the monsoon cycle with the reactivation and increased inputs from rivers in North Africa, especially the Nile. This leads to enhanced freshwater and nutrient input into the Eastern Mediterranean Basin.

Conclusiones

En líneas generales, esta tesis aporta resultados significativos en dos líneas clave, como la integración de múltiples indicadores para mejorar las interpretaciones paleoambientales de oxigenación del medio, y la comprensión de los procesos de formación asi como la correlación entre los Sapropeles (sedimentos orgánicos) del Este del Mar Mediterráneo y las "Capas Ricas en Materia Orgánica" (ORL, por sus siglas en inglés) del Oeste. Los hallazgos indican que las ORL son el resultado de condiciones ambientales variables, exhibiendo una considerable variabilidad en términos de la cantidad de oxígeno presente en las aguas del fondo. Esta variabilidad se observa tanto temporal como espacialmente (profundidad y situación geográfica). Sin embargo, los Sapropels parecen ser eventos más consistentes en el tiempo y el espacio, producidos por acción de los monzones y su influencia en la salinidad del agua en el este del Mar Mediterráneo, lo que aumenta la disponibilidad de nutrientes. En las ORL, sin embargo, no parecen existir una relación directa en el tiempo y en el espacio, lo que dificulta su estudio.

El uso de scripts de Python en el análisis de imágenes aplicado al análisis icnológico automático y semiautomático en fotografías de testigos de sondeos marinos de sedimentos recientes presenta un gran potencial para la mejora en las interpretaciones paleoambientales, facilitando el estudio de las dinámicas y procesos ambientales y, a través de su comparación con otros indicadores, contribuyendo a una interpretación integral de los registros sedimentarios y sus implicaciones ambientales. Los métodos desarrollados en esta tesis mejoran el análisis de la icnofábricas.

El uso de un enfoque multi-indicador que integra las características icnológicas presentadas de forma continua, la composición geoquímica, las asociaciones de foraminíferos bénticos, el color del sedimento, y propiedades magnéticas, se ha revelado como una herramienta de gran utilidad para evaluar cambios paleoclimáticas, oceanográficos o ambientales, permitiendo además una reconstrucción detallada de las condiciones de oxigenación en sedimentos marinos.

Además, la investigación llevada a cabo ha permitido realizar una interpretación de la variabilidad ambiental en las condiciones del agua de fondo en las cuencas del Mar Mediterráneo durante el Último Ciclo Glacial. Los resultados de esta tesis han corroborado que el Último Ciclo Glaciar fue un periodo caracterizado por importantes variaciones en las condiciones ambientales en la cuenca profunda del Mar Mediterráneo, lo que viene indicado por cambios significativos observados en los proxies utilizados. Además, estas variaciones estuvieron probablemente controladas por importantes fenómenos climáticos observados en este periodo.

Asimismo, se ha puesto de manifiesto la correlación existente entre la información icnológica y otros indicadores climáticos en la Cuenca del Mar de Alborán, habiéndose comparado entre otros con registros bien definidos como los de temperatura superficial del mar mediante

alquenonas los perfiles de $\delta^{18}O$. Esta correlación se observa no solo durante el Último Ciclo Glacial, sino también en ciclos que ocurren a escalas temporales más cortas, como los Eventos de Heinrich, el Drías Reciente y los intervalos de formación de ORL. Se ha observado que los estadios fríos están generalmente asociados con un aumento en la ventilación de las aguas profundas, observándose una reacción de la comunidad bentónica responsable de la bioturbación.

En base a los resultados, se han diferenciado tres tipos de ORLs, que reflejan parámetros paleoambientales variables, como las fluctuaciones significativas en los niveles de oxígeno entre los diferentes eventos acaecidos en el Oeste del Mar Mediterráneo:

• Tipo 1, caracterizado por un espesor intermedio, corresponde a intervalos con niveles moderados a altos de bioturbación, lo que indica disponibilidad de oxígeno que permite la presencia de una comunidad bentónica de organismos bioturbadores bien desarrollada.

• Tipo 2 se refiere a ORLs con mayor potencia, que presentan una alternancia de secciones con bioturbación moderada a alta, indicando fluctuaciones en las condiciones de oxígeno durante el mismo evento, desde estados con una moderada falta de oxígeno hasta ambientes disóxicos o subóxicos.

• Tipo 3 se caracteriza por ORLs de muy bajo espesor, las cuales muestran una estructura laminada sin signos de bioturbación, asociadas con condiciones anóxicas o subóxicas y un hábitat macrobentónico desfavorable para la presencia de organismos bioturbadores.

Además, los análisis icnológicos y del color permitieron refinar tentativamente la descripción inicial de las capas ORLs, observando la existencia de capas potencialmente similares a ORL no descritas previamente en la Cuenca del Mar de Alborán. Asimismo, se ha puesto de manifiesto una variabilidad interna importante en las ORLs observadas en estudios previos. El refinamiento de los registros de las ORLs demuestra una mejor correlación entre la variación climática, especialmente entre los ciclos de Dansgaard-Oeschger y los Eventos Heinrich, y el depósito de ORLs durante el Último Ciclo Glacial.

Esta variabilidad interna de las ORLs se ha confirmado en la ORL1, que abarca desde hace unos 15,000 años hasta hace unos 8,000 años, con eventos de breve reoxigenación del medio que parecen estar asociados a los cambios climáticos que ocurrieron durante ese intervalo, Estos periodos permitieron la bioturbación y la removilización de metales traza dentro del sedimento. Estos eventos de reoxigenacion están asociados con las transiciones entre condiciones frías y cálidas de alta frecuencia que ocurrieron durante el periodo. Durante el final del Último Ciclo Glacial al menos uno de estos eventos de reoxigenación ocurrió en la fase fría GI-1d, como indican los cambios en las señales de metales traza redox y modificaciones en las asociaciones de foraminíferos. Durante el Drías Reciente, se reconoce una fase significativa de reoxigenación. Los resultados muestran que, al menos, las ORL1 y ORL2 no fueron períodos de constante baja oxigenación, si no que experimentaron importantes fluctuaciones relacionadas con cambios climáticos de corta duración.

En la Cuenca del Mediterráneo Oriental, específicamente en las zonas cercanas al Golfo de Sirta y al Canal de Sicilia, cambios abruptos en la oceanografía tuvieron un impacto en la concentración de oxígeno en el agua del fondo. Estas variaciones produjeron importantes cambios en las características icnológicas y en la composición geoquímica del sedimento, y determinaron la formación de sapropeles junto con cambios en la productividad. Se ha observado que existe variabilidad icnológica y geoquímica entre los distintos sapropeles estudiados (S3, S4 y S5 bien desarrollados, y S2 débilmente registrado), implicando por tanto que los sapropeles, al menos a la profundidad estudiada, tuvieron diferentes condiciones durante y tras su formación. Además, el flujo bentónico tiene una gran importancia en la determinación del grado de retrabajamiento y registro de los sapropeles.

La comparación entre el Mediterráneo Oriental y Occidental demuestra que los factores de variabilidad entre ambas cuencas podrían presentar cierto grado de correlación durante determinados periodos. En el Mediterráneo Occidental, las ORLs se correlacionaron con las transiciones estadio-interestadio y los Eventos de Heinrich durante el Último Ciclo Glacial debido a la reducción de la renovación de la Agua Profunda del Mediterráneo Occidental asociada al calentamiento, la bajada en salinidad y el desplazamiento de los vientos dominantes del Atlántico, lo cual afecta a la evaporación y la flotabilidad de las aguas superficiales y la capacidad de la agua superficial para hundirse a zonas profundas. El Mediterráneo Oriental experimentó la influencia de esta variabilidad climática del hemisferio norte, pero se ve también fuertemente afectado por los monzones, y el efecto en la reactivación de los ríos del norte de África y el consecuente el aumento de los aportes de agua dulce y nutrientes a la cuenca, siendo especialmente importantes los aportes del Nilo.

References

Adloff, F., Mikolajewicz, U., Kučera, M., Grimm, R., Maier-Reimer, E., Schmiedl, G., Emeis, K.-C. (2011). Upper ocean climate of the Eastern Mediterranean Sea during the Holocene Insolation Maximum – a model study. Climate of the Past 7, 1103–1122. https://doi.org/10.5194/cp-7-1103-2011

Aksu, A.E., Jenner, G., Hiscott, R.N., İşler, E.B. (2008). Occurrence, stratigraphy and geochemistry of Late Quaternary tephra layers in the Aegean Sea and the Marmara Sea. Marine Geology 252, 174–192. https://doi.org/10.1016/j.margeo.2008.04.004

Algeo, T.J., Li, C. (2020). Redox classification and calibration of redox thresholds in sedimentary systems. Geochimica et Cosmochimica Acta 287, 8–26. https://doi.org/10.1016/j.gca.2020.01.055

Algeo, T.J., Liu, J. (2020). A re-assessment of elemental proxies for paleoredox analysis. Chemical Geology 540, 119549. https://doi.org/10.1016/j.chemgeo.2020.119549

Algeo, T.J., Lyons, T.W. (2006). Mo-total organic carbon covariation in modern anoxic marine environments: Implications for analysis of paleoredox and paleohydrographic conditions. Paleoceanography 21, PA1016 . https://doi.org/10.1029/2004PA001112

Algeo, T.J., Maynard, J.B. (2004). Trace-element behavior and redox facies in core shales of Upper Pennsylvanian Kansas-type cyclothems. Chemical Geology 206, 289–318. https://doi.org/
10.1016/j.chemgeo.2003.12.009

Algeo, T.J., Owens, J.D. Morford, J.L., Dickson, A.J. (2020). New developments in geochemical proxies for paleoceanographic research. Geochimica et Cosmochimica Acta 287, 1–7. https://doi.org/10.1016/j.gca.2020.07.010

Algeo, T.J., Tribovillard, N. (2009). Environmental analysis of paleoceanographic systems based on molybdenum–uranium covariation. Chemical Geology 268, 211–225. https://doi.org/10.1016/j.chemgeo.2009.09.001

Allard, J.L., Hughes, P.D., Woodward, J.C. (2021). Heinrich Stadial aridity forced Mediterranean-wide glacier retreat in the last cold stage. Nature Geoscience 14, 197–205. https://doi.org/10.1038/s41561-021-00703-6

Allen, J.R.M., Brandt, U., Brauer, A., Hubberten, H.-W., Huntley, B., Keller, J., Kraml, M., Mackensen, A., Mingram, J., Negendank, J.F.W., Nowaczyk, N.R., Oberhänsli, H., Watts, W.A., Wulf, S., Zolitschka, B. (1999). Rapid environmental changes in southern Europe during the last glacial period. Nature 400, 740–743. https://doi.org/10.1038/23432

Aller, R.C. (1982). The Effects of Macrobenthos on Chemical Properties of Marine Sediment and Overlying Water. In: McCall, P.L., Tevesz, M.J.S. (Eds.), Animal-Sediment Relations. Topics in Geobiology. Boston: Springer, pp. 53–102. https://doi.org/10.1007/978-1-4757-1317-6_2

Alley, R.B. (1998). Icing the North Atlantic. Nature 392, 335–337. https://doi.org/10.1038/32781

Alley, R.B., Marotzke, J., Nordhaus, W.D., Overpeck, J.T., Peteet, D.M., Pielke, R.A., Pierrehumbert, R.T., Rhines, P.B., Stocker, T.F., Talley, L.D., Wallace, J.M. (2003). Abrupt Climate Change. Science 299, 2005–2010. https://doi.org/10.1126/science.1081056

Alley, R.B., Mayewski, P.A. Sowers, T., Stuiver, M., Taylor, K.C., Clark, P.U. (1997). Holocene climatic instability: A prominent, widespread event 8200 yr ago. Geology 25, 483–486. https://doi.org/10.1130/0091-7613(1997)025<0483:HCIAPW>2.3.CO;2

Allison, E.H., Bassett, H.R. (2015). Climate change in the oceans: Human impacts and responses. Science 350, 778–782. https://doi.org/10.1126/science.aac8721

Almogi-Labin, A., Bar-Matthews, M., Shriki, D., Kolosovsky, E., Paterne, M., Schilman, B., Ayalon, A., Aizenshtat, Z., Matthews, A. (2009). Climatic variability during the last ~90ka of the southern and northern Levantine Basin as evident from marine records and speleothems. Quaternary Science Reviews 28, 2882–2896. https://doi.org/10.1016/j.quascirev.2009.07.017

Alonso, B., Juan, C., Ercilla, G., Cacho, I., López-González, N., Rodríquez-Tovar, F.J., Dorador, J., Francés, G., Casas, D., Vandorpe, T., Vázquez, J.T. (2021). Paleoceanographic and paleoclimatic variability in the Western Mediterranean during the last 25 cal. kyr BP. New insights from contourite drifts. Marine Geology 437, 106488. https://doi.org/10.1016/j.margeo.2021.106488

Alvarez-Marron, J. (1999). Pliocene to Holocene structure of the Eastern Alboran Sea (Western Mediterranean). Proceedings of the Ocean Drilling Program 161, 345–355. https://doi.org/10.2973/odp.proc.sr.161.224.1999

Amitai, Y., Ashkenazy, Y., Gildor, H. (2021). The Effect of the Source of Deep Water in the Eastern Mediterranean on Western Mediterranean Intermediate and Deep Water. Frontiers in Marine Science 7, 615975 https://doi.org/10.3389/fmars.2020.615975

Andersen, K.K., Azuma, N., Barnola, J.-M., Bigler, M., Biscaye, P., Caillon, N., Chappellaz, J., Clausen, H.B., Dahl-Jensen, D., Fischer, H., Flückiger, J., Fritzsche, D., Fujii, Y., Goto-Azuma, K., Grønvold, K., Gundestrup, N.S., Hansson, M., Huber, C., Hvidberg, C.S., ... White, J.W.C., North Greenland Ice Core Project members (2004). High-resolution record of Northern Hemisphere climate extending into the last interglacial period. Nature 431, 147–151. https://doi.org/10.1038/nature02805

Andersen, K.K., Svensson, A., Johnsen, S.J., Rasmussen, S.O., Bigler, M., Röthlisberger, R., Ruth, U., Siggaard-Andersen, M.-L., Peder Steffensen, J., Dahl-Jensen, D., Vinther, B.M., Clausen, H.B. (2006). The Greenland Ice Core Chronology 2005, 15–42ka. Part 1: constructing the time scale. Quaternary Science Reviews, 25, 3246–3257. https://doi.org/10.1016/j.quascirev.2006.08.002

Andersen, M.B., Matthews, A., Bar-Matthews, M., Vance, D. (2020). Rapid onset of ocean anoxia shown by high U and low Mo isotope compositions of sapropel S1. Geochemical Perspectives Letters 15, 10–14. https://doi.org/10.7185/geochemlet.2027

Andersen, M.B., Matthews, A., Vance, D., Bar-Matthews, M., Archer, C., de Souza, G.F. (2018). A 10-fold decline in the deep Eastern Mediterranean thermohaline overturning

circulation during the last interglacial period. Earth and Planetary Science Letters 503, 58–67. https://doi.org/10.1016/j.epsl.2018.09.013

Andrews, J.T., Voelker, A.H.L. (2018). "Heinrich events" (& sediments): A history of terminology and recommendations for future usage. Quaternary Science Reviews 187, 31–40. https://doi.org/10.1016/j.quascirev.2018.03.017

Arndt, S., Jørgensen, B.B.B., LaRowe, D.E.E., Middelburg, J.J.J., Pancost, R.D.D., Regnier, P. (2013). Quantifying the degradation of organic matter in marine sediments: A review and synthesis. Earth-Science Reviews 123, 53–86. https://doi.org/10.1016/j.earscirev.2013.02.008

Arrhenius, G. (1952). Sediment cores from the east Pacific. Reports of the Swedish Deep-Sea Expedition, 1947-1948 5, 189–201.

Arz, H.W., Pätzold, J., Wefer, G. (1998). Correlated Millennial-Scale Changes in Surface Hydrography and Terrigenous Sediment Yield Inferred from Last-Glacial Marine Deposits off Northeastern Brazil. Quaternary Research 50, 157–166. https://doi.org/10.1006/qres.1998.1992

Ausín, B., Flores, J.A., Sierro, F.J., Bárcena, M.A., Hernández-Almeida, I., Francés, G., Gutiérrez-Arenillas, E., Martrat, B., Grimalt, J.O., Cacho, I. (2015a). Coccolithophore productivity and surface water dynamics in the Alboran Sea during the last 25kyr. Palaeogeography, Palaeoclimatology, Palaeoecology 418, 126–140. https://doi.org/10.1016/j.palaeo.2014.11.011

Ausín, B., Flores, J.A., Sierro, F.J., Cacho, I., Hernández-Almeida, I., Martrat, B., Grimalt, J.O. (2015b). Atmospheric patterns driving Holocene productivity in the Alboran Sea (Western Mediterranean): A multiproxy approach. The Holocene 25, 583–595. https://doi.org/10.1177/0959683614565952

Baas, J.H., Mienert, J., Abrantes, F., Prins, M.A. (1997). Late Quaternary sedimentation on the Portuguese continental margin: climate-related processes and products. Palaeogeography, Palaeoclimatology, Palaeoecology 130, 1–23. https://doi.org/10.1016/S0031-0182(96)00135-6

Baas, J.H., Schönfeld, J., Zahn, R. (1998). Mid-depth oxygen drawdown during Heinrich events: evidence from benthic foraminiferal community structure, trace-fossil tiering, and benthic δ13C at the Portuguese Margin. Marine Geology 152, 25–55. https://doi.org/10.1016/S0025-3227(98)00063-2

Bagniewski, W., Meissner, K.J., Menviel, L. (2017). Exploring the oxygen isotope fingerprint of Dansgaard-Oeschger variability and Heinrich events. Quaternary Science Reviews 159, 1–14. https://doi.org/10.1016/j.quascirev.2017.01.007

Bahr, A., Kaboth, S., Jiménez-Espejo, F.J., Sierro, F.J., Voelker, A.H.L., Lourens, L., Röhl, U., Reichart, G.J., Escutia, C., Hernández-Molina, F.J., Pross, J., Friedrich, O. (2015). Persistent monsoonal forcing of Mediterranean Outflow Water dynamics during the late Pleistocene. Geology 43, 951–954. https://doi.org/10.1130/G37013.1

Bahr, A., Lamy, F., Arz, H., Kuhlmann, H., Wefer, G. (2005). Late glacial to Holocene climate and sedimentation history in the NW Black Sea. Marine Geology 214, 309–322. https://doi.org/10.1016/j.margeo.2004.11.013

Bajo, P., Drysdale, R.N., Woodhead, J.D., Hellstrom, J.C., Hodell, D., Ferretti, P., Voelker, A.H.L., Zanchetta, G., Rodrigues, T., Wolff, E., Tyler, J., Frisia, S., Spötl, C., Fallick,

A.E. (2020). Persistent influence of obliquity on ice age terminations since the Middle Pleistocene transition. Science 367, 1235–1239. https://doi.org/10.1126/science.aaw1114

Bakker, N.L., Drake, N.A., Bristow, C.S. (2019). Evaluating the relative importance of northern African mineral dust sources using remote sensing. Atmospheric Chemistry and Physics 19, 10525–10535. https://doi.org/10.5194/acp-19-10525-2019

Bárcena, M.A., Cacho, I., Abrantes, F., Sierro, F.J., Grimalt, J.O., Flores, J.A. (2001). Paleoproductivity variations related to climatic conditions in the Alboran Sea (western Mediterranean) during the last glacial–interglacial transition: the diatom record. Palaeogeography, Palaeoclimatology, Palaeoecology 167, 337–357. https://doi.org/10.1016/S0031-0182(00)00246-7

Baringer, M.O., Price, J.F. (1999). A review of the physical oceanography of the Mediterranean outflow. Marine Geology 155, 63–82. https://doi.org/10.1016/S0025-3227(98)00141-8

Barker, S., Chen, J., Gong, X., Jonkers, L., Knorr, G., Thornalley, D. (2015). Icebergs not the trigger for North Atlantic cold events. Nature 520, 333–336. https://doi.org/10.1038/nature14330

Bar-Matthews, M., Ayalon, A., Kaufman, A. (2000). Timing and hydrological conditions of Sapropel events in the Eastern Mediterranean, as evident from speleothems, Soreq cave, Israel. Chemical Geology 169, 145–156. https://doi.org/10.1016/S0009-2541(99)00232-6

Bar-Matthews, M., Ayalon, A., Kaufman, A. (1997). Late Quaternary Paleoclimate in the Eastern Mediterranean Region from Stable Isotope Analysis of Speleothems at Soreq Cave, Israel. Quaternary Research 47, 155–168. https://doi.org/10.1006/qres.1997.1883

Bartolomé, M., Moreno, A., Sancho, C., Stoll, H.M., Cacho, I., Spötl, C., Belmonte, Á., Edwards, R.L., Cheng, H., Hellstrom, J.C. (2015). Hydrological change in Southern Europe responding to increasing North Atlantic overturning during Greenland Stadial 1. Proceedings of the National Academy of Sciences 112, 6568–6572. https://doi.org/10.1073/pnas.1503990112

Batchelor, C.L., Margold, M., Krapp, M., Murton, D.K., Dalton, A.S., Gibbard, P.L., Stokes, C.R., Murton, J.B., Manica, A. (2019). The configuration of Northern Hemisphere ice sheets through the Quaternary. Nature Communications 10, 3713. https://doi.org/10.1038/s41467-019-11601-2

Baucon, A., Bednarz, M., Dufour, S., Felletti, F., Malgesini, G., Neto de Carvalho, C., Niklas, K.J., Wehrmann, A., Batstone, R., Bernardini, F., Briguglio, A., Cabella, R., Cavalazzi, B., Ferretti, A., Zanzerl, H., McIlroy, D. (2020). Ethology of the trace fossil Chondrites: Form, function and environment. Earth-Science Reviews 202, 102989. https://doi.org/10.1016/j.earscirev.2019.102989

Bazzicalupo, P., Maiorano, P., Girone, A., Marino, M., Combourieu-Nebout, N., Incarbona, A. (2018). High-frequency climate fluctuations over the last deglaciation in the Alboran Sea, Western Mediterranean: Evidence from calcareous plankton assemblages. Palaeogeography, Palaeoclimatology, Palaeoecology 506, 226–241. https://doi.org/10.1016/j.palaeo.2018.06.042

Bazzicalupo, P., Sicre, M.-A., Checa, H., Maiorano, P., Margaritelli, G., Klein, V., Pena, L.D., Cacho, I., Frigola, J., Bonomo, S., Cascella, A., Lirer, F. (2022). Climate evolution in the Adriatic Sea across the last deglaciation: A multiproxy approach combining biomarkers

and calcareous plankton. Palaeogeography, Palaeoclimatology, Palaeoecology 608, 111291. https://doi.org/10.1016/j.palaeo.2022.111291

Benkovitz, A., Matthews, A., Teutsch, N., Poulton, S.W., Bar-Matthews, M., Almogi-Labin, A. (2020). Tracing water column euxinia in Eastern Mediterranean Sapropels S5 and S7. Chemical Geology 545, 119627. https://doi.org/10.1016/j.chemgeo.2020.119627

Bennett, W.W., Canfield, D.E. (2020). Redox-sensitive trace metals as paleoredox proxies: A review and analysis of data from modern sediments. Earth-Science Reviews 204, 103175. https://doi.org/10.1016/j.earscirev.2020.103175

Bensi, M., Velaoras, D., Meccia, V.L., Cardin, V. (2016). Effects of the Eastern Mediterranean Sea circulation on the thermohaline properties as recorded by fixed deep-ocean observatories. Deep Sea Research Part I: Oceanographic Research Papers 112, 1–13. https://doi.org/10.1016/j.dsr.2016.02.015

Béranger, K., Drillet, Y., Houssais, M.-N., Testor, P., Bourdallé-Badie, R., Alhammoud, B., Bozec, A., Mortier, L., Bouruet-Aubertot, P., Crépon, M. (2010). Impact of the spatial distribution of the atmospheric forcing on water mass formation in the Mediterranean Sea. Journal of Geophysical Research: Oceans 115. https://doi.org/10.1029/2009JC005648

Béranger, K., Mortier, L., Crépon, M. (2005). Seasonal variability of water transport through the Straits of Gibraltar, Sicily and Corsica, derived from a high-resolution model of the Mediterranean circulation. Progress in Oceanography 66, 341–364. https://doi.org/10.1016/j.pocean.2004.07.013

Bergamasco, A., Malanotte-Rizzoli, P. (2010). The circulation of the Mediterranean Sea: a historical review of experimental investigations. Advances in Oceanography and Limnology 1, 11–28. https://doi.org/10.1080/19475721.2010.491656

Berger, A. (1988). Milankovitch Theory and climate. Reviews of Geophysics 26, 624–657. https://doi.org/10.1029/RG026i004p00624

Berger, A., Loutre, M.F. (1991). Insolation values for the climate of the last 10 million years. Quaternary Science Reviews 10, 297–317. https://doi.org/10.1016/0277-3791(91)90033-Q

Berger, A.L. (1992). Astronomical theory of Paleoclimates and the last glacial-interglacial cycle. Quaternary Science Reviews 11, 571–581. https://doi.org/10.1016/0277-3791(92)90014-Y

Berger, B., Crucifix, M., Hodell, D.A., Mangili, C., McManus, J.F., Otto-Bliesner, B.L., Pol, K., Raynaud, D., Skinner, L.C., Tzedakis, P.C., Wolff, E.W., Yin, Q.Z., Abe-Ouchi, A., Barbante, C., Brovkin, V., Cacho, I., Capron, E., Ferretti, P., Ganopolski, A., ...Vazquez Riveiros, N. (2016). Interglacials of the last 800,000 years. Reviews of Geophysics 54, 162–219. https://doi.org/10.1002/2015RG000482

Berner, E.K., Berner, R.A. (2012). Global Environment Water, Air, and Geochemical Cycles. Princeton: Princeton University Press, 464 pp.

Berner, R.A. (2003). The long-term carbon cycle, fossil fuels and atmospheric composition. Nature 426, 323–326. https://doi.org/10.1038/nature02131

Berner, R.A. (1971). Principles of chemical sedimentology. New York: McGraw-Hill, 240 pp.

Bertling, M., Braddy, S.J., Bromley, R.G., Demathieu, G.R., Genise, J., Mikuláš, R., Nielsen, J.K., Nielsen, K.S.S., Rindsberg, A.K., Schlirf, M., Uchman, A. (2006). Names for trace fossils: a uniform approach. Lethaia 39, 265–286. https://doi.org/10.1080/00241160600787890

Bethoux, J.P. (1979). Budgets of the Mediterranean Sea. Their dependence on local climate and on the characteristics of Atlantic waters. Oceanologica Acta 9, 59–67.

Bethoux, J.P., Gentili, B. (1999). Functioning of the Mediterranean Sea: past and present changes related to freshwater input and climate changes. Journal of Marine Systems 20, 33–47. https://doi.org/10.1016/S0924-7963(98)00069-4

Bethoux, J.P., Gentili, B. (1994) The Mediterranean Sea, a Test Area for Marine and Climatic Interactions, in: Malanotte-Rizzoli, P., Robinson, A.R. (eds) Ocean Processes in Climate Dynamics: Global and Mediterranean Examples. NATO ASI Series 419, Springer: Dordrecht, pp. 239–254. https://doi.org/10.1007/978-94-011-0870-6_11

Bethoux, J.P., Gentili, B., Morin, P., Nicolas, E., Pierre, C., Ruiz-Pino, D. (1999). The Mediterranean Sea: a miniature ocean for climatic and environmental studies and a key for the climatic functioning of the North Atlantic. Progress in Oceanography 44, 131–146. https://doi.org/10.1016/S0079-6611(99)00023-3

Bethoux, J.P., Gentili, B., Raunet, J., Tailliez, D. (1990). Warming trend in the western Mediterranean deep water. Nature 347, 660–662. https://doi.org/10.1038/347660a0

Béthoux, J.-P., Pierre, C. (1999). Mediterranean functioning and sapropel formation: respective influences of climate and hydrological changes in the Atlantic and the Mediterranean. Marine Geology 153, 29–39. https://doi.org/10.1016/S0025-3227(98)00091-7

Beuvier, J., Sevault, F., Herrmann, M., Kontoyiannis, H., Ludwig, W., Rixen, M., Stanev, E., Branger, K., Somot, S. (2010). Modeling the Mediterranean Sea interannual variability during 1961-2000: Focus on the Eastern Mediterranean Transient. Journal of Geophysical Research: Oceans 115. https://doi.org/10.1029/2009JC005950

Bijma, J., Pörtner, H.-O., Yesson, C., Rogers, A.D. (2013). Climate change and the oceans – What does the future hold? Marine Pollution Bulletin, The Global State of the Ocean; Interactions Between Stresses, Impacts and Some Potential Solutions. Synthesis papers from the International Programme on the State of the Ocean 2011 and 2012 Workshops 74, 495–505. https://doi.org/10.1016/j.marpolbul.2013.07.022

Björck, S., Walker, M.J.C., Cwynar, L.C., Johnsen, S., Knudsen, K.-L., Lowe, J.J., Wohlfarth, B. (1998). An event stratigraphy for the Last Termination in the North Atlantic region based on the Greenland ice-core record: a proposal by the INTIMATE group. Journal of Quaternary Science 13, 283–292. https://doi.org/10.1002/(SICI)1099-1417(199807/08)13:4<283::AID-JQS386>3.0.CO;2-A

Blair, N.E., Aller, R.C. (2012). The Fate of Terrestrial Organic Carbon in the Marine Environment. Annual Review of Marine Science 4, 401–423. https://doi.org/10.1146/annurev-marine-120709-142717

Blanchet, C.L., Osborne, A.H., Tjallingii, R., Ehrmann, W., Friedrich, T., Timmermann, A., Brückmann, W., Frank, M. (2021). Drivers of river reactivation in North Africa during the last glacial cycle. Nature Geoscience 14, 97–103. https://doi.org/10.1038/s41561-020-00671-3

Blockley, S.P.E., Lane, C.S., Hardiman, M., Rasmussen, S.O., Seierstad, I.K., Steffensen, J.P., Svensson, A., Lotter, A.F., Turney, C.S.M., Bronk Ramsey, C. (2012). Synchronisation of palaeoenvironmental records over the last 60,000 years, and an extended INTIMATE1 event stratigraphy to 48,000 b2k. Quaternary Science Reviews, 36, 2–10. https://doi.org/10.1016/j.quascirev.2011.09.017

Blunier, T., Brook, E.J. (2001). Timing of millennial-scale climate change in Antarctica and Greenland during the last glacial period. Science 291, 109–112. https://doi.org/10.1126/science.291.5501.109

Boers, N., Ghil, M., Rousseau, D.-D. (2018). Ocean circulation, ice shelf, and sea ice interactions explain Dansgaard–Oeschger cycles. Proceedings of the National Academy of Sciences 115, E11005–E11014. https://doi.org/10.1073/pnas.1802573115

Bohn, H.L., O'Connor, G.A., McNean, B.L. (1979). Soil chemistry. New York: John Willey.

Bond, G., Broecker, W., Johnsen, S., McManus, J., Labeyrie, L., Jouzel, J., Bonani, G. (1993). Correlations between climate records from North Atlantic sediments and Greenland ice. Nature 365, 143–147. https://doi.org/10.1038/365143a0

Bond, G., Heinrich, H., Broecker, W.S., Labeyrie, L., McManus, J., Andrews, J.T., Huon, S., Jantschik, R., Clasen, S., Simet, C., Tedesco, K., Klas, M., Bonani, G., Ivy, S. (1992). Evidence for massive discharges of icebergs into the North Atlantic Ocean during the last glacial period. Nature 360, 245–249. https://doi.org/10.1038/360245a0

Bond, G., Showers, W., Cheseby, M., Lotti, R., Almasi, P., deMenocal, P., Priore, P., Cullen, H., Hajdas, I., Bonani, G. (1997). A Pervasive Millennial-Scale Cycle in North Atlantic Holocene and Glacial Climates. Science 278, 1257–1266. https://doi.org/10.1126/science.278.5341.1257

Bond, G.C., Lotti, R. (1995). Iceberg Discharges into the North Atlantic on Millennial Time Scales During the Last Glaciation. Science 267, 1005–1010. https://doi.org/10.1126/science.267.5200.1005

Bopp, L., Resplandy, L., Orr, J.C., Doney, S.C., Dunne, J.P., Gehlen, M., Halloran, P., Heinze, C., Ilyina, T., Séférian, R., Tjiputra, J., Vichi, M. (2013). Multiple stressors of ocean ecosystems in the 21st century: projections with CMIP5 models. Biogeosciences 10, 6225–6245. https://doi.org/10.5194/bg-10-6225-2013

Borreggine, M., Myhre, S.E., Mislan, K.A.S., Deutsch, C., Davis, C.V. (2017). A database of paleoceanographic sediment cores from the North Pacific, 1951–2016. Earth System Science Data 9, 739–749. https://doi.org/10.5194/essd-9-739-2017

Bosmans, J.H.C., Drijfhout, S.S., Tuenter, E., Hilgen, F.J., Lourens, L.J. (2015). Response of the North African summer monsoon to precession and obliquity forcings in the EC-Earth GCM. Climate Dynamics 44, 279–297. https://doi.org/10.1007/s00382-014-2260-z

Bottjer, D.J., Droser, M.L. (1991). Ichnofabric and Basin Analysis. PALAIOS 6, 199-205. https://doi.org/10.2307/3514901

Bout-Roumazeilles, V., Combourieu-Nebout, N., Desprat, S., Siani, G., Turon, J.L., Essallami, L. (2013). Tracking atmospheric and riverine terrigenous supplies variability during the last glacial and the Holocene in central Mediterranean. Climate of the Past 9, 1065–1087. https://doi.org/10.5194/CP-9-1065-2013

Box, M.R., Krom, M.D., Cliff, R.A., Bar-Matthews, M., Almogi-Labin, A., Ayalon, A., Paterne, M. (2011). Response of the Nile and its catchment to millennial-scale climatic change since the LGM from Sr isotopes and major elements of East Mediterranean sediments. Quaternary Science Reviews 30, 431–442. https://doi.org/10.1016/J.QUASCIREV.2010.12.005

Bramlette, M.N., Bradley, W.H. (1940). Geology and Biology of North Atlantic Deep-sea Cores Between Newfoundland and Ireland. Part 1. Lithology and geologic interpretations. US Geological Survey Professional Paper 196A, 1–34.

Breitburg, D., Levin, L.A., Oschlies, A., Grégoire, M., Chavez, F.P., Conley, D.J., Garçon, V., Gilbert, D., Gutiérrez, D., Isensee, K., Jacinto, G.S., Limburg, K.E., Montes, I., Naqvi, S.W.A., Pitcher, G.C., Rabalais, N.N., Roman, M.R., Rose, K.A., Seibel, B.A., Telszewski, M., Yasuhara, M., Zhang, J. (2018). Declining oxygen in the global ocean and coastal waters. Science 359, eaam7240. https://doi.org/10.1126/science.aam7240

Broecker, W., Putnam, A.E. (2012). How did the hydrologic cycle respond to the two-phase mystery interval? Quaternary Science Reviews 57, 17–25. https://doi.org/10.1016/j.quascirev.2012.09.024

Broecker, W.S. (1992). Defining the Boundaries of the Late-Glacial Isotope Episodes. Quaternary Research 38, 135–138. https://doi.org/10.1016/0033-5894(92)90036-I

Broecker, W.S., Bond, G., Klas, M., Bonani, G., Wolfli, W. (1990). A salt oscillator in the glacial Atlantic? 1. The concept. Paleoceanography 5, 469–477. https://doi.org/10.1029/PA005i004p00469

Bromley, R.G. (1996). Trace Fossils: Biology, Taxonomy and Applications. London: Taylor and Francis, 378 pp. https://doi.org/10.4324/9780203059890

Bromley, R.G., Ekdale, A.A. (1986). Composite ichnofabrics and tiering of burrows. Geological Magazine 123, 59–65. https://doi.org/10.1017/S0016756800026534

Bromley, R.G., Ekdale, A.A. (1984). Chondrites: a trace fossil indicator of anoxia in sediments. Science 224, 872–874. https://doi.org/10.1126/science.224.4651.872

Bromley, R.G., Ekdale, A.A., Asgaard, U. (1999). Zoophycos in the Upper Cretaceous chalk of Denmark and Sweden. Greifswalder Geowissenschaftliche Beiträge (ekkehard Herrig Festschrift) 6.

Bromley, R.G., Hanken, N.-M., Asgaard, U. (1990). Shallow marine bioerosion: preliminary results of an experimental study. Bulletin of the Geological Society of Denmark 38, 85–99. https://doi.org/10.37570/bgsd-1990-38-09

Brumsack, H.-J. (2006). The trace metal content of recent organic carbon-rich sediments: Implications for Cretaceous black shale formation. Palaeogeography, Palaeoclimatology, Palaeoecology 232, 344–361. https://doi.org/10.1016/j.palaeo.2005.05.011

Bryden, H.L., Kinder, T.H. (1991). Steady two-layer exchange through the Strait of Gibraltar. Deep Sea Research Part A. Oceanographic Research Papers 38, S445–S463. https://doi.org/10.1016/S0198-0149(12)80020-3

Buatois, L.A., Mángano, M.G. (2011). Ichnology. Cambridge: Cambridge University Press,. https://doi.org/10.1017/CBO9780511975622

Buzas, M.A., Culver, S.J., Jorissen, F.J. (1993). A statistical evaluation of the microhabitats of living (stained) infaunal benthic foraminifera. Marine Micropaleontology 20, 311–320. https://doi.org/10.1016/0377-8398(93)90040-5

Cacho, I., Grimalt, J.O., Canals, M. (2002). Response of the Western Mediterranean Sea to rapid climatic variability during the last 50,000 years: a molecular biomarker approach. Journal of Marine Systems 33–34, 253–272. https://doi.org/10.1016/S0924-7963(02)00061-1

Cacho, I., Grimalt, J.O., Pelejero, C., Canals, M., Sierro, F.J., Flores, J.A., Shackleton, N. (1999). Dansgaard-Oeschger and Heinrich event imprints in Alboran Sea paleotemperatures. Paleoceanography 14, 698–705. https://doi.org/10.1029/1999PA900044

Cacho, I., Grimalt, J.O., Sierro, F.J., Shackleton, N., Canals, M. (2000). Evidence for enhanced Mediterranean thermohaline circulation during rapid climatic coolings. Earth and Planetary Science Letters 183, 417–429. https://doi.org/10.1016/S0012-821X(00)00296-X

Cacho, I., Shackleton, N., Elderfield, H., Sierro, F.J., Grimalt, J.O. (2006). Glacial rapid variability in deep-water temperature and δ18O from the Western Mediterranean Sea. Quaternary Science Reviews 25, 3294–3311. https://doi.org/10.1016/j.quascirev.2006.10.004

Calvert, S.E. (1987). Oceanographic controls on the accumulation of organic matter in marine sediments. Geological Society, London, Special Publications 26, 137–151. https://doi.org/10.1144/GSL.SP.1987.026.01.08

Calvert, S.E., Fontugne, M.R. (2001). On the late Pleistocene-Holocene sapropel record of climatic and oceanographic variability in the Eastern Mediterranean. Paleoceanography 16, 78–94. https://doi.org/10.1029/1999PA000488

Calvert, S.E., Nielsen, B., Fontugne, M.R. (1992). Evidence from nitrogen isotope ratios for enhanced productivity during formation of eastern Mediterranean sapropels. Nature 359, 223–225. https://doi.org/10.1038/359223a0

Calvert, S.E., Pedersen, T.F. (2007). Elemental Proxies for Palaeoclimatic and Palaeoceanographic Variability in Marine Sediments: Interpretation and Application, in: Claude Hillaire–Marcel (Ed). Proxies in Late Cenozoic Paleoceanography. Amsterdam: Elsevier, Developments in Marine Geology 1, pp. 568–644.

Calvert, S.E., Pedersen, T.F. (1993). Geochemistry of Recent oxic and anoxic marine sediments: Implications for the geological record. Marine Geology 113, 67–88. https://doi.org/10.1016/0025-3227(93)90150-T

Campins, J., Genovés, A., Picornell, M.A., Jansà, A. (2011). Climatology of Mediterranean cyclones using the ERA-40 dataset. International Journal of Climatology 31, 1596–1614. https://doi.org/10.1002/joc.2183

Camuera, J., Jiménez-Moreno, G., Ramos-Román, M.J., García-Alix, A., Jiménez-Espejo, F.J., Toney, J.L., Anderson, R.S. (2021). Chronological control and centennial-scale climatic subdivisions of the Last Glacial Termination in the western Mediterranean region. Quaternary Science Reviews 255, 106814. https://doi.org/10.1016/j.quascirev.2021.106814

Camuera, J., Jiménez-Moreno, G., Ramos-Román, M.J., García-Alix, A., Toney, J.L., Anderson, R.S., Jiménez-Espejo, F., Bright, J., Webster, C., Yanes, Y., Carrión, J.S. (2019). Vegetation and climate changes during the last two glacial-interglacial cycles in the western Mediterranean: A new long pollen record from Padul (southern Iberian Peninsula). Quaternary Science Reviews 205, 86–105. https://doi.org/10.1016/J.QUASCIREV.2018.12.013

Camuera, J., Ramos-Román, M.J., Jiménez-Moreno, G., García-Alix, A., Ilvonen, L., Ruha, L., Gil-Romera, G., González-Sampériz, P., Seppä, H. (2022). Past 200 kyr hydroclimate variability in the western Mediterranean and its connection to the African Humid Periods. Scientific Reports 12, 9050. https://doi.org/10.1038/s41598-022-12047-1

Canfield, D.E. (1994). Factors influencing organic carbon preservation in marine sediments. Chemical Geology 114, 315–329. https://doi.org/10.1016/0009-2541(94)90061-2

Caralp, M.-H. (1988). Late glacial to recent deep-sea benthic foraminifera from the northeastern Atlantic (Cadiz Gulf) and western Mediterranean (Alboran Sea): Paleooceanographic results. Marine Micropaleontology 13, 265–289. https://doi.org/10.1016/0377-8398(88)90006-0

Carmona, N.B., Mángano, M.G., Buatois, L.A., Bromley, R.G., Ponce, J.J., Asgaard, U., Bellosi, E. (2020). Scolicia and its producer in shallow-marine deposits of the Miocene Chenque Formation (Patagonia, Argentina): functional morphology and implications for understanding burrowing behavior. Ichnos 27, 290–299. https://doi.org/10.1080/10420940.2020.1744589

Carter, S.C., Paytan, A., Griffith, E.M. (2020). Toward an improved understanding of the marine barium cycle and the application of marine barite as a paleoproductivity proxy. Minerals 10, 421. https://doi.org/10.3390/min10050421

Casanova-Arenillas, S. (2019). SantiCa/ichAnTool-Project (Version 2.1). https://doi.org/10.5281/zenodo.3518837

Casanova-Arenillas, S., Rodríguez-Tovar, F.J., Martínez-Ruiz, F. (2022). Ichnological evidence for bottom water oxygenation during organic rich layer deposition in the westernmost Mediterranean over the Last Glacial Cycle. Marine Geology 443, 106673. https://doi.org/10.1016/j.margeo.2021.106673

Casanova-Arenillas, S., Rodríguez-Tovar, F.J., Martínez-Ruiz, F. (2021). Ichnological analysis as a tool for assessing deep-sea circulation in the westernmost Mediterranean over the Last Glacial Cycle. Palaeogeography, Palaeoclimatology, Palaeoecology 562, 110082. https://doi.org/10.1016/j.palaeo.2020.110082

Casanova-Arenillas, S., Rodríguez-Tovar, F.J., Martínez-Ruiz, F. (2020). Applied ichnology in sedimentary geology: Python scripts as a method to automatize ichnofabric analysis in marine core images. Computers & Geosciences 136, 104407. https://doi.org/10.1016/j.cageo.2020.104407

Casford, J.S.L.S.L., Rohling, E.J., Abu-Zied, R.H., Fontanier, C., Jorissen, F.J., Leng, M.J., Schmiedl, G., Thomson, J. (2003). A dynamic concept for eastern Mediterranean circulation and oxygenation during sapropel formation. Palaeogeography, Palaeoclimatology, Palaeoecology 190, 103–119. https://doi.org/10.1016/S0031-0182(02)00601-6

Castañeda, I.S., Schouten, S., Pätzold, J., Lucassen, F., Kasemann, S., Kuhlmann, H., Schefuß, E. (2016). Hydroclimate variability in the Nile River Basin during the past 28,000 years. Earth and Planetary Science Letters 438, 47–56. https://doi.org/10.1016/j.epsl.2015.12.014

Cattaneo, A., Badhani, S., Caradonna, C., Bellucci, M., Leroux, E., Babonneau, N., Garziglia, S., Poort, J., Akhmanov, G.G., Bayon, G., Dennielou, B., Jouet, G., Migeon, S., Rabineau, M., Droz, L., Clare, M. (2020). The Last Glacial Maximum Balearic Abyssal Plain megabed revisited. Geological Society, London, Special Publications 500, 341–357. https://doi.org/10.1144/SP500-2019-188

Cisneros, M., Cacho, I., Frigola, J., Sánchez-Vidal, A., Calafat, A., Pedrosa-Pàmies, R., Rumín-Caparrós, A., Canals, M. (2019). Deep-water formation variability in the north-western Mediterranean Sea during the last 2500 yr: A proxy validation with present-day data. Global and Planetary Change 177, 56–68. https://doi.org/10.1016/j.gloplacha.2019.03.012

Cita, M.B., Vergnaud-Grazzini, C., Robert, C., Chamley, H., Ciaranfi, N., d'Onofrio, S. (1977). Paleoclimatic Record of a Long Deep Sea Core from the Eastern Mediterranean. Quaternary Research 8, 205–235. https://doi.org/10.1016/0033-5894(77)90046-1

Clark, A. (2019). Python Imaging Library. URL: http://www.pythonware.com/products/pil/

Clark, P.U., Dyke, A.S., Shakun, J.D., Carlson, A.E., Clark, J., Wohlfarth, B., Mitrovica, J.X., Hostetler, S.W., McCabe, A.M. (2009). The Last Glacial Maximum. Science 325, 710–714. https://doi.org/10.1126/science.1172873

Clark, P.U., Pisias, N.G., Stocker, T.F., Weaver, A.J. (2002). The role of the thermohaline circulation in abrupt climate change. Nature 415, 863–869. https://doi.org/10.1038/415863a

Clarkson, M.O., Poulton, S.W., Guilbaud, R., Wood, R.A. (2014). Assessing the utility of Fe/Al and Fe-speciation to record water column redox conditions in carbonate-rich sediments. Chemical Geology 382, 111–122. https://doi.org/10.1016/j.chemgeo.2014.05.031

CLIMAP project (1981). Seasonal reconstructions of the Earth`s surface at the last glacial maximum. Geological Society of America.

CLIMAP project members (1976). The Surface of the Ice-Age Earth. Science 191, 1131–1137. https://doi.org/10.1126/science.191.4232.1131

COHMAP members (1988). Climatic Changes of the Last 18,000 Years: Observations and Model Simulations. Science 241, 1043–1052. https://doi.org/10.1126/science.241.4869.1043

Colley, S., Thomson, J. (1985). Recurrent uranium relocations in distal turbidites emplaced in pelagic conditions. Geochimica et Cosmochimica Acta 49, 2339–2348.

https://doi.org/10.1016/0016-7037(85)90234-0

Comas, M., Platt, J.P., Soto, J.I., Watts, A.B. (1999). The origin and tectonic history of the Alboran Basin: Insights from Leg 161 results. Proceedings of the Ocean Drilling Program 161, 555–580. https://doi.org/10.2973/odp.proc.sr.161.262.1999

Comas, M.C., García-Dueñas, V., Jurado, M.J. (1992). Neogene tectonic evolution of the Alboran Sea from MCS data. Geo-Marine Letters 12, 157–164. https://doi.org/10.1007/BF02084927

Comas-Bru, L., Hernández, A. (2018). Reconciling North Atlantic climate modes: revised monthly indices for the East Atlantic and the Scandinavian patterns beyond the 20th century. Earth System Science Data 10, 2329–2344. https://doi.org/10.5194/essd-10-2329-2018

Combourieu Nebout, N., Peyron, O., Dormoy, I., Desprat, S., Beaudouin, C., Kotthoff, U., Marret, F. (2009). Rapid climatic variability in the west Mediterranean during the last 25 000 years from high resolution pollen data. Climate of the Past 5, 503–521. https://doi.org/
10.5194/cp-5-503-2009

Cornuault, M., Tachikawa, K., Vidal, L., Guihou, A., Siani, G., Deschamps, P., Bassinot, F., Revel, M. (2018). Circulation Changes in the Eastern Mediterranean Sea Over the Past 23,000 Years Inferred From Authigenic Nd Isotopic Ratios. Paleoceanography and Paleoclimatology 33, 264–280. https://doi.org/10.1002/2017PA003227

Cornuault, M., Vidal, L., Tachikawa, K., Licari, L., Rouaud, G., Sonzogni, C., Revel, M. (2016). Deep water circulation within the eastern Mediterranean Sea over the last 95 kyr: New insights from stable isotopes and benthic foraminiferal assemblages. Palaeogeography, Palaeoclimatology, Palaeoecology 459, 1–14. https://doi.org/10.1016/j.palaeo.2016.06.038

Correns, C.W. (1937). Wissenschaftliche Ergebnisse der Deutsche Atlantische Expedition "'Meteor"', 1925–1927, in: Die Sedimente Des Aquatorialen Atlantischen Ozeans. II. Geochemie Der Sedimente. pp. 205–245.

Corrick, E.C., Drysdale, R.N., Hellstrom, J.C., Capron, E., Rasmussen, S.O., Zhang, X., Fleitmann, D., Couchoud, I., Wolff, E. (2020). Synchronous timing of abrupt climate changes during the last glacial period. Science 369, 963–969. https://doi.org/10.1126/science.aay5538

Cortina, A., Sierro, F.J., Flores, J.A., Martrat, B., Grimalt, J.O. (2015). The response of SST to insolation and ice sheet variability from MIS 3 to MIS 11 in the northwestern Mediterranean Sea (Gulf of Lions). Geophysical Research Letters 42, 10366–10374. https://doi.org/10.1002/2015GL065539

Costa, K.M., Anderson, R.F., McManus, J.F., Winckler, G., Middleton, J.L., Langmuir, C.H. (2018). Trace element (Mn, Zn, Ni, V) and authigenic uranium (aU) geochemistry reveal sedimentary redox history on the Juan de Fuca Ridge, North Pacific Ocean. Geochimica et Cosmochimica Acta, Chemistry of oceans past and present: A Special Issue in tribute to Harry Elderfield 236, 79–98. https://doi.org/10.1016/j.gca.2018.02.016

Costa, K.M., Nielsen, S.G., Wang, Y., Lu, W., Hines, S.K.V., Jacobel, A.W., Oppo, D.W. (2023). Marine sedimentary uranium to barium ratios as a potential quantitative proxy for Pleistocene bottom water oxygen concentrations. Geochimica et Cosmochimica Acta 343, 1–16. https://doi.org/10.1016/j.gca.2022.12.022

Cramer, W., Guiot, J., Fader, M., Garrabou, J., Gattuso, J.-P., Iglesias, A., Lange, M.A., Lionello, P., Llasat, M.C., Paz, S., Peñuelas, J., Snoussi, M., Toreti, A., Tsimplis, M.N., Xoplaki, E. (2018). Climate change and interconnected risks to sustainable development

in the Mediterranean. Nature Climate Change 8, 972–980. https://doi.org/10.1038/s41558-018-0299-2

Cramp, A., O'Sullivan, G. (1999). Neogene sapropels in the Mediterranean: a review. Marine Geology 153, 11–28. https://doi.org/10.1016/S0025-3227(98)00092-9

Criado-Aldeanueva, F., Soto-Navarro, F.J., García-Lafuente, J. (2014). Large-Scale Atmospheric Forcing Influencing the Long-Term Variability of Mediterranean Heat and Freshwater Budgets: Climatic Indices. Journal of Hydrometeorology 15, 650–663. https://doi.org/10.1175/JHM-D-13-04.1

Criado-Aldeanueva, F., Soto-Navarro, F.J., García-Lafuente, J. (2012). Seasonal and interannual variability of surface heat and freshwater fluxes in the Mediterranean Sea: budgets and exchange through the Strait of Gibraltar. International Journal of Climatology 32, 286–302. https://doi.org/10.1002/joc.2268

Criado-Aldeanueva, F., Soto-Navarro, J. (2020). Climatic Indices over the Mediterranean Sea: A Review. Applied Sciences 10, 5790. https://doi.org/10.3390/app10175790

Crocker, A.J., Naafs, B.D.A., Westerhold, T., James, R.H., Cooper, M.J., Röhl, U., Pancost, R.D., Xuan, C., Osborne, C.P., Beerling, D.J., Wilson, P.A. (2022). Astronomically controlled aridity in the Sahara since at least 11 million years ago. Nature Geoscience 15, 671–676. https://doi.org/10.1038/s41561-022-00990-7

Crusius, J., Thomson, J. (2000). Comparative behavior of authigenic Re, U, and Mo during reoxidation and subsequent long-term burial in marine sediments. Geochimica et Cosmochimica Acta 64, 2233–2242. https://doi.org/10.1016/S0016-7037(99)00433-0

Dansgaard, W. 1987. Ice Core Evidence of Abrupt Climatic Changes, in: Berger E.H., Labyrie L.D. (Eds), Abrupt Climatic Change. Dordrecht: Springer, pp. 223–233. https://doi.org/10.1007/978-94-009-3993-6_21

Dansgaard, W., Clausen, H.B., Gundestrup, N., Hammer, C.U., Johnsen, S.F., Kristinsdottir, P.M., Reeh, N. (1982). A New Greenland Deep Ice Core. Science 218, 1273–1277. https://doi.org/10.1126/science.218.4579.1273

Dansgaard, W., Johnsen, S.J., Clausen, H.B., Dahl-jensen, D., Gundestrup, N., Hammer, C.U., Oeschger, H. (1984). North Atlantic climatic oscillations revealed by deep Greenland ice cores. Climate Processes and Climate Sensitivity 29, 288–298. https://doi.org/10.1029/GM029p0288

Dansgaard, W., Johnsen, S.J., Clausen, H.B., Dahl-Jensen, D., Gundestrup, N.S., Hammer, C.U., Hvidberg, C.S., Steffensen, J.P., Sveinbjörnsdottir, A.E., Jouzel, J., Bond, G. (1993). Evidence for general instability of past climate from a 250-kyr ice-core record. Nature 364, 218–220. https://doi.org/10.1038/364218a0

Dauwe, B., Middelburg, J.J., Herman, P.M.J. (2001). Effect of oxygen on the degradability of organic matter in subtidal and intertidal sediments of the North Sea area. Marine Ecology Progress Series 215, 13–22. https://doi.org/10.3354/meps215013

De Lange, G.J., Thomson, J., Reitz, A., Slomp, C.P., Speranza Principato, M., Erba, E., Corselli, C. (2008). Synchronous basin-wide formation and redox-controlled preservation of a Mediterranean sapropel. Nature Geoscience 1, 606–610. https://doi.org/10.1038/ngeo283

De Lange, G.J., Van Os, B., Pruysers, P.A., Middelburg, J.J., Castradori, D., Van Santvoort, P., Müller, P.J., Eggenkamp, H., Prahl, F.G. (1994). Possible Early Diagenetic Alteration of Palaeo Proxies, in: Zahn, R., Pedersen, T.F., Kaminski, M.A., Labeyrie, L. (Eds.), Carbon Cycling in the Glacial Ocean: Constraints on the Ocean's Role in Global Change. Berlin: Springer, NATO ASI Series 17, pp. 225–258. https://doi.org/10.1007/978-3-642-78737-9_10

Degens, E.T. (1965). Geochemistry of sediments., New Jersey: Prentice Hall Inc, 342 pp.

deMenocal, P., Ortiz, J., Guilderson, T., Adkins, J., Sarnthein, M., Baker, L., Yarusinsky, M. (2000). Abrupt onset and termination of the African Humid Period: rapid climate responses to gradual insolation forcing. Quaternary Science Reviews 19, 347–361. https://doi.org/10.1016/S0277-3791(99)00081-5

Dercourt, J., Zonenshain, L.P., Ricou, L.-E., Kazmin, V.G., Le Pichon, X., Knipper, A.L., Grandjacquet, C., Sbortshikov, I.M., Geyssant, J., Lepvrier, C., Pechersky, D.H., Boulin, J., Sibuet, J.-C., Savostin, L.A., Sorokhtin, O., Westphal, M., Bazhenov, M.L., Lauer, J.P., Biju-Duval, B. (1986). Geological evolution of the tethys belt from the Atlantic to the pamirs since the LIAS. Tectonophysics, Evolution of the Tethys 123, 241–315. https://doi.org/10.1016/0040-1951(86)90199-X

Dermawan, D., Wang, Y.-F., You, S.-J., Jiang, J.-J., Hsieh, Y.-K. (2022). Impact of climatic and non-climatic stressors on ocean life and human health: A review. Science of The Total Environment 821, 153387. https://doi.org/10.1016/j.scitotenv.2022.153387

Di Donato, V., Sgarrella, F., Sprovieri, R., Di Stefano, E., Martín-Fernández, J.A., Incarbona, A. (2022). High-frequency modification of the central Mediterranean seafloor environment over the last 74 ka. Palaeogeography, Palaeoclimatology, Palaeoecology 593, 110924. https://doi.org/10.1016/j.palaeo.2022.110924

Dinarès-Turell, J., Hoogakker, B.A.A., Roberts, A.P., Rohling, E.J., Sagnotti, L. (2003). Quaternary climatic control of biogenic magnetite production and eolian dust input in cores from the Mediterranean Sea. Palaeogeography, Palaeoclimatology, Palaeoecology 190, 195–209. https://doi.org/10.1016/S0031-0182(02)00605-3

Dominik, J., Mangini, A. (1979). Late quaternary sedimentation rate variations on the Mediterranean Ridge, as results from the 230Th excess method. Sedimentary Geology 23, 95–112. https://doi.org/10.1016/0037-0738(79)90008-3

Dorador, J., Rodríguez-Tovar, F.J. (2018). High-resolution image treatment in ichnological core analysis: Initial steps, advances and prospects. Earth-Science Reviews 177, 226–237. https://doi.org/10.1016/j.earscirev.2017.11.020

Dorador, J., Rodríguez-Tovar, F.J. (2016a). High resolution digital image treatment to color analysis on cores from IODP Expedition 339: Approaching lithologic features and bioturbational influence. Marine Geology 377, 127–135. https://doi.org/10.1016/j.margeo.2016.02.005

Dorador, J., Rodríguez-Tovar, F.J. (2016b). Stratigraphic variation in ichnofabrics at the "Shackleton Site" (IODP Site U1385) on the Iberian Margin: Paleoenvironmental implications. Marine Geology 377, 118–126. https://doi.org/10.1016/j.margeo.2015.09.008

Dorador, J., Rodríguez-Tovar, F.J. (2015). Application of digital image tratement to the characterization and differentiation of deep-sea ichnofacies. Spanish Journal of Paleontology 30, 265–274.

Dorador, J., Rodríguez-Tovar, F.J. (2014a). Quantitative estimation of bioturbation based on digital image analysis. Marine Geology 349, 55–60. https://doi.org/10.1016/j.margeo.2014.01.003

Dorador, J., Rodríguez-Tovar, F.J. (2014b). Digital image treatment applied to ichnological analysis of marine core sediments. Facies 60, 39–44. https://doi.org/10.1007/s10347-013-0383-z

Dorador, J., Rodríguez-Tovar, F.J. (2014c). A novel application of digital image treatement by quantitative pxel analysis to trace fossil research in marine cores. PALAIOS 29, 533–538. https://doi.org/10.2110/palo.2014.044

Dorador, J., Wetzel, A., Rodríguez-Tovar, F.J. (2016). Zoophycos in deep-sea sediments indicates high and seasonal primary productivity: Ichnology as a proxy in palaeoceanography during glacial–interglacial variations. Terra Nova 28, 323–328. https://doi.org/10.1111/ter.12224

Douglas, G.B., Adeney, J.A. (2000). Diagenetic cycling of trace elements in the bottom sediments of the Swan River Estuary, Western Australia. Applied Geochemistry 15, 551–566. https://doi.org/10.1016/S0883-2927(99)00070-0

Droser, M.L., Bottjer, D.J. (1989). Ichnofabric of Sandstones Deposited in High-Energy Nearshore Environments: Measurement and Utilization. PALAIOS 4, 598. https://doi.org/10.2307/3514750

Droser, M.L., Bottjer, J.D. (1986). A semiquantitative field classification of ichnofabric. Journal of Sedimentary Research 56, 448–449. https://doi.org/10.1306/212F89C2-2B24-11D7-8648000102C1865D

Duhamel, M., Colin, C., Revel, M., Siani, G., Dapoigny, A., Douville, E., Wu, J., Zhao, Y., Liu, Z., Montagna, P. (2020). Variations in eastern Mediterranean hydrology during the last climatic cycle as inferred from neodymium isotopes in foraminifera. Quaternary Science Reviews 237, 106306. https://doi.org/10.1016/j.quascirev.2020.106306

Dünkeloh, A., Jacobeit, J. (2003). Circulation dynamics of Mediterranean precipitation variability 1948–98. International Journal of Climatology 23, 1843–1866. https://doi.org/10.1002/joc.973

Durrieu de Madron, X., Guieu, C., Sempéré, R., Conan, P., Cossa, D., D'Ortenzio, F., Estournel, C., Gazeau, F., Rabouille, C., Stemmann, L., Bonnet, S., Diaz, F., Koubbi, P., Radakovitch, O., Babin, M., Baklouti, M., Bancon-Montigny, C., Belviso, S., Bensoussan, N., ... Verney, R. (2011). Marine ecosystems' responses to climatic and anthropogenic forcings in the Mediterranean. Progress in Oceanography 91, 97–166. https://doi.org/10.1016/j.pocean.2011.02.003

Durrieu de Madron, X., Houpert, L., Puig, P., Sanchez-Vidal, A., Testor, P., Bosse, A., Estournel, C., Somot, S., Bourrin, F., Bouin, M.N., Beauverger, M., Beguery, L., Calafat, A., Canals, M., Cassou, C., Coppola, L., Dausse, D., D'Ortenzio, F., Font, J., ... Raimbault, P. (2013). Interaction of dense shelf water cascading and open-sea convection in the northwestern Mediterranean during winter 2012. Geophysical Research Letters 40, 1379–1385. https://doi.org/10.1002/grl.50331

Dymond, J., Suess, E., Lyle, M. (1992). Barium in Deep-Sea Sediment: A Geochemical Proxy for Paleoproductivity. Paleoceanography 7, 163–181. https://doi.org/10.1029/92PA00181

Dypvik, H., Harris, N.B. (2001). Geochemical facies analysis of fine-grained siliciclastics using Th/U, Zr/Rb and (Zr+Rb)/Sr ratios. Chemical Geology 181, 131–146. https://doi.org/10.1016/S0009-2541(01)00278-9

Ehrenberg, K. (1944). Ergänzende Bemerkungen zu den seinerzeit aus dem Miozän von Burgschleinitz beschriebenen Gangkernen und Bauten dekapoder Krebse. Paläontologische Zeitschrift 23, 354–359.

Ehrmann, W., Schmiedl, G. (2021). Nature and dynamics of North African humid and dry periods during the last 200,000 years documented in the clay fraction of Eastern Mediterranean deep-sea sediments. Quaternary Science Reviews 260, 106925. https://doi.org/10.1016/j.quascirev.2021.106925

Ehrmann, W., Seidel, M., Schmiedl, G. (2013). Dynamics of Late Quaternary North African humid periods documented in the clay mineral record of central Aegean Sea sediments. Global and Planetary Change 107, 186–195. https://doi.org/10.1016/j.gloplacha.2013.05.010

Einsele, G. (2000). Sedimentary Basins: Evolution, Facies, and Sediment Budgets. Heidelberg:Springer-Verlag, 727 pp. http://dx.doi.org/10.1007/978-3-662-04029-4

Ekdale, A.A., Bromley, R.G. (2003). Paleoethologic interpretation of complex Thalassinoides in shallow-marine limestones, Lower Ordovician, southern Sweden. Palaeogeography, Palaeoclimatology, Palaeoecology 192, 221–227. https://doi.org/10.1016/S0031-0182(02)00686-7

Ekdale, A.A., Bromley, R.G. (1991). Analysis of composite ichnofabrics; an example in Uppermost Cretaceous chalk of Denmark. PALAIOS 6, 232–249. https://doi.org/10.2307/3514904

Ekdale, A.A., Bromley, R.G. (1983). Trace fossils and ichnofabric in the Kjolby Gaard Marl, uppermost Cretaceous, Denmark. Bulletin of the Geological Society of Denmark 31, 107–119. https://doi.org/10.37570/bgsd-1982-31-08

Ekdale, A.A., Bromley, R.G., Knaust, D. (2012). The Ichnofabric Concept, in: Knaust, D., Bromley, R.G. (Eds.). Trace Fossils as Indicators of Sedimentary Environments. pp. 139–155. https://doi.org/10.1016/B978-0-444-53813-0.00005-8

Ekdale, A.A., Bromley, R.G., Pemberton, S.G. (1984). Ichnology: The Use of Trace Fossils in Sedimentology and Stratigraphy. SEPM Society for Sedimentary Geology. SEPM short course notes 15, 317 pp. https://doi.org/10.2110/scn.84.15

Ekdale, A.A., Lewis, D.W. (1991). The New Zealand Zoophycos revisited: Morphology, ethology, and paleoecology. Ichnos 1, 183–194. https://doi.org/10.1080/10420949109386351

Emeis, K.-C., Sakamoto, T., Wehausen, R., Brumsack, H.-J. (2000). The sapropel record of the eastern Mediterranean Sea — results of Ocean Drilling Program Leg 160. Palaeogeography, Palaeoclimatology, Palaeoecology 158, 371–395.

https://doi.org/10.1016/S0031-0182(00)00059-6

Emerson, S.R., Huested, S.S. (1991). Ocean anoxia and the concentrations of molybdenum and vanadium in seawater. Marine Chemistry 34, 177–196. https://doi.org/10.1016/0304-4203(91)90002-E

Emis, K.-C., Weissert, H. (2009). Tethyan-Mediterranean organic carbon-rich sediments from Mesozoic black shales to sapropels. Sedimentology 56, 247–266. https://doi.org/10.1111/j.1365-3091.2008.01026.x

Ercilla, G., Juan, C., Hernández-Molina, F.J., Bruno, M., Estrada, F., Alonso, B., Casas, D., Farran, Marcel. lí, Llave, E., García, M., Vázquez, J.T., D'Acremont, E., Gorini, C., Palomino, D., Valencia, J., El Moumni, B., Ammar, A. (2016). Significance of bottom currents in deep-sea morphodynamics: An example from the Alboran Sea. Marine Geology 378, 157–170. https://doi.org/10.1016/j.margeo.2015.09.007

Ercilla, G., Juan, C., Periáñez, R., Alonso, B., Abril, J.M., Estrada, F., Casas, D., Vázquez, J.T., D'Acremont, E., Gorini, C., El Moumni, B., Do Couto, D., Valencia, J. (2019). Influence of alongslope processes on modern turbidite systems and canyons in the Alboran Sea (southwestern Mediterranean). Deep Sea Research Part I: Oceanographic Research Papers 144, 1–16. https://doi.org/10.1016/j.dsr.2018.12.002

Evan, A.T., Flamant, C., Gaetani, M., Guichard, F. (2016). The past, present and future of African dust. Nature 531, 493–495. https://doi.org/10.1038/nature17149

Evangelinos, D., Escutia, C., Etourneau, J., Hoem, F., Bijl, P., Boterblom, W., van de Flierdt, T., Valero, L., Flores, J.-A., Rodriguez-Tovar, F.J., Jimenez-Espejo, F.J., Salabarnada, A., López-Quirós, A. (2020). Late Oligocene-Miocene proto-Antarctic Circumpolar Current dynamics off the Wilkes Land margin, East Antarctica. Global and Planetary Change 191, 103221. https://doi.org/10.1016/j.gloplacha.2020.103221

Evans, M.E., Heller, F. (2003). Environmental Magnetism: Principles and Applications of Enviromagnetics. Amsterdam:Elsevier, 299 pp.

Fabres, J., Calafat, A., Sanchez-Vidal, A., Canals, M., Heussner, S. (2002). Composition and spatio-temporal variability of particle fluxes in the Western Alboran Gyre, Mediterranean Sea. Journal of Marine Systems 33–34, 431–456. https://doi.org/10.1016/S0924-7963(02)00070-2

Filippidi, A., Triantaphyllou, M.V., De Lange, G.J. (2016). Eastern-Mediterranean ventilation variability during sapropel S1 formation, evaluated at two sites influenced by deep-water formation from Adriatic and Aegean Seas. Quaternary Science Reviews 144, 95–106. https://doi.org/10.1016/j.quascirev.2016.05.024

Fischer, H., Fundel, F., Ruth, U., Twarloh, B., Wegner, A., Udisti, R., Becagli, S., Castellano, E., Morganti, A., Severi, M., Wolff, E., Littot, G., Röthlisberger, R., Mulvaney, R., Hutterli, M.A., Kaufmann, P., Federer, U., Lambert, F., Bigler, M., ... Wagenbach, D. (2007). Reconstruction of millennial changes in dust emission, transport and regional sea ice coverage using the deep EPICA ice cores from the Atlantic and Indian Ocean sector of Antarctica. Earth and Planetary Science Letters 260, 340–354. https://doi.org/10.1016/j.epsl.2007.06.014

Fischer, H., Wahlen, M., Smith, J., Mastroianni, D., Deck, B. (1999). Ice Core Records of Atmospheric CO2 Around the Last Three Glacial Terminations. Science 293, 1712–1714. https://doi.org/10.1126/science.283.5408.1712

Fletcher, William J., Sánchez Goñi, M.F., Allen, J.R.M., Cheddadi, R., Combourieu-Nebout, N., Huntley, B., Lawson, I., Londeix, L., Magri, D., Margari, V., Müller, U.C., Naughton, F., Novenko, E., Roucoux, K., Tzedakis, P.C. (2010). Millennial-scale variability during the last glacial in vegetation records from Europe. Quaternary Science Reviews, 29, 2839–2864. https://doi.org/10.1016/j.quascirev.2009.11.015

Fletcher, W. J., Sanchez Goñi, M.F., Peyron, O., Dormoy, I. (2010). Abrupt climate changes of the last deglaciation detected in a Western Mediterranean forest record. Climate of the Past 6, 245–264. https://doi.org/10.5194/cpd-5-203-2009

Flocas, H.A., Simmonds, I., Kouroutzoglou, J., Keay, K., Hatzaki, M., Bricolas, V., Asimakopoulos, D. (2010). On Cyclonic Tracks over the Eastern Mediterranean. Journal of Climate 23, 5243–5257. https://doi.org/10.1175/2010JCLI3426.1

Frey, R.W., Curran, A.H., Pemberton, S.G. (1984). Tracemaking activities of crabs and their environmental significance: the ichnogenus Psilonichnus. Journal of Paleontology 58, 333–354.

Frigola, J., Moreno, A., Cacho, I., Canals, M., Sierro, F.J., Flores, J.A., Grimalt, J.O. (2008). Evidence of abrupt changes in Western Mediterranean Deep Water circulation during the last 50kyr: A high-resolution marine record from the Balearic Sea. Quaternary International 181, 88–104. https://doi.org/10.1016/j.quaint.2007.06.016

Fronval, T., Jansen, E. (1997). Eemian and Early Weichselian (140–60 ka) Paleoceanography and paleoclimate in the Nordic Seas with comparisons to Holocene conditions. Paleoceanography 12, 443–462. https://doi.org/10.1029/97PA00322

Fu, S., Werner, F. (2000). Distribution, ecology and taphonomy of the organism trace, Scolicia, in northeast Atlantic deep-sea sediments. Palaeogeography, Palaeoclimatology, Palaeoecology 156, 289–300. https://doi.org/10.1016/S0031-0182(99)00146-7

Gallego-Torres, D., Martínez-Ruiz, F., De Lange, G.J., Jiménez-Espejo, F.J., Ortega-Huertas, M. (2010). Trace-elemental derived paleoceanographic and paleoclimatic conditions for Pleistocene Eastern Mediterranean sapropels. Palaeogeography, Palaeoclimatology, Palaeoecology 293, 76–89. https://doi.org/10.1016/j.palaeo.2010.05.001

García-Alix, A., Camuera, J., Ramos-Román, M.J., Toney, J.L., Sachse, D., Schefuß, E., Jiménez-Moreno, G., Jiménez-Espejo, F.J., López-Avilés, A., Anderson, R.S., Yanes, Y. (2021). Paleohydrological dynamics in the Western Mediterranean during the last glacial cycle. Global and Planetary Change 202, 103527. https://doi.org/10.1016/j.gloplacha.2021.103527

Gascard, J.C. (1978). Mediterranean deep water formation baroclinic instability and oceanic eddies. Oceanologica Acta 1, 315–330.

Gascard, J.C., Richez, C. (1985). Water masses and circulation in the Western Alboran sea and in the Straits of Gibraltar. Progress in Oceanography 15, 157–216. https://doi.org/10.1016/0079-6611(85)90031-X

Giannetti, A., McCann, T. (2010). The Upper Paleocene of the Zumaya Section (Northern Spain): Review of the Ichnological Content and Preliminary Palaeoecological Interpretation. Ichnos 17, 137–161. https://doi.org/10.1080/10420941003659550

Gilman, C., Garrett, C. (1994). Heat flux parameterizations for the Mediterranean Sea: The role of atmospheric aerosols and constraints from the water budget. Journal of Geophysical Research: Oceans 99, 5119–5134. https://doi.org/10.1029/93JC03069

Giorgi, F. (2006). Climate change hot-spots. Geophysical Research Letters 33, L08707. https://doi.org/10.1029/2006GL025734

Goldberg, E.D. (1963). Mineralogy and chemistry of marine sedimentation., in: Shepard, F.P. (Ed.), Submarine Geology. New York: Harper and Row, pp. 436–466.

Goldberg, E.D. (1954). Marine geochemistry, I. Chemical scavengers of the sea. Journal of Geology, 62, 249–265.

Goldberg, E.D., Arrhenius, G.O.S. (1958). Chemistry of Pacific pelagic sediments. Geochimica et Cosmochimica Acta 13, 153–212.

Goudie, A.S., Middleton, N.J. (2001). Saharan dust storms: nature and consequences. Earth-Science Reviews 56, 179–204. https://doi.org/10.1016/S0012-8252(01)00067-8

Govin, A., Holzwarth, U., Heslop, D., Ford Keeling, L., Zabel, M., Mulitza, S., Collins, J.A., Chiessi, C.M. (2012). Distribution of major elements in Atlantic surface sediments (36°N-49°S): Imprint of terrigenous input and continental weathering. Geochemistry, Geophysics, Geosystems 13, Q01013. https://doi.org/10.1029/2011GC003785

Grant, K.M. (2013). Sea-level change, monsoon variability, and eastern Mediterranean climate over the Late Pleistocene. Doctoral Thesis, University of Southampton, Southampton 176 pp.

Grant, K.M., Amarathunga, U., Amies, J.D., Hu, P., Qian, Y., Penny, T., Rodriguez-Sanz, L., Zhao, X., Heslop, D., Liebrand, D., Hennekam, R., Westerhold, T., Gilmore, S., Lourens, L.J., Roberts, A.P., Rohling, E.J. (2022). Organic carbon burial in Mediterranean sapropels intensified during Green Sahara Periods since 3.2 Myr ago. Communications Earth & Environment 3, 1–9. https://doi.org/10.1038/s43247-021-00339-9

Grant, K.M., Grimm, R., Mikolajewicz, U., Marino, G., Ziegler, M., Rohling, E.J. (2016). The timing of Mediterranean sapropel deposition relative to insolation, sea-level and African monsoon changes. Quaternary Science Reviews 140, 125–141. https://doi.org/10.1016/j.quascirev.2016.03.026

Gregory, B.R.B., Patterson, R.T., Reinhardt, E.G., Galloway, J.M., Roe, H.M. (2019). An evaluation of methodologies for calibrating Itrax X-ray fluorescence counts with ICP-MS concentration data for discrete sediment samples. Chemical Geology 521, 12–27. https://doi.org/10.1016/j.chemgeo.2019.05.008

Griffith, E.M., Paytan, A. (2012). Barite in the ocean – occurrence, geochemistry and palaeoceanographic applications. Sedimentology 59, 1817–1835. https://doi.org/10.1111/J.1365-3091.2012.01327.X

Grimm, R., Maier-Reimer, E., Mikolajewicz, U., Schmiedl, G., Müller-Navarra, K., Adloff, F., Grant, K.M., Ziegler, M., Lourens, L.J., Emeis, K.-C. (2015). Late glacial initiation of Holocene eastern Mediterranean sapropel formation. Nature Communications 6, 7099. https://doi.org/10.1038/ncomms8099

Hällberg, L.P., Stevens, T., Almqvist, B., Snowball, I., Wiers, S., Költringer, C., Lu, H., Zhang, H., Lin, Z. (2020). Magnetic susceptibility parameters as proxies for desert sediment provenance. Aeolian Research 46, 100615. https://doi.org/10.1016/j.aeolia.2020.100615

Halpern, B.S., Frazier, M., Afflerbach, J., Lowndes, J.S., Micheli, F., O'Hara, C., Scarborough, C., Selkoe, K.A. (2019). Recent pace of change in human impact on the world's ocean. Scientific Reports 9, 11609. https://doi.org/10.1038/s41598-019-47201-9

Häntzschel, W. (1975). Miscellanea, Supplement 1 Trace Fossils and Problematica. Part W. Treatise on Invertebrate Paleontology, Kansas: The Geological Society of America, 269 pp.

Hays, J.D., Imbrie, J., Shackleton, N.J. (1976). Variations in the Earth's Orbit: Pacemaker of the Ice Ages. Science 194, 1121–1132. https://doi.org/10.1126/science.194.4270.1121

Heburn, G.W., La Violette, P.E. (1990). Variations in the structure of the anticyclonic gyres found in the Alboran Sea. Journal of Geophysical Research 95, 1599. https://doi.org/10.1029/JC095iC02p01599

Hedges, J.I., Keil, R.G. (1995). Sedimentary organic matter preservation: an assessment and speculative synthesis. Marine Chemistry 49, 81–115. https://doi.org/10.1016/0304-4203(95)00008-F

Hedges, J.I., Keil, R.G., Benner, R. (1997). What happens to terrestrial organic matter in the ocean?. Organic Geochemistry 27, 195–212. https://doi.org/10.1016/S0146-6380(97)00066-1

Hedges, J.I., Oades, J.M. (1997). Comparative organic geochemistries of soils and marine sediments. Organic Geochemistry 27, 319–361. https://doi.org/10.1016/S0146-6380(97)00056-9

Heinrich, H. (1988). Origin and consequences of cyclic ice rafting in the Northeast Atlantic Ocean during the past 130,000 years. Quaternary Research 29, 142–152. https://doi.org/10.1016/0033-5894(88)90057-9

Helz, G.R., Bura-Nakić, E., Mikac, N., Ciglenečki, I. (2011). New model for molybdenum behavior in euxinic waters. Chemical Geology 284, 323–332. https://doi.org/10.1016/j.chemgeo.2011.03.012

Hemming, S.R. (2004). Heinrich events: Massive late Pleistocene detritus layers of the North Atlantic and their global climate imprint. Reviews of Geophysics 42, RG1005. https://doi.org/10.1029/2003RG000128

Henkel, S., Mogollón, J.M., Nöthen, K., Franke, C., Bogus, K., Robin, E., Bahr, A., Blumenberg, M., Pape, T., Seifert, R., März, C., de Lange, G.J., Kasten, S. (2012). Diagenetic barium cycling in Black Sea sediments – A case study for anoxic marine environments. Geochimica et Cosmochimica Acta 88, 88–105. https://doi.org/10.1016/j.gca.2012.04.021

Hennekam, R., Sweere, T., Tjallingii, R., de Lange, G.J., Reichart, G.-J. (2019). Trace metal analysis of sediment cores using a novel X-ray fluorescence core scanning method. Quaternary International 514, 55–67. https://doi.org/10.1016/j.quaint.2018.10.018

Hennekam, R., van der Bolt, B., van Nes, E.H., de Lange, G.J., Scheffer, M., Reichart, G.-J. (2020). Early-Warning Signals for Marine Anoxic Events. Geophysical Research Letters 47, e2020GL089183. https://doi.org/10.1029/2020GL089183

Henry, L.G., McManus, J.F., Curry, W.B., Roberts, N.L., Piotrowski, A.M., Keigwin, L.D. (2016). North Atlantic ocean circulation and abrupt climate change during the last glaciation. Science 353, 470–474. https://doi.org/10.1126/science.aaf5529

Hermelin, J.O.R. (1991). Hyalinea balthica (Schroeter) in lower Pliocene sediments of the Northwest Arabian Sea. Journal of Foraminiferal Research 21, 244–251. https://doi.org/10.2113/gsjfr.21.3.244

Hernández-Molina, F.J., Stow, D.A.V., Alvarez-Zarikian, C.A., Acton, G.D., Bahr, A., Balestra, B., Ducassou, E., Flood, R., Flores, J.-A., Furota, S., Grunert, P., Hodell, D., Jiménez-Espejo, F.J., Kim, J.K., Krissek, L., Kuroda, J., Li, B., Llave, E., Lofi, J., ... Xuan, C. (2014). Onset of Mediterranean outflow into the North Atlantic. Science 344, 1244–1250. https://doi.org/10.1126/science.1251306

Hertweck, G., Wehrmann, A., Liebezeit, G. (2007). Bioturbation structures of polychaetes in modern shallow marine environments and their analogues to Chondrites group traces. Palaeogeography, Palaeoclimatology, Palaeoecology 245, 382–389. https://doi.org/10.1016/j.palaeo.2006.09.001

Hesse, R., Schacht, U. (2011). Early Diagenesis of Deep-Sea Sediments, in: HüNeke, H., Mulder, T. (Eds). Deep-Sea Sediments. Amsterdam: Elsevier. Developments in Sedimentology 63, pp. 557–713. https://doi.org/10.1016/B978-0-444-53000-4.00009-3

Higgs, N.C., Thomson, J., Wilson, T.R.S., Croudace, I.W. (1994). Modification and complete removal of eastern Mediterranean sapropels by postdepositional oxidation. Geology 22, 423–426. https://doi.org/10.1130/0091-7613(1994)022<0423:MACROE>2.3.CO;2

Hilgen, F.J. (1991). Extension of the astronomically calibrated (polarity) time scale to the Miocene/Pliocene boundary. Earth and Planetary Science Letters 107, 349–368. https://doi.org/10.1016/0012-821X(91)90082-S

Hilgen, F.J., Abdul Aziz, H., Krijgsman, W., Raffi, I., Turco, E. (2003). Integrated stratigraphy and astronomical tuning of the Serravallian and lower Tortonian at Monte dei Corvi (Middle–Upper Miocene, northern Italy). Palaeogeography, Palaeoclimatology, Palaeoecology 199, 229–264. https://doi.org/10.1016/S0031-0182(03)00505-4

Hodell, D.A., Crowhurst, S.J., Lourens, L., Margari, V., Nicolson, J., Rolfe, J.E., Skinner, L.C., Thomas, N.C., Tzedakis, P.C., Mleneck-Vautravers, M.J., Wolff, E.W. (2023). A 1.5-million-year record of orbital and millennial climate variability in the North Atlantic. Climate of the Past 19, 607–636. https://doi.org/10.5194/cp-19-607-2023

Hodell, D.A., Nicholl, J.A., Bontognali, T.R.R.R., Danino, S., Dorador, J., Dowdeswell, J.A., Einsle, J., Kuhlmann, H., Martrat, B., Mleneck-Vautravers, M.J., Rodríguez-Tovar, F.J., Röhl, U. (2017). Anatomy of Heinrich Layer 1 and its role in the last deglaciation. Paleoceanography 32, 284–303. https://doi.org/10.1002/2016PA003028

Hoerling, M.P., Hurrell, J.W., Xu, T., Bates, G.T., Phillips, A.S. (2004). Twentieth century North Atlantic climate change. Part II: Understanding the effect of Indian Ocean warming. Climate Dynamics 23, 391–405. https://doi.org/10.1007/s00382-004-0433-x

Hoffman, J.S., Clark, P.U., Parnell, A.C., He, F. (2017). Regional and global sea-surface temperatures during the last interglaciation. Science 355, 276–279. https://doi.org/10.1126/science.aai8464

Hoogakker, B.A.A., Rothwell, R.G., Rohling, E.J., Paterne, M., Stow, D.A.V., Herrle, J.O., Clayton, T. (2004). Variations in terrigenous dilution in western Mediterranean Sea pelagic sediments in response to climate change during the last glacial cycle. Marine Geology 211, 21–43. https://doi.org/10.1016/j.margeo.2004.07.005

Horner, T.J., Little, S.H., Conway, T.M., Farmer, J.R., Hertzberg, J.E., Janssen, D.J., Lough, A.J.M., McKay, J.L., Tessin, A., Galer, S.J.G., Jaccard, S.L., Lacan, F., Paytan, A., Wuttig, K., GEOTRACES–PAGES Biological Productivity Working Group Members. (2021). Bioactive Trace Metals and Their Isotopes as Paleoproductivity Proxies: An Assessment Using GEOTRACES-Era Data. Global Biogeochemical Cycles 35, e2020GB006814. https://doi.org/10.1029/2020GB006814

Hughes, P.D., Gibbard, P.L. (2018). Global glacier dynamics during 100 ka Pleistocene glacial cycles. Quaternary Research 90, 222–243. https://doi.org/10.1017/qua.2018.37

Hughes, P.D., Gibbard, P.L., Ehlers, J. (2013). Timing of glaciation during the last glacial cycle: Evaluating the concept of a global "Last Glacial Maximum" (LGM). Earth-Science Reviews 125, 171–198. https://doi.org/10.1016/j.earscirev.2013.07.003

Hüneke, H., Henrich, R. (2011). Pelagic Sedimentation in Modern and Ancient Oceans. In: in: HüNeke, H., Mulder, T. (Eds). Deep-Sea Sediments. Amsterdam: Elsevier. Developments in Sedimentology 63, pp. 215–351. https://doi.org/10.1016/B978-0-444-53000-4.00004-4

Hunter, J.D. (2007). Matplotlib: A 2D Graphics Environment. Computing in Science & Engineering 9, 90–95. https://doi.org/10.1109/MCSE.2007.55

Imbrie, J., Berger, A., Boyle, E.A., Clemens, S.C., Duffy, A., Howard, W.R., Kukla, G., Kutzbach, J., Martinson, D.G., McIntyre, A., Mix, A.C., Molfino, B., Morley, J.J., Peterson, L.C., Pisias, N.G., Prell, W.L., Raymo, M.E., Shackleton, N.J., Toggweiler, J.R. (1993). On the structure and origin of major glaciation cycles 2. The 100,000-year cycle. Paleoceanography 8, 699–735. https://doi.org/10.1029/93PA02751

Incarbona, A., Sprovieri, M. (2020). The Postglacial Isotopic Record of Intermediate Water Connects Mediterranean Sapropels and Organic-Rich Layers. Paleoceanography and Paleoclimatology 35, e2020PA004009. https://doi.org/10.1029/2020PA004009

IPCC, 2021. Climate Change 2021: The Physical Science Basis. Contribution of Working Group I to the Sixth Assessment Report of the Intergovernmental Panel on Climate Change. Cambridge: Cambridge University Press.

Ivanovic, R.F., Valdes, P.J., Gregoire, L., Flecker, R., Gutjahr, M. (2014). Sensitivity of modern climate to the presence, strength and salinity of Mediterranean-Atlantic exchange in a global general circulation model. Climate Dynamics 42, 859–877. https://doi.org/10.1007/s00382-013-1680-5

Ivy-Ochs, S., Kerschner, H., Reuther, A., Preusser, F., Heine, K., Maisch, M., Kubik, P.W., Schlüchter, C. (2008). Chronology of the last glacial cycle in the European Alps. Journal of Quaternary Science 23, 559–573. https://doi.org/10.1002/jqs.1202

Jacobel, A.W., Anderson, R.F., Jaccard, S.L., McManus, J.F., Pavia, F.J., Winckler, G. (2020). Deep Pacific storage of respired carbon during the last ice age: Perspectives from bottom water oxygen reconstructions. Quaternary Science Reviews 230, 106065. https://doi.org/10.1016/j.quascirev.2019.106065

Jacobel, A.W., McManus, J.F., Anderson, R.F., Winckler, G. (2017). Repeated storage of respired carbon in the equatorial Pacific Ocean over the last three glacial cycles. Nature Communications 8, 1727. https://doi.org/10.1038/s41467-017-01938-x

Jaeschke, A., Rühlemann, C., Arz, H., Heil, G., Lohmann, G. (2007). Coupling of millennial-scale changes in sea surface temperature and precipitation off northeastern Brazil with

high-latitude climate shifts during the last glacial period. Paleoceanography 22. https://doi.org/10.1029/2006PA001391

Jenkins, W.J. (2003). Tracers of Ocean Mixing, in: Holland, H.D., Turekian, K.K. (Eds). The Oceans and Marine Geochemistry. Amsterdam:Elsevier. Treatise on Geochemistry 6, pp. 223–246. https://doi.org/10.1016/B0-08-043751-6/06110-7

Jenkyns, H.C. (2010). Geochemistry of oceanic anoxic events. Geochemistry, Geophysics, Geosystems 11, Q03004. https://doi.org/10.1029/2009GC002788

Jewell, A.M., Cooper, M.J., Milton, J.A., James, R.H., Crocker, A.J., Wilson, P.A. (2022). Chemical isolation and isotopic analysis of terrigenous sediments with emphasis on effective removal of contaminating marine phases including barite. Chemical Geology 589, 120673. https://doi.org/10.1016/j.chemgeo.2021.120673

Jilbert, T., Reichart, G.-J., Aeschlimann, B., Günther, D., Boer, W., de Lange, G. (2010). Climate-controlled multidecadal variability in North African dust transport to the Mediterranean. Geology 38, 19–22. https://doi.org/10.1130/G25287.1

Jiménez-Espejo, F.J., García-Alix, A., Jiménez-Gómez, F., Rodrigo-Gámiz, M., Anderson, R.S., Rodríguez-Tovar, F.J., Martínez-Ruiz, F., Giralt, S., Delgado Huertas, A., Pardo-Igúzquiza, E. (2014). Saharan aeolian input and effective humidity variations over western Europe during the Holocene from a high altitude record. Chemical Geology 374–375, 1–12. https://doi.org/10.1016/j.chemgeo.2014.03.001

Jiménez-Espejo, F.J., Martinez-Ruiz, F., Rogerson, M., González-Donoso, J.M., Romero, O.E., Linares, D., Sakamoto, T., Gallego-Torres, D., Rueda Ruiz, J.L., Ortega-Huertas, M., Perez Claros, J.A. (2008). Detrital input, productivity fluctuations, and water mass circulation in the westernmost Mediterranean Sea since the Last Glacial Maximum. Geochemistry, Geophysics, Geosystems 9, Q11U02. https://doi.org/10.1029/2008GC002096

Jiménez-Espejo, F.J., Martínez-Ruiz, F., Sakamoto, T., Iijima, K., Gallego-Torres, D., Harada, N. (2007). Paleoenvironmental changes in the western Mediterranean since the last glacial maximum: High resolution multiproxy record from the Algero–Balearic basin. Palaeogeography, Palaeoclimatology, Palaeoecology 246, 292–306. https://doi.org/10.1016/j.palaeo.2006.10.005

Jiménez-Espejo, F.J., Pardos-Gené, M., Martínez-Ruiz, F., García-Alix, A., van de Flierdt, T., Toyofuku, T., Bahr, A., Kreissig, K. (2015). Geochemical evidence for intermediate water circulation in the westernmost Mediterranean over the last 20kyrBP and its impact on the Mediterranean Outflow. Global and Planetary Change 135, 38–46. https://doi.org/10.1016/j.gloplacha.2015.10.001

Johnsen, S.J. (1999). GRIP Oxygen Isotopes. https://doi.org/10.1594/PANGAEA.55091

Johnsen, S.J., Clausen, H.B., Dansgaard, W., Fuhrer, K., Gundestrup, N., Hammer, C.U., Iversen, P., Jouzel, J., Stauffer, B., Steffensen, J.P. (1992). Irregular glacial interstadials recorded in a new Greenland ice core. Nature 359, 311–313. https://doi.org/10.1038/359311a0

Jones, B., Manning, D.A.C. (1994). Comparison of geochemical indices used for the interpretation of palaeoredox conditions in ancient mudstones. Chemical Geology 111, 111–129. https://doi.org/10.1016/0009-2541(94)90085-X

Jones, P.D., Jonsson, T., Wheeler, D. (1997). Extension to the North Atlantic oscillation using early instrumental pressure observations from Gibraltar and south-west Iceland. International Journal of Climatology 17, 1433–1450. https://doi.org/10.1002/(SICI)1097-0088(19971115)17:13<1433::AID-JOC203>3.0.CO;2-P

Jorissen, F.J., Fontanier, C., Thomas, E. (2007). Paleoceanographical Proxies Based on Deep-Sea Benthic Foraminiferal Assemblage Characteristics, in: Hillarie-Marcel, C., De Vernal, A. (Eds.) Proxies in Late Cenozoic Paleoceanography. Amsterdam: Elsevier Developments in Marine Geology 1, pp. 263–325. https://doi.org/10.1016/S1572-5480(07)01012-3

Josey, S.A. (2003). Changes in the heat and freshwater forcing of the eastern Mediterranean and their influence on deep water formation. Journal of Geophysical Research 108, 3237, https://doi.org/10.1029/2003JC001778

Josey, S.A., Somot, S., Tsimplis, M. (2011). Impacts of atmospheric modes of variability on Mediterranean Sea surface heat exchange. Journal of Geophysical Research 116, C02032. https://doi.org/10.1029/2010JC006685

Juan, C., Ercilla, G., Estrada, F., Alonso, B., Casas, D., Vázquez, J.T., d'Acremont, E., Medialdea, T., Hernández-Molina, F.J., Gorini, C., El Moumni, B., Valencia, J. (2020). Multiple factors controlling the deep marine sedimentation of the Alboran Sea (SW Mediterranean) after the Zanclean Atlantic Mega-flood. Marine Geology 423, 106138. https://doi.org/10.1016/j.margeo.2020.106138

Jung, M., Ilmberger, J., Mangini, A., Emeis, K.-C. (1997). Why some Mediterranean sapropels survived burn-down (and others did not). Marine Geology 141, 51–60. https://doi.org/10.1016/S0025-3227(97)00031-5

Keighley, D.G., Pickerill, R.K. (1995). The ichnotaxa Paleophycus and Planolites: historical perspectives and recommendations. Ichnos 3, 301–309. https://doi.org/10.1080/10420949509386400

Kennedy, M.J., Pevear, D.R., Hill, R.J. (2002). Mineral Surface Control of Organic Carbon in Black Shale. Science 295, 657–660. https://doi.org/10.1126/science.1066611

Kidd, R.B., Cita, M.B., Ryan, W.B.F. (1978). Stratigraphy of eastern Mediterranean sapropel sequences recovered during Leg 42A and their paleoenvironmental significance, in: Initial Reports of the Deep-Sea Drilling Project Project 42A, pp. 421–443.

Kindler, P., Guillevic, M., Baumgartner, M., Schwander, J., Landais, A., Leuenberger, M. (2014). Temperature reconstruction from 10 to 120 kyr b2k from the NGRIP ice core. Climate of the Past 10, 887–902. https://doi.org/10.5194/cp-10-887-2014

King, S.L., Froelich, P.N., Jahnke, R.A. (2000). Early diagenesis of germanium in sediments of the Antarctic South Atlantic: in search of the missing Ge sink. Geochimica et Cosmochimica Acta 64, 1375–1390. https://doi.org/10.1016/S0016-7037(99)00406-8

Knaust, D. (2017). Atlas of Trace Fossils in Well Core. Springer Cham, 209 pp. https://doi.org/10.1007/978-3-319-49837-9

Knaust, D. (2012). Methodology and Techniques, in: Knaust, D., Bromley, R.G. (Eds.). Trace Fossils as Indicators of Sedimentary Environments. Elsevier, Developments in Sedimentology 64, pp. 245–271. https://doi.org/10.1016/B978-0-444-53813-0.00009-5

Knaust, D. (2009). Ichnology as a tool in carbonate reservoir characterization: A case study from the Permian–Triassic Khuff Formation in the Middle East. GeoArabia 14, 17–38. https://doi.org/10.2113/geoarabia140317

Knaust, D., Bromley, R.G. (2012). Trace fossils as indicators of sedimentary environments. Amsterdam: Elsevier, 960 pp.

Kodama, K.P., Hinnov, L.A. (2014). Rock Magnetic Cyclostratigraphy. John Wiley & Sons, 165 pp.

Konijnendijk, T.Y.M., Ziegler, M., Lourens, L.J. (2015). On the timing and forcing mechanisms of late Pleistocene glacial terminations: Insights from a new high-resolution benthic stable oxygen isotope record of the eastern Mediterranean. Quaternary Science Reviews 129, 308–320. https://doi.org/10.1016/j.quascirev.2015.10.005

Kotake, N. (2014). Changes in lifestyle and habitat of Z oophycos -producing animals related to evolution of phytoplankton during the Late Mesozoic: geological evidence for the 'benthic-pelagic coupling model. Lethaia 47, 165–175. https://doi.org/10.1111/let.12046

Krijgsman, W. (2002). The Mediterranean: Mare Nostrum of Earth sciences. Earth and Planetary Science Letters 205, 1–12. https://doi.org/10.1016/S0012-821X(02)01008-7

Krijgsman, W., Hilgen, F.J., Langereis, C.G., Santarelli, A., Zachariasse, W.J. (1995). Late Miocene magnetostratigraphy, biostratigraphy and cyclostratigraphy in the Mediterranean. Earth and Planetary Science Letters 136, 475–494. https://doi.org/10.1016/0012-821X(95)00206-R

Krishnamurthy, R.V., Meyers, P.A., Lovan, N.A. (2000). Isotopic evidence of sea-surface freshening, enhanced productivity, and improved organic matter preservation during sapropel deposition in the Tyrrhenian Sea. Geology 28, 263. https://doi.org/10.1130/0091-7613(2000)28<263:IEOSFE>2.0.CO;2

Krokos, G., Velaoras, D., Korres, G., Perivoliotis, L., Theocharis, A. (2014). On the continuous functioning of an internal mechanism that drives the Eastern Mediterranean thermohaline circulation: The recent activation of the Aegean Sea as a dense water source area. Journal of Marine Systems 129, 484–489. https://doi.org/10.1016/j.jmarsys.2013.10.002

Kubin, E., Poulain, P.-M., Mauri, E., Menna, M., Notarstefano, G. (2019). Levantine Intermediate and Levantine Deep Water Formation: An Argo Float Study from 2001 to 2017. Water 11, 1781. https://doi.org/10.3390/w11091781

Kusch, S., Eglinton, T.I., Mix, A.C., Mollenhauer, G. (2010). Timescales of lateral sediment transport in the Panama Basin as revealed by radiocarbon ages of alkenones, total organic carbon and foraminifera. Earth and Planetary Science Letters 290, 340–350. https://doi.org/10.1016/j.epsl.2009.12.030

Kuypers, M.M.M., Pancost, R.D., Nijenhuis, I.A., Sinninghe Damsté, J.S. (2002). Enhanced productivity led to increased organic carbon burial in the euxinic North Atlantic basin during the late Cenomanian oceanic anoxic event. Paleoceanography 17, 1051. https://doi.org/10.1029/2000PA000569

Lacombe, H., Tchernia, P. (1974). Les zones de formation d'eau profonde oceanique caracteres-processus-problemes, in: processus form. eaux oceaniques profondes en particulier mediterranee occident. Colloquium international. C.N.R.S., Paris, 1974, pp. 249-262.

Lacombe, H., Tchernia, P., Gamberoni, L. (1985). Variable bottom water in the Western Mediterranean basin. Progress in Oceanography 14, 319–338. https://doi.org/10.1016/0079-6611(85)90015-1

Langgut, D., Almogi-Labin, A., Bar-Matthews, M., Pickarski, N., Weinstein-Evron, M. (2018). Evidence for a humid interval at ~56–44 ka in the Levant and its potential link to modern humans dispersal out of Africa. Journal of Human Evolution 124, 75–90. https://doi.org/10.1016/j.jhevol.2018.08.002

LaRowe, D.E., Arndt, S., Bradley, J.A., Estes, E.R., Hoarfrost, A., Lang, S.Q., Lloyd, K.G., Mahmoudi, N., Orsi, W.D., Shah Walter, S.R., Steen, A.D., Zhao, R. (2020). The fate of organic carbon in marine sediments - New insights from recent data and analysis. Earth-Science Reviews 204, 103146. https://doi.org/10.1016/j.earscirev.2020.103146

Larrasoaña, J.C., Roberts, A.P., Hayes, A., Wehausen, R., Rohling, E.J. (2006). Detecting missing beats in the Mediterranean climate rhythm from magnetic identification of oxidized sapropels (Ocean Drilling Program Leg 160). Physics of the Earth and Planetary Interiors 156, 283–293. https://doi.org/10.1016/j.pepi.2005.04.017

Larrasoaña, J.C., Roberts, A.P., Rohling, E.J. (2008). Magnetic susceptibility of eastern Mediterranean marine sediments as a proxy for Saharan dust supply? Marine Geology 254, 224–229. https://doi.org/10.1016/j.margeo.2008.06.003

Larrasoaña, J.C., Roberts, A.P., Rohling, E.J., Winklhofer, M., Wehausen, R. (2003). Three million years of monsoon variability over the northern Sahara. Climate Dynamics 21, 689–698. https://doi.org/10.1007/s00382-003-0355-z

Lascaratos, A., Williams, R.G., Tragou, E. (1993). A mixed-layer study of the formation of Levantine intermediate water. Journal of Geophysical Research 98, 14739–14749. https://doi.org/10.1029/93JC00912

Łaska, W., Rodríguez-Tovar, F.J., Uchman, A. (2017). Evaluating macrobenthic response to the Cretaceous–Palaeogene event: A high-resolution ichnological approach at the Agost section (SE Spain). Cretaceous Research 70, 96–110. https://doi.org/10.1016/j.cretres.2016.10.003

Le Treut, H., Ghil, M. (1983. Orbital forcing, climatic interactions, and glaciation cycles. Journal of Geophysical Research: Oceans 88, 5167–5190. https://doi.org/10.1029/JC088iC09p05167

Leeder, M.R., McNeill, L.C., Ll Collier, R.E., Portman, C., Rowe, P.J., Andrews, J.E., Gawthorpe, R.L. (2003). Corinth rift margin uplift: New evidence from Late Quaternary marine shorelines. Geophysical Research Letters 30, 1611. https://doi.org/10.1029/2003GL017382

Lejeusne, C., Chevaldonné, P., Pergent-Martini, C., Boudouresque, C.F., Pérez, T. (2010). Climate change effects on a miniature ocean: the highly diverse, highly impacted Mediterranean Sea. Trends in Ecology & Evolution 25, 250–260. https://doi.org/10.1016/j.tree.2009.10.009

Lenton, T.M., Ciscar, J.-C. (2013). Integrating tipping points into climate impact assessments. Climatic Change 117, 585–597. https://doi.org/10.1007/s10584-012-0572-8

Lenton, T.M., Held, H., Kriegler, E., Hall, J.W., Lucht, W., Rahmstorf, S., Schellnhuber, H.J. (2008). Tipping elements in the Earth's climate system. Proceedings of the National Academy of Sciences 105, 1786–1793. https://doi.org/10.1073/pnas.0705414105

Levin, L.A. (2018). Manifestation, Drivers, and Emergence of Open Ocean Deoxygenation. Annual Review of Marine Science 10, 229–260. https://doi.org/10.1146/annurev-marine-121916-063359

Li, C., Born, A. (2019). Coupled atmosphere-ice-ocean dynamics in Dansgaard-Oeschger events. Quaternary Science Reviews 203, 1–20. https://doi.org/10.1016/j.quascirev.2018.10.031

Lifland, J. (2003). The North Atlantic Oscillation: Climatic Significance and Environmental Impact. Eos, Transactions, American Geophysical Union 84, 73–73. https://doi.org/10.1029/2003EO080005

Lionello, P. (2012). The Climate of the Mediterranean Region: From the Past to the Future. Amsterdam: Elsevier, 502pp. https://doi.org/10.1016/C2011-0-06210-5

Lionello, P., Giorgi, F., Rohling, E., Seager, R. (2023). Mediterranean climate: past, present and future, in: Schroeder, K., Chiggiato, J. (Eds.), Oceanography of the Mediterranean Sea: An Introductory Guide. Amsterdam: Elsevier, pp. 41–91. https://doi.org/10.1016/B978-0-12-823692-5.00011-X

Lionello, P., Malanotte-Rizzoli, P., Boscolo, R., Alpert, P., Artale, V., Li, L., Luterbacher, J., May, W., Trigo, R., Tsimplis, M., Ulbrich, U., Xoplaki, E. (2006). The Mediterranean climate: An overview of the main characteristics and issues, in: Lionello, P., Malanotte-Rizzoli, P., Boscolo, R. (Eds.). Developments in Earth and Environmental Sciences, Mediterranean. Amsterdam: Elsevier, pp. 1–26. https://doi.org/10.1016/S1571-9197(06)80003-0

Lionello, P., Trigo, I.F., Gil, V., Liberato, M.L.R., Nissen, K.M., Pinto, J.G., Raible, C.C., Reale, M., Tanzarella, A., Trigo, R.M., Ulbrich, S., Ulbrich, U. (2016). Objective climatology of cyclones in the Mediterranean region: a consensus view among methods with different system identification and tracking criteria. Tellus A: Dynamic Meteorology and Oceanography 68, 29391. https://doi.org/10.3402/tellusa.v68.29391

Lisiecki, L.E. (2010). Links between eccentricity forcing and the 100,000-year glacial cycle. Nature Geoscience 3, 349–352. https://doi.org/10.1038/ngeo828

Litt, T., Krastel, S., Sturm, M., Kipfer, R., Örcen, S., Heumann, G., Franz, S.O., Ülgen, U.B., Niessen, F. (2009). 'PALEOVAN', International Continental Scientific Drilling Program (ICDP): site survey results and perspectives. Quaternary Science Reviews 28, 1555–1567. https://doi.org/10.1016/j.quascirev.2009.03.002

Liu, J., Algeo, T.J. (2020). Beyond redox: Control of trace-metal enrichment in anoxic marine facies by watermass chemistry and sedimentation rate. Geochimica et Cosmochimica Acta 287, 296–317. https://doi.org/10.1016/j.gca.2020.02.037

Liu, Q., Roberts, A.P., Larrasoaña, J.C., Banerjee, S.K., Guyodo, Y., Tauxe, L., Oldfield, F. (2012. Environmental magnetism: Principles and applications. Reviews of Geophysics 50, RG4002. https://doi.org/10.1029/2012RG000393

Lolis, C.J., Bartzokas, A., Katsoulis, B.D. (2002). Spatial and temporal 850 hPa air temperature and sea-surface temperature covariances in the Mediterranean region and their connection to atmospheric circulation. International Journal of Climatology 22, 663–676. https://doi.org/10.1002/joc.759

Loon, H. van, Rogers, J.C. (1978). The Seesaw in Winter Temperatures between Greenland and Northern Europe. Part I: General Description. Monthly Weather Review 106, 296–310. https://doi.org/10.1175/1520-0493(1978)106<0296:TSIWTB>2.0.CO;2

López-González, N., Alonso, B., Juan, C., Ercilla, G., Bozzano, G., Cacho, I., Casas, D., Palomino, D., Vázquez, J.-T., Estrada, F., Bárcenas, P., D'Acremont, E., Gorini, C., Moumni, B.E. (2019). 133,000 Years of Sedimentary Record in a Contourite Drift in the Western Alboran Sea: Sediment Sources and Paleocurrent Reconstruction. Geosciences 9, 345. https://doi.org/10.3390/geosciences9080345

Lourens, L.J., Antonarakou, A., Hilgen, F.J., Van Hoof, A. a. M., Vergnaud-Grazzini, C., Zachariasse, W.J. (1996). Evaluation of the Plio-Pleistocene astronomical timescale. Paleoceanography 11, 391–413. https://doi.org/10.1029/96PA01125

Loutre, M.-F., Paillard, D., Vimeux, F., Cortijo, E. (2004). Does mean annual insolation have the potential to change the climate? Earth and Planetary Science Letters 221, 1–14. https://doi.org/10.1016/S0012-821X(04)00108-6

Lowe, J.J., Rasmussen, S.O., Björck, S., Hoek, W.Z., Steffensen, J.P., Walker, M.J.C., Yu, Z.C., INTIMATE group (2008). Synchronisation of palaeoenvironmental events in the North Atlantic region during the Last Termination: a revised protocol recommended by the INTIMATE group, Quaternary Science Reviews 27, Issues 1–2, 6-17. https://doi.org/10.1016/j.quascirev.2007.09.016

Löwemark, L. (2015). Testing ethological hypotheses of the trace fossil Zoophycos based on Quaternary material from the Greenland and Norwegian Seas. Palaeogeography, Palaeoclimatology, Palaeoecology 425, 1–13. https://doi.org/10.1016/j.palaeo.2015.02.025

Löwemark, L. (2012). Ethological analysis of the trace fossil Zoophycos: hints from the Arctic Ocean. Lethaia 45, 290–298. https://doi.org/10.1111/j.1502-3931.2011.00282.x

Löwemark, L., Jakobsson, M., Mörth, M., Backman, J. (2008). Arctic Ocean manganese contents and sediment colour cycles. Polar Research 27, 105–113. https://doi.org/10.3402/polar.v27i2.6169

Löwemark, L., Lin, Y., Chen, H.-F., Yang, T.-N., Beier, C., Werner, F., Lee, C.-Y., Song, S.-R., Kao, S.-J. (2006). Sapropel burn-down and ichnological response to late Quaternary sapropel formation in two ~400 ky records from the eastern Mediterranean Sea. Palaeogeography, Palaeoclimatology, Palaeoecology 239, 406–425. https://doi.org/10.1016/j.palaeo.2006.02.013

Löwemark, L., Schönfeld, J., Werner, F., Schäfer, P. (2004). Trace fossils as a paleoceanographic tool: evidence from Late Quaternary sediments of the southwestern Iberian margin. Marine Geology 204, 27–41. https://doi.org/10.1016/S0025-3227(03)00351-7

Lowery, C.M., Bralower, T.J., Owens, J.D., Rodríguez-Tovar, F.J., Jones, H., Smit, J., Whalen, M.T., Claeys, P., Farley, K., Gulick, S.P.S., Morgan, J.V., Green, S., Chenot, E., Christeson, G.L., Cockell, C.S., Coolen, M.J.L., Ferrière, L., Gebhardt, C., Goto, K., Kring, D.A., ... Zylberman, W. (2018). Rapid recovery of life at ground zero of the end-Cretaceous mass extinction. Nature 558, 288–291. https://doi.org/10.1038/s41586-018-0163-6

Lyons, R., Oldfield, F., Williams, E. (2012). The possible role of magnetic measurements in the discrimination of Sahara/Sahel dust sources. Earth Surface Processes and Landforms 37, 594–606. https://doi.org/10.1002/esp.2268

Lyons, T.W., Severmann, S. (2006). A critical look at iron paleoredox proxies: New insights from modern euxinic marine basins. Geochimica et Cosmochimica Acta 70, 5698–5722. https://doi.org/10.1016/j.gca.2006.08.021

MacAyeal, D.R. (1993). Binge/purge oscillations of the Laurentide Ice Sheet as a cause of the North Atlantic's Heinrich events. Paleoceanography 8, 775–784. https://doi.org/10.1029/93PA02200

MacEachern, J.A., Bann, K.L., Gingras, M.K., Zonneveld, J.-Paul., Dashtgard, S.E., Pemberton, S.G. (2012). The Ichnofacies Paradigm, in: Knaust, D., Bromley, R.G. (Eds.). Trace Fossils as Indicators of Sedimentary Environments. Amsterdam: Elsevier. Developments in Sedimentology 6, pp 103–138. https://doi.org/10.1016/B978-0-444-53813-0.00004-6

MacEachern, J.A., Zaitlin, B.A., Pemberton, S.G. (1999). A sharp-based sandstone of the Viking Formation, Joffre Field, Alberta, Canada; criteria for recognition of transgressively incised shoreface complexes. Journal of Sedimentary Research 69, 876–892. https://doi.org/10.2110/jsr.69.876

Macias, D., Garcia-Gorriz, E., Stips, A. (2016). The seasonal cycle of the Atlantic Jet dynamics in the Alboran Sea: direct atmospheric forcing versus Mediterranean thermohaline circulation. Ocean Dynamics 66, 137–151. https://doi.org/10.1007/s10236-015-0914-y

Magwood, J.P.A., Ekdale, A.A. (1994). Computer-Aided Analysis of Visually Complex Ichnofabrics in Deep-Sea Sediments. PALAIOS 9, 102–115. https://doi.org/10.2307/3515083

Maher, B.A., Thompson, R. Ed. (1999). Quaternary Climates, Environments and Magnetism. Cambridge: Cambridge University Press, 390 pp.

Maheras, P., Xoplaki, E., Davies, T., Martin-Vide, J., Bariendos, M., Alcoforado, M.J. (1999). Warm and cold monthly anomalies across the Mediterranean basin and their relationship with circulation; 1860–1990. International Journal of Climatology 19, 1697–1715. https://doi.org/10.1002/(SICI)1097-0088(199912)19:15<1697::AID-JOC442>3.0.CO;2-S

Malanotte-Rizzoli, P., Artale, V., Borzelli-Eusebi, G.L., Brenner, S., Crise, A., Gacic, M., Kress, N., Marullo, S., Ribera D'Alcalà, M., Sofianos, S., Tanhua, T., Theocharis, A., Alvarez, M., Ashkenazy, Y., Bergamasco, A., Cardin, V., Carniel, S., Civitarese, G., ... Triantafyllou, G. (2014). Physical forcing and physical/biochemical variability of the Mediterranean Sea: A review of unresolved issues and directions for future research. Ocean Science 10, 281–322. https://doi.org/10.5194/OS-10-281-2014

Malanotte-Rizzoli, P., Bergamasco, A. (1991). The wind and thermally driven circulation of the eastern Mediterranean Sea. Part II: the Baroclinic case. Dynamics of Atmospheres and Oceans, 15, 355–419. https://doi.org/10.1016/0377-0265(91)90026-C

Mángano, M.G., Buatois, L.A. (2012). A Multifaceted Approach to Ichnology. Ichnos 19, 121–126. https://doi.org/10.1080/10420940.2012.685566

Mangini, A., Jung, M., Laukenmann, S. (2001). What do we learn from peaks of uranium and of manganese in deep sea sediments? Marine Geology 177, 63–78.

https://doi.org/10.1016/S0025-3227(01)00124-4

Mariotti, A., Arkin, P. (2007). The North Atlantic Oscillation and oceanic precipitation variability. Climate Dynamics 28, 35–51. https://doi.org/10.1007/s00382-006-0170-4

Martínez-García, P., Soto, J.I., Comas, M. (2011). Recent structures in the Alboran Ridge and Yusuf fault zones based on swath bathymetry and sub-bottom profiling: Evidence of active tectonics. Geo-Marine Letters 31, 19–36. https://doi.org/10.1007/s00367-010-0212-0

Martínez-Ruiz, F., Jroundi, F., Paytan, A., Guerra-Tschuschke, I., Abad, M. del M., González-Muñoz, M.T. (2018). Barium bioaccumulation by bacterial biofilms and implications for Ba cycling and use of Ba proxies. Nature Communications 9, 1619. https://doi.org/10.1038/s41467-018-04069-z

Martínez-Ruiz, F., Kastner, M., Gallego-Torres, D., Rodrigo-Gámiz, M., Nieto-Moreno, V., Ortega-Huertas, M. (2015). Paleoclimate and paleoceanography over the past 20,000 yr in the Mediterranean Sea Basins as indicated by sediment elemental proxies. Quaternary Science Reviews 107, 25–46. https://doi.org/10.1016/j.quascirev.2014.09.018

Martínez-Ruiz, F., Kastner, M., Paytan, A., Ortega-Huertas, M., Bernasconi, S.M. (2000). Geochemical evidence for enhanced productivity during S1 sapropel deposition in the eastern Mediterranean. Paleoceanography 15, 200–209. https://doi.org/10.1029/1999PA000419

Martrat, B., Grimalt, J.O., Lopez-Martínez, C., Cacho, I., Sierro, F.J., Flores, J.A., Zahn, R., Canals, M., Curtis, J.H., Hodell, D.A. (2004). Abrupt temperature changes in the Western Mediterranean over the past 250,000 years. Science 306, 1762–1765. https://doi.org/
10.1126/science.1101706

Martrat, B., Grimalt, J.O., Shackleton, N.J., de Abreu, L., Hutterli, M.A., Stocker, T.F. (2007. Four Climate Cycles of Recurring Deep and Surface Water Destabilizations on the Iberian Margin. Science 317, 502–507. https://doi.org/10.1126/science.1139994

Martrat, B., Jimenez-Amat, P., Zahn, R., Grimalt, J.O. (2014). Similarities and dissimilarities between the last two deglaciations and interglaciations in the North Atlantic region. Quaternary Science Reviews 99, 122–134. https://doi.org/10.1016/j.quascirev.2014.06.016

Maslin, M. (2016). Forty years of linking orbits to ice ages. Nature 540, 208–209. https://doi.org/10.1038/540208a

Masqué, P., Fabres, J., Canals, M., Sanchez-Cabeza, J.A., Sanchez-Vidal, A., Cacho, I., Calafat, A.M., Bruach, J.M. (2003). Accumulation rates of major constituents of hemipelagic sediments in the deep Alboran Sea: a centennial perspective of sedimentary dynamics. Marine Geology 193, 207–233. https://doi.org/10.1016/S0025-3227(02)00593-5

Massalongo, A. (1855). Zoophycos, novum genus plantarum fossilium. Monographia. Typis Antonellianis, Veronae 45–52.

Mauffrey, M.A., Berné, S., Jouet, G., Giresse, P., Gaudin, M. (2015). Sea-level control on the connection between shelf-edge deltas and the Bourcart canyon head (western

Mediterranean) during the last glacial/interglacial cycle. Marine Geology 370, 1–19. https://doi.org/10.1016/j.margeo.2015.09.010

Mavropoulou, A.-M., Vervatis, V., Sofianos, S. (2020). Dissolved oxygen variability in the Mediterranean Sea. Journal of Marine Systems 208, 103348. https://doi.org/10.1016/j.jmarsys.2020.103348

Mayer, L.M., Schick, L.L., Allison, M.A., Ruttenberg, K.C., Bentley, S.J. (2007). Marine vs. terrigenous organic matter in Louisiana coastal sediments: The uses of bromine: organic carbon ratios. Marine Chemistry 107, 244–254. https://doi.org/10.1016/j.marchem.2007.07.007

McCave, I.N. (2007. Chapter One Deep-Sea Sediment Deposits and Properties Controlled by Currents, in: Hillaire-Marcel, C., De Vernal, A. (Eds.). Proxies in Late Cenozoic Paleoceanography. Amsterdam: Elsevier Developments in Marine Geology 1, pp. 19–62. https://doi.org/10.1016/S1572-5480(07)01006-8

McHugh, C.M.G., Gurung, D., Giosan, L., Ryan, W.B.F., Mart, Y., Sancar, U., Burckle, L., Çagatay, M.N. (2008). The last reconnection of the Marmara Sea (Turkey) to the World Ocean: A paleoceanographic and paleoclimatic perspective. Marine Geology 255, 64–82. https://doi.org/10.1016/j.margeo.2008.07.005

McLennan, S.M. (2001). Relationships between the trace element composition of sedimentary rocks and upper continental crust. Geochemistry, Geophysics, Geosystems 2. https://doi.org/10.1029/2000GC000109

McManus, J., Berelson, W.M., Klinkhammer, G.P., Hammond, D.E., Holm, C. (2005). Authigenic uranium: Relationship to oxygen penetration depth and organic carbon rain. Geochimica et Cosmochimica Acta 69, 95–108. https://doi.org/10.1016/j.gca.2004.06.023

McManus, J., Berelson, W.M., Klinkhammer, G.P., Johnson, K.S., Coale, K.H., Anderson, R.F., Kumar, N., Burdige, D.J., Hammond, D.E., Brumsack, H.J., McCorkle, D.C., Rushdi, A. (1998). Geochemistry of barium in marine sediments: implications for its use as a paleoproxy. Geochimica et Cosmochimica Acta 62, 3453–3473. https://doi.org/10.1016/S0016-7037(98)00248-8

McManus, J.F., Francois, R., Gherardi, J.-M., Keigwin, L.D., Brown-Leger, S. (2004). Collapse and rapid resumption of Atlantic meridional circulation linked to deglacial climate changes. Nature 428, 834–837. https://doi.org/10.1038/nature02494

Medoc Group, Lacombe, H., Tehernia, P., Ribet, M., Bonnot, J., Frassetto, R., Swallow, J.C., Miller, A.R., Stommel, H., Medoc Group (1970). Observation of Formation of Deep Water in the Mediterranean Sea, 1969. Nature 227, 1037–1040. https://doi.org/10.1038/2271037a0

Mellado-Cano, J., Barriopedro, D., García-Herrera, R., Trigo, R.M., Hernández, A. (2019). Examining the North Atlantic Oscillation, East Atlantic Pattern, and Jet Variability since 1685. Journal of Climate 32, 6285–6298. https://doi.org/10.1175/JCLI-D-19-0135.1

Menviel, L., Timmermann, A., Friedrich, T., England, M.H. (2014). Hindcasting the continuum of Dansgaard–Oeschger variability: mechanisms, patterns and timing. Climate of the Past 10, 63–77. https://doi.org/10.5194/cp-10-63-2014

Menviel, L.C., Skinner, L.C., Tarasov, L., Tzedakis, P.C. (2020. An ice–climate oscillatory framework for Dansgaard–Oeschger cycles. Nature Reviews Earth & Environment 1, 677–693. https://doi.org/10.1038/s43017-020-00106-y

Mesa-Fernández, J.M., Martínez-Ruiz, F., Rodrigo-Gámiz, M., Jiménez-Espejo, F.J., García, M., Sierro, F.J. (2022). Paleocirculation and paleoclimate conditions in the western Mediterranean basins over the last deglaciation: new insights from sediment composition variations. Global and Planetary Change 209, 103732. https://doi.org/10.1016/j.gloplacha.2021.103732

Meyers, P.A. (2006). Paleoceanographic and paleoclimatic similarities between Mediterranean sapropels and Cretaceous black shales. Palaeogeography, Palaeoclimatology, Palaeoecology 235, 305–320. https://doi.org/10.1016/j.palaeo.2005.10.025

Meyers, P.A., Arnaboldi, M. (2005). Trans-Mediterranean comparison of geochemical paleoproductivity proxies in a mid-Pleistocene interrupted sapropel. Palaeogeography, Palaeoclimatology, Palaeoecology 222, 313–328. https://doi.org/10.1016/j.palaeo.2005.03.020

Meyers, S.R., Malinverno, A. (2018). Proterozoic Milankovitch cycles and the history of the solar system. Proceedings of the National Academy of Sciences 115, 6363–6368. https://doi.org/10.1073/pnas.1717689115

Meyers, S.R., Sageman, B.B. (2007). Quantification of deep-time orbital forcing by average spectral misfit. American Journal of Science 307, 773–792. https://doi.org/10.2475/05.2007.01

Michel, J., Borgomano, J., Reijmer, J.J.G. (2018). Heterozoan carbonates: When, where and why? A synthesis on parameters controlling carbonate production and occurrences. Earth-Science Reviews 182, 50–67. https://doi.org/10.1016/j.earscirev.2018.05.003

Middelburg, J.J. (2018). Reviews and syntheses: to the bottom of carbon processing at the seafloor. Biogeosciences 15, 413–427. https://doi.org/10.5194/bg-15-413-2018

Middelburg, J.J. (1989). A simple rate model for organic matter decomposition in marine sediments. Geochimica et Cosmochimica Acta 53, 1577–1581. https://doi.org/10.1016/0016-7037(89)90239-1

Middelburg, J.J., Nieuwenhuize, J., Van Breugel, P. (1999). Black carbon in marine sediments. Marine Chemistry 65, 245–252. https://doi.org/10.1016/S0304-4203(99)00005-5

Middelburg, J.J., Vlug, T., Jaco, F., van der Nat, W.A. (1993). Organic matter mineralization in marine systems. Global and Planetary Change 8, 47–58. https://doi.org/10.1016/0921-8181(93)90062-S

Middleton, N.J., Goudie, A.S. (2001). Saharan dust: sources and trajectories. Transactions of the Institute of British Geographers 26, 165–181. https://doi.org/10.1111/1475-5661.00013

Miguez-Salas, O., Vardaro, M. F., Rodríguez-Tovar, F. J., Pérez-Claros, J. A., & Huffard, C. L. (2022). Deep-sea echinoid trails and seafloor nutrient distribution: present and past implications. Frontiers in Marine Science, 9, 903864. https://doi.org/10.3389/fmars.2022.903864

Miguez-Salas, O., Dorador, J., Rodríguez-Tovar, F.J. (2019). Introducing Fiji and ICY image processing techniques in ichnological research as a tool for sedimentary basin analysis. Marine Geology 413, 1–9. https://doi.org/10.1016/j.margeo.2019.03.013

Miguez-Salas, O., Rodríguez-Tovar, F.J., Duarte, L.V. (2018). Ichnological analysis at the Fonte Coberta section (Lusitanian Basin, Portugal): Approaching depositional

environment during the Toarcian oceanic anoxic event (T-OAE). Spanish Journal of Palaeontology 33, 261–276. https://doi.org/10.7203/sjp.33.2.13602

Miguez-Salas, O., Rodríguez-Tovar, F.J., Duarte, L.V. (2017). Selective incidence of the toarcian oceanic anoxic event on macroinvertebrate marine communities: a case from the Lusitanian basin, Portugal. Lethaia 50, 548–560. https://doi.org/10.1111/let.12212

Mikolajewicz, U. (2011). Modeling Mediterranean Ocean climate of the Last Glacial Maximum. Climate of the Past 7, 161–180. https://doi.org/10.5194/cp-7-161-2011

Milliman, J.D., Meade, R.H. (1983). World-Wide Delivery of River Sediment to the Oceans. The Journal of Geology 91, 1–21. https://doi.org/10.1086/628741

Millot, C. (2014). Heterogeneities of in- and out-flows in the Mediterranean Sea. Progress in Oceanography 120, 254–278. https://doi.org/10.1016/j.pocean.2013.09.007

Millot, C. (1999). Circulation in the Western Mediterranean Sea. Journal of Marine Systems 20, 423–442. https://doi.org/10.1016/S0924-7963(98)00078-5

Millot, C. (1990). The Gulf of Lions' hydrodynamics. Continental Shelf Research 10, 885–894. https://doi.org/10.1016/0278-4343(90)90065-T

Millot, C., Candela, J., Fuda, J.-L., Tber, Y. (2006). Large warming and salinification of the Mediterranean outflow due to changes in its composition. Deep Sea Research Part I: Oceanographic Research Papers 53, 656–666. https://doi.org/10.1016/j.dsr.2005.12.017

Millot, C., Taupier-Letage, I. (2005). Circulation in the Mediterranean Sea. In: Saliot, A. (Ed.), The Mediterranean Sea. Handbook of Environmental Chemistry. Berlin: Springer, pp. 29–66. https://doi.org/10.1007/b107143

Mollenhauer, G., Inthorn, M., Vogt, T., Zabel, M., Sinninghe Damsté, J.S., Eglinton, T.I. (2007). Aging of marine organic matter during cross-shelf lateral transport in the Benguela upwelling system revealed by compound-specific radiocarbon dating. Geochemistry, Geophysics, Geosystems 8. https://doi.org/10.1029/2007GC001603

Monaco, P., Rodríguez-Tovar, F., Uchman, A. (2016). Environmental fluctuations during the latest Cenomanian (Bonarelli Level) in the Gubbio area (central Italy) based on an ichnofabric approach, in: Menichetti, M., Coccioni, R., Montanari, A. (Eds) The Stratigraphic Record of Gubbio: Integrated Stratigraphy of the Late Cretaceous–Paleogene Umbria-Marche Pelagic Basin. The Geological Society of America Special Pappers 524, pp. 97–103. https://doi.org/10.1130/2016.2524(07)

Monaco, P., Rodríguez-Tovar, F.J., Uchman, A. (2012). Ichnological analysis of lateral environmental heterogeneity within the Bonarelli Level (Uppermost Cenomanian) in the classical localities near Gubbio, Central Apennines Italy. PALAIOS 27, 48–54. https://doi.org/10.2110/palo.2011.p11-018r

Monedero-Contreras, R.D., Martínez-Ruiz, F., Rodríguez-Tovar, F.J. (2023). Role of climate variability on deep-water dynamics and deoxygenation during sapropel deposition: New insights from a palaeoceanographic empirical approach. Palaeogeography, Palaeoclimatology, Palaeoecology 622, 111601. https://doi.org/10.1016/j.palaeo.2023.111601

Moodley, L., Middelburg, J.J., Herman, P.M.J., Soetaert, K., de Lange, G.J. (2005). Oxygenation and organic-matter preservation in marine sediments: Direct experimental

evidence from ancient organic carbon–rich deposits. Geology 33, 889–892. https://doi.org/10.1130/G21731.1

Moore, G.W.K., Renfrew, I.A. (2012). Cold European winters: interplay between the NAO and the East Atlantic mode. Atmospheric Science Letters 13, 1–8. https://doi.org/10.1002/asl.356

Morcillo-Montalbá, L., Rodrigo-Gámiz, M., Martínez-Ruiz, F., Ortega-Huertas, M., Schouten, S., Sinninghe Damsté, J.S. (2021). Rapid Climate Changes in the Westernmost Mediterranean (Alboran Sea) Over the Last 35 kyr: New Insights from Four Lipid Paleothermometers (UK'37, TEXH86, RI-OH', and LDI). Paleoceanography and Paleoclimatology 36, e2020PA004171. https://doi.org/10.1029/2020PA004171

Moreno, A., Cacho, I., Canals, M., Grimalt, J.O., Sánchez-Goñi, M.F., Shackleton, N., Sierro, F.J. (2005). Links between marine and atmospheric processes oscillating on a millennial time-scale. A multi-proxy study of the last 50,000yr from the Alboran Sea (Western Mediterranean Sea). Quaternary Science Reviews 24, 1623–1636. https://doi.org/10.1016/j.quascirev.2004.06.018

Moreno, A., Cacho, I., Canals, M., Prins, M.A., Sánchez-Goñi, M.-F., Grimalt, J.O., Weltje, G.J. (2002). Saharan Dust Transport and High-Latitude Glacial Climatic Variability: The Alboran Sea Record. Quaternary Research 58, 318–328. https://doi.org/10.1006/qres.2002.2383

Morford, J.L., Emerson, S. (1999). The geochemistry of redox sensitive trace metals in sediments. Geochimica et Cosmochimica Acta 63, 1735–1750. https://doi.org/10.1016/S0016-7037(99)00126-X

Morford, J.L., Martin, W.R., Carney, C.M. (2009a). Uranium diagenesis in sediments underlying bottom waters with high oxygen content. Geochimica et Cosmochimica Acta 73, 2920–2937. https://doi.org/10.1016/j.gca.2009.02.014

Morford, J.L., Martin, W.R., François, R., Carney, C.M. (2009b). A model for uranium, rhenium, and molybdenum diagenesis in marine sediments based on results from coastal locations. Geochimica et Cosmochimica Acta 73, 2938–2960. https://doi.org/10.1016/j.gca.2009.02.029

Morgan, J.V., Gulick, S.P.S., Bralower, T., Chenot, E., Christeson, G., Claeys, P., Cockell, C., Collins, G.S., Coolen, M.J.L., Ferrière, L., Gebhardt, C., Goto, K., Jones, H., Kring, D.A., Le Ber, E., Lofi, J., Long, X., Lowery, C., Mellett, C., ... Zylberman, W. (2016). The formation of peak rings in large impact craters. Science 354, 878–882. https://doi.org/10.1126/science.aah6561

Morigi, C., Jorissen, F.J., Fraticelli, S., Horton, B.P., Principi, M., Sabbatini, A., Capotondi, L., Curzi, P.V., Negri, A. (2005). Benthic foraminiferal evidence for the formation of the Holocene mud-belt and bathymetrical evolution in the central Adriatic Sea. Marine Micropaleontology 57, 25–49. https://doi.org/10.1016/j.marmicro.2005.06.001

Müller, P.J., Suess, E. (1979). Productivity, sedimentation rate, and sedimentary organic matter in the oceans—I. Organic carbon preservation. Deep Sea Research Part A. Oceanographic Research Papers 26, 1347–1362. https://doi.org/10.1016/0198-0149(79)90003-7

Müller, U.C., Pross, J., Tzedakis, P.C., Gamble, C., Kotthoff, U., Schmiedl, G., Wulf, S., Christanis, K. (2011. The role of climate in the spread of modern humans into Europe.

Quaternary Science Reviews 30, 273–279. https://doi.org/10.1016/j.quascirev.2010.11.016

Murat, A. (1999). Pliocene-Pleistocene occurrence of sapropels in the Western Mediterranean Sea and their relation to eastern Mediterranean sapropels. Proceedings of the Ocean Drilling Program 161, 519–527. https://doi.org/10.2973/odp.proc.sr.161.244.1999

Murray, J.W. (2006). Exology and Applications of Benthic Foraminifera. Cambridge: Cambridge University Press, 436 pp. https://doi.org/10.1017/CBO9780511535529

Murray, J.W. (1973). Distribution and Ecology of Living Benthic Foraminiferids. London: Heinemann Educational Publishers, 283 pp.

Murray, S.J., Renard, A.F. (1891). Report on Deep-sea Deposits Based on the Specimens Collected During the Voyage of H.M.S. Challenger in the Years 1872 to 1876. H.M. Stationery Office.

Naranjo, C., García Lafuente, J., Sánchez Garrido, J.C., Sánchez Román, A., Delgado Cabello, J. (2012). The Western Alboran Gyre helps ventilate the Western Mediterranean Deep Water through Gibraltar. Deep Sea Research Part I: Oceanographic Research Papers 63, 157–163. https://doi.org/10.1016/j.dsr.2011.10.003

Naranjo, C., Sammartino, S., García-Lafuente, J., Bellanco, M.J., Taupier-Letage, I. (2015). Mediterranean waters along and across the Strait of Gibraltar, characterization and zonal modification. Deep Sea Research Part I: Oceanographic Research Papers 105, 41–52. https://doi.org/10.1016/j.dsr.2015.08.003

Narcisi, B., Vezzoli, L. (1999). Quaternary stratigraphy of distal tephra layers in the Mediterranean—an overview. Global and Planetary Change 21, 31–50. https://doi.org/10.1016/S0921-8181(99)00006-5

Nicholson, H.A. (1873). Contributions to the study of the Errant Anelides of the Older Paleozoic rocs. Proceedings of the royal society of London 21, 299–290.

Nickell, L., Atkinson, R. (1995). Functional morphology of burrows and trophic modes of three thalassinidean shrimp species, and a new approach to the classification of thalassinidean burrow morphology. Marine Ecology Progress Series 128, 181–197. https://doi.org/10.3354/meps128181

Nielsen, J.N. (1912). Hidrography of the Mediterranean and adjacent waters, in: Report of the Danish Oceanographic Expedition 1908- 1910 to the Mediterranean and Adjacent Waters. Copenhagen, pp. 72–191.

Nieto-Moreno, V., Martínez-Ruiz, F., Giralt, S., Jiménez-Espejo, F.J., Gallego-Torres, D., Rodrigo-Gámiz, M., García-Orellana, J., Ortega-Huertas, M., de Lange, G.J. (2011). Tracking climate variability in the western Mediterranean during the Late Holocene: a multiproxy approach. Climate of the Past 7, 1395–1414. https://doi.org/10.5194/cp-7-1395-2011

Nijenhuis, I.A., Becker, J., De Lange, G.J. (2001). Geochemistry of coeval marine sediments in Mediterranean ODP cores and a land section: Implications for sapropel formation models. Palaeogeography, Palaeoclimatology, Palaeoecology 165, 97–112. https://doi.org/10.1016/S0031-0182(00)00155-3

Nijenhuis, I.A., Schenau, S.J., Van der Weijden, C.H., Hilgen, F.J., Lourens, L.J., Zachariasse, W.J. (1996). On the origin of Upper Miocene sapropelites: A case study from the

Faneromeni Section, Crete (Greece). Paleoceanography 11, 633–645. https://doi.org/10.1029/96PA01963

Nocquet, J.-M., Calais, E. (2004). Geodetic Measurements of Crustal Deformation in the Western Mediterranean and Europe. Pure and applied geophysics, 161, 661–681. https://doi.org/10.1007/s00024-003-2468-z

Oldfield, F. (2003). A high resolution late Holocene palaeoenvironmental record from the central Adriatic Sea. Quaternary Science Reviews 22, 319–342. https://doi.org/10.1016/S0277-3791(02)00088-4

Oldfield, F., Chiverrell, R.C., Lyons, R., Williams, E., Shen, Z., Bristow, C., Bloemendal, J., Torrent, J., Boyle, J.F. (2014). Discriminating dusts and dusts sources using magnetic properties and hematite: Goethite ratios of surface materials and dust from North Africa, the Atlantic and Barbados. Aeolian Research 13, 91–104. https://doi.org/10.1016/j.aeolia.2014.03.010

Pälike, H. (2005). EARTH | Orbital Variation (Including Milankovitch Cycles), in: Selley, R.C., Cocks, L.R.M., Plimer, I.R. (Eds.), Encyclopedia of Geology. Elsevier, pp. 410–421. https://doi.org/10.1016/B0-12-369396-9/00123-4

Papadopoulos, V.P., Josey, S.A., Bartzokas, A., Somot, S., Ruiz, S., Drakopoulou, P. (2012). Large-Scale Atmospheric Circulation Favoring Deep- and Intermediate-Water Formation in the Mediterranean Sea. Journal of Climate 25, 6079–6091. https://doi.org/10.1175/JCLI-D-11-00657.1

Pastor, F., Valiente, J.A., Khodayar, S. (2020). A Warming Mediterranean: 38 Years of Increasing Sea Surface Temperature. Remote Sensing 12, 2687. https://doi.org/10.3390/rs12172687

Paterne, M., Guichard, F., Duplessy, J.C., Siani, G., Sulpizio, R., Labeyrie, J. (2008). A 90,000–200,000 yrs marine tephra record of Italian volcanic activity in the Central Mediterranean Sea. Journal of Volcanology and Geothermal Research 177, 187–196. https://doi.org/10.1016/j.jvolgeores.2007.11.028

Paterne, M., Guichard, F., Labeyrie, J. (1988). Explosive activity of the South Italian volcanoes during the past 80,000 years as determined by marine tephrochronology. Journal of Volcanology and Geothermal Research 34, 153–172. https://doi.org/10.1016/0377-0273(88)90030-3

Paytan, A., Griffith, E.M. (2007). Marine barite: Recorder of variations in ocean export productivity. Deep-Sea Research Part II: Topical Studies in Oceanography 54, 687–705. https://doi.org/10.1016/j.dsr2.2007.01.007

Peck, V.L., Hall, I.R., Zahn, R., Grousset, F., Hemming, S.R., Scourse, J.D. (2007). The relationship of Heinrich events and their European precursors over the past 60ka BP: a multi-proxy ice-rafted debris provenance study in the North East Atlantic. Quaternary Science Reviews 26, 862–875. https://doi.org/10.1016/j.quascirev.2006.12.002

Pedersen, T.F., Calvert, S.E. (1990). Anoxia vs. Productivity: What Controls the Formation of Organic-Carbon-Rich Sediments and Sedimentary Rocks? AAPG Bulletin 74, 454–466. https://doi.org/10.1306/0C9B232B-1710-11D7-8645000102C1865D

Pemberton, S.G., Frey, R.W. (1982). Trace fossil nomenclature and the Planolites-Palaeophycus dilemma. Journal of Paleontology 56, 843–881.

Pe-Piper, G., Piper, D.J.W. (2002). The igneous rocks of Greece. The anatomy of an orogen. Beiträge zur regionalen Geologie der Erde. Schweizerbart Science Publishers, Stuttgart, Germany.

Pérez-Asensio, J.N. (2021). Quantitative palaeobathymetric reconstructions based on foraminiferal proxies: a case study from the Neogene of south-west Spain. Palaeontology 64, 475–488. https://doi.org/10.1111/pala.12538

Pérez-Asensio, J.N., Aguirre, J. (2010). Benthic foraminiferal assemblages in temperate coral-bearing deposits from the Late Pliocene. Journal of Foraminiferal Research 40, 61–78. https://doi.org/10.2113/gsjfr.40.1.61

Pérez-Asensio, J.N., Frigola, J., Pena, L.D., Sierro, F.J., Reguera, M.I., Rodríguez-Tovar, F.J., Dorador, J., Asioli, A., Kuhlmann, J., Huhn, K., Cacho, I. (2020). Changes in western Mediterranean thermohaline circulation in association with a deglacial Organic Rich Layer formation in the Alboran Sea. Quaternary Science Reviews 228, 106075. https://doi.org/10.1016/j.quascirev.2019.106075

Pérez-Folgado, M., Sierro, F.J., Flores, J.A., Grimalt, J.O., Zahn, R. (2004). Paleoclimatic variations in foraminifer assemblages from the Alboran Sea (Western Mediterranean) during the last 150 ka in ODP Site 977. Marine Geology 212, 113–131. https://doi.org/10.1016/
j.margeo.2004.08.002

Perkel, J.M. (2015). Programming: Pick up Python. Nature 518, 125–126. https://doi.org/10.1038/518125a

Perkins, H., Kinder, T., Violette, P.L. (1990). The Atlantic inflow in the Western Alboran Sea. Journal of Physical Oceanography 20, 242–263. https://doi.org/10.1175/1520-0485(1990)020<0242:TAIITW>2.0.CO;2

Pierau, R., Hanebuth, T.J.J., Krastel, S., Henrich, R. (2010). Late Quaternary climatic events and sea-level changes recorded by turbidite activity, Dakar Canyon, NW Africa. Quaternary Research 73, 385–392. https://doi.org/10.1016/j.yqres.2009.07.010

Pinardi, N., Cessi, P., Borile, F., Wolfe, C.L.P. (2019). The Mediterranean Sea Overturning Circulation. Journal of Physical Oceanography 49, 1699–1721. https://doi.org/10.1175/JPO-D-18-0254.1

Pinardi, N., Masetti, E. (2000). Variability of the large scale general circulation of the Mediterranean Sea from observations and modelling: a review. Palaeogeography, Palaeoclimatology, Palaeoecology 158, 153–173. https://doi.org/10.1016/S0031-0182(00)00048-1

Pinardi, N., Zavatarelli, M., Adani, M., Coppini, G., Fratianni, C., Oddo, P., Simoncelli, S., Tonani, M., Lyubartsev, V., Dobricic, S., Bonaduce, A. (2015). Mediterranean Sea large-scale low-frequency ocean variability and water mass formation rates from 1987 to 2007: A retrospective analysis. Progress in Oceanography 132, 318–332. https://doi.org/10.1016/j.pocean.2013.11.003

Plaza-Morlote, M., Rey, D., Santos, J.F., Ribeiro, S., Heslop, D., Bernabeu, A., Mohamed, K.J., Rubio, B., Martíns, V. (2017). Southernmost evidence of large European Ice Sheet-derived freshwater discharges during the Heinrich Stadials of the Last Glacial Period (Galician Interior Basin, Northwest Iberian Continental Margin). Earth and Planetary Science Letters 457, 213–226. https://doi.org/10.1016/j.epsl.2016.10.020

Polovina, J.J., Howell, E.A., Abecassis, M. (2008). Ocean's least productive waters are expanding. Geophysical Research Letters 35, L03618. https://doi.org/10.1029/2007GL031745

Poulos, S.E., Voulgaris, G., Kapsimalis, V., Collins, M., Evans, G. (2002). Sediment fluxes and the evolution of a riverine-supplied tectonically-active coastal system: Kyparissiakos Gulf, Ionian Sea (eastern Mediterranean). Geological Society, London, Special Publications 191, 247–266. https://doi.org/10.1144/GSL.SP.2002.191.01.17

Pozo-Vázquez, D., Esteban-Parra, M.J., Rodrigo, F.S., Castro-Díez, Y. (2001). The Association between ENSO and Winter Atmospheric Circulation and Temperature in the North Atlantic Region. Journal of Climate 14, 3408–3420. https://doi.org/10.1175/1520-0442(2001)014<3408:TABEAW>2.0.CO;2

Pusceddu, A., Mea, M., Gambi, C., Bianchelli, S., Canals, M., Sanchez-Vidal, A., Calafat, A., Heussner, S., De Madron, X.D., Avril, J., Thomsen, L., Garcìa, R., Danovaro, R. (2010). Ecosystem effects of dense water formation on deep Mediterranean Sea ecosystems: an overview. Advances in Oceanography and Limnology 1, 67–83. https://doi.org/10.1080/19475721003735765

Qian, Y., Heslop, D., Roberts, A.P., Hu, P., Zhao, X., Liu, Y., Li, J., Grant, K.M., Rohling, E.J. (2021). Low-Temperature Magnetic Properties of Marine Sediments—Quantifying Magnetofossils, Superparamagnetism, and Maghemitization: Eastern Mediterranean Examples. Journal of Geophysical Research: Solid Earth 126, e2021JB021793. https://doi.org/10.1029/2021JB021793

Quatrefages, M.A. (1849). Note sur la Scolicia prisca (A. de Q.) annélide fossile de la Craie. Annales des Sciences Naturalles 3 série. Zoologie 12, 265–266.

Rae, J.W.B., Zhang, Y.G., Liu, X., Foster, G.L., Stoll, H.M., Whiteford, R.D.M. (2021). Atmospheric CO2 over the Past 66 Million Years from Marine Archives. Annual Review of Earth and Planetary Sciences 49, 609–641. https://doi.org/10.1146/annurev-earth-082420-063026

Railsback, L.B., Gibbard, P.L., Head, M.J., Voarintsoa, N.R.G., Toucanne, S. (2015). An optimized scheme of lettered marine isotope substages for the last 1.0 million years, and the climatostratigraphic nature of isotope stages and substages. Quaternary Science Reviews 111, 94–106. https://doi.org/10.1016/j.quascirev.2015.01.012

Rasmussen, S.O., Andersen, K.K., Svensson, A.M., Steffensen, J.P., Vinther, B.M., Clausen, H.B., Siggaard-Andersen, M.-L., Johnsen, S.J., Larsen, L.B., Dahl-Jensen, D., Bigler, M., Röthlisberger, R., Fischer, H., Goto-Azuma, K., Hansson, M.E., Ruth, U. (2006). A new Greenland ice core chronology for the last glacial termination. Journal of Geophysical Research: Atmospheres 111, D06102. https://doi.org/10.1029/2005JD006079

Rasmussen, S.O., Bigler, M., Blockley, S.P., Blunier, T., Buchardt, S.L., Clausen, H.B., Cvijanovic, I., Dahl-Jensen, D., Johnsen, S.J., Fischer, H., Gkinis, V., Guillevic, M., Hoek, W.Z., Lowe, J.J., Pedro, J.B., Popp, T., Seierstad, I.K., Steffensen, J.P., Svensson, A.M., ...Winstrup, M. (2014). A stratigraphic framework for abrupt climatic changes during the Last Glacial period based on three synchronized Greenland ice-core records: refining and extending the INTIMATE event stratigraphy. Quaternary Science Reviews 106, 14–28. https://doi.org/10.1016/j.quascirev.2014.09.007

Reed, D.C., Slomp, C.P., de Lange, G.J. (2011). A quantitative reconstruction of organic matter and nutrient diagenesis in Mediterranean Sea sediments over the Holocene. Geochimica et Cosmochimica Acta 75, 5540–5558. https://doi.org/10.1016/j.gca.2011.07.002

Reineck, H.E. (1963. Sedimentgefüge im Bereich der südlichen Nordsee. Abhandlungen der Senckenbergischen Naturforschenden Gesellschaft 505, 1–138.

Reineck, H.E., Singh, I.B. (1967). Primary sedimentary structures in the recent sediments of the Jade, North Sea. Marine Geology 5, 227–235. https://doi.org/10.1016/0025-3227(67)90084-9

Reitz, A., de Lange, G.J. (2006). Abundant Sr-rich aragonite in eastern Mediterranean sapropel S1: Diagenetic vs. detrital/biogenic origin. Palaeogeography, Palaeoclimatology, Palaeoecology 235, 135–148. https://doi.org/10.1016/j.palaeo.2005.10.024

Reolid, M., Emanuela, M., Nieto, L.M., Rodríguez-Tovar, F.J. (2014). The Early Toarcian Oceanic Anoxic Event in the External Subbetic (Southiberian Palaeomargin, Westernmost Tethys): Geochemistry, nannofossils and ichnology. Palaeogeography, Palaeoclimatology, Palaeoecology 411, 79–94. https://doi.org/10.1016/j.palaeo.2014.06.023

Revel, M., Colin, C., Bernasconi, S., Combourieu-Nebout, N., Ducassou, E., Grousset, F.E., Rolland, Y., Migeon, S., Bosch, D., Brunet, P., Zhao, Y., Mascle, J. (2014). 21,000 Years of Ethiopian African monsoon variability recorded in sediments of the western Nile deep-sea fan. Regional Environmental Change 14, 1685–1696. https://doi.org/10.1007/s10113-014-0588-x

Revel, M., Ducassou, E., Grousset, F.E., Bernasconi, S.M., Migeon, S., Revillon, S., Mascle, J., Murat, A., Zaragosi, S., Bosch, D. (2010). 100,000 Years of African monsoon variability recorded in sediments of the Nile margin. Quaternary Science Reviews 29, 1342–1362. https://doi.org/10.1016/j.quascirev.2010.02.006

Rhein, M. (1995). Deep water formation in the western Mediterranean. Journal of Geophysical Research 100, 6943. https://doi.org/10.1029/94JC03198

Ridgwell, A.J., Watson, A.J., Raymo, M.E. (1999). Is the spectral signature of the 100 kyr glacial cycle consistent with a Milankovitch origin?. Paleoceanography 14, 437–440. https://doi.org/10.1029/1999PA900018

Riedinger, N., Pfeifer, K., Kasten, S., Garming, J.F.L., Vogt, C., Hensen, C. (2005). Diagenetic Alteration of Magnetic Signals by Anaerobic Oxidation of Methane Related to a Change in Sedimentation Rate. Geochimica et Cosmochimica Acta 69, 4117–4126. https://doi.org/10.1016/J.GCA.2005.02.004

Roberts, N. (1998). The Holocene: Environmental History. Oxford: Blackwell Publishers.

Robinson, A.R., Golnaraghi, M. (1994). The Physical and Dynamical Oceanography of the Mediterranean Sea, in: Malanotte-Rizzoli, P., Robinson, A.R. (Eds.), Ocean Processes in Climate Dynamics: Global and Mediterranean Examples. Dordrecht: Springer, NATO ASI Series, pp. 255–306. https://doi.org/10.1007/978-94-011-0870-6_12

Robinson, A.R., Malanotte-Rizzoli, P., Hecht, A., Michelato, A., Roether, W., Theocharis, A., Ünlüata, Ü., Pinardi, N., Artegiani, A., Bergamasco, A., Bishop, J., Brenner, S., Christianidis, S., Gacic, M., Georgopoulos, D., Golnaraghi, M., Hausmann, M., Junghaus, H.-G., Lascaratos, A, ... Osman, M. (1992). General circulation of the Eastern

Mediterranean. Earth-Science Reviews 32, 285–309. https://doi.org/10.1016/0012-8252(92)90002-B

Robinson, D. (2017). The Incredible Growth of Python | Stack Overflow. stackoverflow.blog.

Rodrigo-Gámiz, M., Martínez-Ruiz, F., Chiaradia, M., Jiménez-Espejo, F.J., Ariztegui, D. (2015). Radiogenic isotopes for deciphering terrigenous input provenance in the western Mediterranean. Chemical Geology 410, 237–250. https://doi.org/10.1016/j.chemgeo.2015.06.004

Rodrigo-Gámiz, M., Martínez-Ruiz, F., Jiménez-Espejo, F.J., Gallego-Torres, D., Nieto-Moreno, V., Romero, O., Ariztegui, D. (2011). Impact of climate variability in the western Mediterranean during the last 20,000 years: oceanic and atmospheric responses. Quaternary Science Reviews 30, 2018–2034. https://doi.org/10.1016/j.quascirev.2011.05.011

Rodrigo-Gámiz, M., Martínez-Ruiz, F., Rodríguez-Tovar, F.J., Jiménez-Espejo, F.J., Pardo-Igúzquiza, E. (2014). Millennial- to centennial-scale climate periodicities and forcing mechanisms in the westernmost Mediterranean for the past 20,000 yr. Quaternary Research 81, 78–93. https://doi.org/10.1016/j.yqres.2013.10.009

Rodríguez-Tovar, F.J. (2022). Ichnological analysis: A tool to characterize deep-marine processes and sediments. Earth-Science Reviews 228, 104014. https://doi.org/10.1016/j.earscirev.2022.104014

Rodríguez-Tovar, F.J. (2021). Ichnology of the Toarcian Oceanic Anoxic Event: An understimated tool to assess palaeoenvironmental interpretations. Earth-Science Reviews 216, 103579. https://doi.org/10.1016/j.earscirev.2021.103579

Rodríguez-Tovar, F.J., Dorador, J. (2015). Ichnofabric characterization in cores: a method of digital image treatment. Annales Societatis Geologorum Poloniae 85, 465–471. https://doi.org/10.14241/asgp.2015.010

Rodríguez-Tovar, F.J., Dorador, J. (2014). Ichnological analysis of Pleistocene sediments from the IODP Site U1385 "Shackleton Site" on the Iberian margin: Approaching paleoenvironmental conditions. Palaeogeography, Palaeoclimatology, Palaeoecology 409, 24–32. https://doi.org/10.1016/j.palaeo.2014.04.027

Rodríguez-Tovar, F.J., Dorador, J., Grunert, P., Hodell, D.A. (2015). Deep-sea trace fossil and benthic foraminiferal assemblages across glacial Terminations 1, 2 and 4 at the "Shackleton Site" (IODP Expedition 339, Site U1385). Global and Planetary Change 133, 359–370. https://doi.org/10.1016/j.gloplacha.2015.05.003

Rodríguez-Tovar, F.J., Dorador, J., Hodell, D.A.V. (2019a). Trace fossils evidence of a complex history of nutrient availability and oxygen conditions during Heinrich Event 1. Global and Planetary Change 174, 26–34. https://doi.org/0.1016/j.gloplacha.2019.01.003

Rodríguez-Tovar, F.J., Dorador, J., Mena, A., Francés, G. (2020a). Regional and global changes during Heinrich Event 1 affecting macrobenthic habitat: Ichnological evidence of sea-bottom conditions at the Galicia Interior Basin. Global and Planetary Change 192, 103227. https://doi.org/10.1016/j.gloplacha.2020.103227

Rodríguez-Tovar, F.J., Dorador, J., Mena, A., Hernández-Molina, F.J. (2018). Lateral variability of ichnofabrics in marine cores: Improving sedimentary basin analysis using

Computed Tomography images and high-resolution digital treatment. Marine Geology 397, 72–78. https://doi.org/10.1016/j.margeo.2017.12.006

Rodríguez-Tovar, F.J., Hernández-Molina, F.J. (2018). Ichnological analysis of contourites: Past, present and future. Earth-Science Reviews 182, 28–41. https://doi.org/10.1016/j.earscirev.2018.05.008

Rodríguez-Tovar, F.J., Hernández-Molina, F.J., Hüneke, H., Llave, E., Stow, D. (2019b). Contourite facies model: Improving contourite characterization based on the ichnological analysis. Sedimentary Geology 384, 60–69. https://doi.org/10.1016/j.sedgeo.2019.03.010

Rodríguez-Tovar, F.J., Löwemark, L., Pardo-Igúzquiza, E. (2011). Zoophycos cyclicity during the last 425ka in the northeastern South China Sea: Evidence for monsoon fluctuation at the Milankovitch scale. Palaeogeography, Palaeoclimatology, Palaeoecology 305, 256–263. https://doi.org/10.1016/j.palaeo.2011.03.006

Rodríguez-Tovar, F.J., Miguez-Salas, O., Dorador, J., Duarte, L.V. (2019c). Opportunistic behaviour after the Toarcian Oceanic Anoxic Event: The trace fossil Halimedides. Palaeogeography, Palaeoclimatology, Palaeoecology 520, 240–250. https://doi.org/10.1016/j.palaeo.2019.01.036

Rodríguez-Tovar, F.J., Miguez-Salas, O., Duarte, L.V. (2017). Toarcian Oceanic Anoxic Event induced unusual behaviour and palaeobiological changes in Thalassinoides tracemakers. Palaeogeography, Palaeoclimatology, Palaeoecology 485, 46–56. https://doi.org/10.1016/j.palaeo.2017.06.002

Rodríguez-Tovar, F.J., Puga-Bernabéu, Á., Buatois, L.A. (2008). Large burrow systems in marine Miocene deposits of the Betic Cordillera (Southeast Spain). Palaeogeography, Palaeoclimatology, Palaeoecology 268, 19–25. https://doi.org/10.1016/j.palaeo.2008.07.022

Rodríguez-Tovar, F.J., Uchman, A. (2017). The Faraoni event (latest Hauterivian) in ichnological record: The Río Argos section of southern Spain. Cretaceous Research 79, 109–121. https://doi.org/10.1016/j.cretres.2017.07.018

Rodríguez-Tovar, F.J., Uchman, A. (2011). Ichnological data as a useful tool for deep-sea environmental characterization: a brief overview and an application to recognition of small-scale oxygenation changes during the Cenomanian–Turonian anoxic event. Geo-Marine Letters 31, 525–536. https://doi.org/10.1007/s00367-011-0237-z

Rodríguez-Tovar, F.J., Uchman, A. (2010). Ichnofabric evidence for the lack of bottom anoxia during the Lower Toarcian oceanic anoxic event in the Fuente de la Vidriera section, Betic Cordillera, Spain. PALAIOS 25, 576–587. https://doi.org/10.2110/palo.2009.p09-153r

Rodríguez-Tovar, F.J., Uchman, A., Martín-Algarra, A. (2009). Oceanic Anoxic Event at the Cenomanian-Turonian boundary interval (OAE-2): ichnological approach from the Betic Cordillera, southern Spain. Lethaia 42, 407–417. https://doi.org/10.1111/j.1502-3931.2009.00159.x

Rodríguez-Tovar, F.J., Uchman, A., Reolid, M., Sánchez-Quiñónez, C.A. (2020b). Ichnological analysis of the Cenomanian–Turonian boundary interval in a collapsing slope setting: A case from the Rio Fardes section, southern Spain. Cretaceous Research 106, 104262. https://doi.org/10.1016/j.cretres.2019.104262

Rodwell, M.J., Hoskins, B.J. (2001). Subtropical Anticyclones and Summer Monsoons. Journal of Climate 14, 3192–3211. https://doi.org/10.1175/1520-0442(2001)014<3192:SAASM>2.0.CO;2

Roegner, G.C., Needoba, J.A., Baptista, A.M. (2011). Coastal Upwelling Supplies Oxygen-Depleted Water to the Columbia River Estuary. PLOS ONE 6, e18672. https://doi.org/10.1371/journal.pone.0018672

Roether, W., Klein, B., Manca, B.B., Theocharis, A., Kioroglou, S. (2007). Transient Eastern Mediterranean deep waters in response to the massive dense-water output of the Aegean Sea in the 1990s. Progress in Oceanography 74, 540–571. https://doi.org/10.1016/j.pocean.2007.03.001

Roether, W., Manca, B.B., Klein, B., Bregant, D., Georgopoulos, D., Beitzel, V., Kovačević, V., Luchetta, A. (1996). Recent Changes in Eastern Mediterranean Deep Waters. Science 271, 333–335. https://doi.org/10.1126/science.271.5247.333

Roether, W., Schlitzer, R. (1991). Eastern Mediterranean deep water renewal on the basis of chlorofluoromethane and tritium data. Dynamics of Atmospheres and Oceans, The Mediterranean Sea 15, 333–354. https://doi.org/10.1016/0377-0265(91)90025-B

Rogerson, M., Cacho, I., Jiménez-Espejo, F.J., Reguera, M.I., Sierro, F.J., Martínez-Ruiz, F., Frigola, J., Canals, M. (2008). A dynamic explanation for the origin of the western Mediterranean organic-rich layers. Geochemistry, Geophysics, Geosystems 9, Q07U01. https://doi.org/10.1029/2007GC001936

Rogerson, M., Rohling, E.J., Bigg, G.R., Ramirez, J. (2012). Paleoceanography of the Atlantic-Mediterranean exchange: Overview and first quantitative assessment of climatic forcing. Reviews of Geophysics 50, RG2003. https://doi.org/10.1029/2011RG000376

Rögl, F. (1999). Mediterranean and Parathetys Paleogeography during the Oligocene and Miocene, in: Agustí, J., Rook, L., Andrews, P. (Eds.). The Evolution of Neogene Terrestrial Ecosystems in Europe. Cambridge Cambridge:University Press. Hominoid Evolution and Climatic Change in Europe 1, pp. 9–23.

Rohling, E.J. (1994). Review and new aspects concerning the formation of eastern Mediterranean sapropels. Marine Geology 122, 1–28. https://doi.org/10.1016/0025-3227(94)90202-X

Rohling, E.J., Abu-Zied, R.H., Casford, C.S.L., Hayes, A., Hoogakker, B.A.A. (2009). The mediterranean Sea. Present and past, in: Oxford Regional Environments: Physical Geography of the Mediterranean Basin. Oxford: Oxford University Press, 704 pp.

Rohling, E.J., Grant, K., Hemleben, C., Siddall, M., Hoogakker, B. A. A., Bolshaw, M., Kucera, M. (2008). High rates of sea-level rise during the last interglacial period. Nature Geoscience 1, 38–42. https://doi.org/10.1038/ngeo.2007.28

Rohling, E.J., Hayes, A., De Rijk, S., Kroon, D., Zachariasse, W.J., Eisma, D. (1998). Abrupt cold spells in the northwest Mediterranean. Paleoceanography 13, 316–322. https://doi.org/10.1029/98PA00671

Rohling, E.J., Hilgen, F.J. (1991). The eastern Mediterranean climate at times of sapropel formation: a review. Geologie en Mijnbouw 70, 253–264.

Rohling, E.J., Marino, G., Grant, K.M. (2015). Mediterranean climate and oceanography, and the periodic development of anoxic events (sapropels). Earth-Science Reviews 143, 62–97. https://doi.org/10.1016/j.earscirev.2015.01.008

Rosenbaum, G., Lister, G.S. (2004). Neogene and Quaternary rollback evolution of the Tyrrhenian Sea, the Apennines, and the Sicilian Maghrebides. Tectonics 23, TC1013. https://doi.org/10.1029/2003TC001518

Rosenbaum, G., Lister, G.S., Duboz, C. (2002). Relative motions of Africa, Iberia and Europe during Alpine orogeny. Tectonophysics 359, 117–129. https://doi.org/10.1016/S0040-1951(02)00442-0

Rossignol-Strick, M. (1985). Mediterranean Quaternary sapropels, an immediate response of the African monsoon to variation of insolation. Palaeogeography, Palaeoclimatology, Palaeoecology 49, 237–263. https://doi.org/10.1016/0031-0182(85)90056-2

Rossignol-Strick, M. (1983). African monsoons, an immediate climate response to orbital insolation. Nature 304, 46–49. https://doi.org/10.1038/304046a0

Rossignol-Strick, M., Nesteroff, W., Olive, P., Vergnaud-Grazzini, C. (1982). After the deluge: Mediterranean stagnation and sapropel formation. Nature 295, 105–110. https://doi.org/10.1038/295105a0

Rossignol-Strick, M., Paterne, M. (1999). A synthetic pollen record of the eastern Mediterranean sapropels of the last 1 Ma: implications for the time-scale and formation of sapropels. Marine Geology 153, 221–237. https://doi.org/10.1016/S0025-3227(98)00080-2

Rothwell, R.G., Croudace, I.W. (2015). Micro-XRF Studies of Sediment Cores. Dordrecht: Springer. https://doi.org/10.1007/978-94-017-9849-5_1.

Rothwell, R.G., Hoogakker, B., Thomson, J., Croudace, I.W., Frenz, M. (2006). Turbidite emplacement on the southern Balearic Abyssal Plain (western Mediterranean Sea) during Marine Isotope Stages 1–3: an application of ITRAX XRF scanning of sediment cores to lithostratigraphic analysis. Geological Society, London, Special Publications 267, 79–98. https://doi.org/10.1144/GSL.SP.2006.267.01.06

Rousseau, D.-D., Bagniewski, W., Ghil, M. (2022). Abrupt climate changes and the astronomical theory: are they related? Climate of the Past 18, 249–271. https://doi.org/10.5194/cp-18-249-2022

Ruddiman, W.F. (2006). Orbital changes and climate. Quaternary Science Reviews 25, 3092–3112. https://doi.org/10.1016/j.quascirev.2006.09.001

Ruddiman, W.F., Raymo, M.E., Martinson, D.G., Clement, B.M., Backman, J. (1989). Pleistocene evolution: Northern hemisphere ice sheets and North Atlantic Ocean. Paleoceanography 4, 353–412. https://doi.org/10.1029/PA004i004p00353

Sabatier, P., Nicolle, M., Piot, C., Colin, C., Debret, M., Swingedouw, D., Perrette, Y., Bellingery, M.-C., Chazeau, B., Develle, A.-L., Leblanc, M., Skonieczny, C., Copard, Y., Reyss, J.-L., Malet, E., Jouffroy-Bapicot, I., Kelner, M., Poulenard, J., Didier, J., Arnaud, F., Vannière, B. (2020). Past African dust inputs in the western Mediterranean area controlled by the complex interaction between the Intertropical Convergence Zone, the North Atlantic Oscillation, and total solar irradiance. Climate of the Past 16, 283–298. https://doi.org/10.5194/cp-16-283-2020

Sahami, M., Dumais, S., Heckerman, D., Horvitz, E. (1998). A Bayesian Approach to Filtering Junk E-Mail. Microsoft Research.

Salby, M.L. (2011). Physics of the Atmosphere and Climate, Physics of the Atmosphere and Climate. Cambridge: Cambridge University Press. https://doi.org/10.1017/CBO9781139005265

Sánchez Goñi, M., Cacho, I., Turon, J., Guiot, J., Sierro, F.J., Peypouquet, J., Grimalt, J., Shackleton, N. (2002). Synchroneity between marine and terrestrial responses to millennial scale climatic variability during the last glacial period in the Mediterranean region. Climate Dynamics 19, 95–105. https://doi.org/10.1007/s00382-001-0212-x

Sánchez Goñi, M.F. (2022). An overview of the Last Glacial Cycle, in: Palacios, D., Hughes, P. D., García-Ruiz, J. M., Andrés, N. (Eds). European Glacial Landscapes. Amsterdam:Elsevier, pp 165–169. https://doi.org/10.1016/B978-0-12-823498-3.00012-1

Sánchez Goñi, M.F., Ferretti, P., Polanco-Martínez, J.M., Rodrigues, T., Alonso-García, M., Rodríguez-Tovar, F.J., Dorador, J., Desprat, S. (2019). Pronounced northward shift of the westerlies during MIS 17 leading to the strong 100-kyr ice age cycles. Earth and Planetary Science Letters 511, 117–129. https://doi.org/10.1016/j.epsl.2019.01.032

Sanchez Goñi, M.F., Harrison, S.P. (2010). Millennial-scale climate variability and vegetation changes during the Last Glacial: Concepts and terminology. Quaternary Science Reviews 29, 2823–2827. https://doi.org/10.1016/j.quascirev.2009.11.014

Sarhan, T. (2000). Upwelling mechanisms in the northwestern Alboran Sea. Journal of Marine Systems 23, 317–331. https://doi.org/10.1016/S0924-7963(99)00068-8

Sarmiento, J.L., Gruber, N. (2006). Ocean Biogeochemical Dynamics. Princeton: Princeton U. Press.

Satow, C., Tomlinson, E.L., Grant, K.M., Albert, P.G., Smith, V.C., Manning, C.J., Ottolini, L., Wulf, S., Rohling, E.J., Lowe, J.J., Blockley, S.P.E., Menzies, M.A. (2015). A new contribution to the Late Quaternary tephrostratigraphy of the Mediterranean: Aegean Sea core LC21. Quaternary Science Reviews 117, 96–112. https://doi.org/10.1016/j.quascirev.2015.04.005

Savrda, C.E. (2016). Composite ichnofabrics: categorization based on number of ichnocoenoses and their temporal incongruence. PALAIOS 31, 92–96. https://doi.org/20160309203344370000

Savrda, C.E. (2007). Trace Fossils and Marine Benthic Oxygenation, in: Miller, W. (Ed). Trace Fossils. Amsterdam: Elsevier, pp. 149–158. https://doi.org/10.1016/B978-044452949-7/50135-2

Savrda, C.E. (1995). Ichnologic applications in paleoceanographic, paleoclimatic, and sea-level studies. PALAIOS 10, 565–577. https://doi.org/10.2307/3515095

Savrda, C.E. (1992). Trace Fossils and Benthic Oxygenation. Short Courses in Paleontology 5, 172–196. https://doi.org/10.1017/S2475263000002348

Savrda, C.E., Bottjer, D.J. (1991). Oxygen-related biofacies in marine strata: an overview and update. Geological Society, London, Special Publications 58, 201–219. https://doi.org/10.1144/GSL.SP.1991.058.01.14

Savrda, C.E., Bottjer, D.J. (1989). Trace-fossil model for reconstructing oxygenation histories of ancient marine bottom waters: Application to Upper Cretaceous Niobrara formation, Colorado. Palaeogeography, Palaeoclimatology, Palaeoecology 74, 49–74. https://doi.org/10.1016/0031-0182(89)90019-9

Savrda, C.E., Bottjer, D.J. (1987). Trace fossils as indicators of bottom-water redox conditions in ancient marine environments, in: New Concepts in the Use of Biogenic Sedimentary Structures for Paleoenvironmental Interpretation. Society for Sedimentary Geology, Pacific Section, pp. 3–26.

Savrda, C.E., Bottjer, D.J. (1986). Trace-fossil model for reconstruction of paleo-oxygenation in bottom waters. Geology 14, 3-6. https://doi.org/10.1130/0091-7613(1986)14<3:TMFROP>2.0.CO;2

Schindelin, J., Arganda-Carreras, I., Frise, E., Kaynig, V., Longair, M., Pietzsch, T., Preibisch, S., Rueden, C., Saalfeld, S., Schmid, B., Tinevez, J.-Y., White, D.J., Hartenstein, V., Eliceiri, K., Tomancak, P., Cardona, A. (2012). Fiji: an open-source platform for biological-image analysis. Nature Methods 9, 676–682. https://doi.org/10.1038/nmeth.2019

Schlirf, M. (2000). Upper Jurassic trace fossils from the Boulonnais (northern France). Geologica et Palaeontologica 34, 145–213.

Schmiedl, G., Mitschele, A., Beck, S., Emeis, K.-C., Hemleben, C., Schulz, H., Sperling, M., Weldeab, S. (2003). Benthic foraminiferal record of ecosystem variability in the eastern Mediterranean Sea during times of sapropel S5 and S6 deposition. Palaeogeography Palaeoclimatology Palaeoecology 190, 139–164. https://doi.org/10.1016/S0031-0182(02)00603-X

Schmitz, W.J. (1996). On the World Ocean Circulation. Volume 1. Some Global Features / North Atlantic Circulation. Woods Hole Oceanographic Institution Technical Report WHOI-96-03, 149 pp.

Schoepfer, S.D., Shen, J., Wei, H., Tyson, R.V., Ingall, E., Algeo, T.J. (2015). Total organic carbon, organic phosphorus, and biogenic barium fluxes as proxies for paleomarine productivity. Earth-Science Reviews 149, 23–52. https://doi.org/10.1016/J.EARSCIREV.2014.08.017

Schönfeld, J., Zahn, R., de Abreu, L. (2003). Surface and deep water response to rapid climate changes at the Western Iberian Margin. Global and Planetary Change 36, 237–264. https://doi.org/10.1016/S0921-8181(02)00197-2

Schott, F., Visbeck, M., Send, U., Fischer, J., Stramma, L., Desaubies, Y. (1996). Observations of Deep Convection in the Gulf of Lions, Northern Mediterranean, during the Winter of 1991/92. Journal of Physical Oceanography 26, 505–524. https://doi.org/10.1175/1520-0485(1996)026<0505:OODCIT>2.0.CO;2

Schroeder, K., Chiggiato, J. (Eds.) (2022). Oceanography of the Mediterranean Sea. Amsterdam:Elsevier, 584pp.

Schroeder, K., Chiggiato, J., Josey, S.A., Borghini, M., Aracri, S., Sparnocchia, S. (2017). Rapid response to climate change in a marginal sea. Scientific Reports 7, 4065. https://doi.org/10.1038/s41598-017-04455-5

Schroeder, K., Garcìa-Lafuente, J., Josey, S.A., Artale, V., Nardelli, B.B., Carrillo, A., Gačić, M., Gasparini, G.P., Herrmann, M., Lionello, P., Ludwig, W., Millot, C., Özsoy, E.,

Pisacane, G., Sánchez-Garrido, J.C., Sannino, G., Santoleri, R., Somot, S., Struglia, M., Stanev, E., Taupier-Letage, I., Tsimplis, M.N., Vargas-Yáñez, M., Zervakis, V., Zodiatis, G. (2012). Circulation of the Mediterranean Sea and its Variability, in: Lionello, P. (Ed). The Climate of the Mediterranean Region. Amsterdam: Elsevier, pp 187–256. https://doi.org/10.1016/B978-0-12-416042-2.00003-3

Schroeder, K., Ribotti, A., Borghini, M., Sorgente, R., Perilli, A., Gasparini, G.P. (2008). An extensive western Mediterranean deep water renewal between 2004 and 2006. Geophysical Research Letters 35, L18605. https://doi.org/10.1029/2008GL035146

Schroeder, K., Tanhua, T., Chiggiato, J., Velaoras, D., Josey, S.A., García Lafuente, J., Vargas-Yáñez, M. (2022). The forcings of the Mediterranean Sea and the physical properties of its water masses, in: Schroeder, K., Chiggiato, J. (Eds.), The Oceanography of the Mediterranean Sea: An Introductory Guide. Amsterdam:Elsevier, pp. 93–123. https://doi.org/10.1016/B978-0-12-823692-5.00005-4

scikit-learn: machine learning in Python (2023). URL: https://scikit-learn.org/stable/index.html

Seilacher, A. (1990). Aberrations in bivalve evolution related to photo- and chemosymbiosis. Historical Biology 3, 289–311. https://doi.org/10.1080/08912969009386528

Seilacher, A. (1967). Fossil behaviour. Scientific American 217, 72–80.

Seilacher, A. (1964). Biogenic sedimentary structures. Approaches to Paleoecology 296–316.

Send, U., Font, J., Krahmann, G., Millot, C., Rhein, M., Tintoré, J. (1999). Recent advances in observing the physical oceanography of the western Mediterranean Sea. Progress in Oceanography 44, 37–64. https://doi.org/10.1016/S0079-6611(99)00020-8

Serreze, M.C., Carse, F., Barry, R.G., Rogers, J.C. (1997). Icelandic Low Cyclone Activity: Climatological Features, Linkages with the NAO, and Relationships with Recent Changes in the Northern Hemisphere Circulation. Journal of Climate 10, 453–464.

https://doi.org/10.1175/1520-0442(1997)010<0453:ILCACF>2.0.CO;2

Sha, L., Ait Brahim, Y., Wassenburg, J.A., Yin, J., Peros, M., Cruz, F.W., Cai, Y., Li, H., Du, W., Zhang, H., Edwards, R.L., Cheng, H. (2019). How Far North Did the African Monsoon Fringe Expand During the African Humid Period? Insights From Southwest Moroccan Speleothems. Geophysical Research Letters 46, 14093–14102. https://doi.org/10.1029/2019GL084879

Shackleton, N.J., Opdyke, N.D. (1977). Oxygen isotope and palaeomagnetic evidence for early Northern Hemisphere glaciation. Nature 270, 216–219. https://doi.org/10.1038/270216a0

Shackleton, N.J., Opdyke, N.D. (1973). Oxygen Isotope and Palaeomagnetic Stratigraphy of Equatorial Pacific Core V28-238: Oxygen Isotope Temperatures and Ice Volumes on a 105 Year and 106 Year Scale. Quaternary Research 3, 39–55. https://doi.org/10.1016/0033-5894(73)90052-5

Shackleton, N.J., Sánchez-Goñi, M.F., Pailler, D., Lancelot, Y. (2003). Marine Isotope Substage 5e and the Eemian Interglacial. Global and Planetary Change 36, 151–155. https://doi.org/10.1016/S0921-8181(02)00181-9

Shao, Y., Zhang, J., Ishizuka, M., Mikami, M., Leys, J., Huang, N. (2020). Dependency of particle size distribution at dust emission on friction velocity and atmospheric boundary-layer stability. Atmospheric Chemistry and Physics 20, 12939–12953.

https://doi.org/10.5194/acp-20-12939-2020

Shin, J.Y., Yu, Y., Seo, I., Hyeong, K., Lim, D., Kim, W. (2018). Magnetic Properties of Deep-Sea Sediments From the North Pacific: A Proxy of Glacial Deep-Water Ventilation. Geochemistry, Geophysics, Geosystems 19, 4433–4443. https://doi.org/10.1029/2018GC007735

Shipboard Scientific Party (1996a). Site 977. Proceedings of the Ocean Drilling Program 161, 299–353. https://doi.org/10.2973/odp.proc.ir.161.107.1996

Shipboard Scientific Party (1996b). Site 976. Proceedings of the Ocean Drilling Program 161, 179–297. https://doi.org/10.2973/odp.proc.ir.161.106.1996

Siddall, M., Rohling, E.J., Almogi-Labin, A., Hemleben, C., Meischner, D., Schmelzer, I., Smeed, D.A. (2003). Sea-level fluctuations during the Last Glacial Cycle. Nature 423, 853–8. https://doi.org/10.1038/nature01690

Sierro, F.J., Flores, J.A., Zamarreño, I., Vázquez, A., Utrilla, R., Francés, G., Hilgen, F.J., Krijgsman, W. (1999). Messinian pre-evaporite sapropels and precession-induced oscillations in western Mediterranean climate. Marine Geology 153, 137–146. https://doi.org/10.1016/S0025-3227(98)00085-1

Sierro, F.J., Hodell, D.A., Andersen, N., Azibeiro, L.A., Jimenez-Espejo, F.J., Bahr, A., Flores, J.A., Ausin, B., Rogerson, M., Lozano-Luz, R., Lebreiro, S.M., Hernandez-Molina, F.J., Jimenez-Espejo, F.J., Bahr, A., Flores, J.A., Ausin, B., Rogerson, M., Lozano-Luz, R., Lebreiro, S.M., Hernandez-Molina, F.J. (2020). Mediterranean Overflow Over the Last 250 kyr: Freshwater Forcing From the Tropics to the Ice Sheets. Paleoceanography and Paleoclimatology 35, e2020PA003931. https://doi.org/10.1029/2020PA003931

Sierro, F.J., Hodell, D.A., Curtis, J.H., Flores, J.A., Reguera, I., Colmenero-Hidalgo, E., Bárcena, M.A., Grimalt, J.O., Cacho, I., Frigola, J., Canals, M. (2005). Impact of iceberg melting on Mediterranean thermohaline circulation during Heinrich events. Paleoceanography 20. https://doi.org/10.1029/2004PA001051

Sigl, W., Chamley, H., Fabricius, F., Ghislaine, G. d'Argoud, Müller, J. (1978). Sedimentology and environmental conditions of sapropels, in: Deep Sea Drilling Project Initial Reports 42 Part 1. pp. 445–465.

Singh, A.K., Marcantonio, F., Lyle, M. (2011). Sediment focusing in the Panama Basin, Eastern Equatorial Pacific Ocean. Earth and Planetary Science Letters 309, 33–44. https://doi.org/10.1016/j.epsl.2011.06.020

Skliris, N., Sofianos, S., Lascaratos, A. (2007). Hydrological changes in the Mediterranean Sea in relation to changes in the freshwater budget: A numerical modelling study. Journal of Marine Systems 65, 400–416. https://doi.org/10.1016/j.jmarsys.2006.01.015

Somot, S., Houpert, L., Sevault, F., Testor, P., Bosse, A., Taupier-Letage, I., Bouin, M.-N., Waldman, R., Cassou, C., Sanchez-Gomez, E., Durrieu de Madron, X., Adloff, F., Nabat, P., Herrmann, M. (2018). Characterizing, modelling and understanding the climate variability of the deep water formation in the North-Western Mediterranean Sea. Climate Dynamics 51, 1179–1210. https://doi.org/10.1007/s00382-016-3295-0

Spears, D.A., Kanaris-Sotiriou, R. (1976). Titanium in some Carboniferous sediments from Great Britain. Geochimica et Cosmochimica Acta 40, 345–351. https://doi.org/10.1016/0016-7037(76)90212-X

Stanley, D.J. (1972). The Mediterranean Sea: A natural sedimentation laboratory. Stroudsburg:Hutchinson & Ross. 765 p. https://doi.org/10.4319/lo.1974.19.3.0547a

Stata corp. Stata Statistical Software.

Steffensen, J.P., Andersen, K.K., Bigler, M., Clausen, H.B., Dahl-Jensen, D., Fischer, H., Goto-Azuma, K., Hansson, M., Johnsen, S.J., Jouzel, J., Masson-Delmotte, V., Popp, T., Rasmussen, S.O., Röthlisberger, R., Ruth, U., Stauffer, B., Siggaard-Andersen, M.-L., Sveinbjörnsdóttir, Á.E., Svensson, A., White, J.W.C. (2008). High-Resolution Greenland ice core data show abrupt climate change happens in few years. Science 321, 680–684. https://doi.org/10.1126/science.1157707

Stein, R. (1990). Organic carbon content/sedimentation rate relationship and its paleoenvironmental significance for marine sediments. Geo-Marine Letters 10, 37–44. https://doi.org/10.1007/BF02431020

Sternberg, E., Jeandel, C., Miquel, J.-C., Gasser, B., Souhaut, M., Arraes-Mescoff, R., Francois, R. (2007). Particulate barium fluxes and export production in the northwestern Mediterranean. Marine Chemistry 105, 281–295. https://doi.org/10.1016/j.marchem.2007.03.003

Stewart, J.R., Stringer, C.B. (2012. Human Evolution Out of Africa: The Role of Refugia and Climate Change. Science 335, 1317–1321. https://doi.org/10.1126/science.1215627

Stramma, L., Prince, E.D., Schmidtko, S., Luo, J., Hoolihan, J.P., Visbeck, M., Wallace, D.W.R., Brandt, P., Körtzinger, A. (2012). Expansion of oxygen minimum zones may reduce available habitat for tropical pelagic fishes. Nature Climate Change 2, 33–37. https://doi.org/10.1038/nclimate1304

Stríkis, N.M., Chiessi, C.M., Cruz, F.W., Vuille, M., Cheng, H., de Souza Barreto, E.A., Mollenhauer, G., Kasten, S., Karmann, I., Edwards, R.L., Bernal, J.P., Sales, H. dos R. (2015). Timing and structure of Mega-SACZ events during Heinrich Stadial 1. Geophysical Research Letters 42, 5477-5484. https://doi.org/10.1002/2015GL064048

Stuut, J.-B.W., Temmesfeld, F., De Deckker, P. (2014). A 550 ka record of aeolian activity near North West Cape, Australia: inferences from grain-size distributions and bulk chemistry of SE Indian Ocean deep-sea sediments. Quaternary Science Reviews 83, 83–94. https://doi.org/10.1016/j.quascirev.2013.11.003

Suc, J.-P. (1984). Origin and evolution of the Mediterranean vegetation and climate in Europe. Nature 307, 429–432. https://doi.org/10.1038/307429a0

Svensson, A., Andersen, K.K., Bigler, M., Clausen, H.B., Dahl-Jensen, D., Davies, S.M., Johnsen, S.J., Muscheler, R., Parrenin, F., Rasmussen, S.O., Röthlisberger, R., Seierstad, I., Steffensen, J.P., Vinther, B.M. (2008). A 60 000 year Greenland stratigraphic ice core chronology. Climate of the Past 4, 47–57. https://doi.org/10.5194/cp-4-47-2008

Sweere, T., Hennekam, R., Vance, D., Reichart, G.-J. (2021). Molybdenum isotope constraints on the temporal development of sulfidic conditions during Mediterranean sapropel intervals | Geochemical Perspectives Letters. Geochemical Perspectives Letters 17, 16–20. https://doi.org/10.7185/geochemlet.2108

Tachikawa, K., Vidal, L., Cornuault, M., Garcia, M., Pothin, A., Sonzogni, C., Bard, E., Menot, G., Revel, M. (2015). Eastern Mediterranean Sea circulation inferred from the conditions of S1 sapropel deposition. Climate of the Past 11, 855–867. https://doi.org/10.5194/cp-11-855-2015

Tanaka, T., Togashi, S., Kamioka, H., Amakawa, H., Kagami, H., Hamamoto, T., Yuhara, M., Orihashi, Y., Yoneda, S., Shimizu, H., Kunimaru, T., Takahashi, K., Yanagi, T., Nakano, T., Fujimaki, H., Shinjo, R., Asahara, Y., Tanimizu, M., Dragusanu, C. (2000). JNdi-1: a neodymium isotopic reference in consistency with LaJolla neodymium. Chemical Geology 168, 279–281. https://doi.org/10.1016/S0009-2541(00)00198-4

Taylor, A., Goldring, R., Gowland, S. (2003). Analysis and application of ichnofabrics. Earth-Science Reviews 60, 227–259. https://doi.org/10.1016/S0012-8252(02)00105-8

Taylor, A.M., Goldring, R. (1993). Description and analysis of bioturbation and ichnofabric. Journal of the Geological Society 150, 141–148. https://doi.org/10.1144/gsjgs.150.1.0141

Taylor, S.R., McLennan, S.M. (1985). The continental crust: Its composition and evolution. Oxford:Lackwell Scientific Publications, , 312 pp.

Tesi, T., Asioli, A., Minisini, D., Maselli, V., Dalla Valle, G., Gamberi, F., Langone, L., Cattaneo, A., Montagna, P., Trincardi, F. (2017). Large-scale response of the Eastern Mediterranean thermohaline circulation to African monsoon intensification during sapropel S1 formation. Quaternary Science Reviews 159, 139–154. https://doi.org/10.1016/j.quascirev.2017.01.020

The MathWorks (2019). MathWorks - Makers of MATLAB and Simulink - MATLAB & Simulink.

The R Foundation (1999). R: The R Project for Statistical Computing.

Thompson, R., Oldfield, F. (1986). Environmental Magnetism. London:Allen&Unwin, 228 pp.

Thomsen, E., Vorren, T.O. (1984). Pyritization of tubes and burrows from Late Pleistocene continental shelf sediments off North Norway. Sedimentology 31, 481–492. https://doi.org/10.1111/j.1365-3091.1984.tb01814.x

Thomson, J., Croudace, I.W., Rothwell, R.G. (2006). A geochemical application of the ITRAX scanner to a sediment core containing eastern Mediterranean sapropel units. Geological Society, London, Special Publications 267, 65–77. https://doi.org/10.1144/GSL.SP.2006.267.01.05

Thomson, J., Higgs, N.C., Croudace, I.W., Colley, S., Hydes, D.J. (1993). Redox zonation of elements at an oxic/post-oxic boundary in deep-sea sediments. Geochimica et Cosmochimica Acta 57, 579–595. https://doi.org/10.1016/0016-7037(93)90369-8

Thomson, J., Higgs, N.C., Wilson, T.R.S., Croudace, I.W., De Lange, G.J., Van Santvoort, P.J.M. (1995). Redistribution and geochemical behaviour of redox-sensitive elements around S1, the most recent eastern Mediterranean sapropel. Geochimica et Cosmochimica Acta 59, 3487–3501. https://doi.org/10.1016/0016-7037(95)00232-O

Thomson, J., Mercone, D., De Lange, G.J., Van Santvoort, P.J.M. (1999). Review of recent advances in the interpretation of eastern Mediterranean sapropel S1 from geochemical evidence. Marine Geology 153, 77–89. https://doi.org/10.1016/S0025-3227(98)00089-9

Thomson J, Crudeli D, De Lange G, Slomp CP, Erba E, Corselli C, Calvert SE (2004) Florisphaera profunda and the origin and diagenesis of carbonate phases in eastern

Mediterranean sapropel units. Paleoceanography 19, PA3003. https://doi.org/doi:10.1029/2003PA000976

Thunell, R., Benitez-Nelson, C., Varela, R., Astor, Y., Muller-Karger, F. (2007). Particulate organic carbon fluxes along upwelling-dominated continental margins: Rates and mechanisms. Global Biogeochemical Cycles 21, GB1022. https://doi.org/10.1029/2006GB002793

Thunell, R.C., Williams, D.F., Kennett, J.P. (1977). Late Quaternary paleoclimatology, stratigraphy and sapropel history in eastern Mediterranean deep-sea sediments. Marine Micropaleontology 2, 371–388. https://doi.org/10.1016/0377-8398(77)90018-4

Tierney, J.E., Pausata, F.S.R., De Menocal, P.B. (2017). Rainfall regimes of the Green Sahara. Science Advances 3, e160150. https://doi.org/10.1126/sciadv.1601503

Timmer, E.R., Gingras, M.K., Zonneveld, J.-P. (2016a). PYCHNO: A Core-Image Quantitative Ichnology Logging Software. PALAIOS 31, 525–532. https://doi.org/2016111403064744000

Timmer, E.R., Gingras, M.K., Zonneveld, J.P. (2016b). Spatial and temporal significance of process ichnology data from silty-mudstone beds of inclined heterolithic stratification, Lower Cretaceous McMurray Formation, NE Alberta, Canada. PALAIOS 31, 533–548. https://doi.org/10.2110/palo.2015.089

Toucanne, S., Angue Minto'o, C.M., Fontanier, C., Bassetti, M.-A., Jorry, S.J., Jouet, G. (2015). Tracking rainfall in the northern Mediterranean borderlands during sapropel deposition. Quaternary Science Reviews 129, 178–195. https://doi.org/10.1016/j.quascirev.2015.10.016

Trias-Navarro, S., Pena, L.D., de la Fuente, M., Paredes, E., Garcia-Solsona, E., Frigola, J., Català, A., Caruso, A., Lirer, F., Haghipour, N., Pérez-Asensio, J.N., Cacho, I. (2023). Eastern Mediterranean water outflow during the Younger Dryas was twice that of the present day. Nature Communications Earth & Environment 4, 1–9. https://doi.org/10.1038/s43247-023-00812-7

Tribovillard, N., Algeo, T.J., Baudin, F., Riboulleau, A. (2012). Analysis of marine environmental conditions based on molybdenum–uranium covariation—Applications to Mesozoic paleoceanography. Chemical Geology 324–325, 46–58. https://doi.org/10.1016/j.chemgeo.2011.09.009

Tribovillard, N., Algeo, T.J., Lyons, T., Riboulleau, A. (2006). Trace metals as paleoredox and paleoproductivity proxies: An update. Chemical Geology 232, 12–32. https://doi.org/10.1016/j.chemgeo.2006.02.012

Trigo, I.F., Davies, T.D., Bigg, G.R. (1999). Objective Climatology of Cyclones in the Mediterranean Region. Journal of Climate 12, 1685–1696. https://doi.org/10.1175/1520-0442(1999)012<1685:OCOCIT>2.0.CO;2

Trigo, R.M., Valente, M.A., Trigo, I.F., Miranda, P.M.A., Ramos, A.M., Paredes, D., García-Herrera, R. (2008). The Impact of North Atlantic Wind and Cyclone Trends on European Precipitation and Significant Wave Height in the Atlantic. Annals of the New York Academy of Sciences 1146, 212–234. https://doi.org/10.1196/annals.1446.014

Tromp, T.K., Van Cappellen, P., Key, R.M. (1995). A global model for the early diagenesis of organic carbon and organic phosphorus in marine sediments. Geochimica et Cosmochimica Acta 59, 1259–1284. https://doi.org/10.1016/0016-7037(95)00042-X

Tsimplis, M.N., Bryden, H.L. (2000). Estimation of the transports through the Strait of Gibraltar. Deep Sea Research Part I: Oceanographic Research Papers 47, 2219–2242. https://doi.org/10.1016/S0967-0637(00)00024-8

Tsimplis, M.N., Zervakis, V., Josey, S.A., Peneva, E.L., Struglia, M.V., Stanev, E.V., Theocharis, A., Lionello, P., Malanotte-Rizzoli, P., Artale, V., Tragou, E., Oguz, T. (2006). Chapter 4 Changes in the oceanography of the Mediterranean Sea and their link to climate variability. Developments in Earth and Environmental Sciences 4, 227–282. https://doi.org/10.1016/S1571-9197(06)80007-8

Tyson, R.V. (2001). Sedimentation rate, dilution, preservation and total organic carbon: some results of a modelling study. Organic Geochemistry 32, 333–339. https://doi.org/10.1016/S0146-6380(00)00161-3

Tyson, R.V., Pearson, T.H. (1991). Modern and ancient continental shelf anoxia: An overview. Geological Society Special Publication 58, 1–24. https://doi.org/10.1144/GSL.SP.1991.058.01.01

Uchman, A., Bak, K., Rodríguez-Tovar, F.J. (2008). Ichnological record of deep-sea palaeoenvironmental changes around the Oceanic Anoxic Event 2 (Cenomanian-Turonian boundary): An example from the Barnasiówka section, Polish Outer Carpathians. Palaeogeography, Palaeoclimatology, Palaeoecology 262, 61–71. https://doi.org/10.1016/j.palaeo.2008.02.002

Uchman, A., Rodríguez-Tovar, F.J., Machaniec, E., Kędzierski, M. (2013a). Ichnological characteristics of Late Cretaceous hemipelagic and pelagic sediments in a submarine high around the OAE-2 event: A case from the Rybie section, Polish Carpathians. Palaeogeography, Palaeoclimatology, Palaeoecology 370, 222–231. https://doi.org/10.1016/j.palaeo.2012.12.013

Uchman, A., Rodríguez-Tovar, F.J., Oszczypko, N. (2013b). Exceptionally favourable life conditions for macrobenthos during the Late Cenomanian OAE-2 event: Ichnological record from the Bonarelli Level in the Grajcarek Unit, Polish Carpathians. Cretaceous Research 46, 1–10. https://doi.org/10.1016/j.cretres.2013.08.007

Uchman, A., Wetzel, A. (2012). Deep-sea fans, in: Knaust, D., Bromley, R.G. (Eds), Trace Fossils as Indicators of Sedimentary Environments. Amsterdam:Elsevier. Developments in Sedimentology 64, pp. 643–671. https://doi.org/10.1016/B978-0-444-53813-0.00021-6

Uchman, A., Wetzel, A. (2011). Deep-Sea Ichnology: The Relationships Between Depositional Environment and Endobenthic Organisms, in: Hüneke, H., Mulder, T. (Eds.). Deep-Sea Sediments. Amsterdam:Elsevier, Developments in Sedimentology 63, pp. 517–546.

Ulbrich, U., Lionello, P., Belušić, D., Jacobeit, J., Knippertz, P., Kuglitsch, F.G., Leckebusch, G.C., Luterbacher, J., Maugeri, M., Maheras, P., Nissen, K.M., Pavan, V., Pinto, J.G., Saaroni, H., Seubert, S., Toreti, A., Xoplaki, E., Ziv, B. (2012). Climate of the Mediterranean, in: Lionello, P. (Ed), The Climate of the Mediterranean Region: From the past to the future. Amsterdam:Elsevier, pp. 301–346. https://doi.org/10.1016/B978-0-12-416042-2.00005-7

UNEP/MAP, Plan Bleu. (2020). State of the Environment and Development in the Mediterranean: Summary for Decision Makers. Nairobi.

Vadsaria, T., Ramstein, G., Dutay, J. -C., Li, L., Ayache, M., Richon, C. (2019). Simulating the Occurrence of the Last Sapropel Event (S1): Mediterranean Basin Ocean Dynamics Simulations Using Nd Isotopic Composition Modeling. Paleoceanography and Paleoclimatology 34, 237–251. https://doi.org/10.1029/2019PA003566

van der Walt, S., Colbert, S.C., Varoquaux, G. (2011). The NumPy Array: A Structure for Efficient Numerical Computation. Computing in Science & Engineering 13, 22–30. https://doi.org/10.1109/MCSE.2011.37

Van der Zwaan, G.J., Duijnstee, I.A.P., den Dulk, M., Ernst, S.R., Jannink, N.T., Kouwenhoven, T.J. (1999). Benthic foraminifers: proxies or problems? A review of paleocological concepts. Earth-Science Reviews 46, 213–236. https://doi.org/10.1016/S0012-8252(99)00011-2

Van Morkhoven, F.P.C.M., Berggren, W.A., Edwards, A.S. (1986). Cenozoic cosmopolitan deep-water benthic foraminifera. Bulletin des centres de recherche exploration-production Elf-Aquitaine 11.

Van Os, B.J.H., Lourens, L.J., Hilgen, F.J., De Lange, G.J., Beaufort, L. (1994). The formation of Pliocene sapropels and carbonate cycles in the Mediterranean: Diagenesis, dilution, and productivity. Paleoceanography 9, 601–617. https://doi.org/10.1029/94PA00597

Van Santvoort, P.J.M., De Lange, G.J., Langereis, C.G., Dekkers, M.J., Paterne, M. (1997). Geochemical and paleomagnetic evidence for the occurrence of "missing" sapropels in eastern Mediterranean sediments. Paleoceanography 12, 773–786. https://doi.org/10.1029/
97PA01351

Vance, D., Thirlwall, M. (2002). An assessment of mass discrimination in MC-ICPMS using Nd isotopes. Chemical Geology 185, 227–240. https://doi.org/10.1016/S0009-2541(01)00402-8

Vine, J.D., Tourtelot, E.B. (1970). Geochemistry of black shale deposits; a summary report. Economic Geology 65, 253–272. https://doi.org/10.2113/gsecongeo.65.3.253

Vinn, O., Bendella, M., Benyoucef, M., Zhang, L.-J., Bouchemla, I., Ferré, B., Lagnaoui, A. (2020). Abundant Zoophycos and Chondrites from the Messinian (Upper Miocene) of northwestern Algeria. Journal of African Earth Sciences 171, 103921. https://doi.org/10.1016/j.jafrearsci.2020.103921

Voelker, A., Lebreiro, S., Schonfeld, J., Cacho, I., Erlenkeuser, H., Abrantes, F. (2006). Mediterranean outflow strengthening during northern hemisphere coolings: A salt source for the glacial Atlantic? Earth and Planetary Science Letters 245, 39–55. https://doi.org/10.1016/j.epsl.2006.03.014

Vogel, H., Zanchetta, G., Sulpizio, R., Wagner, B., Nowaczyk, N. (2010). A tephrostratigraphic record for the last glacial–interglacial cycle from Lake Ohrid, Albania and Macedonia. Journal of Quaternary Science 25, 320–338. https://doi.org/10.1002/jqs.1311

von Grafenstein, R., Zahn, R., Tiedemann, R., Murat, A. (1999). Planktonic δ18O records at Sites 976 and 977, Alboran Sea: stratigraphy, forcing, and paleoceanographic

implications. Proceedings of the Ocean Drilling Program 161, 469–479. https://doi.org/10.2973/odp.proc.sr.161.233.1999

von Sternberg, K.G. (1833). Versuch einer geognostisch–botanischen Darstellung der Flora der Vorwelt. Fr. Fleischer, Leipzig, Prague 5–8.

Vorlicek, T.P., Kahn, M.D., Kasuya, Y., Helz, G.R. (2004). Capture of molybdenum in pyrite-forming sediments: role of ligand-induced reduction by polysulfides 1 1Associate editor: M. Goldhaber. Geochimica et Cosmochimica Acta 68, 547–556. https://doi.org/10.1016/S0016-7037(03)00444-7

Vörösmarty, C.J., Fekete, B.M., Tucker, B.A. (1998). Global River Discharge, 1807-1991, Version 1.1 (RivDIS). https://doi.org/10.3334/ORNLDAAC/199

Wang, B., Ding, Q. (2008). Global monsoon: Dominant mode of annual variation in the tropics. Dynamics of Atmospheres and Oceans, 44, 165–183. https://doi.org/10.1016/j.dynatmoce.2007.05.002

Wang, P.X., Wang, B., Cheng, H., Fasullo, J., Guo, Z., Kiefer, T., Liu, Z. (2017). The global monsoon across time scales: Mechanisms and outstanding issues. Earth-Science Reviews 174, 84–121. https://doi.org/10.1016/j.earscirev.2017.07.006

Warning, B., Brumsack, H.-J. (2000). Trace metal signatures of eastern Mediterranean sapropels. Palaeogeography, Palaeoclimatology, Palaeoecology 158, 293–309. https://doi.org/10.1016/S0031-0182(00)00055-9

Washington, R., Bouet, C., Cautenet, G., Mackenzie, E., Ashpole, I., Engelstaedter, S., Lizcano, G., Henderson, G.M., Schepanski, K., Tegen, I. (2009). Dust as a tipping element: The Bodélé Depression, Chad. Proceedings of the National Academy of Sciences 106, 20564–20571. https://doi.org/10.1073/pnas.0711850106

Wasmund, E. (1930). Bitumen, Sapropel und Gyttja. Geologiska Föreningen i Stockholm Förhandlingar 52, 315–350. https://doi.org/10.1080/11035893009448185

Wedepohl, K.H. (1995). The composition of the continental crust. Geochimica et Cosmochimica Acta 59, 1217–1232. https://doi.org/10.1016/0016-7037(95)00038-2

Wedepohl, K.H. (1971). Environmental influences on the chemical composition of shales and clay, in: Ahrens, L.H., Press, F., Runcorn, S.K., Urey, H.C. (Eds.). Physics and Chemistry of the Earth. Oxford: Pergamon, pp. 307–331.

Wedepohl, K.H. (1960. Spurenanalytische Untersuchungen an Tiefseetonen aus dem Atlantik. Geochimica et Cosmochimica Acta 200–231.

Weldeab, S., Siebel, W., Wehausen, R., Emeis, K.-C., Schmiedl, G., Hemleben, C. (2003). Late Pleistocene sedimentation in the Western Mediterranean Sea: implications for productivity changes and climatic conditions in the catchment areas. Palaeogeography, Palaeoclimatology, Palaeoecology 190, 121–137. https://doi.org/10.1016/S0031-0182(02)00602-8

Weltje, G.J., Bloemsma, M.R., Tjallingii, R., Heslop, D., Röhl, U., Croudace, I.W. (2015). Prediction of Geochemical Composition from XRF Core Scanner Data: A New Multivariate Approach Including Automatic Selection of Calibration Samples and Quantification of Uncertainties, in: Croudace, I.W., Rothwell, R.G. (Eds.). Micro-XRF Studies of Sediment Cores: Applications of a Non-Destructive Tool for the Environmental

Sciences. Dordrecht:Springer, pp. 507–534. https://doi.org/10.1007/978-94-017-9849-5_21

Westerhold, T., Marwan, N., Drury, A.J., Liebrand, D., Agnini, C., Anagnostou, E., Barnet, J.S.K., Bohaty, S.M., De Vleeschouwer, D., Florindo, F., Frederichs, T., Hodell, D.A., Holbourn, A.E., Kroon, D., Lauretano, V., Littler, K., Lourens, L.J., Lyle, M., Pälike, H., Röhl, U., Tian, J., Wilkens, R.H., Wilson, P.A., Zachos, J.C. (2020). An astronomically dated record of Earth's climate and its predictability over the last 66 million years. Science 369, 1383–1387. https://doi.org/10.1126/science.aba6853

Wetzel, A. (2010). Deep-sea ichnology: Observations in modern sediments to interpret fossil counterparts. Acta Geologica Polonica 60, 125–138.

Wetzel, A. (2008). Recent Bioturbation in The Deep South China Sea: A Uniformitarian Ichnologic Approach. PALAIOS 23, 601–615. https://doi.org/10.2110/palo.2007.p07-096r

Wetzel, A. (1991). Ecologic interpretation of deep-sea trace fossil communities. Palaeogeography, Palaeoclimatology, Palaeoecology 85, 47–69. https://doi.org/10.1016/0031-0182(91)90025-M

Wetzel, A. (1983). Biogenic Sedimentary Structures in a Modern Upwelling Region: Northwest African Continental Margin, in: NATO Conference Series, (Series) 4: Marine Sciences. pp. 123–144.

Wetzel, A., Tjallingii, R., Wiesner, M.G. (2011). Bioturbational structures record environmental changes in the upwelling area off Vietnam (South China Sea) for the last 150,000years. Palaeogeography, Palaeoclimatology, Palaeoecology 311, 256–267. https://doi.org/10.1016/j.palaeo.2011.09.003

Wetzel, A., Uchman, A. (2012). Hemipelagic and Pelagic Basin Plains, in: Developments in Sedimentology. pp. 673–701. https://doi.org/10.1016/B978-0-444-53813-0.00022-8

Whitmore, L.M., Shiller, A.M., Horner, T.J., Xiang, Y., Auro, M.E., Bauch, D., Dehairs, F., Lam, P.J., Li, J., Maldonado, M.T., Mears, C., Newton, R., Pasqualini, A., Planquette, H., Rember, R., Thomas, H. (2022). Strong Margin Influence on the Arctic Ocean Barium Cycle Revealed by Pan-Arctic Synthesis. Journal of Geophysical Research: Oceans 127, e2021JC017417. https://doi.org/10.1029/2021JC017417

Wolff, E.W., Chappellaz, J., Blunier, T., Rasmussen, S.O., Svensson, A. (2010). Millennial-scale variability during the last glacial: The ice core record. Quaternary Science Reviews 29, 2828–2838. https://doi.org/10.1016/j.quascirev.2009.10.013

Woodward, J. (Ed.) (2009). The physical Geography of the Mediterranean. Oxford: Oxford University Press. https://doi.org/10.1093/oso/9780199268030.001.0001,

Wu, J., Böning, P., Pahnke, K., Tachikawa, K., De Lange, G. (2017). Eolian and riverine contributions to central-Mediterranean sediments: a high-resolution Holocene record. 19th proceedings from EGU General Assembly 2017, Vienna, Austria. p.3836.

Wu, J., Böning, P., Pahnke, K., Tachikawa, K., de Lange, G.J. (2016). Unraveling North-African riverine and eolian contributions to central Mediterranean sediments during Holocene sapropel S1 formation. Quaternary Science Reviews 152, 31–48. https://doi.org/10.1016/j.quascirev.2016.09.029

Wu, J., Filippidi, A., Davies, G.R., de Lange, G.J. (2018). Riverine supply to the eastern Mediterranean during last interglacial sapropel S5 formation: A basin-wide perspective. Chemical Geology 485, 74–89. https://doi.org/10.1016/j.chemgeo.2018.03.037

Wu, J., Pahnke, K., Böning, P., Wu, L., Michard, A., de Lange, G.J. (2019. Divergent Mediterranean seawater circulation during Holocene sapropel formation – Reconstructed using Nd isotopes in fish debris and foraminifera. Earth and Planetary Science Letters 511, 141–153. https://doi.org/10.1016/j.epsl.2019.01.036

Wu, P., Haines, K. (1996). Modeling the dispersal of Levantine Intermediate Water and its role in Mediterranean deep water formation. Journal of Geophysical Research: Oceans 101, 6591–6607. https://doi.org/10.1029/95JC03555

Wüst, G. (1961). On the vertical circulation of the Mediterranean Sea. Journal of Geophysical Research 66, 3261–3271. https://doi.org/10.1029/jz066i010p03261

Xoplaki, E., González-Rouco, J.F., Luterbacher, J., Wanner, H. (2004). Wet season Mediterranean precipitation variability: influence of large-scale dynamics and trends. Climate Dynamics 23, 63–78. https://doi.org/10.1007/s00382-004-0422-0

Xoplaki, E., Trigo, R.M., García-Herrera, R., Barriopedro, D., D'Andrea, F., Fischer, E.M., Gimeno, L., Gouveia, C., Hernández, E., Kuglitsch, F.G., Mariotti, A., Nieto, R., Pinto, J.G., Pozo-Vázquez, D., Saaroni, H., Toreti, A., Trigo, I.F., Vicente-Serrano, S.M., Yiou, P., Ziv, B. (2012). Large-Scale Atmospheric Circulation Driving Extreme Climate Events in the Mediterranean and its Related Impacts, in: Lionello P. (Ed). The Climate of the Mediterranean Region. Amsterdam: Elsevier, pp. 347–417. https://doi.org/10.1016/B978-0-12-416042-2.00006-9

Zahn, R., Schönfeld, J., Kudrass, H.-R., Park, M.-H., Erlenkeuser, H., Grootes, P. (1997). Thermohaline instability in the North Atlantic during meltwater events: Stable isotope and ice-rafted detritus records from Core SO75-26KL, Portuguese Margin. Paleoceanography 12, 696–710. https://doi.org/10.1029/97PA00581

Zaragosi, S., Bourillet, J.-F., Eynaud, F., Toucanne, S., Denhard, B., Van Toer, A., Lanfumey, V. (2006). The impact of the last European deglaciation on the deep-sea turbidite systems of the Celtic-Armorican margin (Bay of Biscay). Geo-Marine Letters 26, 317–329. https://doi.org/10.1007/s00367-006-0048-9

Zhao, Y., Colin, C., Liu, Z., Paterne, M., Siani, G., Xie, X. (2012). Reconstructing precipitation changes in northeastern Africa during the Quaternary by clay mineralogical and geochemical investigations of Nile deep-sea fan sediments. Quaternary Science Reviews 57, 58–70. https://doi.org/10.1016/j.quascirev.2012.10.009

Zheng, Y., Anderson, R.F., Van Geen, A., Fleisher, M.Q. (2002). Remobilization of authigenic uranium in marine sediments by bioturbation. Geochimica et Cosmochimica Acta 66, 1759–1772. https://doi.org/10.1016/S0016-7037(01)00886-9

Ziegler, M., Jilbert, T., de Lange, G.J., Lourens, L.J., Reichart, G.-J. (2008). Bromine counts from XRF scanning as an estimate of the marine organic carbon content of sediment cores. Geochemistry, Geophysics, Geosystems 9. https://doi.org/10.1029/2007GC001932

Ziegler, M., Lourens, L.J., Tuenter, E., Hilgen, F., Reichart, G.-J., Weber, N. (2010). Precession phasing offset between Indian summer monsoon and Arabian Sea productivity linked to changes in Atlantic overturning circulation. Paleoceanography 25. https://doi.org/10.1029/2009PA001884

Zielhofer, C., von Suchodoletz, H., Fletcher, W.J., Schneider, B., Dietze, E., Schlegel, M., Schepanski, K., Weninger, B., Mischke, S., Mikdad, A. (2017). Millennial-scale fluctuations in Saharan dust supply across the decline of the African Humid Period. Quaternary Science Reviews 171, 119–135. https://doi.org/10.1016/j.quascirev.2017.07.010

Ziemen, F.A., Kapsch, M.-L., Klockmann, M., Mikolajewicz, U. (2019). Heinrich events show two-stage climate response in transient glacial simulations. Climate of the Past 15, 153–168. https://doi.org/10.5194/cp-15-153-2019

Zirks, E., Krom, M.D., Zhu, D., Schmiedl, G., Goodman-Tchernov, B.N. (2019). Evidence for the Presence of Oxygen-Depleted Sapropel Intermediate Water across the Eastern Mediterranean during Sapropel S1. ACS Earth Space Chemistry 3, 2287–2297. https://doi.org/10.1021/acsearthspacechem.9b00128

Zonneveld, K.A.F.F., Versteegh, G.J.M.M., Kasten, S., Eglinton, T.I., Emeis, K.-C., Huguet, C., Koch, B.P., de Lange, G.J., de Leeuw, J.W., Middelburg, J.J., Mollenhauer, G., Prahl, F.G., Rethemeyer, J., Wakeham, S.G. (2010). Selective preservation of organic matter in marine environments; processes and impact on the sedimentary record. Biogeosciences 7, 483–511. https://doi.org/10.5194/bg-7-483-2010

Zwiep, K.L., Hennekam, R., Donders, T.H., van Helmond, N.A.G.M., de Lange, G.J., Sangiorgi, F. (2018). Marine productivity, water column processes and seafloor anoxia in relation to Nile discharge during sapropels S1 and S3. Quaternary Science Reviews 200, 178–190. https://doi.org/10.1016/j.quascirev.2018.08.026

List of Acronyms

AHP	African Humid Period
AMOC	Atlantic Meridional Overturning Circulation
AW	Atlantic Water
BA	Bølling–Allerød interstadial
BI	Bioturbation Index
BP	Before Present
CPS	Counts per second
EA	East Atlantic Pattern
EA-WR	East Atlantic-West Russia pattern
EF	Enrichment Factor
EMDW	Eastern Mediterranean Deep Water
ETP	Eccentricity-Tilt-Precession
DO	Dansgaard-Oeschger Oscillation
DSDP	Deep Sea Drilling Project
GI	Glacial/Greenland Interstadial
GS	Glacial/Greenland Stadial
HE	Heinrich Events
HS	Heinrich Stadial
ICP-MS	Inductively coupled plasmas mass spectrometry
IODP	International Ocean Drilling Program
ITCZ	Intertropical Convergence Zone
LGM	Last Glacial Maximum
LGC	Last Glacial Cycle
LIW	Levantine Intermediate Water
MAW	Modified Atlantic Water
mbsl	meters below sea level
mcd	meters composite depth
MIS	Marine Isotope Stage
MMC	Mediterranean Meridional Oscillation
MO	Mediterranean Oscillation
MOW	Mediterranean Outflow Water

NAO	North Atlantic Oscillation
NN	Neural network
OD	Older Dryas
ODP	Ocean Drilling Program
OM	Organic Matter
ORL	Organic Rich Layer
PC	Principal Component
PCA	Principal Component Analysis
RGB	Red Green Blue
RSL	Relative Sea Level
S1, S2...	Sapropel 1, Sapropel 2...
T1, T2...	Termination I, II...
TOC	Total Organic Carbon
WDXRF	Wavelength dispersion X-Ray fluorescence
WMDW	Western Mediterranean Deep Water
XRF	X-Ray Fluorescence
YD	Younger Dryas Stadial

Appendix

Radiogenic isotopes of Eastern Mediterranean: additional work initiated during this thesis.

A.1. Introduction:

The core under investigation in this study was LC21 (see Fig. A1), which was recovered in the northern region of Crete. This particular core was subjected to extensive research in the past, as documented in studies (e.g., Satow et al., 2015; Grant et al., 2016). The well-established age model of LC21 provides a reliable foundation for our analysis. Moreover, the core's known tephra layers are of significant importance for our radiogenic analysis, as they can potentially influence the radiogenic signal.

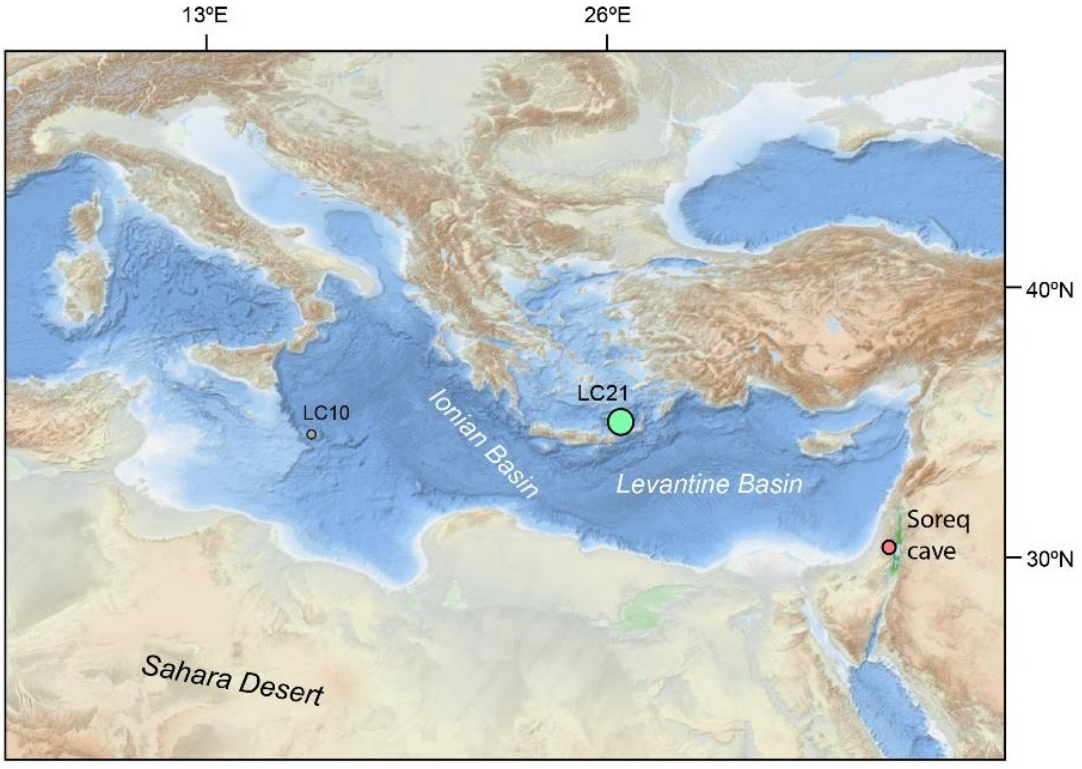

Figure A1. LC21's location is in the Eastern Mediterranean.

During my research, I had the opportunity to conduct two visits to the National Oceanography Centre (NOC) in Southampton, collaborating with the Paleoclimate and Palaeoceanography Group at the University of Southampton on a study investigating the provenance of the detrital fraction in the Eastern Mediterranean. We employed a novel technique involving the use of radiogenic isotopes of samarium and neodymium. It involved a series of steps aimed at eliminating any potential radiogenic isotopic signals that were not associated with the detrital fraction. These steps included various chemical treatments, in addition to the previously employed ones, to specifically target the removal of marine barite (Jewell et al., 2022). The crucial work carried out included core and sample selection, sampling procedures, sample preparation, application of methodologies to eliminate non-detrital signals, and the use of cation exchange columns. Throughout these processes, I closely collaborated with the personnel from NOCs, who provided invaluable support and expertise.

The studies undertaken had multiple objectives:

To investigate the provenance of the detrital fraction during periods of maximum and minimum insolation in the northern hemisphere. This analysis aimed to provide insights into how insolation influenced humidity patterns in the Mediterranean region. By examining precipitation patterns during these periods, we aimed to enhance our understanding of the impact of insolation on regional climate dynamics.

Understanding how the redox conditions during sapropel formation could affect the preservation of radiogenic isotopic signals. The methodology employed in this study involved several steps designed to remove organic matter. Yet further investigation was necessary to determine whether these methods developed for sediments with lower organic carbon content could be directly applied to highly organic-rich sapropels. Alternatively, adjustments to the methodology might be required to account for the unique characteristics of sapropel sediments with high organic carbon content.

A.2. Methodology used for radiogenic isotope analysis

For radiogenic isotope analysis, the samples must first be processed to remove all the marine contaminants that could affect the Sr and Nd signal of the terrigenous fraction (Fig. A2).

The samples were treated with different reactions in several steps following the method elaborated by Jewel et al. (2022), with the sample being rinsed in MilliQ water between each treatment. The first step is the drying sample; we select around 3 gr. The second step is decarbonating the sample with a 10% acetic acid over 24 hours. The third step involves

removing possible organic carbon with an H_2O_2 solution diluted at 10% over 48 hours at 65°C. The fourth step consists of removing the iron and manganese oxides that exist as authigenic coatings, adding a buffer to PH4 Hydroxylamine Na-EDTA and acetic acid solution, and using NaOH to control the PH. The fifth step is the removal of biogenic silica; this is done by adding 1.5M NaOH solution and sonicating the sample for 10 minutes, then letting it react for 2 hours in a bath at 85°C, repeating these processes 2 times and then letting it react for 24 hours at 65°C. The sixth step is the cation exchange wash with 1M $MgCl_2$ to remove the Sr signal, so it does not contaminate the cation columns associated with seawater; this is accomplished by treating the sample with 1 molar magnesium chloride for 24 hours. The next step, and the last before the freeze drying, is to remove marine barite, which is accomplished using 0.2 M diethylene triamine pentaacetic acid (DTPA) (Jewell et al., 2022). If this is the first time working on the site, the amount of DTPA treatment will have to be determined by splitting the sample and treating each split a different number of times; the treatment must be the minimum possible, but making sure all the barite is removed and that $^{86}Sr/^{87}Sr$ stabilises. Hence, these splits of the selected samples must be run until the end (through all the cation columns).

Nd and Sr were isolated using chromatographic column separation (Fig A3). Mother solutions were screened using an ICP obtaining the Ba, Nd and Sr in ppm; this value was used to select the amount of solution to subsample to have a minimum of 1 µg of Sr and 200 ng of Nd. Thus, a different amount of solution was sampled to run in the columns, attending to the screening results.

The solution was passed through a cation column containing Bio-Rad AG-50 W-X8 resin 200-400 µm mesh to remove Barium in the sample fraction isolated for isotopic analysis.

Nd was then isolated using a reverse phase column containing Ln-spec resin 50–100 µm (Pin and Zalduegui, 1997) to ensure good separation of the rare earth elements (REEs), especially Ce, and minimal interference during mass spectrometry. Sr was isolated using Eichrom Sr-spec resin, with an approximate recovery of 99.8%.

The Sr fraction was dried and loaded onto an outgassed Ta filament with 1 ml of a Ta activator solution. The samples were analysed on a ThermoScientific Triton Thermal Ionisation Mass Spectrometer using a multi-dynamic procedure and an ^{88}Sr beam of 2V. Fractionation was corrected using an exponential correction normalised to $^{86}Sr/^{88}Sr = 0.1194$.

Nd isotopes were measured using a multi-collector inductively coupled plasma mass spectrometer (MC-ICP-MS, Thermo Scientific Neptune). Corrected Nd isotopic compositions were obtained using a method based on Vance and Thirlwall (2002), adjusting to a $^{146}Nd/^{144}Nd$ ratio of 0.7219 and a secondary normalisation $^{142}Nd/^{144}Nd = 1.141876$. Results for the JNdi-1 reference standard (Tanaka et al., 2000) measured as an unknown were 0.512115 with an external reproducibility of ±0.000006 (2SD) across 6 analysis sessions over 2 years.

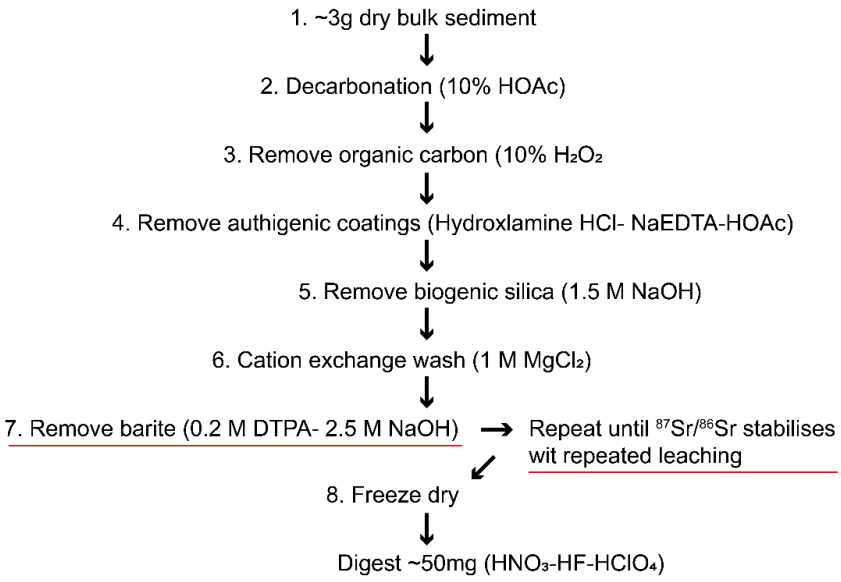

Figure A2. Sample preparation for radiogenic isotope analysis.

Figure A3. The setting of cation exchange columns in a clean laboratory.

A.3. Preliminary results and discussion

The analysis yielded interesting results regarding the variations in the detrital fraction within the Eastern Mediterranean, particularly the associations observed with humidity during sapropel formation. These findings shed light on the dynamic nature of the region and provide valuable insights into how the detrital fraction has changed over time.

For instance, as shown in Figure A4, the $^{86}Sr/^{87}Sr$ greatly decreased during the sapropel S5 and S1, also decreasing during MIS4. εNd, however, shows the same pattern during S5 and S1 but not during MIS2. In general, Nd is stable except for sapropels S5 and S1, while Sr isotopic composition seems more variable, with lows in sapropels at the end of MIS 2 and 3 and during MIS4.

In one instance during S5 (refer to Fig. A4), a significant decoupling was observed between the $^{86}Sr/^{87}Sr$ and εNd values. This decoupling suggests that these elements responded differently, potentially indicating a specific event or input of high ^{86}Sr into the basin. This punctual input of high ^{86}Sr could be responsible for the observed decoupling and warrants further investigation to understand the underlying processes and their implications.

When comparing the results with the known composition in the provenance areas (refer to Fig. A5), a consistent composition suggests a source from the central Sahara or a mixture of material from paleo-rivers and dust. However, during S5, the composition gradually shifts towards a higher proportion of riverine input. This observation aligns with the increased discharge during that period (Wu et al., 2017, 2018; Blanchet et al., 2021). Still, it is important to note that this response is not observed in S1, suggesting that the riverine discharge did not extend as far north during this period. Alternatively, other contributing factors in S5 may be responsible for the observed riverine signal. Further investigation is required to better understand the factors influencing the differences in the observed signals between S1 and S5.

S1, on the other hand, does exhibit a smaller response, suggesting an increase in riverine input. However, this response is not observed in sapropel S4, indicating markedly different conditions between interglacial and glacial sapropels. A preliminary interpretation could be that the variation in northern margin humidity was less significant during glacial periods, as suggested by previous studies (e.g., De Lange et al., 2008).

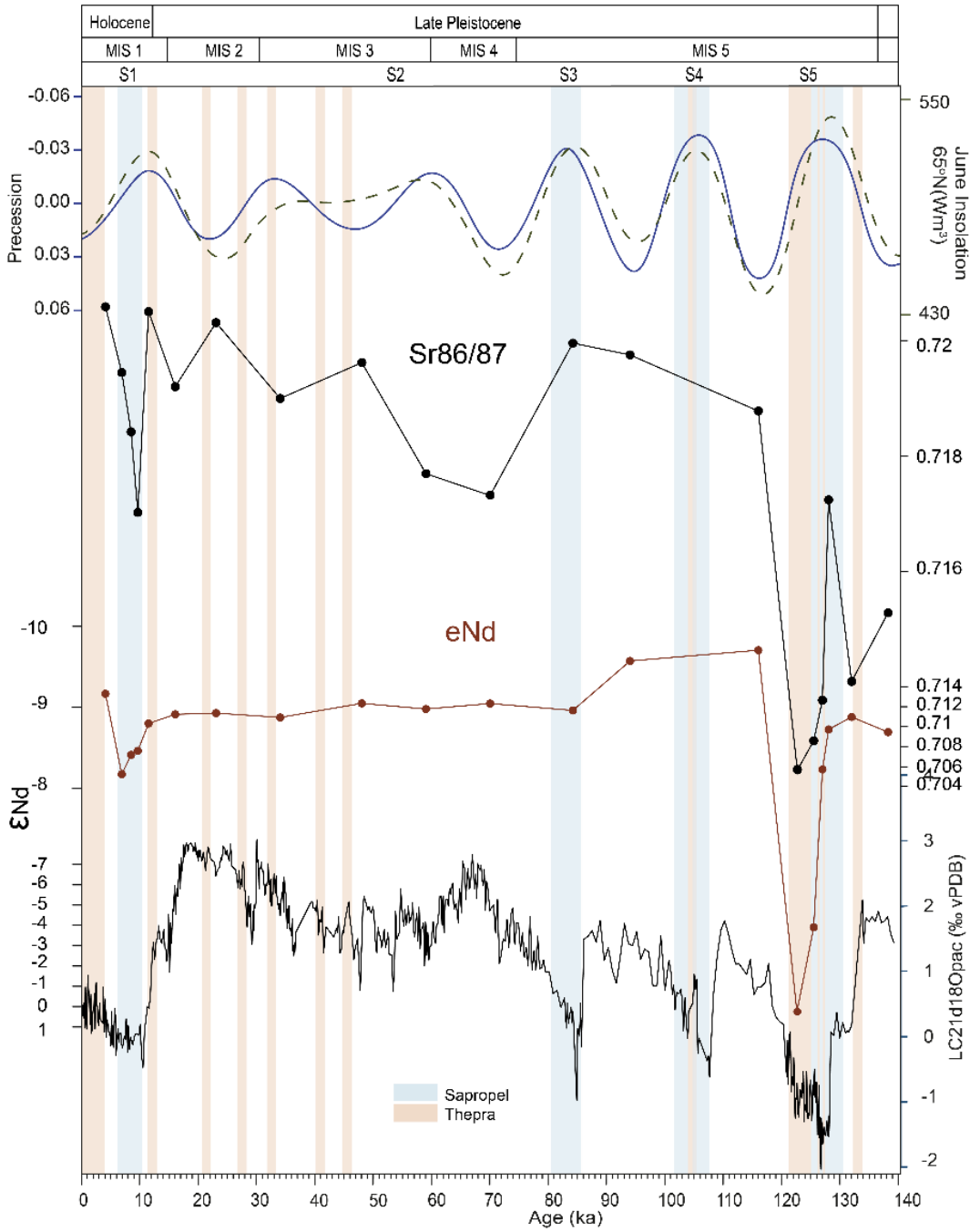

Figure A4. Variation of 86Sr/87Sr and εNd over time during the Last Glacial Cycle. Correlation with sapropels, marine oxygen isotope values and Insolation over the North Hemisphere.

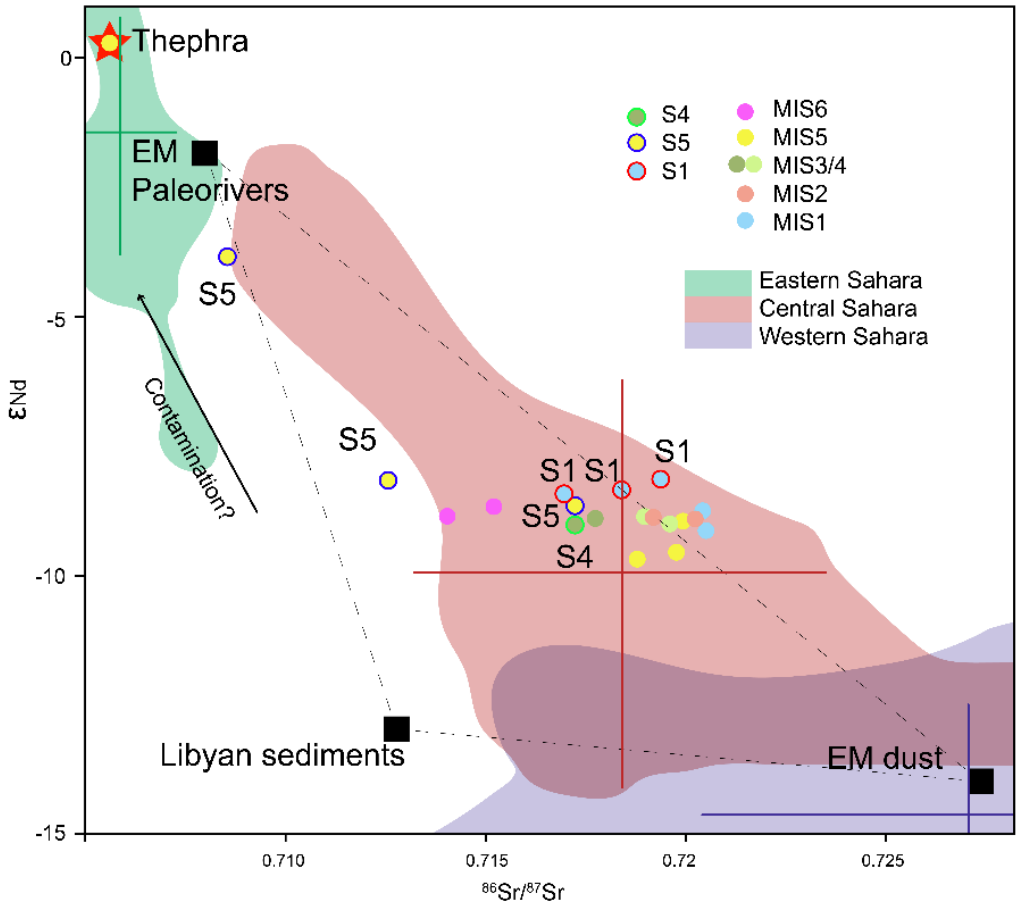

Figure A5. Projection of the values of $^{86}Sr/^{87}Sr$ and εNd and comparison with the values from precedence areas. Data for precedence area values from Blanchet et al. (2021).

Appendix references

Blanchet, C.L., Osborne, A.H., Tjallingii, R., Ehrmann, W., Friedrich, T., Timmermann, A., Brückmann, W., Frank, M. (2021). Drivers of river reactivation in North Africa during the last glacial cycle. Nature Geoscience 14, 97–103. https://doi.org/10.1038/s41561-020-00671-3

De Lange, G.J., Thomson, J., Reitz, A., Slomp, C.P., Speranza Principato, M., Erba, E., Corselli, C. (2008). Synchronous basin-wide formation and redox-controlled preservation of a Mediterranean sapropel. Nature Geoscience 1, 606–610. https://doi.org/10.1038/ngeo283

Grant, K.M., Grimm, R., Mikolajewicz, U., Marino, G., Ziegler, M., Rohling, E.J. (2016). The timing of Mediterranean sapropel deposition relative to insolation, sea-level and African monsoon changes. Quaternary Science Reviews 140, 125–141. https://doi.org/10.1016/j.quascirev.2016.03.026

Jewell, A.M., Cooper, M.J., Milton, J.A., James, R.H., Crocker, A.J., Wilson, P.A. (2022). Chemical isolation and isotopic analysis of terrigenous sediments with emphasis on effective removal of contaminating marine phases including barite. Chemical Geology 589, 120673. https://doi.org/10.1016/j.chemgeo.2021.120673

Pin, C., Zalduegui, J.S. (1997). Sequential separation of light rare-earth elements, thorium and uranium by miniaturized extraction chromatography: Application to isotopic analyses of silicate rocks. Analytica Chimica Acta 339, 79–89. https://doi.org/10.1016/S0003-2670(96)00499-0

Satow, C., Tomlinson, E.L., Grant, K.M., Albert, P.G., Smith, V.C., Manning, C.J., Ottolini, L., Wulf, S., Rohling, E.J., Lowe, J.J., Blockley, S.P.E., Menzies, M.A. (2015). A new contribution to the Late Quaternary tephrostratigraphy of the Mediterranean: Aegean Sea core LC21. Quaternary Science Reviews 117, 96–112. https://doi.org/10.1016/j.quascirev.2015.04.005

Wu, J., Filippidi, A., Davies, G.R., de Lange, G.J. (2018). Riverine supply to the eastern Mediterranean during last interglacial sapropel S5 formation: A basin-wide perspective. Chemical Geology 485, 74–89. https://doi.org/10.1016/j.chemgeo.2018.03.037

Wu, J., Böning, P., Pahnke, K., Tachikawa, K., De Lange, G. (2017). Eolian and riverine contributions to central-Mediterranean sediments: a high-resolution Holocene record. 19th proceedings from EGU General Assembly 2017, Vienna, Austria. p.3836.